GPR STUDIES ALONG ACTIVE FAULTS IN KACHCHH, WESTERN INDIA

A
Thesis
submitted to
THE M. S. UNIVERSITY OF BARODA
for the degree of
DOCTOR OF PHILOSOPHY
in Geology

BY

VIKAS CHOWKSEY

Department of Geology
Faculty of Science
The M. S. University of Baroda
Vadodara - 390 002
2013

CERTIFICATE

This is to certify that the contents of this thesis comprise original research of the candidate and have at no time been submitted for any other degree.

(Vikas Chowksey)	(D. M. Maurya)	(L. S. Chamyal)
Candidate	Guide	Head

ACKNOWLEDGMENTS

Foremost, I am deeply indebted to my guide Dr. D.M. Maurya for his endless enthusiasm and constant support during the present study. He not only introduced me to neotectonic of Kachchh in a simple manner but also made my vision broader and efficiently guided me in each aspect of my research work. The present study would not have been possible without his active involvement.

I am grateful to Prof. L. S. Chamyal, Head- Department of Geology, who inspired me to take up research. On and off discussions with him significantly improved my understanding in the field of Quaternary geology.

I am very thankful to Dr. Atul Patidar for their valuable discussion and suggestions during the course of study. Special thanks are due to my dear friends Mr. Nitesh N. Khonde and Miss Parul N. Joshi who provided invaluable help in the field. Ms. Mamta Tiwari helped in carrying out remote sensing analysis. I would also like to thank Mr. Vishal M. Ukey, Siddharth P. Prizomwala and Miss. Jaquilin Joseph who were always there when it mattered the most. Extensive GPR studies were mainly possible due to active help provided by Mr. Sanjay Rohit (Field Assistant). I would also like to thank Mr. Mayank Joshi and Mr. Tathagata Ghosh for providing all help and support as and when required. I also want to thanks my hostel colleagues Dhrumil, Pranav, Anand, Bhavesh, Chetan Bhai and Chintan for their kind support during the study.

I gratefully acknowledge the financial support received from the Department of Science and Technology (DST), and Ministry of Earth Sciences (MoES) in the form of research projects sanctioned to Dr. D. M. Maurya, for carrying out the present study.

I would also like to thank all my colleagues of Sub Surface Team, ONGC, Cambay for their support and encouragement ever since I joined them a couple of years back. My sincere gratitude to Mr. K. L. Jagetia, I/c SST, ONGC, Cambay for providing all the necessary support required to complete my doctoral work. I would also like to thank Dr. D. K. Baishya, Manager (Res) ONGC, Cambay for his constant encouragement to pursue my research work. I am thankful to all my colleagues who offloaded me with office workload in the final phase so that I can concentrate on completing my thesis.

At the end I am indebted to my family for their constant love and affection. This work is mainly the result of the blessings of my parents who have always motivated me in some of the frustrating part of my life. I would also like to thank my elder brother, my sister, and my maternal uncle who have shouldered all the responsibilities of family. Last

but not least, I would like to thank my fiancée Sweta Goswami for her love and support during the final phase of the study.

Vikas Chowksey

CONTENTS

PART – A BACKGROUND INFORMATION

	Page No.
CHAPTER-1 INTRODUCTION	**1-11**
The Rationale	1
The Kachchh seismic zone	3
Scope and objectives	5
Study area	6
Approach and methodology	10
CHAPTER-2 REGIONAL GEOLOGY AND STRUCTURE	**12-24**
Structural Setup	12
Regional geology	15
Mesozoic stratigraphy	15
Northern mainland	15
Wagad	18
Island Belt	20
Tertiary stratigraphy	22
Khari Nadi Formation	23
Kankawati Formation	24

PART-B KACHCHH MAINLAND FAULT (KMF)

CHAPTER-3 NEOTECTONIC SETTING	**25-36**
Morphotectonic segments	26
Fluvial geomorphology	27
The KMF scarp	30
Field setting of the KMF	32
CHAPTER-4 QUATERNARY STRATIGRAPHY	**37-62**
Nirona - Jhura segment	38
Kunaria - Lodai segment	43
Lodai - Jawaharnagar segment	49
Jawaharnagar - Khirasara segment	52
Khirsara - Devisar segment	54
Lithostratigraphy	55
Neotectonic implications	60
CHAPTER-5 GROUND PENETRATING RADAR (GPR) STUDIES	**63-89**
Importance of GPR technique in active fault studies	63
GPR studies along KMF	64
GPR data acquisition and processing strategy	65
Radar characterisation of Quaternary sediments	67
Mapping the KMF using GPR	74
Recognition of KMF in GPR data	75
Nirona - Jhura segment (Segment-I)	77
Kunaria - Lodai segment (Segment-II)	80
Lodai - Jawaharnagar segment (Segment-III)	80
Jawaharnagar - Khirsara segment (Segment-IV)	84
Khirsara - Devisar segment (Segment-V)	86

CHAPTER-6 EVIDENCE FOR EASTWARD EXTENSION AND PROPAGATION OF THE KMF **90-102**
Tectonic-Geomorphology-Segment VI 90
Geomorphic analysis 91
Drainage characteristics 94
GPR studies 97

PART-C SOUTH WAGAD FAULT (SWF)

CHAPTER-7 FIELD AND GPR STUDIES ALONG SOUTH WAGAD FAULT (SWF) **103-120**
The South Wagad Fault 105
Geomorphology and Quaternary sediments 107
GPR data acquisition 111
Near surface trace of SWF 112
GPR studies 113

PART-D SURFACE DEFORMATION RELATED TO KMF-SWF INTERACTION

CHAPTER-8 TECTONIC GEOMORPHOLOGY OF THE SAMAKHIALI-LAKADIA PLAIN **121-132**
Landscape characteristics 122
The Samakhiali Plain 123
The Lakadia Plain 124
Drainage characteristics 126
The Samakhiali Plain 127
The Lakadia Plain 128
Longitudinal River profiles 131

CHAPTER-9 LANDSCAPE ANALYSIS OF SAMAKHIALI-LAKADIA PLAIN USING REMOTE SENSING AND GIS **133-151**
Morphometric analysis 133
Drainages of the Samakhiali plain 135
Drainages of the Lakadia plain 136
Terrain analysis 137
DEM analysis 139
Geomorphic indices 141
Results and interpretation 151

PART-E GEDI FAULT

CHAPTER-10 FIELD AND GPR STUDIES ALONG THE GEDI FAULT **154-170**
Tectonic geomorphology 154
The Gedi Fault 157
GPR studies 157
Velocity analysis 158
Nature of Gedi fault and neotectonic implications 160

PART-F NEOTECTONICS OF THE ISLAND BELT FAULT (IBF)

CHAPTER-11 BELA AND KHADIR ISLANDS **171-185**

Tectonic geomorphology 172
The IBF scarp 172
Fluvial geomorphology 177
Bela island 178
Khadir and Bhanjada islands 180
Geomorphic evidence for Holocene uplift 182
Raised intertidal flats 182
Marine Erosional Features 183

CHAPTER-12 PACHHAM ISLAND **186-205**

Tectonic geomorphology 186
Fluvial geomorphology 191
Quaternary sediments 193
Lithostratigraphy 202
Evidence for neotectonic reactivation of IBF 203

PART-G INTERPRETATION AND SYNTHESIS

CHAPTER-13 DISCUSSION **206-218**

Neotectonic evolution of active fault zones 206
Towards a neotectonic model of Kachchh 211
Possible cause of high seismicity in Kachchh basin 217

CHAPTER-14 CONCLUSIONS **219-221**

APPENDIX **222-237**

REFERENCES **238-249**

LIST OF PUBLICATIONS OF VIKAS CHOWKSEY **250**

List of Figures

		Page No.
Figure 1.1	Map of Kachchh basin showing the general geomorphic configuration and various uplift bounding faults (based on Biswas, 1987). The boxed area (continuous line) shows the extent of the presently active Kachchh Seismic Zone as delineated by Mandal and Chadha (2008). Smaller boxes (dashed line) indicate the faults zones and area covered in the present study. A-KMF zone, B- SWF zone, C-Samakhilai-Lakadia plain, D-GF zone, E-IBF zone. (Inset-Location map).	2
Figure 1.2	Spatial distribution of 470 focal mechanisms in the Kachchh seismic zone. Smaller beach ball represents solutions for the aftershocks of Mw3.0-5.8. Medium size beach balls represent the focal mechanism solutions of the 7th March 2006 Mw 5.6 Gedi event and the 15th December 2007 Mw4.5 ABF event. And, the largest beach ball marks the focal mechanism solution of the 2001 Mw7.7 Bhuj mainshock. Solid lines mark the known faults i.e. NPF, KMF, ABF, IBF, BF and KHF (after Mandal, 2009).	05
Figure 2.1	Structural map of Kachchh showing various faults and epicentres of recent seismic activity (after Biswas and Khattri, 2002). Locations of epicentres of major earthquake are shown by stars (1819A: Rajendran and Rajendran, 2001; 1819B: Quittmeyer and Jacob, 1979; 1819C: Chandra, 1977).	13
Figure 2.2	Geological map of Kachchh basin (after Biswas and Deshpande, 1970)	16
Figure 3.1	**(a)** DEM of the eastern part of the Northern Hill Range. Note the close correspondence between the individual structures and the physiography. Also seen is the sharp physiographic contrast provided by the north facing scarps at the northern margin of the range and the flat terrain of the Banni plain which tends to die out at the eastern margin. The morphotectonic segments (I-VI) as delineated in the present study are also shown. Note that the KMF has no geomorphic expression in the segment-VI. **(b)** Generalised geomorphological map of the Northern Hill Range and the KMF zone. The KMF zone is marked by a narrow belt of Quaternary sediments between the scarps and the Banni plain. The domes shows typical radial drainage patterns conforming to the structure. Also shown are the numerous small streams that arise from the scarp region and flow northward traversing the Quaternary sediment cover. All drainages disappear in the Banni plain. 1-15 marks the locations of the lithologs of the exposed Quaternary sediments described in the next chapter.	28
Figure 3.2	Longitudinal river profiles of north flowing streams in various segments of KMF zone. The steepness of the profiles is observed to consistently reduce from segment-I to segment-V.	29
Figure 3.3	**(a)** Topographic profile drawn over the **c**rest of the E-W trending KMF scarps. The superimposed geological formations are not representative of the lithology of the scarps. Instead, the formations shown depict the depth of dissection down to maximum stratigraphic level in the respective part of the segments. The formations are schematically plotted based on the geological description of Biswas (1977). The figure shows eastward decreasing depth of dissection thereby progressive exposing younger formations. This correlates with the prominent decreasing height of the KMF scarps in the eastward direction. **(b)** Thickness of the Quaternary sediments developed in various segments of KMF.	31
Figure 3.4	**(a)** View of the KMF in a large artificially dug pit to the SW of Jhura showing it reverse nature. Note the sharp lithological contact between the softer Tertiary shales on the right (north) side and the compact Mesozoic rocks to the left (south) side of the fault plane. **(b)** View of a small outcrop showing the reverse nature of the fault plane of the KMF along a small stream to the north of Devisar. **(c)** View across the Lotia stream (west of	34

	Jawaharnagar)) showing the overturned (south diping) northern limb of the flexure which points to reverse nature of the KMF (not exposed here). Cliff section shows the flat surface over Quaternary sediments overlapping the Mesozoic rocks. The KMF scarp is visible at the far end. **(d)** Vertically dipping sheared Mesozoic rocks to the east of Jawaharnagar indicating the surface trace of the KMF. **(e)** View of a small exposure of the KMF in segment-V. **(f)** View of the Quaternary sediments overlying the south dipping Tertiary rocks (west of Jawaharnagar).	
Figure 3.5	**(a)** View of a stream section to the east of Khirsara showing the KMF expressed as a steep northward dipping fault marking the sharp lithotectonic contact between the near vertical Mesozoic rocks to the south and Tertiary rocks to the north. **(b)** The exposed fault plane of the KMF forming a scarp. **(c)** View of the low incised cliffs exposing Quaternary alluvial sediments reflecting the thin sediment cover. Also visible are the Tertiary rocks in the stream bed and the scarp (shown in previous photograph) in the background. **(d)** Northward view of the same stream showing incision in Mesozoic rocks and the almost flat topography beyond the fault line. The person is standing exactly along fault plane of the KMF shown in a.	35
Figure 4.1	Lithologs of Quaternary sediments exposed in Segment-I. Location of the lithologs is shown in Fig. 3.1b.	38
Figure 4.2	**(a)** Close view of clast supported bouldery gravel at the base of the exposed cliff section in Kaila river to the south of Jhura. **(b)** Close view of the largest boulder observed. The size of the clast is 0.6 m. **(c)** Tilted sediment succession of Quaternary deposits exposed in a lower order stream in segment-I. **(d)** View of aeolian miliolite forming the floor of the incised valley shown in (c). Note the fine grained nature of the deposit and the aeolian cross bedding. **(e)** Close view showing the aeolian cross bedding in the miliolite deposit shown in (d).	39
Figure 4.3	**(a)** Panoramic view of the KMF zone showing the field setting of the Quaternary colluvio-fluvial deposits along the Falay River. Note the flat surface formed over the colluvio-fluvial deposits exposed along the incised cliff of the river. Also seen are the vertical to sub vertical sheared Mesozoic rocks in the river bed and the sharp unconformable contact with the overlying stratified colluvio-fluvial deposits. **(b)** Close view of the colluvio-fluvial deposits resting unconformably over the Mesozoic rocks in Falay river. **(c)** View of the clast supported gravel in Falay river. Note the coarse nature of the deposit and the angular nature of the clasts. **(d)** View of a knick point in Falay river showing the sedimentary succession. Note the valley-fill miliolite dividing the colluvio-fluvial deposits into two distinct phases. Location of the knick point is about half kilometer upstream of the photographs in (a), (b) and (c).	44
Figure 4.4	Lithologs of Quaternary sediments exposed in Falay river in Segment-II. Location of the lithologs is shown in Fig. 3.1b. The vertical scale is in meters.	45
Figure 4.5	Lithologs of Quaternary sediments in Segment-II. Location of the lithologs is shown in Fig. 4.1b. The vertical scale is in meters.	48
Figure 4.6	Lithologs of Quaternary sediments in Segments III and IV. Lithologs 11-13 are from Segment-III while lithologs 14-15 are from Segment-IV. The vertical scale is in meters.	51
Figure 4.7	**(a)** Downstream view of large entrenched meander formed in Quaternary deposits to the north of the KMF scarp in Segment- IV. Note the deep incision and overall fine grained nature of the sediment succession exposed in the cliff which is in contrast to the sediments in segments to the west shown in earlier photographs. **(b)** View of a small incised meander in close	53

to the Banni plain. The KMF scarp is seen in the background. Note the sharp decrease in incision as compared with the incision shown in a. Rapid decrease in depth of incision in less than two kilometers suggests that neotectonic movements along the KMF are responsible for the incision of Quaternary sediments.

Figure 4.8 Lateral correlation of the Quaternary sediments exposed in the KMF zone. Note the clear distinct three phases of aggradation. The vertical scale is in meters. 57

Figure 4.9 Composite lithostratigraphic log of the Quaternary sediments occurring along the KMF zone in the study area. The vertical scale is in meters. 59

Figure 5.1 **(a)** Processed CMP profile taken over the cliff section of a stream near Dhrang. **(b)** Velocity diagram of the CMP profile shown in (a). **(c)** Processed CMP profile taken over the cliff section of Falay river. **(d)** Velocity diagram of the CMP profile shown in (b). 66

Figure 5.2 **(a)** Geomorphological map of KMF zone to the north of Habo dome. Locations of the sections studied and GPR sites are also shown. **(b)** Panoramic view of the KMF zone showing the field setting of the Quaternary colluvio-fluvial deposits along the Falay River. Note the flat surface in the front of the KMF scarps formed over the colluvio-fluvial deposits exposed along the incised cliffs of the river. Also seen are the vertical to sub vertical highly sheared Mesozoic rocks marking the KMF and the sharp unconformable contact with the overlying stratified colluvio-fluvial deposits. GPR survey (site 1) was carried out at the left hand corner of the photograph. **(c)** View of the incision of colluvio-fluvial surface by a stream to the east of Dhrang. **(d)** View of the exposed section in the incised cliff shown in b. Note the Mesozoic shales at the base and the distinct depositional phases. Height of the person in the picture is 170 cms.` 68

Figure 5.3 Lithologs of exposed sections of Quaternary colluvio-fluvial deposits at sites 1 to 4. Site 1, 2 and 4 are of river cliff sections while 3 is from a pit section. Location of lithologs is shown in Fig. 5.2a. 70

Figure 5.4 200 MHz monostatic antenna GPR profiles in wiggle mode. Various radar facies and corresponding lithologies are indicated against each profile. Location of sites is shown in Fig. 5.1a. **(a)** S-N profile from site 1 near the Falay River showing three distinct radar facies. **(b)** S-N profile from site 2 showing three distinct radar facies. 71

Figure 5.5 nonostatic antenna GPR profiles in wiggle mode. Various radar facies and corresponding lithologies are indicated against each profile. Location of sites is shown in Fig. 5.1a. **(a)** S-N profile from site 3. Photograph shows the exposed pit section. The rectangular box in the profile corresponds to the exposed pit section. **(b)** S-N profile from site 4 with photograph of the river section. Height of the person in the picture is 1.58 m. 73

Figure 5.6 Digital Elevation Model (DEM) of the study area prepared from Aster data highlighting the geomorphic set up of the KMF zone along with various morphotectonic segments of Kachchh Mainland Fault (KMF). 1-12 are the locations of the GPR survey transects. 75

Figure 5.7 **(a)** GPR profile taken from the northward flowing stream to the east of Palanpur village with 200 MHz antenna, location of site is shown in Fig. 5.5. Note the strong reflections emanating from the fault plane. **(b)** Oscilloscope of a single scan emanating from of the Mesozoic rocks **(c)** Oscilloscope of a single scan emanating from of the Tertiary rocks. **(d)** The boxed portion of (a) is shown in a Wiggle mode. 77

Figure 5.8 **(a)** GPR profile taken from South of Jhura village with 200 MHz antenna, location of site is shown in Fig. 5.5. Note the strong reflections emanating from the fault plane. **(b)** Oscilloscope of a single scan emanating from of the Mesozoic rocks **(c)** Oscilloscope of a single scan emanating from of the 79

Tertiary rocks. **(d)** The boxed portion of (a) is shown in a Wiggle mode.

Figure 5.9 **(a)** GPR profile taken from cliff section of the Falay river with 200 MHz antenna, location of site is shown in Fig. 5.5. Note the strong reflections emanating from the fault plane. **(b)** Oscilloscope of a single scan emanating from of the Mesozoic rocks **(c)** Oscilloscope of a single scan emanating from of the Tertiary rocks. **(d)** The boxed portion of (a) is shown in a Wiggle mode. 81

Figure 5.10 **(a)** GPR profile taken from south of Khengarpar with 200 MHz antenna, location of site is shown in Fig. 5.5. Note the strong reflections emanating from the fault plane. **(b)** Oscilloscope of a single scan emanating from of the Mesozoic rocks **(c)** Oscilloscope of a single scan emanating from of the Tertiary rocks. **(d)** The boxed portion of (a) is shown in a Wiggle mode. 82

Figure 5.11 **(a)** GPR profile taken from a cliff section of a distributary of the Dharampur stream near the Lotia dam with 35 MHz bistatic antenna in a point mode, location of site is shown in Fig. 5.5. Note the strong reflections emanating from the fault plane. **(b)** The boxed portion of (a) is shown in a Wiggle mode. **(c)** Oscilloscope of a single scan emanating from of the Mesozoic rocks **(d)** Oscilloscope of a single scan emanating from of the Tertiary rocks.` 83

Figure 5.12 **(a)** GPR profile taken from a cliff section of a north flowing stream near Jawaharnagar, location of site is shown in Fig. 5.5 with 80 MHz bistatic antenna in a point mode. Note the strong reflections emanating from the fault plane. **(b)** Oscilloscope of a single scan emanating from of the Mesozoic rocks **(c)** Oscilloscope of a single scan emanating from of the Tertiary rocks. **(d)** The boxed portion of (a) is shown in a Wiggle mode. 85

Figure 5.13 **(a)** GPR profile taken from north of Khirsara with 200 MHz antenna, location of site is shown in Fig. 5.5. Note the strong reflections emanating from the fault plane. **(b)** Oscilloscope of a single scan emanating from of the Mesozoic rocks **(c)** Oscilloscope of a single scan emanating from of the Tertiary rocks. **(d)** The boxed portion of (a) is shown in a Wiggle mode. 86

Figure 5.14 **(a)** GPR profile taken from south of Morwan village with 80 MHz bistatic antenna in a point mode, location of site is shown in Fig. 5.5. Note the strong reflections emanating from the fault plane. **(b)** Oscilloscope of a single scan emanating from of the Mesozoic rocks **(c)** Oscilloscope of a single scan emanating from of the Tertiary rocks. **(d)** The boxed portion of (a) is shown in a Wiggle mode. 87

Figure 5.15 **(a)** GPR profile taken from a north flowing stream south of Amrapar village with 80 MHz bistatic antenna in a point mode, location of site is shown in Fig. 5.5. Note the strong reflections emanating from the fault plane. **(b)** Oscilloscope of a single scan emanating from of the Mesozoic rocks **(c)** Oscilloscope of a single scan emanating from of the Tertiary rocks. **(d)** The boxed portion of (a) is shown in a Wiggle mode. 89

Figure 6.1 Digital Elevation Model (DEM) of Segment VI. The lines aa'-ff' are the location of the N-S topographic profiles shown in Fig. 6.2 while AA'-DD' are the location of E-W topographic profiles shown in Fig. 6.3. The thick red lines (10-12) denote the sites of GPR surveys described in this chapter. 91

Figure 6.2 N-S topographic profiles showing the prominent northward slope. Note the absence of surface indication of the KMF. The highest part of the slope consists of Mesozoic rocks with thin alluvial cover. The location of profiles is shown in Fig. 6.1. 93

Figure 6.3 E-W topographic profiles along the length of segment VI. location of the profile is shown in the Fig. 6.1. Note a prominent topographic low in the western part of the segment interpreted as a saddle. The topographically high central and eastern parts of the segment correspond to Mesozoic rocks in shallow depth and is interpreted as a structural high in the buried 94

Northern Hill Range.
Figure 6.4 Drainage map of the segment-VI. Note the parallel north flowing streams consistent with the slope direction. The streams emerge from the nearly flat suggesting recent uplift along the KMF buried at shallow depth. 95
Figure 6.5 Photographs showing the geomorphic characteristics of a small north flowing stream near Krishnanagar (east of Amardi) in segment-VI. **(a)** Upstream view of the narrow gorge like channel formed by the stream in caompact Mesozoic bedrock. **(b)** Visibly broadened channel of the same stream further north after it emerges from the Mesozoic rocks. The stream bed in the foreground shows patchy exposures of Tertiary rocks. GPR survey was carried out in this reach (site 2) for demarcating the near surface trace of the KMF. **(c)** E-W trending extensional ground cracks developed on alluvial surface in the vicinity of the GPR site 3 at Sikra. **(d)** Close view of the cracks **(e)** E-W trending cracks stream bed near the GPR site 2 shown in b **(f)** Close view of the crack in the stream bed. 96
Figure 6.6 Log of Trench 1 excavated by Rajendran et al. 2008 across the lateral spread during 2001 earthquake near Budharmora. 99
Figure 6.7 **(a)** GPR profile obtained north of Budharmora The profile was collected with 200 MHz antenna over close to the trench section shown in Fig. 6.5. Location of site is shown in Fig. 6.1. **(b)** Oscilloscope of a single scan emanating from of the Mesozoic rocks **(c)** Oscilloscope of a single scan emanating from of the Tertiary rocks. **(d)** The boxed portion of (a) is shown in wiggle mode. 99
Figure 6.8 **(a)** GPR profile taken east of Amardi. The profile is collected with 80 MHz bistatic antenna. Location of site is shown in Fig. 6.1. **(b)** Oscilloscope of a single scan emanating from of the Mesozoic rocks **(c)** Oscilloscope of a single scan emanating from of the Tertiary rocks. **(d)** The boxed portion of (a) is shown in wiggle mode. 101
Figure 6.9 **(a)** GPR profile taken to the west of Sikra village. The profile was collected with 200 MHz antenna. Location of site is shown in Fig. 6.1. **(b)** The boxed portion of (a) is shown in wiggle mode. **(c)** A 80 MHz bistatic antenna profile collected in a point mode **(d)** Oscilloscope of a single scan emanating from of the Mesozoic rocks **(e)** Oscilloscope of a single scan emanating from of the Tertiary rocks. 102
Figure 7.1 Geological map of Wagad region (after Biswas, 1993) 103
Figure 7.2 DEM of the SWF zone showing the sharp physiographic contrast along the fault. The sites of GPR survey are also shown. 106
Figure 7.3 **(a)** North facing view of the surface developed over the Quaternary sediments in the SWF zone to the east of Adhoi. The low ridge at the far end marks the SWF scarp which exposes steeply dipping Mesozoic rocks. **(b)** View of the SWF zone near Adhoi village showing the Tertiary rocks overlain by Quaternary sediments as exposed in a pit in the foreground. The prominent surface abuts upslope with the SWF scarp seen as a low ridge at the far end. **(c)** Upstream view of Adhoi river showing semi-compacted aeolian miliolite exposed in the river bed. **(d)** Upstream view of the incised channel of Kara Vokra river near Halra village in SWF zone exposing Quaternary alluvial deposits. The linear ridge at the far end marks the SWF scarp. 107
Figure 7.4 **(a)** Exposure of the SWF along a stream at the SE margin of the Chitrod dome. Note the almost vertical sheared Mesozoic rocks and the Tertiary rocks exposed in the cliff section on the downstream side. **(b)** Southward view of the dissected topography. The SWF is seen in the foreground. **(c)** Vertical sheared Mesozoic rocks marking the SWF zone. Wamka village is seen in the background. **(d)** Upstream view of the knick point formed along the SWF by a small south flowing stream near Shivlakha **(e)** Narrow chasm 108

carved out by the stream across the knick point shown in e.
Figure 7.5 Drainage map of the SWF zone. 109
Figure 7.6 **(a)** Processed CMP profile recorded near Mewasa **(b)** Velocity diagram of the CMP profile shown in (a). 111
Figure 7.7 **(a)** GPR profile obtained from east of Wamka village with 200 MHz antenna, location of site is shown in Fig. 7.2. Note the strong reflections emanating from the fault plane. **(b)** Oscilloscope of a single scan emanating from of the Mesozoic rocks **(c)** Oscilloscope of a single scan emanating from of the Tertiary rocks. **(d)** The boxed portion of (a) is shown in a Wiggle mode. 112
Figure 7.8 **(a)** GPR profile taken from south of Halra dome with 40 MHz bistatic antenna, location of site is shown in Fig. 7.2. Note the strong reflections emanating from the fault plane. **(b)** Oscilloscope of a single scan emanating from of the Mesozoic rocks **(c)** Oscilloscope of a single scan emanating from of the Tertiary rocks. **(d)** The boxed portion of (a) is shown in a Wiggle mode. 114
Figure 7.9 **(a)** GPR profile taken near the bank of Adhoi river with 80 MHz bistatic antenna, location of site is shown in Fig. 7.2. Note the strong reflections emanating from the fault plane. **(b)** Oscilloscope of a single scan emanating from of the Mesozoic rocks **(c)** Oscilloscope of a single scan emanating from of the Tertiary rocks. **(d)** The boxed portion of (a) is shown in a wiggle mode. 115
Figure 7.10 **(a)** GPR profile taken from east of Adhoi town with 40 MHz bistatic antenna, location of site is shown in Fig. 7.2. Note the strong reflections emanating from the fault plane. **(b)** Oscilloscope of a single scan emanating from of the Mesozoic rocks **(c)** Oscilloscope of a single scan emanating from of the Tertiary rocks. **(d)** The boxed portion of (a) is shown in a Wiggle mode. 116
Figure 7.11 **(a)** GPR profile taken from south of Shivlakha dome with 80 MHz bistatic antenna, location of site is shown in Fig. 7.2. Note the strong reflections emanating from the fault plane. **(b)** Oscilloscope of a single scan emanating from of the Mesozoic rocks **(c)** Oscilloscope of a single scan emanating from of the Tertiary rocks. **(d)** The boxed portion of (a) is shown in a Wiggle mode. 118
Figure 7.12 **(a)** GPR profile taken from south of Chitrod dome near Khanpar village with 200 MHz antenna, location of site is shown in Fig. 7.2. Note the strong reflections emanating from the fault plane. **(b)** Oscilloscope of a single scan emanating from of the Mesozoic rocks **(c)** Oscilloscope of a single scan emanating from of the Tertiary rocks. **(d)** The boxed portion of (a) is shown in a Wiggle mode. 119
Figure 7.13 **(a)** GPR profile taken near Mewasa with 80 MHz monostatic antenna, location of site is shown in Fig. 7.2. Note the strong reflections emanating from the fault plane. **(b)** Oscilloscope of a single scan emanating from of the Mesozoic rocks **(c)** Oscilloscope of a single scan emanating from of the Tertiary rocks. **(d)** The boxed portion of (a) is shown in a Wiggle mode. 120
Figure 8.1 Contour map of Samakhiali-Lakadia plain. Note the wider spacing of contours in the eastern part (Samakhiali plain) indicating gentle slope and relatively closely spaced contours in the western part (Lakadia plain) indicating steeper slope. 122
Figure 8.2 N-S topographic sections across Samakhiali plain showing the subtle geomorphic high in response to the rising KMF ridge in the subsurface. 123
Figure 8.3 N-S topographic profiles across the Lakadia Plain. 124
Figure 8.4 Drainage map of Samakhiali-Lakadia plain. The E-W trending zone of drainage disruption in Samakhiali plain is also shown. 125
Figure 8.5 **(a)** View of the steeply dipping Mesozoic rocks in the SWF zone. **(b)** View 128

	of broad indistinct channel of the Adhoi river in the zone of disruption. **(c)** Upstream view of the well defined channel with incised cliffs of the Adhoi river in the upstream part. **(d)** Upstream view of the channel of Adhoi river (Gupt river) near Chhadwala to the south of zone of disruption where the channel is again reappears. **(e)** View of the straight and narrow channel of the Kara Vokra river in the zone of disruption. **(f)** View of the shallow broad channel of the Khari Vokra river which flows westward through the central part of the Samakhiali graben.	
Figure 8.6	**(a)** View of the geomorphic high to the east of Lakadia with erosional gullies exposing Tertiary rocks. **(b)** Downstream view of the Khari river incising through Tertiary rocks near Lakadia. **(c)** View of the incised cliff section exposing Quaternary alluvial sediments along a stream to the south of Khanpar.	129
Figure 8.7	Longitudinal profiles of the rivers in Samakhiali plain	131
Figure 8.8	Longitudinal profiles of the rivers in Lakadia plain	131
Figure 9.1	Drainage map of the Khari Vokra basin.	135
Figure 9.2	Drainage map of the Adhoi basin.	136
Figure 9.3	Drainage map of the Khari basin.	137
Figure 9.4	Flow chart showing the methodology adopted in the present study.	138
Figure 9.5	Digital Elevation Model (DEM) of the Samakhiali-Lakadia plain.	139
Figure 9.6	Slope map of the Samakhiali-Lakadia plain.	139
Figure 9.7	Aspect map of the Samakhiali-Lakadia plain.	140
Figure 9.8	Hillshade map of the Samakhiali-Lakadia plain.	141
Figure 9.9	Schematic diagrams elaborating the method used for calculation of various geomorphic indices included in the present study.	142
Figure 9.10	Hypsometric curves of the drainage basins of Samakhiali-Lakadia plain.	143
Figure 9.11	Map of drainage basins showing AF values.	145
Figure 9.12	Map of drainage basins showing locations and values of T.	146
Figure 9.13	Contour map showing drainages and midpoints for which SL index calculated.	147
Figure 9.14	SL index map for the 64 drainages of the Samakhiali-Lakadia plain.	150
Figure 9.15	Interpolated SL index map of Samakhiali-Lakadia plain.	151
Figure 10.1	**(a)** DEM of the study area. The E-W trending low relief terrain of the Desalpar flexure zone is seen**. (b)** Drainage map of study area. Note the poorly developed drainage in the central part in contrast to the eastern part. Also note the radial drainage in Gangta bet in the extreme west. 1-6 are the locations of the GPR survey transects.	155
Figure 10.2	**(a)** Photomosaic showing the general geomorphology of the Gedi Fault zone. The mound like topography of the Quaternary miliolite deposits almost completely overwhelms the low relief fault scarp. The exposure of the Tertiary rocks shown is exposed due to the excavation done for the construction of a pond. (Loc. between Nagalpar and Gedi). **(b)** View of the north dipping strata of the overturned southern limb of the flexure. Also seen is the overlying thin sheet of aeolian miliolite deposits. **(c)** View of a well section showing the semi compacted aeolian miliolite deposits overlying the Mesozoic rocks. Note the southward steepening of dips of the Mesozoic strata due to the effect of the Gedi Fault which is located further left of the photograph. (Loc. west of Gedi).	156
Figure 10.3	**(a)** Exposure of the Gedi Fault in a shallow stream to the south of Nagalpar. Note the subvertical contact between the Mesozoic rocks and the Tertiary rocks marking the Gedi Fault. **(b)** View of the Gedi Fault exposed in an artificial excavation between Nagalpar and Gedi. Note the steep northward dipping fault plane and the Mesozoic rocks riding over the Tertiary sediments. **(c)** Photograph showing the reverse nature of the Gedi Fault in Gangta bet. Note the steep northward dip of the compact Mesozoic strata	158

	and the softer Tertiary sediments. **(d)** View of the GPR survey using Multi Low Frequency (MLF) antenna over the miliolite deposits.	
Figure 10.4	**(a)** Processed CMP profile taken over the Mesozoic rocks at Mayawandh. **(b)** Velocity diagram of the CMP profile shown in a. **(c)** Processed CMP profile taken over the Tertiary rocks at Mayawandh. **(d)** Velocity diagram of the CMP profile shown in (b).	159
Figure 10.5	**(a)** GPR profile taken to the north of Lakdaki Wandh using 40 MHz bistatic antenna. Note the strong reflections emanating from the fault plane. **(b)** Interpreted section of the profile shown in (a).	161
Figure 10.6	**(a)** Oscilloscope of a single scan emanating from of the Mesozoic rocks at site 2. **(b)** Oscilloscope of a single scan emanating from of the Tertiary rocks at site 1.	162
Figure 10.7	**(a)** GPR profile taken to the south of Mayawandh using 80 MHz antenna. Note the strong reflections emanating from the fault plane. **(b)** Interpreted section of the profile shown in (a).	162
Figure 10.8	**(a)** Oscilloscope of a single scan emanating from of the Mesozoic rocks at site 2. **(b)** Oscilloscope of a single scan emanating from of the Tertiary rocks at site 1.	163
Figure 10.9	**(a)** GPR profile taken to the north of Davari using 80 MHz antenna. Note the sharp amplitude contrast marking the trace of the Gedi Fault. Also seen is the tendency of the fault to become reverse near the surface. **(b)** Interpreted section of the profile shown in (a).	164
Figure 10.10	**(a)** Oscilloscope of a single scan emanating from of the Mesozoic rocks at site 3. **(b)** Oscilloscope of single scan emanating from the Tertiary rocks at site 2.	164
Figure 10.11	**(a)** 200 MHz profile obtained to the south of Nagalpar. Note the thin Quaternary sediment cover and the vertical nature of the fault. **(b)** Interpreted section of the profile shown in (a).	165
Figure 10.12	**(a)** Oscilloscope of a single scan emanating from of the Mesozoic rocks at site 4. **(b)** Oscilloscope of a single scan emanating from the Tertiary rocks at site 3.	166
Figure 10.13	**(a)** 200 MHz GPR profile taken to the west of Gedi. **(b)** Interpreted section of the profile shown in a. **(c)** Enlarged area of fault location marked in (a).	166
Figure 10.14	**(a)** Oscilloscope of a single scan emanating from of the Mesozoic rocks at site 5. **(b)** Oscilloscope of a single scan emanating from of the Tertiary rocks at site 4.	167
Figure 10.15	**(a)** 80 MHz GPR profile taken to the south of Bhojnari Dhar. The fault is marked by the amplitude contrast between the Mesozoic rocks and Tertiary sediments. **(b)** Interpreted section of the profile shown in (a).	168
Figure 10.16	**(a)** Oscilloscope of a single scan emanating from of the Mesozoic rocks at site 6. **(b)** Oscilloscope of single scan emanating from the Tertiary rocks at site 5.	168
Figure 11.1	Geological map of Bela, Khadir and Bhanjada islands (after Biswas, 1993) with Quaternary deposits around the margins of the islands.	172
Figure 11.2	**2** Digital Elevation Model (DEM) prepared from Aster Data showing the Bela, Khadir and Bhanjada islands. Note the prominent north facing escarpment and the south oriented backslopes.	173
Figure 11.3	E-W topographic profiles drawn over the crest of the northern escarpments of Bela (a), Khadir (b) Bhanjada and (c) islands.	174
Figure 11.4	Contour map (20 m interval) of the Bela island showing the landscape. Note the steep northern escarpment and the gorge formed across the scarp and increased spacing of the contours on the backslopes.	175
Figure 11.5	**(a)** Photomosaic of the northern escarpment of the Bela island. In the foreground is the rann surface and the vestiges of the palaeo rocky coast **(b)** Panoramic view showing the marine erosional landscape at the base of the	176

	Bela scarp seen in the background **(c)** View of the Khadir scarp. Note the youthful nature of the escarpment.	
Figure 11.6	Contour map of the Khadir island **(a)** and Bhanjada island **(b)**.	176
Figure 11.7	N-S topographic sections across Bela (a) Khadir (b) Bhanjada and (c) islands. The tilt block structure of the islands is clearly evident.	178
Figure 11.8	Drainage map of the Bela Island. Note the dominant south flowing drainages and the few north flowing drainages. Numbers 1-5 indicate the rivers whose longitudinal profiles of south flowing river shown in Fig. 11.10(a); Number 6-7 indicates the river whose longitudinal profile of north flowing river shown in Fig. 11.10(b).	179
Figure 11.9	Drainage map of the Khadir island. Numbers 1-8 are the rivers whose longitudinal profiles are shown in the Fig. 12.11.	180
Figure 11.10	Longitudinal river profiles of the Bela island, **(a)** showing the south flowing streams which are draining the southern gentle backslope; **(b)** showing the longitudinal profiles of two north flowing streams.	181
Figure 11.11	Longitudinal river profiles of the rivers of Khadir island.	181
Figure 11.12	**(a)** Distant view of the western margin of the Khadir island. In the foreground is the rann surface. **(b)** Close view of the exposed section of the raised inter-tidal sediments. **(c)** Flat terraced surface of the raised intertidal sediments. In the background is the Bhanjada island. **(d)** View of the terraced surface of raised intertidal sediments at the eastern margin of the Bhanjada island.	183
Figure 11.13	Lithologs of raised intertidal sediments at Khadir and Bhanjada islands.	184
Figure 11.14	**(a)** Lower level marine notch lying north of Bela island; **(b)** Upper level marine notch lying north of Bela island; **(c)** Upper level marine notch lying north of Khadir island; **(d)** Rocky platform developed to the north of the Khadir island.	185
Figure 12.1	**(a)** DEM of the Pachham island showing the various morphotectonic units. Note the north facing escarpment at the northern margin of the island and the central valley between the two hill ranges. Line AA' is the transect for the topographic profile shown in (b). **(b)** Topographic section along AA' transect shown in (a). Note the prominent geomorphic high in the central part that corresponds to the subsurface Median high.	187
Figure 12.2	Drainage map of the Pachham island. Note the downward south flowing parallel drainages on the backslopes of the Kaladongar hill range and the radial drainage pattern in the Goradongar hill range controlled by the domal structures. Also seen in the bifurcation of the backslope drainage of the Kaladongar hill range into west flowing and east flowing drainages due to the presence of the geomorphic high in the central valley shown in the Fig. 12.1b. Numbers with star indicates the location of the litho-sections shown in the Fig. 12.6 and 12.8.	189
Figure 12.3	**(a)** Northward view from Goradongar range of the central valley filled with incised Quaternary sediments. Kaladongar hill range can be seen in the background. **(b)** Southward view of the incised cliff section of the Dhorawar stream exposing Quaternary sediments. In the background is the Goradongar hill range.	190
Figure 12.4	Southward view of the incised valley of the Paiya Chhota stream showing two levels of terraces surface. Goradongar hill range is seen in the distant background.	191
Figure 12.5	Longitudinal river profiles of the south flowing rivers draining the back slopes of the Kaladongar Hill Range. Note the prominent convex up segments in all the profiles.	192
Figure 12.6	Lithologs of the Quaternary sediments occurring over the geomorphic high in the central valley. First two lithologs from left are from Harunwandh stream while the other three are from the Paiya chhota stream. Locations of	195

the section are shown in Fig. 12.2.
Figure 12.7 **(a)** A view of the section in the Harunwandh stream showing coarse gravel layers separated by sandy horizons. **(b)** View of the dissected surface developed over aeolian miliolite in the upstream part of the Harunwandh stream. Note sandy present day channel of the river. **(c)** Close view of the unsorted clast supported bouldery gravel overlying the Tertiary rocks at Rabviri to the north of the Goradongar range. 197
Figure 12.8 Lithologs of the exposed Quaternary sediments Location of the section is shown in the Fig. 12.2. 201

List of Tables

		Page No.
Table 2.1	Lithostratigraphy of Mesozoic rock of Kachchh Basin, (after Biswas, 1977).	17
Table 2.2	Stratigraphy of Tertiary sediments of Kachchh basin (after Biswas, 1992).	23
Table 4.1	OSL ages of the exposed Quaternary sediments. Sample PCH-1 is from the Pachham island while the rest are from the Quaternary sediment successions exposed in the KMF zone.	55
Table 9.1	Morphometric parameters, their mathematical expressions and references.	134
Table 9.2	Morphometric parameters for the rivers studied.	134
Table 9.3	Calculated values of parameters for hypsometric curve of the Adhoi basin.	142
Table 9.4	Calculated values of parameters for hypsometric curve of the Khari Vokra basin.	144
Table 9.5	Calculated values of parameters for hypsometric curve of the Khari basin.	144
Table 9.6	SL index values for the drainages of Samakhiali-Lakadia plain.	148
Table 13.1	Summary of the stratigraphy of the Quaternary sediments occurring in the active fault zones of Kachchh.	210

CHAPTER 1

INTRODUCTION

THE RATIONALE

Active tectonics is the prime factor governing the landscape evolution in seismically active areas. Characterization of geomorphic features in such areas is vital for estimating the influence of tectonic movements along faults in recent geologic past (Garcia et al. 2003). However, the landscape response to tectonic movements depends on the nature of uplift that can range from block uplift to tilting due to activity along bounding faults. Moreover, the nature of faults determines the style of structural and landscape deformation occurring in a region. Documenting the geomorphic indicators of active tectonics help in understanding current seismic activity in a neotectonic perspective. Generating geological data along the various active faults to understand their evolutionary history in the recent past is extremely important in view of the renewed conscious and concentrated efforts for evaluating the seismic hazard and mitigation in India (Chadha, 2010)

There is disagreement as to how far back in time 'geologically recent' is, with the common meaning being that neotectonics is the youngest, not yet finished stage in Earth tectonics. A general agreement has been emerging that the actual time frame may be individual for each geological environment and it must be set back in time sufficiently far to fully understand the current tectonic activity. Keeping in view of the fact, that the area of present study is located in Kachchh region, an area well known for recurrent seismic activity, it is imperative that the tectonic history of various faults is known for atleast the Quaternary period. In the present study, therefore, the tectonic activity that has occurred during the Quaternary period is classified as neotectonics. This meaning is implied at all places in the thesis wherever the term neotectonics is used.

The Kachchh basin is a E-W trending palaeo-rift graben that is currently undergoing active coseismic deformation as evidenced by the large scale changes in the landscape caused by large magnitude earthquakes in recent times as exemplified by the 1819 Allahbund earthquake and the 2001 Bhuj earthquake (Oldham, 1926; Bilham, 1998; Mandal and Chadha, 2008). The sedimentary sequence in the basin is approximately 4000 m thick, ranging from Lower Jurassic to Holocene with intervening Upper Cretaceous–Palaeocene basaltic flows of the Deccan Traps (Biswas, 1987). The Kachchh basin was

formed during the middle Jurassic whose subsequent rifting phase in extensional regime continued up to late Cretaceous followed by inversion phase of the Cenozoic have left a profound influence on the landscape.

Presently, the intrabasinal landscape of the Kachchh basin is characterised by major fault bound uplifts which includes the Island Belt Uplift, South Wagad Uplift, Desalpar uplift and the Kachchh Mainland Uplift (Fig. 1.1). These uplifts have prominent geomorphological expression and are bounded by the Island Belt (IBF), South Wagad Fault (SWF), Gedi Fault (GF) and the Kachchh Mainland Fault (KMF) respectively. The tectonic evolution of Kachchh Basin is primarily controlled by movements along three principal sub-parallel faults, namely, Island Belt Fault (IBF), South Wagad Fault system (SWF) and Kachchh Mainland Fault (KMF). The uplifted blocks expose Mesozoic rocks deposited in the rift phase of the basin until late Cretaceous with a pronounced flexure zone comprising asymmetrical domes and anticlines of various shapes and sizes along the generally E-W trending faults bounding the uplifts. In-between these fault bound uplands, the depressions or plains were formed which are occupied by Neogene sediments with thin Quaternary sediment cover.

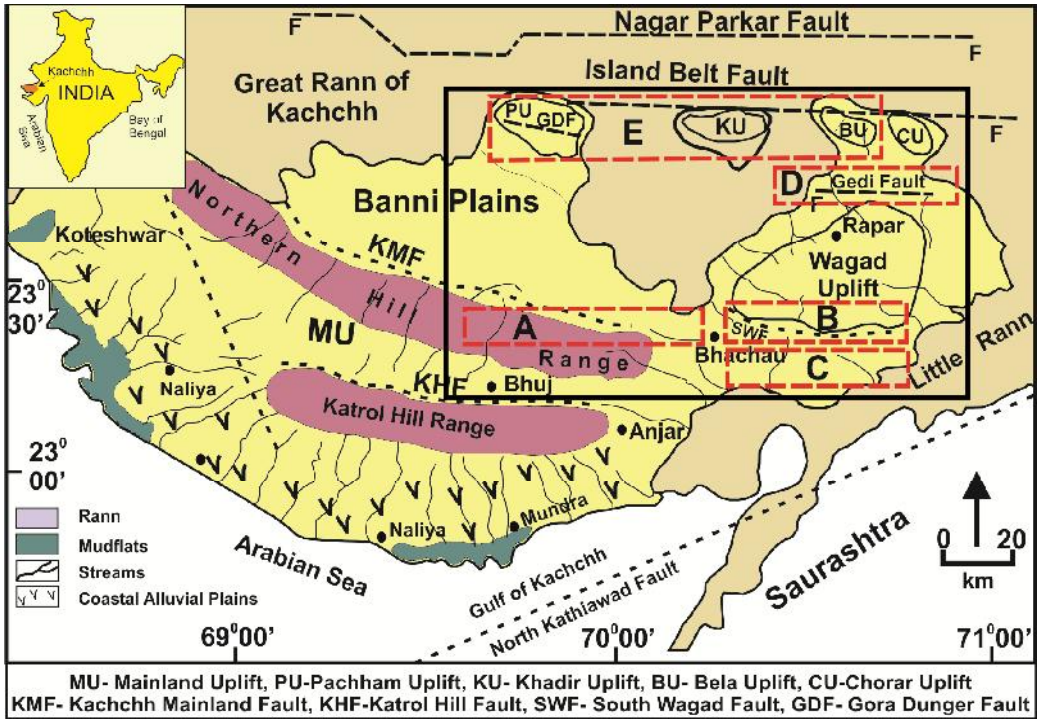

Figure 1.1 Map of Kachchh basin showing the general geomorphic configuration and various uplift bounding faults (based on Biswas, 1987). The boxed area (continuous line) shows the extent of the presently active Kachchh Seismic Zone as delineated by Mandal and Chadha (2008). Smaller boxes (dashed line) indicate the faults zones and area covered in the present study. A- KMF zone, B- SWF zone, C-Samakhiali-Lakadia plain, D-GF zone, E-IBF zone. (Inset-Location map).

PART-A Background Information

The Quaternary deformation in Kachchh basin is generally associated with the Indo-Eurasia collision in the north and the push from the spreading Mid-oceanic Ridge in the south (Thakur and Wesnousky, 2002). However, the Quaternary tectonic activity along the various faults has largely been a much neglected aspect in spite of the high seismic risk. The data available on this aspect is not commensurate with the amount and intense seismic activity witnessed in the Kachchh basin during historic times. This may be partially due to its vastness and remoteness and may be also because of the current political barriers blocking access in some regions. Though, a great deal of information on the pre-Quaternary stratigraphic and tectonic evolution of the basin is available, there are several major issues uninvestigated that can help to reconstruct the tectonic evolution during the Quaternary. Important questions that are unanswered concern the crustal controls on the distribution and kinematics of the various faults, rejuvenation of the fault zones, uplift mechanism, network of active faults including their connectivity, stress transfer and earthquake potential, and the role of tectonism versus climate in the geomorphological evolution of the region.

Despite an increased awareness of the potential for destructive earthquakes from faults within the Kachchh basin, very little information exists about the earthquake histories and recent kinematics of these faults. Specifically, the data available concerns to seismotectonic studies, majority of them carried out after the 2001 event, pre-Quaternary stratigraphic and tectonic evolution and few regional scale geomorphic studies. However, critical data of active fault parameters, recurrence intervals, dates and sizes of past events, slip rates, and kinematics for are non-existent. Furthermore, the exact nature and surficial location of many of these faults is not known. Such database is a primary requirement for constructing realistic probabilistic hazard maps for known active faults.

THE KACHCHH SEISMIC ZONE

On 26 January 2001, one of the deadliest intraplate earthquakes struck the western part of India, with conservative official estimate putting the number of human lives lost at 30,000 and the economic loss at US$ 10 Billion (Gupta et al. 2001; Rajendran et al. 2001; Thakur and Wesnousky, 2002). The epicentre of the earthquake was located at 23.326^{o}N, 70.317^{o}E, 15 km northwest of Bhachau and 60 km east of Bhuj (USGS). The earthquake was not surprising as the Kachchh region has experienced large earthquakes in the historical past (Thakur and Wesnousky, 2002). The May 1668 earthquake completely destroyed the town of Samaji (25^{o}N, 68^{o}E) (Burnes, 1835), and the 16 June 1819 Allahbund earthquake of magnitude > 8 in the Great Rann of Kachchh formed a mound

90 km long and up to 9 m in height (Bilham, 1998). The Allahbund earthquake killed 1500 people in Bhuj and 500 in Ahmedabad (Oldham, 1883). On 19 June 1845, an earthquake shook the walls of the fort at Lakhpat where some lives were lost, and the sea rolled up the Kori creek, overflowing the area westward. During the 1845 earthquake from 19 to 25 June, 66 shocks were counted (Nelson, 1846). The 30 April 1864 earthquake was felt in Wagad, Ahmedabad and Surat (Wynne, 1872). Anjar earthquake of 21 July 1956 which killed about 150 people was the last major earthquake in this region before the 2001 event (Chung and Gao, 1995). Recurrent damaging earthquakes in Kachchh and other parts of India have necessitated the initiation of concrete steps to minimise the impact of seismic hazard (Chadha, 2010)

In the contemporary seismotectonic set up, all intrabasinal faults of the Kachchh basin are believed to be seismically active thereby characterizing the basin as the one with potentially multiple seismogenic sources (Rajendran et al. 2008). Details of the previous earthquakes are scanty, but the 2001 Bhuj earthquake (Mw 7.7) and the prolonged post-earthquake aftershock sequence have been studied in detail (Mandal and Chadha, 2008; Mandal, 2009). The area enclosed by the aftershock activity includes a vast area in the eastern part of the Kachchh basin and has been identified as the Kachchh Seismic Zone (Mandal and Chadha, 2008). The zone encloses several E-W trending fault zones viz, the eastern part of Kachchh Mainland Fault (KMF), South Wagad Fault (SWF), Gedi Fault (GF) and the Island Belt Fault (IBF). These studies reveal progressive northward migration of seismic activity in the last decade which has generated several low to moderate magnitude earthquakes along the Gedi Fault and the Island Belt Fault (IBF) which lie to the north of the epicentral zone of the 2001 Bhuj earthquake (Mandal, 2008).

However, there are no studies available that document the neotectonic setting and history of these faults. Moreover, these faults are poorly constrained in terms of their precise location and shallow subsurface nature. This kind of data is helpful in understanding the neotectonic behaviour and stress accumulation along faults undergoing active coseismic deformation and also for carrying out future trench studies to delineate the palaeoseismic history. The present study is an attempt to delineate the geological parameters of the active faults of Kachchh Seismic Zone in a neotectonic perspective using field and GPR based studies.

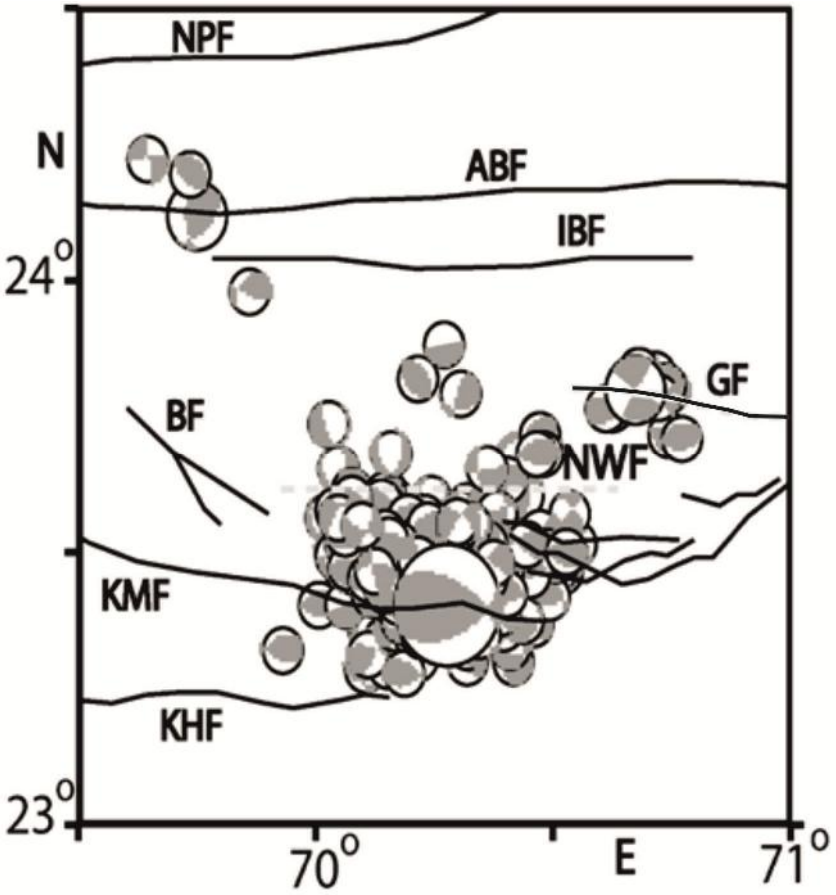

Figure 1.2 Spatial distribution of 470 focal mechanisms in the Kachchh seismic zone. Smaller beach ball represents solutions for the aftershocks of Mw3.0-5.8. Medium size beach balls represent the focal mechanism solutions of the 7th March 2006 Mw 5.6 Gedi event and the 15th December 2007 Mw4.5 ABF event. And, the largest beach ball marks the focal mechanism solution of the 2001 Mw7.7 Bhuj main shock. Solid lines mark the known faults i.e. NPF, KMF, ABF, IBF, BF and KHF (after Mandal, 2009).

SCOPE AND OBJECTIVES

The present study was focused on establishing the location, extent and geometric/structural characteristics of the active faults in the Kachchh Seismic zone using extensive field and GPR based studies. The data generated on neotectonic setting, shallow subsurface fault characteristics, Quaternary stratigraphic development and geomorphic evidences of neotectonic activity are interpreted in conjunction with available seismotectonic studies. The study also attempts to explain based on neotectonic evolution and fault characteristics, the reasons for high and anomalous distribution of seismicity in the basin and vulnerability of the various faults to high magnitude earthquakes in a qualitative sense.

The present study is the first attempt at building up a comprehensive understanding of the active faults in the Kachchh Seismic Zone from a neotectonic

perspective. The primary aim of the present study was to provide constraints on the location, shallow subsurface nature, neotectonic evolution and landscape shaping in the active fault zones of the Kachchh Seismic Zone. The study provides primary data base on geomorphologic, Quaternary stratigraphic, neotectonic evolution, GPR data constraining the precise location of active fault strand of the KMF, SWF, GF and IBF. Eastward lateral extension and propagation of the KMF up to the epicentral area of 2001 earthquake is established on the basis of unequivocal evidence from field and GPR studies. Active surface deformation going on in the Samakhiali-Lakadia plain as a response to KMF-SWF interaction has also been delineated. The data is used for qualitative characterisation of the active faults in terms of their potential to produce large magnitude earthquakes. The study also throws light on the causes of anomalously high and apparently unequal distribution of seismicity in the Kachchh basin as compared to the nearby tectonic terrains of the much fragmented western continental margin of the Indian plate. The data generated and presented in the subsequent chapters is intended to provide a basis for evolving seismic hazard models of the Kachchh basin.

The study was carried out to achieve the following objectives.

1. Delineate the relationship between the structural elements and the landscape configuration along the KMF, SWF, GF and IBF
2. Reconstruct Quaternary stratigraphy of the sediments occurring in the fault zones
3. Precise mapping of the near surface trace of the KMF, SWF, GF and determine their subsurface geometry and nature,
4. Reconstruct the neotectonic history and evolve a model of the Kachchh Seismic zone in contemporary seismotectonic setting.

STUDY AREA

Location

The present study is an attempt to provide neotectonic data on the active faults occurring within the Kachchh Seismic Zone. This zone roughly lies between 69^{o} E and 71^{o} E longitude and 23^{o} and 24^{o}N latitude (Fig.1.1).). Intense aftershock activity, since the post-2001 Bhuj earthquake testify to the active nature of the various faults in the Kachchh Seismic Zone (Mandal and Chadha, 2008). The present study was focussed along the seismically active eastern part of the Kachchh Mainland Fault (KMF), South Wagad Fault (SWF), Gedi Fault (GF) and the Island Belt Fault (IBF), all of which have prominent geomorphic expression as well. Detailed geomorphological studies were also

carried out in the Samakhiali-Lakadia plain to characterise the active deformation caused by the KMF-SWF interaction.

Communication

The area within the Kachchh Seismic zone has a reasonably good network of metalled roads. The Ahmedabad-Kandla National Highway is the only national highway passing through the Kachchh district which connects it with other parts of the country. Some of the important state highways which connect Kachchh with the other districts are the Bhuj-Anjar-Gandhidham road, Bhuj-Mandvi Road and Bhuj-Desalpar-Roha-Naliya-Jakhau road. The small towns and villages are also well connected with a dense network of road. The Great Rann and Banni plain from a largely inaccessible terrain. However, Banni plain is criss-crossed by several tracks connecting various villages which are motorable in dry season. The rail link is also available through Lakadia-Bhachau and Gandhidham-Bhuj rail routes. Bhachau and Bhuj are the major railway stations from which other parts of the area can be accessed by roads. Bhuj airport is the only nearest working civilian airport.

Physiography

Physiographically, the study area can be divided into hilly terrain of Northern Hill Range, Wagad, and Island belt, gently undulating terrain of the Samakhiali-Lakadia plain, Banni plain and the Great Rann. The Northern Hill range marks the northern margin of the Mainland Kachchh which abuts against the Banni plain in the north. The straight north facing escarpment forming the northern margin of the range is the most conspicuous landscape feature of the area. This escarpment marks the geomorphic expression of the Kachchh Mainland Fault, the most significant geomorphological feature of the study area. The Northern Hill Range shows typical mountainous terrain with structurally controlled topography and deep valleys (Fig. 1.1). The Jhura hill forms the highest elevation which is located in the western most segment of the study area. The hill range gradually loses its elevation towards the east and disappears below the Samakhiali-Lakadia plain. The low level flat saline terrain of the Banni-Great Rann sub-basin represents the recently uplifted floor of a palaeo-gulf.

East of the Northern Hill Range lies the Wagad highland which is oval shaped rocky uplifted mass. Wagad is characterized by three main hill ranges named as- the Southern hill range, the Kanthkot hill range and the Northern hill range. Wagad hills are made up of Mesozoic rocks and occur as an isolated uplifted block surrounded by Tertiary rocks, Rann and alluvial sediments. A radial drainage is the characteristic of

Wagad which is in the conformity of structural set up of the area. The drainages rises in the upland part of the Wagad and debouch in either Samakhiali-Lakadia plain or Ranns of Kachchh. Samakhiali-Lakadia plain lies south of the Wagad hill which is a flat surface comprises of thin cover of Quaternary sediments overlying the Tertiary rock. The low relief rocky terrain of the Desalpar Flexure zone lies to the north of Wagad.

The chain of islands comprising the Pachham, Khadir, Bela and Chorar islands together are termed as the Island belt. Pachham island forms the western most island which is characterised by hill range lying north and south margin of the island. The two hill range is separated by central valley which along which the major drainages of the region flows. On the contrary the Bela and Khadir island is characterized by the tilt block type of structure with a steep northern margin and a gentle back slope. Both the islands are characterized by southward flowing parallel drainage.

Drainage

The drainage of Kachchh provides an interesting example of a combination of lithologic and tectonic controls along with the influence of sea level fluctuations during Quaternary period. The drainage density of Kachchh is very high for a hyper arid region. The crest line of the Northern Hill forms the major drainage divide which have resulted in the north and south flowing drainages. The streams originating from the northern slopes of the Central highland, join the streams originated from the Northern hill range and pour their water into the Kaila, Pur, and Kaswali streams which, in turn, debouch into the Ranns. In general, the streams are ephemeral (seasonal) and carry water only during good monsoon. The Wagad region is characterized by the radial drainages reflecting a strong structure control. Adhoi river, Gupt river, Khari Vokra, Khari river forms the major river which rises from the southern margin of Wagad and drains the Samakhiali-Lakadia plain before joining the ranns and the Gulf of Kachchh. Overall, the drainages of the Wagad reflect a strong structural control. While the drainages of the Island belt is dominated by the parallel south flowing drainages developed over the gentle backslopes of the islands. Most of the streams incise through the compact Mesozoic rock forming deep valleys.

Climate

The Kachchh region is known for its arid to hyper-arid climatic conditions. The annual rainfall is about 250-400 mm/year, spread over the entire monsoon months of June to September. May marks the hottest month of the year where the day temperature reaches upto 48^{o}C while January forms the coldest month of the year when the temperature may dip below 10^{o}C. The range of wide temperature fluctuations is on

account of the Tropic of Cancer passing through the Kachchh region. During summer, violent storms are frequently noticed in the area though they are of short duration. NW disturbances may result in prevailing of the cold wave which may result in lowering of temperature below the minimum level. Humidity generally remains high throughout the year which is more in the coastal parts.

Flora

The Kachchh region is very poor in vegetation because of scanty rainfall. The semi-arid desertic climate favours the growth of thorny, non-thorny trees and shrubs which includes *Jal-salvador, Ganzi grenia*, whereas thorny species includes *Baval, Kher, Acacia*, etc. Where in the Acasia Arabia (Gandobaval) covers major portion of the terrain. The coastline exhibits swamps vegetated with mangrove forests and grasses covering dunes and sand flats. The main varieties of flora found in the study area are - Avicennia officinalis (Tavar, Tarvariyan), Leptadenia spartium (Khip), Casuarina Equisetifolia (Saru), Halopyrum mucronatum (Dariyai Kansdo, Dariyai Kans), Melia azadirachta (Limbdo), Acacia arabica (baval), Cassia auriculata (Aval), Sporobolus indicus (Velari charchar), Sueda maritima (Lano, Luno), Euphorbia tirucalli (Thor, Kharsani Thor, Dandalio Thor) Leucoena glauca (Laso baval, Vilayati baval) Butea frondosa (Kesuda no jhad), Zizyphus jujuba (Bordi), Acacia jaquemonti (Tal bavari), Acacia leucophlaea (Harmo baval), Tamarindus indicus (Amli), Sapindus emarginatus (Aritha), Cactus indicus (Hathlo thor), Ficus bengalensis (Vad), Eugenia jambolana (Jambu) etc. Wheat, Cotton, Bajara, Jowar, Mag and Math are common agricultural crops along with various fruits and vegetables.

Fauna

The vast land of Kachchh has long seashore and vast desertic condition which provide Kachchh an extraordinary variety of wild life attracting a large number of avifauna. The chief domestic animals found in the area are horses, camels, oxen, cow, buffaloes, sheep, goats and asses. The wild animals of the region include Panthera pardus (Panther), Chinkara (Gazella Gazella) (local name Chinkara) and the wild asses (Equus Onager Indicus) were found near the little rann of Kachchh. Neelgai or Blue Bull (Bojh), Wild Boar or Jungli Budhar (Sus Scrofa), Indian Wolf (Canis Lepus), Jackal or Shiyad (Canis Auresug), striped Hyena or Jharak (Hyena Hyonna), Desert Hare or Sasla (Lepus Nigricollis Outchensis), Indian Fox (Vulpe Bengalenisis), Mongoose (Herpestus Smithi), besides some jungli cats, desert cats, Pangolin, Indian Porcupine and long eared hedgehod are also found in Kachchh. The Indian Hare (Lepus Nigricollis) is commonly found in the

open fields. The Caracal is the rarest animal found in Kachchh. Many kinds of reptiles including snakes are also found in Kachchh. Some of commonly found reptiles are Crocodile or Mugger, Monitor Lizard or Patla Gho, Kachchh Rock Gecho (Garodi), Desert Monitor Lizard, spiny-tailed lizard or Sanda (Uromastyx Hardwicki), flat-tailed lizard or Khann, Starred Tortoise and fresh water turtle (Lissemus Puctata) along with several varity of snakes both: Poisonous and Non-Poisonous. Black Krait, Black Cobra (Najatripudians), Russels Viper (Vipera Russeli), Saw Scaled Viper (Echlis Carinatus), Sea Snake (Hydrophis Spiralis) etc. are poisonous snakes, while Python (Python Molurus), Sand Boa (Eryx Conicus), Rat Snake (Piyas Mucosus), Royal Snake (Zamenis Diadema) etc. are non-poisonous snakes. The resident and migratory birds are commonly found in Kachchh. The migratory birds are found plentiful during winter season in the organic rich zone of the coastal flats bordering the Gulf of Kachchh and the vast saline expanse of the Little Rann of Kachchh.

People and occupation

Kachchh district is inhabited by various groups and community. Around~ 80% of its population resides in the rural area so people are mainly dependent on agriculture and cattle rearing. The economy of the region is agro based and region is famous for its craft work. The construction of many big ports in the coastal parts of Kachchh has initiated the rapid industrialization between Gandhidham-Mundra and Bhuj-Bhachau during the recent time, which has provided another window of opportunity for the people to earn their livelihood.

APPROACH AND METHODOLOGY

The Kachchh Seismic Zone is ideal for carrying out neotectonic studies. It is essential to employ a comprehensive approach involving geomorphic and stratigraphic data to enable reconstruction of a detailed geomorphic evolutionary history including the nature and timing of tectonic activity along active faults (Chamyal et al., 2002). The present study was carried along the active faults of the Kachchh Seismic Zone viz. the KMF, SWF, GF and IBF, which show significant imprints of neotectonic activities in recent past on the landscape and is affected by a prolonged aftershock sequence since the 2001 Bhuj earthquake. A comprehensive approach involving detailed field mapping of the landforms, DEM modelling and stratigraphic and shallow subsurface studies of the Kachchh Mainland Fault (KMF), South Wagad Fault (SWF) and Gedi Fault (GF) using

PART-A Background Information

GPR has been applied to reconstruct the geomorphic evolution of the study area. The detailed methodology employed for carrying out the present study is described below.

- Available published data on the stratigraphic, structural and seismotectonic aspects of the Kachchh region were critically studied and evaluated to understand the regional geological setting and possible influences of these on the geomorphic set up of the active fault zones.
- Regional scale geomorphic set up of the study area was delineated using Survey of India topographical maps and satellite images.
- Field mapping of various geomorphic features and landforms was carried out. The landforms of the study area were initially categorized into Quaternary and pre-Quaternary geomorphic features and were mapped separately before synthesising them to reconstruct a comprehensive neotectonic evolution of the study area.
- The DEM (Digital elevation models) of the study area were prepared with different resolutions to appreciate the role of various tectonogeomorphic features in landscape evolution.
- The exposed Quaternary sediments were studied with a view to understand the genetic aspects of the landforms and stratigraphic evolution. Both, the fluvial and colluvial sediments were investigated during the course of the study.
- Ground Penetrating Radar (GPR) was used for the precise mapping of the near surface trace of the KMF, SWF and GF and also for determining their nature in the shallow subsurface.
- Detailed remote sensing analysis was carried out for the flat terrain of the Samakhiali- Lakadia plain to delineate the geomorphic signatures of KMF-SWF interaction.
- The morphostratigraphic evolution of the fault zones was reconstructed based on detailed field criteria, field relationships of the various landforms and stratigraphic data. Major tectonic events responsible for the overall geomorphic evolution of the area were also identified.
- The field and GPR data were synthesised and compared to reconstruct the pattern and nature of neotectonic activity along the various fault zones. The results of the studies along the various fault zones were compiled to prepare a neotectonic model of the Kachchh Seismic Zone

CHAPTER 2

REGIONAL GEOLOGY AND STRUCTURE

STRUCTURAL SETUP

The structural setup of the Kachchh basin is mainly controlled by block faulting. The upland forms the tilted block type of structures along the principal faults (Biswas, 1987; 2005). The major uplifts are bounded by five parallel E-W trending faults from north to south (Fig. 2.1) by: (1) Nagar Parkar Fault (NPF), (2) Island Belt Fault (IBF), (3) South Wagad Fault (SWF), (4) Kachchh Mainland Fault (KMF), and (5) North Kathiawar Fault (NKF) respectively. On account of movement along the principle faults there are six major uplifts occur within the Kachchh basin, viz., Pachham, Khadir, Bela and Chorar hill (Island Belt), Wagad highland and Mainland of Kachchh. The lows between the uplifted landmasses are forming the residual depressions as the central valley of Pachham, Rav low land of Wagad. The structure of Kachchh basin described in the following paragraphs is based on detailed work carried out by Biswas (1974; 1977; 1982; 1987; 1993; 2005).

The evolution of the Kachchh rift took place on account of periodic reactivation of the various basement related faults. The rift evolved within the Mid-Proterozoic-Aravalli-Delhi fold belt by reactivation of pre-existing faults along NE–SW trend of Delhi fold belt that swings to E–W in Kachchh region (Biswas, 1977; 1987; 1993; 2005). The rift phase is related to the break up of Gondwanaland which initiated the rifting phase of the Kachchh basin as pericratonic rift within Precambrian mobile belt. Normal faulting formed a series of half-grabens successively from north to south (Biswas, 1987; 2005).

The basin has the typical geometry of an asymmetric rift basin tilted to the south. The Radhanpur-Barmer basement arch forms the hinterland high, which marks the easternmost limit of the rift. To the west, the rift is open, merging with the continental shelf. Rift fill sedimentation continued during the drifting of the plate till Early Cretaceous. In Late Cretaceous, the trailing edge of the Indian plate was uplifted as the leading edge was dragged down towards the Tethyan trench (Biswas, 2005). It has resulted in the inversion of the basin on account of reversed movement of blocks along steep faults (normal faults during rifting). The uplifts came into existence by upthrust of the footwall blocks. The most striking feature of the basin is the occurrence of a first order meridional (NNE-SSW) high (Median High) across the middle of the basin. It

passes transversely across both positive and negative elements of the basin so that the uplifts plunge bilaterally and the sub-basins have a central high or shallow region (Biswas, 1987; 1993). The Median High has controlled the sediment facies and thickness is a tectonized zone along the hinge line of the basin (Biswas, 1987). It shows a strong geomorphologic expression in the present-day landscape.

The tectonic episodes were accompanied by deep crustal magmatic activity. At least two phases of magmatic activity are evident. The first activity took place during extensional stage when ultramafic rocks intruded into the older Jurassic sediments. Presumably at this time the deep-seated magmatic body was emplaced at the site of the mantle rupture close to the basin centre. The other activity took place during Late Cretaceous post-rift uplift stage when plume related alkali and tholeiitic basalts were intruded into the younger Early Cretaceous sediments and extruded as the Deccan Trap flows (Biswas, 2005).

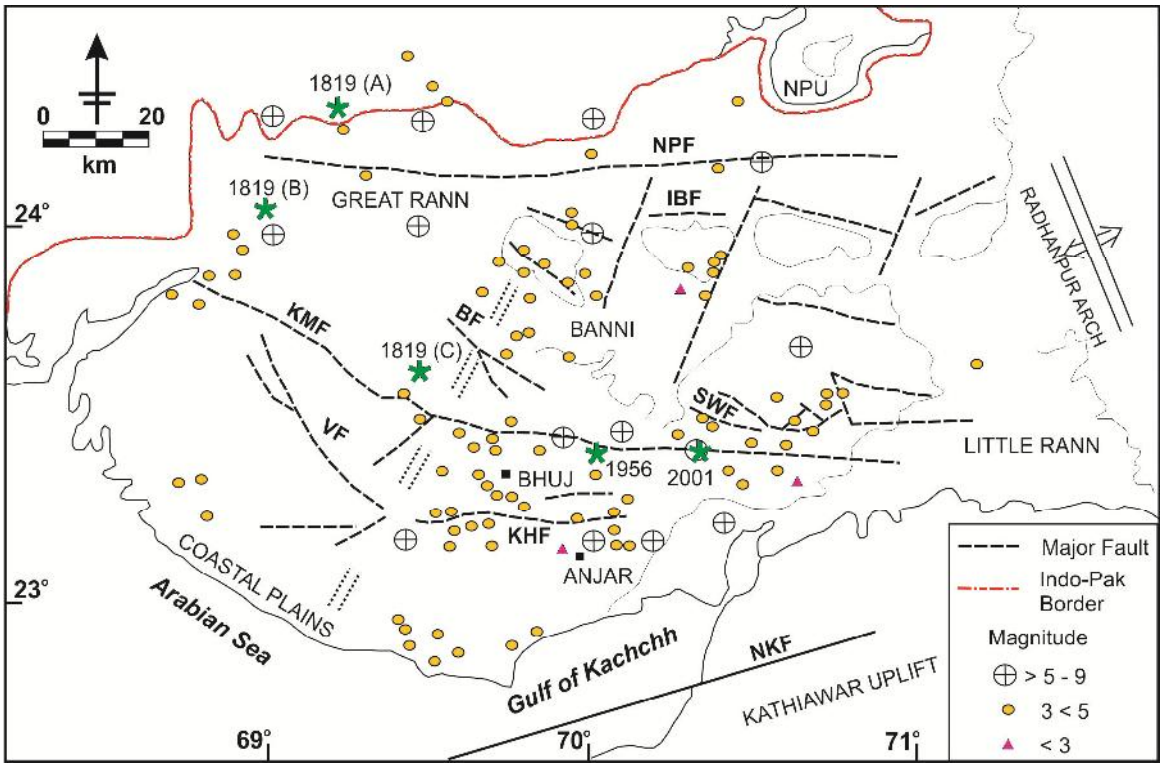

Figure 2.1 Structural map of Kachchh showing various faults and epicentres of recent seismic activity (after Biswas and Khattri, 2002). Locations of epicentres of major earthquake are shown by stars (1819A: Rajendran and Rajendran, 2001; 1819B: Quittmeyer and Jacob, 1979; 1819C: Chandra, 1977).

The Kachchh basin is characterized by E-W tectonic fabric and its tectonic evolution is mainly governed by movements along three principal sub-parallel, vertical to quasi-vertical faults viz. Island Belt Fault (IBF), South Wagad Fault (SWF) and Kachchh Mainland Fault (KMF), whose strike in the eastern part of the basin is E-W which swings

to WNW-ESE in the western margin of the basin. The inversion of the basin has resulted in the fault bounded uplift. The resulted uplift has resulted in the formation of 'Residual Depressions' (Beloussov, 1962) or sub-basins which have acted a depo-centre for the post Mesozoic sedimentary cycle. These sub basins are Great Rann of Kachchh (lies between Nagar-Parkar-Tharad and Island Belt ridges), Banni Basin (lies between Island Belt ridges and Mainland ridges), Little Rann of Kachchh (lies between Wagad ridge and Barmar-Radhanpur Arch) and Gulf of Kachchh (lies between Mainland ridge and Kathiawar high). The continuous compression of the Kachchh basin has resulted in formation of domal and anticlinal structures and gentle flexures along the faulted margin.

The regional trend of the principal faults and associated folds, in the Kachchh, is WNW-ESE in the West, and it tends to swing to E-W near Wagad and further to the East. The Mainland uplift is the biggest uplift followed by the Wagad uplift in term of size. The E–W striking master faults have played a major role during the structural evolution of the basin (Biswas, 2005). All faults are bordered on their upthrown side by a flexure zone comprising domes and anticlines of various shapes and sizes. Major domes among them are Jumara Dome, Jara Dome, Jhura Dome, Chitrod Dome, Mae Dome, Vamka Dome, Halra Dome etc.

The height of the scarp lying north of Northern Hill Range decreases east ward which subsequently disappear below the Samakhiali-Lakadia plain. Wagad is characterised by oval shaped landmass bounded by fault in the north as well as in the south. The Gamdau low land of Wagad and Balasar low land of Bela occupy synclinal depressions. The Desalpar flexure separated the Wagad uplift from the Bela uplift. The Kaladongar, Goradongar and Bela ranges exhibit typical geomorphic features of the hills formed by faulting. The Kaladongar range is characterized by a large asymmetric and doubly plunging anticlinal fold with a steep northern limb and a gentle southern limb. The northern limb of the anticline is down faulted against the E-W trending IBF in the north. The fault is morphologically expressed as E-W trending precipitous scarp forming the northern margin of the Pachham Island. Goradongar Hill is located at the southern periphery of the Pachham Island which is composed of a chain of domal and anticlinal Hills. The northern margin of the range is marked by north facing scarps forming the geomorphic expression of the Goradongar fault. Due to the fault, the domes and anticline have steeper northern limbs with gentle southern limbs.

The northern margin of the Bela and Khadir islands is characterized by E-W trending flexures called the Lodrani and the Khadir anticline (Biswas, 1993). The

escarpment is formed on the southern limb of the anticlines while the northern limb is eroded away. The straight northern margins of the islands are attributed to the E-W trending Island Belt Fault (IBF) in the north, presently buried below the marine sediments of the rann. The remnant of the northern limb of the Bela is exposed north of the Bela scarp. The behaviour of the IBF in the existing compressional stress regime within the Kachchh basin is not known.

REGIONAL GEOLOGY

Kachchh basin is characterized by thick sedimentary succession of sedimentary rock from Middle Jurassic (Bathonian) to Recent. The Kachchh basin is characterized by the Mesozoic rocks which are exposed in the uplifted land masses while Tertiary rock has occupied the structure lows within the basin. The sedimentary deposition of the basin took place in early, syn and post-rift stages of the basin (Biswas, 1977).

Mesozoic stratigraphy

The complete sequence of Mesozoic rock is exposed only in the Mainland of Kachchh. The older Mesozoic sequence (Bathonian to Callovian) is exposed in the northern Island Belt (Pachham, Khadir, Bela and Chorar) and the intermediate rocks in the highland of Wagad. The stratigraphy generally comprises of Mesozoic, Tertiary & Quaternary period (Fig. 2.2). The basement of the Mesozoic rocks is syenite of Precambrian age which is only exposed in Meruda Hill in Great Rann of Kutch. Granitic boulders-conglomerate exposed in Cheriya Bet forms the oldest rock unit of Jurassic age. The Mesozoic stratigraphy of Kachchh is divided into three part viz. Mainland, Pachham Island and Eastern Kachchh. The stratigraphy of Mesozoic rocks of Kachchh basin is given in Table 2.1.

Northern Mainland

The mainland forms the largest geographic entity of the Kachchh basin. It displays the most rugged and most well developed sequence of Mesozoic and Cenozoic rocks. The northern margin of the mainland is bounded by the Kachchh Mainland Fault (KMF) with the domal hilly region, the Northern Hill Range to its south. In the central part, the Katrol Hill Fault (KHF) divides the mainland into southern mainland and northern Mainland Kachchh (Fig. 2.1). The Vigodi Fault and the Naira River fault are the other major fault located in the west and south western part of the mainland. The Mainland outcrop exposes a continuous succession from Bathonian to Santhonian. The oldest sequence from

PART-A Background information

Bathonian to Callovian is exposed in the northernmost part of the Kachchh. The various formations representing deposition in rift during Mesozoic time is briefly described below. The description is based on the Biswas (1977, 1982, 1987, 1993, 2005); Biswas and Raju (1973) and Biswas and Khattri (2002).

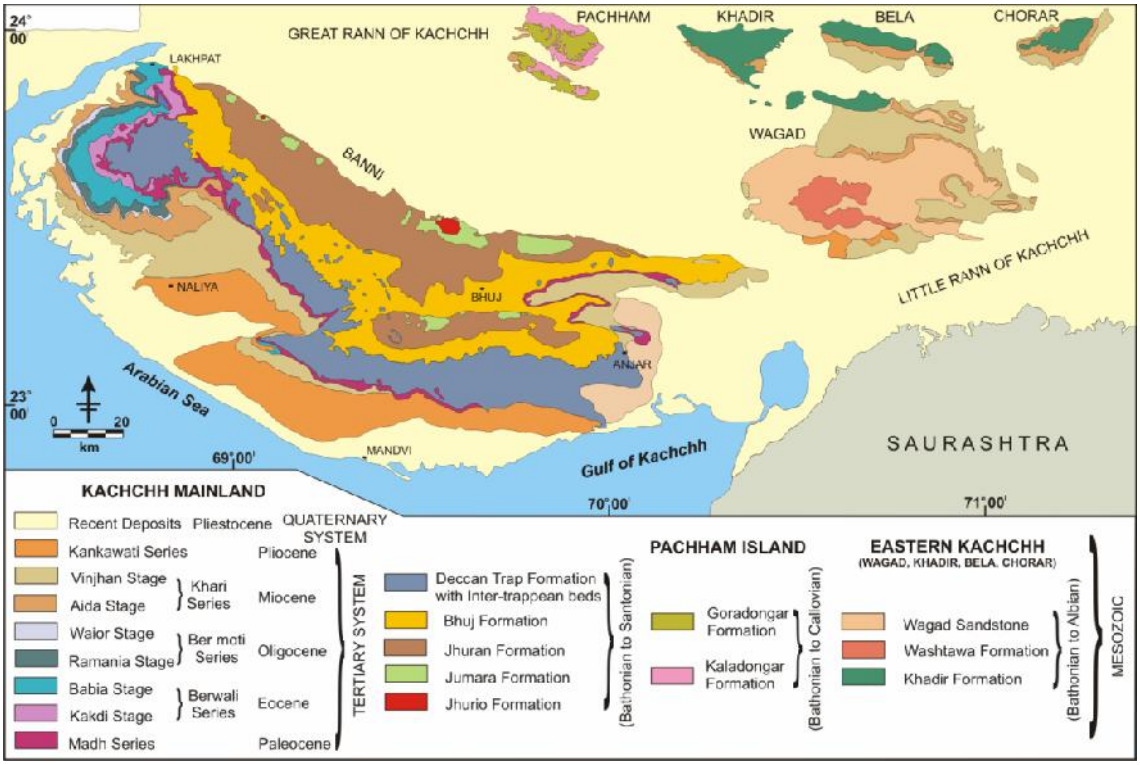

Figure 2.2 Geological map of Kachchh basin (after Biswas and Deshpande, 1970).

Jhurio Formation: A thick sequence of limestone & shale with bands of golden oolites forms the lower part of Mainland stratigraphy, and its name is derived from Jhurio hill in the north central part which forms the type section of this formation (Biswas, 1977). The formation is exposed only as small inliers in three hills, which are large domal structures, along the northern margin of the mainland viz. Habo, Jhurio and Jumara, from east to west. The base of this formation is not exposed anywhere in the basin. Its forms a conformable contact with the overlying Jumara Formation. The physical and biological aspects of the formation indicate littoral to infra-littoral environment. A Bathonian to Callovian age has been assigned based on the fossil assemblages (Biswas, 1977).

***Jumara Formation*:** An argillaceous unit overlies the Jhurio Formation and has been named after its type section in Jumara hill near the Rann, north of Jumara village (Biswas, 1977). It is characterized by monotonous olive-gray, gypseous laminated shales with thin, red ferruginous bands; alternating beds of limestone and occasional sandstone interbeds. Thin fossiliferous oolitic limestone bands occur in the shales, which were called, "Dhosa

Oolite Beds" or "Stage" by earlier workers. These are very characteristics and used as the main key bed in the Mainland stratigraphy. The thickness of the formation is more or less uniform throughout the area varying between 900 to 950 ft. The boundaries of this formation match with those of the Chari Series described earlier by Rajnath (1932) from Jumara hill and they are almost identical units. The Chari Series has been assigned Callovian-Oxfordian age on the basis of ammonites. Ghosh (1969) based on fossil assemblages fixed a Callovian-Argovian age for the Chari Series of Jumara dome. The age of Jumara Formation ranges between Callovian to Oxfordian.

Table 2.1 Lithostratigraphy of Mesozoic rock of Kachchh Basin, (after Biswas, 1977)

<table>
<tr><th colspan="2">Mainland</th><th colspan="2">Pachham Island</th><th colspan="2">Eastern-Kutch (Khadir-Bela-Wagad)</th></tr>
<tr><th>Formation</th><th>Member</th><th>Formation</th><th>Member</th><th>Formation</th><th>Member</th></tr>
<tr><td rowspan="3">Bhuj</td><td>Upper</td><td rowspan="6"></td><td rowspan="6"></td><td colspan="2" rowspan="2"></td></tr>
<tr><td>Ukra</td></tr>
<tr><td>Ghuneri</td><td rowspan="5">Wagad Sandstone</td><td>Gamdau</td></tr>
<tr><td rowspan="4">Jhuran</td><td>Katesar</td><td rowspan="4">Kanthkot</td></tr>
<tr><td>Upper</td></tr>
<tr><td>Middle</td></tr>
<tr><td>Lower</td></tr>
<tr><td rowspan="3">Jhumara</td><td>Dhosa Oolite</td><td>Washtawa</td><td>Bhambhanka shale</td></tr>
<tr><td rowspan="2">Middle</td><td rowspan="5">Khadir (Khadir Island)</td><td rowspan="2">Gadhada</td></tr>
<tr><td rowspan="2">Goradongar</td><td>Modar hill</td></tr>
<tr><td>Lower</td><td>Raimalro</td></tr>
<tr><td rowspan="4">Jhurio</td><td>Upper</td><td>Gadaputa</td><td rowspan="2">Hadibhadang</td></tr>
<tr><td rowspan="2">Middle</td><td>Flagstone</td></tr>
<tr><td rowspan="3">Kaladongar</td><td rowspan="2">Kaladongar Sandstone</td><td rowspan="3">Cheriya bet</td></tr>
<tr><td rowspan="2">Lower</td></tr>
<tr><td>Kuarbet</td></tr>
<tr><td colspan="4"></td><td colspan="2">Precambrian</td></tr>
</table>

***Jhuran Formation*:** It comprises a thick sequence of alternating beds of sandstone and shale (Biswas, 1977). This formation overlies the Dhosa Oolite Member of Jumara

Formation and it is overlain by non-marine sandstones of Bhuj formation. The formation is divided into four in formal member lower, middle, upper and Katesar Members. The formation is extensively exposed along the southern flanks of the northern and central hill ranges in two wide E-W strips. In the extreme west and east they are exposed as small inliers in the Bhuj formation at the central of the domes and anticlines. In the central and western parts of the Mainland, the lower, the middle and the lower part of the upper members are extensively exposed. The middle member is very well exposed in Khari Nadi valley around Rudramata Temple, north of Bhuj. The Lower Member consists of alternating yellow and red sandstone and shale beds in almost equal proportions with thin bands of hard, yellow, fossiliferous, pebbly, calcareous sandstones (Biswas, 1977). The upper member is predominantly arenaceous and composed of red and yellow, massive current-bedded sandstones with intercalations of shale, siltstone and calcareous sandstone bands in the middle. The Katesar Member consists of greenish gray to yellow, massive, current-bedded, sandstones with minor intercalations of shale. Lenticular, hard calcareous bands are also common (Biswas, 1977).

***Bhuj Formation*:** A huge thickness of non-marine sandstones of uniform character constitutes the youngest formation of the Mesozoic stratigraphy of Kachchh (Biswas, 1977). It is named after its type section locality around Bhuj city of Kachchh. This formation is defined by the marine beds of Jhuran formation below and the Deccan trap flows above. The lower member is characterized by cyclic repetition of ferruginous or lateritic bands shales and sandstones. The upper member consists or whitish to pale brown, massive, current bedded, coarse grained well-sorted sandstones with kaolinitic shale and ferruginous band alternations at thick intervals. The Ukra member contains olive green glauconitic sandstones, “green sands” and green and gray shales with thin, fossiliferous bands of purple ironstones, ferruginous mudstone, and gray limestone. These beds pinch out laterally into the sandstones of the Ghuneri and upper members. It is concluded from the lithology, absence of fauna and richness in flora, sedimentary structures, pattern of current-roses, and marine tongues in the down basin direction, that the sediments represent deltaic deposits with distal part (delta front) towards the west and the proximal part (fluvial) to the east in the direction of the land. A Lower Cretaceous (Valanginian) to Santonian time range is assigned for this formation (Biswas, 1977).

Wagad

The Wagad highland is situated between Mainland and the Island Belt. It is characterized by exposed Mesozoic rocks with Tertiary rocks around the periphery of the

Island. Physiographically, Wagad in the north is marked by the Desalpar Flexure zone, while the southern margin is demarcated by the South Wagad Fault (SWF) (Fig. 2.2). Both the faults forms fault bounded flexure zone. The Mesozoic rocks are dissected by several dykes. The Mesozoic rocks of Wagad are classified into following formations.

***Washtawa Formation*:** This rocks of this formation forms the lower most unit of Mesozoic sedimentary succession. Its name is derived on account of its type section exposure in the Washtawa dome, north of Washtawa. A good section is exposed across the valley of Washtawa stream which flows along the strike. The main outcrop is a large oblong inlier in the Wagad Sandstone at the centre of Wagad Highland. The type section generally consists of thickly bedded, cross-laminated, brown and red sandstone and grey, gypseous shale intercalation in the lower part; buff, current-bedded, massive sandstone in the middle part; and yellow, flaggy to fissile sandstone and grey laminated gypseous shales in the upper part. Shale in the upper and lower parts comprises of thin fossiliferous limestone bands. The Washtawa Formation is overlain conformably by the Wagad Sandstone. This boundary between the two is defined by the patchy red fossiliferous marlstone bands in the west and by a yellow, hard, fossiliferous calcareous band in the east. Purple ironstone band exposed near the Chitrod area mark the top of this formation. The facies pattern, lithological association, fauna and its distribution suggest shallowing of depositional environment from sub-littoral to littoral from west to east which should be the direction of the shore.

***Wagad Sandstone*:** Wagad Sandstone conformably overlies the Khadir Formation in the northern part and Washtawa Formation in the Central part of Wagad. It is extensively exposed in Wagad. The formation can be divided into two distinct component members – a lower marine and an upper non-marine, whereas in Eastern part of Wagad only the non-marine sandstones are found. The marine sandstone member, named as Kanthkot Member, passes laterally into non-marine Gamdau Member which is named after the stream by Gamdau village. The lower part of the Kanthkot Member comprises grey, splintery gypseous, fossiliferous shale interlaminated with fine grained red ferruginous sandstones and concretionary layers. The shale pinches out in sandstone towards the east. The upper part of the member is dominated by sandstones. Two distinct sequences of sandstone beds are separated by Kanthkot fossiliferous band which is calcareous in nature and forms a good marker horizon. The upper sandstones comprise of thin inter-beds of grey, gypseous shale and at the top it is capped by a 15 ft. thick Bharodia Astarte Band which is fossiliferous calcareous sandstone.

The gross lithofacies of Gamdau Member of this formation resembles to the lithofacies of Bhuj Formation of the Mainland. It consists of current bedded, buff and pinkish white, medium to coarse grained quartz arenite with lenticular conglomerates, purple concretionary ironstone and lateritic conglomerate bands, lamellar sandstone, and grey silty and white kaolinitic shale forming interbedded repetitive sequence. In the eastern part of Wagad the entire formation shows similar facies as that of Gamdau Member. Wagad sandstone conformably overlies the older formation, while it is overlain unconformably by Neogene rocks under which the top of this formation is buried. The Wagad Sandstone shows the facies of Bhuj formation indicating a similar deltaic environment of deposition. The age of the Wagad Sandstone ranges from Upper Oxfordian to Lower Creataceous (pre-Aptian). The Wagad Sandstone is, therefore, equivalent to the Jhuran Formation and the lower member of the Bhuj Formation of Mainland.

Island Belt

It is located north of Wagad and Mainland Kachchh and comprises of a E-W trending linear chain of four islands surrounded by the Great Rann. These islands from west to east are the Pachham, the Khadir, the Bela and the Chorar islands (Fig. 2.1). The northern margin of all islands is marked by steep north facing escarpments which mark the geomorphic expression of Island Belt Fault. All islands display rugged hilly topography and expose Mesozoic rocks with Tertiary rocks at the fringes of the islands.

Pachham Island

The Pachham Island forms the westernmost island of linear chain of islands viz. Pachham, Bela, Khadir and Chorar Islands. These are basically rocky hill masses exposing laterally correlatable Mesozoic and upper Tertiary (Miocene) rocks rising above the flat rann surface (Biswas, 1993). All the four islands including the Pachham Island are bounded in the north by the Island Belt Fault (IBF), which is concealed below a thick cover of Rann sediments (Fig. 1.2). The Pachham Island is the largest and highest in elevation and also displays a more complicated geological and structural set up in comparison to other islands to the east. The Pachham island is made up of two E-W trending Hill ranges consisting of compacted and structurally deformed Mesozoic rocks with a intervening structural low in between them. The northern half of the island is occupied by the Kaladongar Hill range while the Goradongar Range marks the southern extremity of the island.

Kaladongar Formation: The rocks exposed in the Kaladongar Hill range are grouped as the Kaladongar Formation. The base of the formation is not exposed and the northern scarp exposes a complete stratigraphic succession of this formation. This formation has been divided into three members (Biswas, 1977). The Dingy Hill Member forms the oldest unit which mainly comprises of conglomerate, siltstone, shales and thin fossiliferous sandstone. It is overlain by Kaladongar Sandstone Member with massive medium to coarse grained quartz arenite with some wedges of petromictic conglomerate. The upper most Babia Hill Member has predominant sandstone with subordinate shale. The age of this formation is around Bathonian and indicates littoral depositional environment.

Goradongar Formation: The Goradongar Hill is located at the southern periphery of the Pachham Island which is composed of a chain of domal and anticlinal hills. The northern margin of the range is marked by north facing scarps representing the Goradongar fault. The Hill range is made of Mesozoic rocks classified as the Goradongar Formation which stratigraphically overlies the Kaladongar Formation. It comprises of mainly limestone, shale and sandstone (Biswas, 1977). The formation is divided into four members. The Goradongar Flagstone Member forms the base which consists of thinly bedded to flaggy limestone containing fossils and bands of golden oolite. It is overlain by Gadaputa Sandstone Member which is medium to coarse grained quartz arenites. Raimalro Limestone Member overlies this unit which is basically a calcareous unit mainly comprises of fossiliferous pelsparite with the upper part becoming sandy. The Modar Hill Member forms the top most units with olive grey gypseous shale with some flagstone and ferrigeneous limestone bands along with massive bedded sandstone. Infra-littoral depositional environment and Lower Callovian to Argovian age is inferred from the fossil assemblage (Biswas, 1977). The Tertiary rocks are generally exposed in the eastern and western margin of the central low.

Khadir, Bela and Chorar Islands

The Mesozoic rocks of Khadir, Bela and Chorar islands are classified as follows.

Khadir Formation: The name is given after the Khadir Island which forms its type section. Most of the part of this formation is exposed in the Khadir Island and rest of the formation is exposed in Gangta bet and its top is exposed in the marginal anticline along the Gedi fault, about a kilometer east of Nagalpar. Geomorphologically, the area shows typical expression of this formation is the cuesta type land form. The northern escarpments of the islands have been formed by the thick shale bed protected by the hard

cliff forming sandstones and limestones of the Hadibhadang Sandstone Member. The Cheriya Bet Conglomerates forms the oldest lithology of the Mesozoic rocks of Kachchh. The Khadir formation is mainly divided into following three members-

Hadibhadang Shale Member: The lower part of Hadibhadang Shale is not exposed. The upper part of this shale member is well exposed around Kuda & all along the lower slopes of Bela-Mouvana escarpment and towards east exposure becomes poor. It is characterized by interbeds of siltstone and sandstone is present along with intercalation of thin reddish marlite bands, marlite pebble and nodules. The shale are more silty and gypseous in nature.

Hadibhadang Sandstone Member: It forms the upper part of the escarpment with hard limestone is at the top. This member becomes more argillaceous towards the east. Intercalated shale comprises of variegated, chocolate brown, greenish grey to khaki or yellow with silty beds. Top limestone is thinly bedded containing compact bands of calcareous conglomerate having granite and metamorphic pebbles. Local lenses of golden oolite rock occurs in the lower part of the limestone bed. In western part near Kotada, the limestone bed thins down and become arenaceous and flaky with interbeds of shales. While towards eastern side this limestone bed thickens with consequent reduction of shale.

Gadhada Sandstone Member: It forms the uppermost Jurassic bed exposed in this island. It mainly comprises of sandstone similar to those found in the type section. The basal shale bed is present and the overlying fossiliferous calcareous bed are represented by thin flaky, sandy pelsparite bends occasionally fossiliferous and separated by silty shale followed by pink and buff massive friable feldspathic sandstone with occasionally hard ferruginous sandstone.

Tertiary stratigraphy

The Tertiary rocks occur mainly in the structural lows and unconformably overlie the Mesozoic rocks. The Tertiary rocks occur in Kachchh as narrow strip fringing the Mesozoic outcrops of the highlands. They are best developed in the coastal strips of the southern and western parts of Kachchh Mainland (Fig. 2.2). Tertiaries are also present in surroundings of the Pachham Island, in Khadir it occurs at the periphery of the Island, while almost of two third of the back slope of the Bela Island comprises of Tertiaries. Similarly, narrow strips of Tertiaries occur at the fringes of Wagad and outer periphery of the other uplift; whereas in Great and Little Rann, Samakhiali-Lakadia plain and in Banni

it lies beneath the recent sedimentary cover. They are represented by rocks ranging in age from Palaeocene to Pliocene. The first detailed classification of the Tertiary sediments of Kachchh was presented by Wynne (1872). Biswas (1965) proposed a new Time-Stratigraphic classification of the Tertiary sediments of Kachchh based on chrono-stratotypes and detailed mapping of the time rock units. The classification was later modified by Biswas and Raju (1973). Subsequently, Biswas (1992) proposed a litho-stratigraphic classification of Tertiary sediments of Kachchh introducing a small change of nomenclature (Table 2.2).

Table 2.2 Stratigraphy of Tertiary sediments of Kachchh basin (after Biswas, 1992).

Age	Formation	Members
Pliocene	Sandhan	
Lower Miocene (Burdigalian)	Chhasra	Siltstone
		Claystone
Lower Miocene (Late Aquitanian)	Khari Nadi	
Oligocene	Maniyara Fort	Bermoti
		Coral Limestone Lumpy clay Basal member
Late Middle Eocene	Fulra Limestone	
Middle Eocene	Harudi	
Late Paleocene	Naredi	Ferr. Claystone Assilina Limestone Gypseous Shale
Upper Paleocene	Matanomadh	
Cretaceous–Lower Palaeocene	Deccan Trap	

The Tertiary rocks of Miocene age mainly covers the southern backslope. It mainly comprises of mottled to variegated siltstone and very fine grained sandstones with occasional grey and brown gypseous claystone (Biswas, 1993). The outcrops are however, very limited as they are covered at most places by a cover of Quaternary deposits. The Samakhiali-Lakadia plain lying south of Wagad also consist mainly of Tertiary rocks.

Khari Nadi Formation

The rocks of the Khari Nadi Formation are exposed extensively in eastern Kachchh and mostly they occupy the low lying areas between the uplifts (Biswas, 1993). It is

named after the Khari Nadi where it is exposed along the cliff section along the river. This formation has a distinctive sequence of fine grained to silty, variegated sandstone and occasionally grey and brown gypseous claystone overlying the white foraminiferal limestone of the Fulra and Maniara Fort Formation. In Bela its thickness varies from 15-35m. This formation is deposited in shallow marine stable shelf environment and its age as suggested by fossil study appears to be Late Aquitanian (Biswas, 1993)

Kankawati Formation

The Kankawati Formation represents the sediments deposited in the Pliocene Epoch. The type section is considered at the cliff section in the Kankawati river in between Vinjhan and Sandhan and therefore the name has given as Sandhan Formation. In Lakadia plain, to the south of Wagad, patchy outcrops of these rocks are seen along the faulted edge of Wagad Highland. At these places, some outcrops are seen in the nalas to the east of Lakadia, near Shivlakha to the south-east of Khanpar and Mewasa, and south of Garadongar. Lithologically, the rocks of the Khari Series are dominantly arenaceous. Quartzose sandstone dominates the sequence with subordinate amount of the claystone, shale, siltstone, marlite and calcareous sandstone. The environment of deposition is transitional, estuarine or deltaic to littoral.

CHAPTER 3

NEOTECTONIC SETTING

The northern margin of the Kachchh mainland uplift is marked by a E-W trending structurally controlled hill range called Northern Hill Range that is bounded by the Kachchh Mainland Fault on its northern side. The range extends from Lakhpat in the west to the area around Devisar in the east. The hill range displays a rugged mountainous topography developed in the Mesozoic rocks which form discrete domes of various sizes. The chain of various domal structures comprises the Mundhan dome, Ghuneri dome, Nara dome, Keera dome, Jhura dome, Habo dome, Wantra dome, Devisar dome in addition to several smaller domes (Biswas, 1987; 1993). The domes expose rocks belonging to the Jhurio, Jumara, Jhuran and Bhuj formations that range in age from middle Jurassic to late Cretaceous (Biswas 1987). The formations comprise well compacted and hard sedimentary rocks of various lithologies like sandstones, shales and limestones. The domes are asymmetric in the sense that the northern limb of the domes is steeper as a consequence of the tectonic movements along the KMF that truncates the northern margin of the hill range, while the southern limbs shows gentle dips. The Jhura dome is the largest followed by the Habo dome in terms of the area covered. The domal hills are separated by inter-domal saddles through which major drainages flow northward and disappear in the Banni plain. To the east of Devisar the hill range goes down below the Samakhiali-Lakadia plain.

The present study area is confined to the eastern part of the E-W trending Northern Hill range stretching from the Nirona in the west to Devisar in the east. The present detailed field and GPR based study was concentrated in the eastern part, as it shows a widespread and intense aftershock activity since the 2001 Bhuj earthquake (Mandal and Chadha, 2008). During the present course of study various geomorphic indicators of active tectonics like drainage anomalies, fault scarp, river terraces and fault associated Quaternary deposits were studied in details to delineate the neotectonic setting and neotectonic influences in the landscape development of the KMF zone. In this chapter, salient tectonically generated geomorphic anomalies are described to delineate the spatial variation in the landscape along the KMF zone.

PART-B Kachchh Mainland Fault (KMF)

MORPHOTECTONIC SEGMENTS

The Kachchh Mainland Fault (KMF) is the largest intra-basinal fault of the Kachchh basin that bounds the Mainland uplift in the north beyond which lies the flat expanse of the Banni-Great Rann basin. The fault trends WNW-ESE in the western part while it trends E-W in the eastern part. The fault is known to have suffered several phases of tectonic activity during the Cenozoic (Biswas, 1974; 1987; 1993) and has been found responsible for the several earthquakes in historic times including the 2001 Bhuj earthquake, 1956 Anjar earthquake and the 1819 Allahbund earthquake as well (Chung and Gao, 1995; Bilham, 1998; Biswas and Khattri, 2002). However, Quaternary tectonic evolution of the KMF is not yet precisely understood.

Apart from the north facing scarps marking the KMF, several transverse faults are traceable within the Mesozoic rocks and are evidenced by offset fault scarps of the KMF, beheaded/deflected or offset drainage, sags, shutter ridges and pressure ridges (Maurya et al. 2003a). A significant feature observed is that almost all major transverse faults displacing the KMF and truncating the domes are occupied by a high-order river channel debouching into the Banni plain (Maurya et al. 2003a). For example, the Nirona river, Kaila river, the Pur river and the Kaswali river in the study area flow along the inter-domal transverse fault zones.

The KMF is not a continuous fault, but is laterally displaced by several NNE-SSW to NNW-SSE trending transverse faults (Biswas, 1993). These faults have also been periodically reactivated along with the KMF during the post-rift tectonic evolution of the Mainland Kachchh (Biswas, 1993; Maurya et al. 2003a). Based on the tectonic framework that includes the existence of several transverse faults (Biswas, 1993; Maurya et al. 2003a) and the corresponding geomorphic set up, the KMF zone in the study area is divided into five morphotectonic segments from west to east (Fig. 3.1a). The segment-I is located between Nirona and Pur rivers, segment-II lies between Kunaria and Lodai, segment-III includes the area between Lodai and Jawaharnagar, segment-IV comprises the KMF zone between Jawaharnagar and Khirsara and segment-V is located between Khisara and the area to the east of Devisar. Further east the scarp dies out and the area comprises an almost flat but gently undulating and northward sloping topography that merges with the Samakhiali-Lakadia plain further east. As a result of the field and GPR based studies carried out in the present study, the eastward extension of propagation of KMF is

established. The lateral extension of the KMF has been extended by ~20 kms as a result of the present investigations. The extended part of the KMF delineated has been identified as the Segment-VI and named as the Amrapar-Sikra segment.

From Nirona in Segment-I to Khirsara in Segment-IV, the KMF zone is characterised by thick Quaternary sediments which have buried the KMF below them. The sediments comprise coarse grained colluvio-fluvial to finer grained alluvial sands and silts which are described in details in the next chapter. In the Segment-V (Khirsara-Devisar segment), the alluvial cover is negligible. The Quaternary sediments forms a thin blanket of structureless and unconsolidated alluvial sands and fine gravels averaging 1-2 m in thickness covering the Mesozoic and Tertiary rocks. Major Quaternary aggradation phases evident in other segment are absent though the drainages appear to be of similar characteristics. The general topography of the hill range is also relatively lower (Fig. 3.1) but remains rugged as evidenced by the deeply incised river courses in the bedrock.

The morphotectonic segmentation of the KMF was found necessary to compare the stratigraphic development of the Quaternary sediments in relation to neotectonic activity along various parts of the KMF zone in the study area. The present study indicates that the KMF is not a single continuous fault. Its continuity is broken by several transverse faults which indeed have resulted in several individual segments of KMF. The behaviour of each individual segment is different from the other. Variations within the geomorphic parameters of individual segments are result of differential uplift of the various segments.

FLUVIAL GEOMORPHOLOGY

The drainage configuration in seismically active areas is mainly governed by structural set up. The KMF zone is traversed by several north flowing streams originating in the hilly terrain of the Northern Hill Range (Fig 3.1b). Major rivers of the area flow in the inter-domal depressions, which are fed by streams arising from the gentle southern limbs of the domes. The domal hills are characterized by typical radial drainage patterns (Fig. 3.1b). The north flowing rivers arising in the domal hills, form narrow, deep valleys and gorges within the Mesozoic rocks and follows incised channels to the north of the scarp line.

PART-B Kachchh Mainland Fault (KMF)

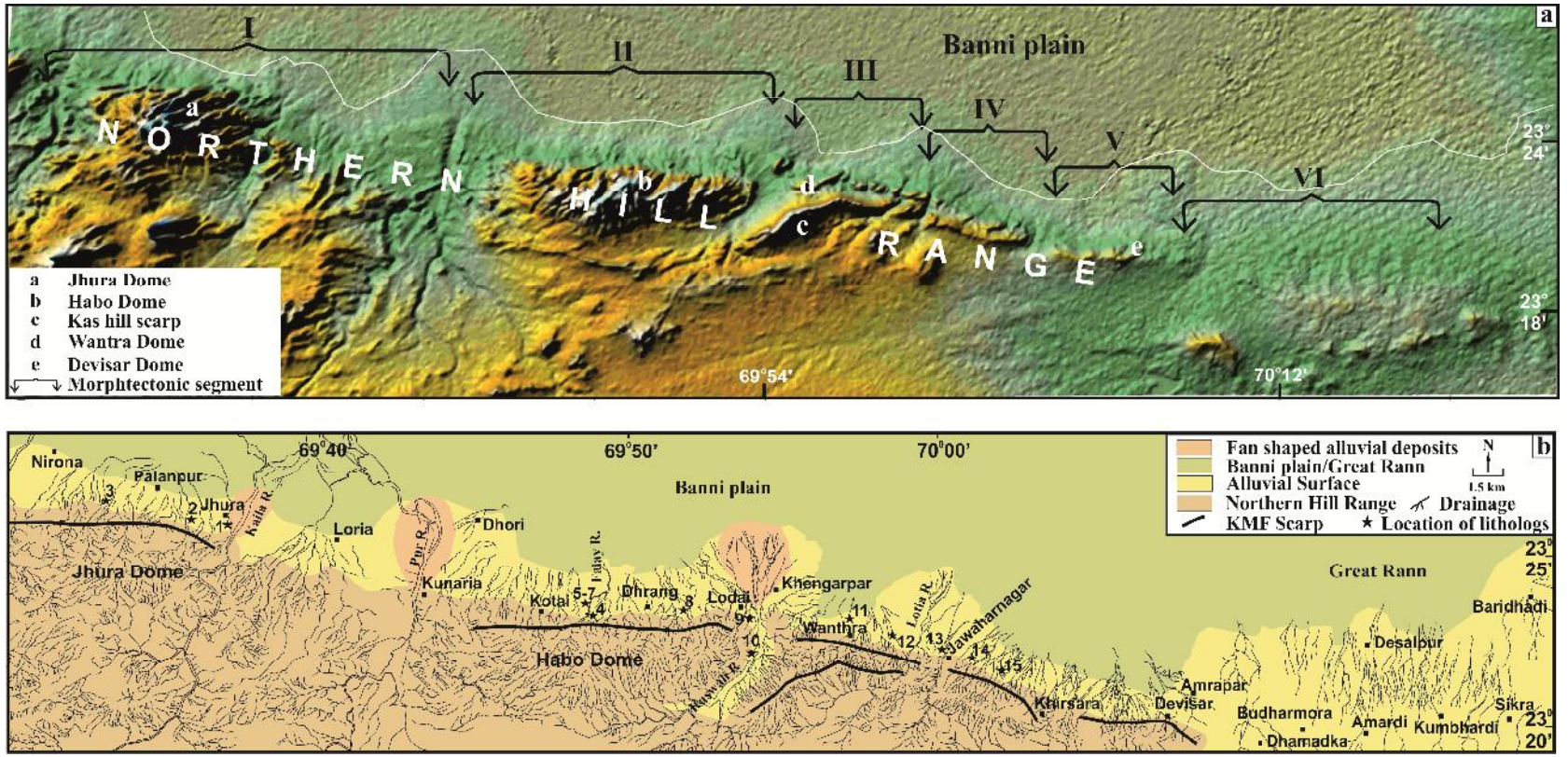

Figure 3.1 (a) DEM of the eastern part of the Northern Hill Range. Note the close correspondence between the individual structures and the physiography. Also seen is the sharp physiographic contrast provided by the north facing scarps at the northern margin of the range and the flat terrain of the Banni plain which tends to die out at the eastern margin. The morphotectonic segments (I-VI) as delineated in the present study are also shown. Note that the KMF has no geomorphic expression in the segment-VI. **(b)** Generalised geomorphological map of the Northern Hill Range and the KMF zone. The KMF zone is marked by a narrow belt of Quaternary sediments between the scarps and the Banni plain. The domes shows typical radial drainage patterns conforming to the structure. Also shown are the numerous small streams that arise from the scarp region and flow northward traversing the Quaternary sediment cover. All drainages disappear in the Banni plain. 1-15 marks the locations of the lithologs of the exposed Quaternary sediments described in the next chapter.

PART-B Kachchh Mainland Fault (KMF)

It is observed that most of the rivers display tight entrenched meanders as they cross the KMF scarp. This phenomenon is on account of the adjustment by the rivers to a sudden change in the gradient induced by neotectonic activity along the KMF. Significantly, the incision is found to rapidly decrease towards north as the streams die out as they reach the Banni plain. This decreasing trend in the incision confirms the tilting of the Quaternary surface due to the rejuvenation of the KMF.

Variation in the concavity of north flowing streams profile is seen in the various morphotectonic segments of KMF (Fig. 3.2). Longitudinal profiles of the streams in the Nirona-Jhura segment, Kunaria-Lodai and Jawaharnagar-Khirsara segments shows steep concavity in the upstream part and are relatively gentler in the lower reaches in comparison to the other easternmost segments. The experimental studies by (Snow and Slingerlands, 1990) reveal that when a river is experiencing uplift in a tilted manner where maximum uplift is towards the upstream side will results in greater erosion at the upstream direction than at downstream end to maintain the equilibrium profile. Thus, this variation can be directly related to the differential uplift within the different morphotectonic segments of KMF.

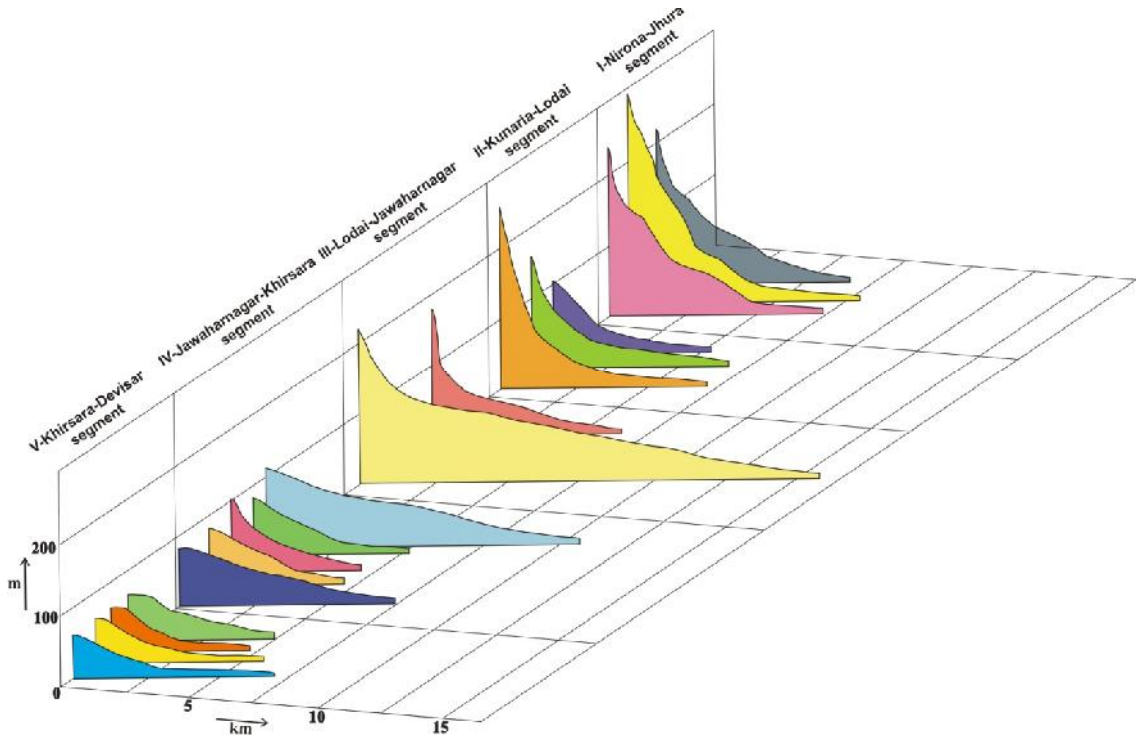

Figure 3.2 Longitudinal river profiles of north flowing streams in various segments of KMF zone. The steepness of the profiles is observed to consistently reduce from segment-I to segment-V.

PART-B Kachchh Mainland Fault (KMF)

THE KMF SCARP

The steep north facing scarps demarcating the northern limit of the Northern Hill Range marks the geomorphic expression of the KMF. The imposing north facing scarp comprises steep north dipping Mesozoic rocks having a trend E-W to ESE-WNW marks a prominent geomorphic expression of the KMF (Fig. 3.1a). Overall, the KMF zone displays the characteristics of a dynamic range front environment that is evident from the steep fault scarp, incised valleys, entrenched meanders, northward sloping alluvial surfaces and predominantly coarse grained colluvio-fluvial deposits.

The topographic profile drawn over the crest of the Northern hill suggests that the Jhura dome has the highest elevation followed by Habo dome which decreases further eastward (Fig. 3.3a). The elevations are the cumulative effect of uplift of the range along the KMF in post-Mesozoic time. Variations in the elevations of the domes are a reflection of the variable magnitude of uplift along the length of the KMF. This suggests that the Jhura dome has undergone maximum uplift which progressively decreases eastward.

The variable uplift also correlates well with the relative ruggedness of the topography and depth of incision in the various domes. Corresponding to the maximum uplift indicated, the Jhura dome shows a highly rugged topography and maximum depth of incision. As shown in the topographic profile, the Jhura dome is not only the largest in size, but it is also the most deeply dissected dome where the dissection extends up to the lowest stratigraphic level whereby the older Mesozoic formations are exposed. The Jhura dome is, in fact, the only dome in the entire Northern Hill Range where all Mesozoic formations are well exposed.

The Habo dome is the second largest dome both in terms of the size and degree of dissection. Fig. 3.3a displays the depth of dissection suffered by the Mesozoic stratigraphic formations (i.e. Jhurio, Jumara, Jhuran and Bhuj Formation) throughout the along the Northern Hill Range. The Jhurio Formation forms the oldest lithology followed by Jumara Formation, both are well exposed in the deep gorges formed by the north flowing stream in Nirona-Jhura segment and Kunaria-Lodai segment (Biswas, 1977). Towards the east the incision by the north flowing streams decreases and thus younger Jhuran and Bhuj Formations are exposed in the entrenched river sections (Biswas, 1977). East of Devisar, the hill range appears to go down below the Samakhiali –Lakadia plain and presumably extends further east in the subsurface.

PART-B Kachchh Mainland Fault (KMF)

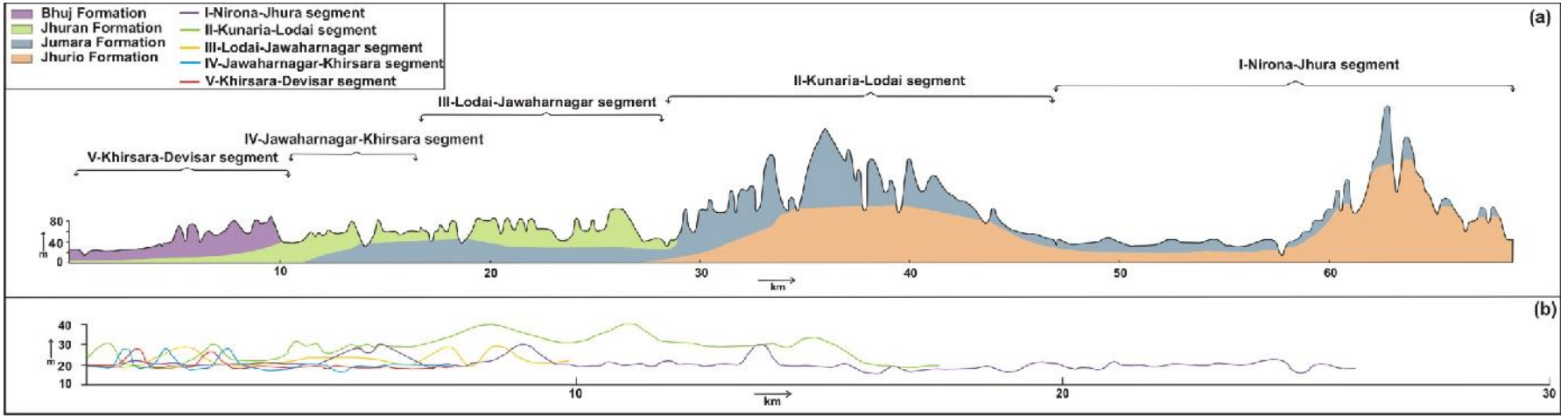

Figure 3.3 (a) Topographic profile drawn over the **c**rest of the E-W trending KMF scarps. The superimposed geological formations are not representative of the lithology of the scarps. Instead, the formations shown depict the depth of dissection down to maximum stratigraphic level in the respective part of the segments. The formations are schematically plotted based on the geological description of Biswas (1977). The figure shows eastward decreasing depth of dissection thereby progressive exposing younger formations. This correlates with the prominent decreasing height of the KMF scarps in the eastward direction. **(b)** Thickness of the Quaternary sediments developed in various segments of KMF.

PART-B Kachchh Mainland Fault (KMF)

The Quaternary surface profile shown in Fig. 3.3b depicts the variation in elevation of Quaternary surface lying to the north of the KMF scarps. The profiles indicate that the Quaternary surface is at the highest elevation in the Kunaria-Lodai segment followed by Nirona-Jhura segment. A sharp decrease in the elevation of Quaternary surface is seen in various eastward segments. The Quaternary surface is at the lowest elevation in the Khirsara-Devisar segment (Fig. 3.3b). The above observations regarding the variation in north flowing river incision in the Mesozoic segment along with the variation in the Quaternary surface development in different morphotectonic segments indicate the differential uplift among the various segments of KMF. Thus, transverse faults have played a dominant role in the segmentation of the KMF and possibly in the dissipation of tectonic stresses in compressional stress regime during the Quaternary.

FIELD SETTING OF THE KMF

The tectonic history of the KMF is intricately linked with the evolution of the Kachchh rift basin. The rift opened during the early Jurassic and witnessed continuous sedimentation during its rifting phase until the late Cretaceous. The KMF along with other intra-basinal faults were formed as vertical normal faults during the active rift phase (Biswas, 1987). Tectonic activity along these faults significantly influenced the pattern and facies distribution of the Mesozoic sediments (Biswas, 1977). As a consequence of the collision of the Indian plate with the Eurasian plate in the north, the rift was inverted at the end of Cretaceous (Biswas and Khattri, 2002). The changeover from extensional stress regime to compressional stress regime, resulted in the formation of intra-basinal uplifts (viz. Mainland uplift, Wagad uplift, Desalpar uplift and Island belt uplift) with corresponding structural lows due to movement along faults (Biswas and Khattri, 2002). Accumulation of the compressive stresses along the intra-basinal faults including the KMF led to the formation of a narrow flexure zone consisting of domes and anticlines on the upthrown sides of the faults (Biswas, 1987). The structural lows that include the Banni-Great Rann basin to the north of the KMF were filled up by thick transgressive marine sediments during the Neogene and Quaternary periods (Biswas, 1993). During the post-Cretaceous inversion phase, the faults bounding the uplifts were periodically reactivated thereby facilitating the deposition of Cenozoic sediments and evolution of the present day landscape (Biswas, 1987).

PART-B Kachchh Mainland Fault (KMF)

The marine Neogene sediments were deformed in a narrow zone all along the KMF during the post-Neogene time under compressive stress regime. Reactivation of the KMF at this time juxtaposed the Neogene sediments against the Mesozoic rocks comprising the Northern Hill Range. The Neogene sediments were subsequently buried under the thick Quaternary sediment pile of the Banni-Great Rann basin and the neotectonically controlled colluvial and alluvial sedimentation in the KMF zone (Chowksey et al. 2011a, b).

Since the KMF zone is for the most part covered by the Quaternary sediments, the surface trace of the KMF is generally marked at the base of scarp. This is mainly because of the lack of subsurface data along the KMF. However, detailed field studies in the various morphotectonic segments revealed that the various north flowing streams incising through of the KMF zone show extremely patchy and poorly exposed Mesozoic and Tertiary rocks below the Quaternary sediments. In view of the consistently thick Quaternary sediments, the trace of the KMF is found to be buried in the segments I to IV. However, sporadic outcrops of the fault were identified on the basis of the observed deformation in the Mesozoic and Tertiary rocks (Fig. 3.4). The rocks were found to attain near vertical to reversed dips especially in the Mesozoic rocks.

An excellent exposure of the fault plane of the KMF was seen in a large artificially excavated pit to the SW of Jhura village (Fig. 3.4a). A sharp lithotectonic contact between the Mesozoic rocks and Tertiary rocks marked the fault plane of the KMF. The KMF is found to be a steep south dipping reverse fault at this location (Fig. 3.4a). The reverse nature of the fault was also observed in a small outcrop along a small stream to the north of Devisar (Fig. 3.4b). Here, the faulted contact of the Mesozoic and Tertiary rocks was found to dip steeply towards the south. The lithologically contrasting rocks occurring on either sides of the fault also showed similar dips. In Lotia stream, the south dipping northern limb of the flexure point to the reverse nature of the KMF (Fig. 3.4c). Significantly, all these exposures are in close vicinity of the transverse faults. This suggests that the zones of intersection of the E-W trending KMF with the transverse faults are the most stressed parts of the KMF. Fig. 3.4 shows the scanty exposures of the KMF observed in segment-I to segment-IV during the detailed field investigations carried out in the present study.

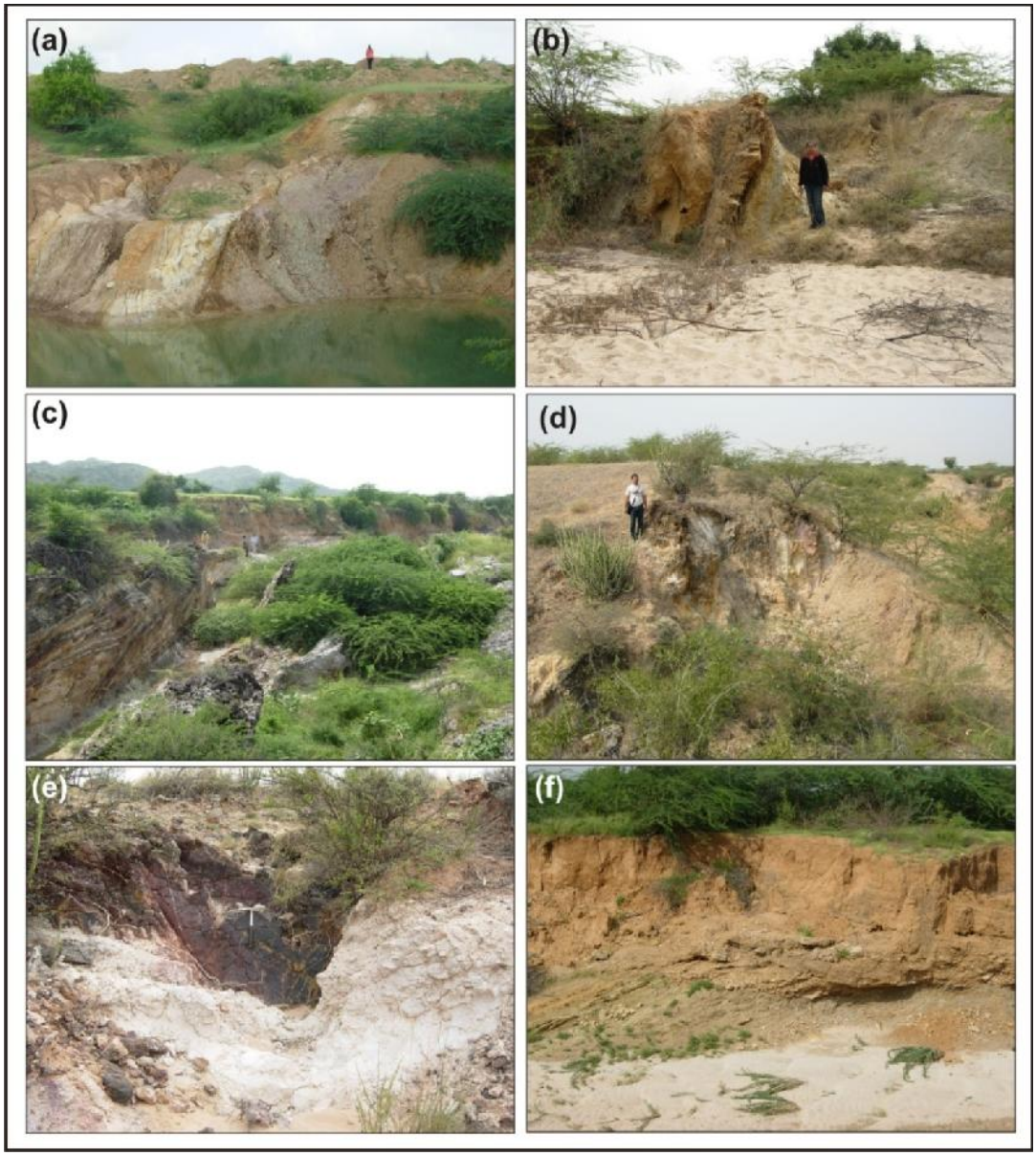

Figure 3.4 (a) View of the KMF in a large artificially dug pit to the SW of Jhura showing it reverse nature. Note the sharp lithological contact between the softer Tertiary shales on the right (north) side and the compact Mesozoic rocks to the left (south) side of the fault plane. **(b)** View of a small outcrop showing the reverse nature of the fault plane of the KMF along a small stream to the north of Devisar. **(c)** View across the Lotia stream (west of Jawaharnagar)) showing the overturned (south diping) northern limb of the flexure which points to reverse nature of the KMF (not exposed here). Cliff section shows the flat surface over Quaternary sediments overlapping the Mesozoic rocks. The KMF scarp is visible at the far end. **(d)** Vertically dipping sheared Mesozoic rocks to the east of Jawaharnagar indicating the surface trace of the KMF. **(e)** View of a small exposure of the KMF in segment-V. **(f)** View of the Quaternary sediments overlying the south dipping Tertiary rocks (west of Jawaharnagar).

PART-B Kachchh Mainland Fault (KMF)

The present field studies, however, revealed that the KMF is ideally exposed in the Khirsara-Devisar segment (segment-V) where the Quaternary sediment cover is negligible (Fig. 3.5). In this segment, the fault plane of the KMF marks the sharp litho-tectonic contact between the Mesozoic rocks and Tertiary (Neogene) rocks (Fig. 3.5a). The fault trace is discontinuously exposed on the surface along several small incising streams flowing northward and disappearing in the Banni plain. The fault is characterized by the sharp contact between the compact sandstones of the Bhuj Formation of late Cretaceous age on the southern side and the semi-compacted Tertiary (Neogene) shales of the Chhasra Formation on the northern side (Biswas, 1993).

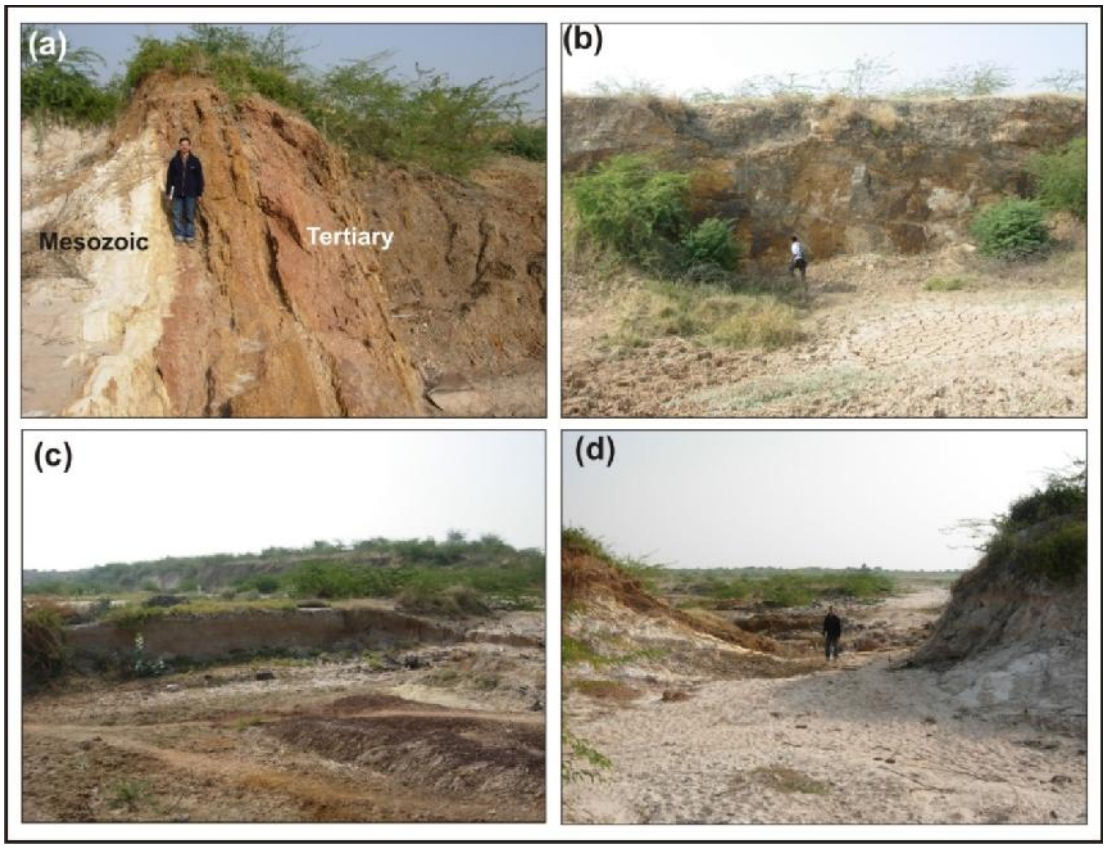

Figure 3.5 (a) View of a stream section to the east of Khirsara showing the KMF expressed as a steep northward dipping fault marking the sharp lithotectonic contact between the near vertical Mesozoic rocks to the south and Tertiary rocks to the north. **(b)** The exposed fault plane of the KMF forming a scarp. **(c)** View of the low incised cliffs exposing Quaternary alluvial sediments reflecting the thin sediment cover. Also visible are the Tertiary rocks in the stream bed and the scarp (shown in previous photograph) in the background. **(d)** Northward view of the same stream showing incision in Mesozoic rocks and the almost flat topography beyond the fault line. The person is standing exactly along fault plane of the KMF shown in a.

PART-B Kachchh Mainland Fault (KMF)

Both formations show near vertical northward dips and are separated by a thin conglomeratic bed. The fault plane shows several slickensided surfaces at many places. The amount of dip of the Neogene rocks rapidly decreases away from the fault and quickly flattens out within few tens of metres before disappearing below the thin Quaternary alluvial cover. It is therefore inferred that the KMF is represented by a single fault strand near the surface marking the litho-tectonic contact between the Mesozoic and Tertiary rocks. This criteria is used for mapping the near surface trace of the KMF using GPR in other morphotectonic segments where it is buried under Quaternary sediments.

CHAPTER 4

QUATERNARY STRATIGRAPHY

Investigations of Quaternary deposits in active fault zones are crucial as they provide critical stratigraphic evidence for reconstructing neotectonic evolution of faults as demonstrated in the case of Katrol Hill Fault in the central part of mainland Kachchh (Leeder et al. 1991; Patidar et al. 2007; 2008). In this chapter, the Quaternary sediments occurring in the eastern part of the KMF zone (Fig. 3.1) are described primarily with a view to delineate its Quaternary evolutionary history. A lithostratigraphic framework supported by chronology of the Quaternary sediments is provided. An attempt is made to identify the phases of neotectonic activity along the KMF as reflected in the stratigraphic development.

The exposed Quaternary sediments in all the morphotectonic segments of the KMF zone in the study area were investigated. The locations of the studied exposed Quaternary sediments in the KMF zone are shown in Fig. 3.1b in the previous chapter. Vertical lithologs were prepared and their lateral variations in sedimentary facies were also documented. OSL dating of the samples collected was also carried out. The occurrence of Quaternary deposits along a 1-3 km wide zone between the KMF scarps and Banni plain is extremely significant (Fig. 3.1b). These deposits average 5-10 m in thickness and display wide variation in lithology, both in the northward direction and laterally along the KMF zone.

The deposits, in general, comprise coarse as well as finer gravelly deposits, sands and aeolian and fluvial miliolites. These deposits together, effectively conceal the KMF fault line below them and form a north sloping surface that merges with the Banni plain. The northward sloping surface developed over the Quaternary deposits is consistent with the decreasing depth of incision in this direction. The Nirona, Kaila, Pur and the Kaswali rivers have given rise to fan shaped alluvial deposits at their mouths near the KMF zone (Fig. 3.1b). These are formed due to dispersal of recent sandy alluvium as the river loses gradient and bifurcate into small indistinct channels before disappearing in the Banni plain. The fan shaped alluvial deposits, therefore, form the stratigraphically youngest Quaternary deposits of the KMF zone. The Quaternary deposits exposed in the cliff sections of the various north flowing streams have great significance for understanding the neotectonic

evolution of the KMF. The Quaternary sediments exposed in various morphotectonic segments are described separately.

NIRONA-JHURA SEGMENT

This segment lies to the north of Jura dome and extends from Nirona in the west to Pur river in the east (Fig. 3.1a). The segment is characterized by a northward sloping surface developed over the Quaternary deposits. The surface abuts against the KMF scarp in the south and gently grades into the flat terrain of the Banni plain in the north. In general, the maximum thickness is exposed closer to the scarps corresponding to the incision pattern which shows a northward decreasing pattern mentioned earlier. Lithologs of the sections studied in this segment are shown in Fig. 4.2.

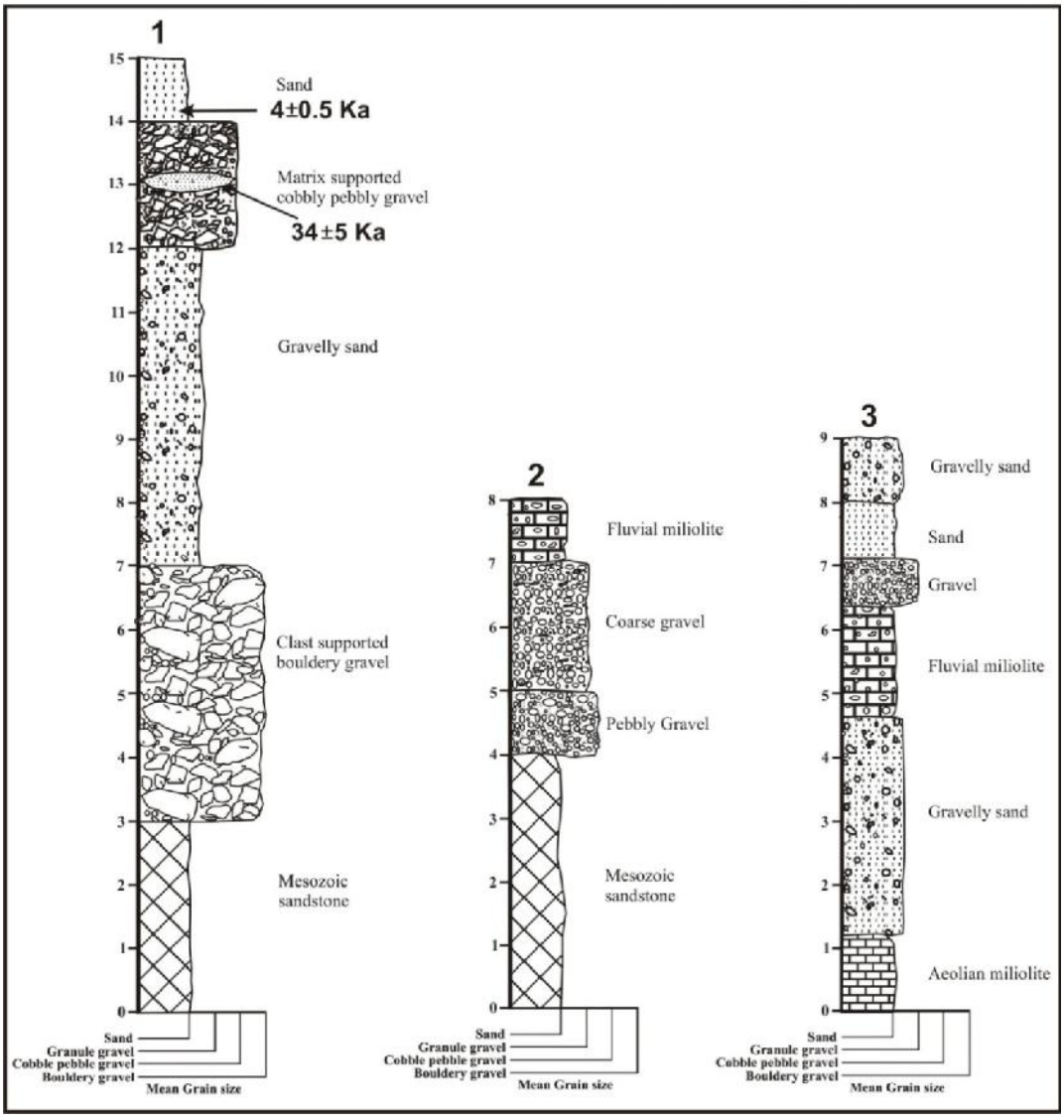

Figure 4.1 Lithologs of Quaternary sediments exposed in Segment-I. Location of the lithologs is shown in Fig. 3.1b.

The maximum thickness of the sediments is exposed along the Kaila river that

flows along the eastern most fringe of the Jhura dome. The Quaternary sediments are exposed in continuous line of vertical cliffs on left bank from Sodha camp to Jhura village in the north (Fig. 3.1b). South of Sodha camp, the cliff exposing Mesozoic rocks of same height are observed. The Quaternary sediments rest unconformably over the northeast dipping Mesozoic sandstones which are also incised (Fig. 4.1, litholog 1). In the upstream reach, the bottommost 2-3 m part of the cliff section comprises of Mesozoic rocks. The overlying ~12 m thick Quaternary sediments is divisible in distinct lithologic units. All units are separated by erosional contacts.

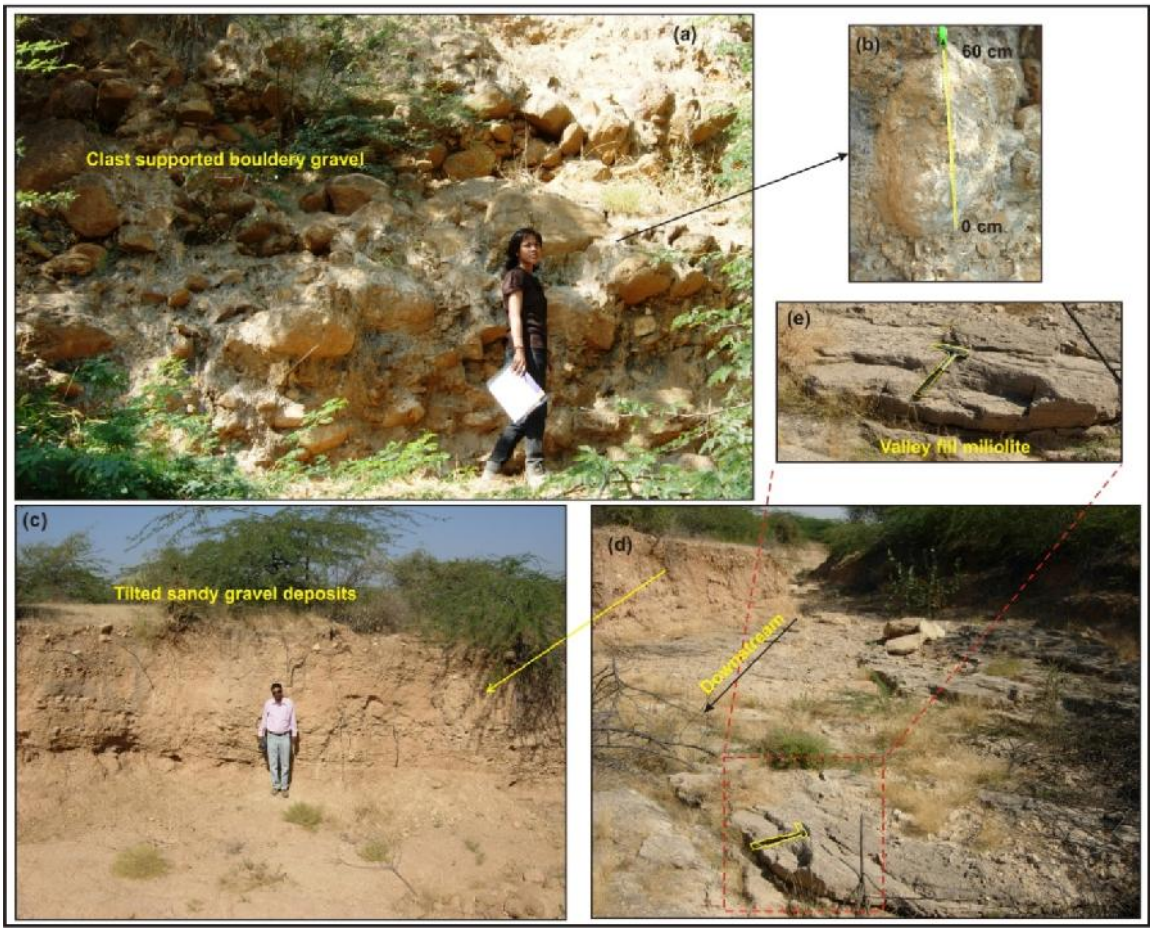

Figure 4.2 **(a)** Close view of clast supported bouldery gravel at the base of the exposed cliff section in Kaila river to the south of Jhura. **(b)** Close view of the largest boulder observed. The size of the clast is 0.6 m. **(c)** Tilted sediment succession of Quaternary deposits exposed in a lower order stream in segment-I. **(d)** View of aeolian miliolite forming the floor of the incised valley shown in (c). Note the fine grained nature of the deposit and the aeolian cross bedding. **(e)** Close view showing the aeolian cross bedding in the miliolite deposit shown in (d).

The succession starts with a 4 m thick clast supported massive bouldery gravel overlying the Mesozoic rocks (Fig. 4.2a). The average size of the boulder is ~50 cm, whereas the largest boulder is approximately 0.6 m (Fig. 4.2b). The large boulders are

enclosed in a matrix of cobble to pebble sized fragments. A small amount of interstitial sand appears to have been introduced subsequently. The lithoclasts are dominantly consisting of Mesozoic sandstones. The clasts are highly angular and sub-rounded. The bigger boulders are concentrated in the basal part of the unit. The vertical change in the clast size is because of the change in shear stress over the bedform. Higher sediment concentration, cohesive matrix and little internal sorting are the indicative of hyperconcentrated pseudoplastic debris flow (Miall, 1996). The higher content of bigger clast size, texture, absence of sedimentary structures indicate cohesionless, non-viscous pseudoplastic debris flow with internal bedload that deposited the poorly graded massive gravel (e.g. Blair and McPherson, 1992; Aziz et al. 2003; Garzione et al. 2003; Dorsey and Roering, 2006; Pope et al. 2008).

The basal boulder gravel unit is overlain by 5 m thick gravelly sand. This unit dominantly comprises several gravel rich layers separated by relatively thinner sandy horizons. The gravel shows angular clasts of pebble size that are enclosed in a matrix of finer gravels and sand. The intervening sands are discontinuous and of lensoid nature. The angular nature of the clasts testifies to the short distance transport which is in conformity with the geomorphic setting of the deposits. The absence of sedimentary structure and occurrence of unorganized pebbles in coarse sandy matrix suggest rapid deposition by sediment gravity flows or debris flows (Rust, 1978; Miall, 1996; e.g. Stokes and Mather, 2000; Aziz et al. 2003; Deynoux et al. 2005). The gravelly sand is overlain by 2 m thick matrix supported cobbly pebbly gravel. The individual clasts are found to be 20-40 cm size. The matrix is composed of rock fragments of smaller size. The clasts and matrix are angular in nature. The unit shows a considerable thickness along the cliff section and a general decrease in clast size towards the north. The presence of matrix suggests the cohesive, viscous nature of depositing flow whereas; the absence of sedimentary structure and the fabric indicate the sediment deposition by debris flows (Rust, 1978; Miall, 1996). All these lithofacies characteristics indicate the deposition by viscous, high strength clast rich debris flows (e.g. Blair and McPherson, 1992; Garzione et al. 2003; Dorsey and Roering, 2006; Pope et al. 2008). OSL sample collected from one of the sand lenses has yielded an age of 34±5 Ka. The top of the section is marked by 1m thick structureless sand deposited by sediment gravity flows which has given an OSL age of 4±0.5 Ka.

The main characteristic of these deposits is their occurrence in imposing cliffs on the left bank of the Kaila River and its dominance of highly angular coarse grained fluvial deposits. A general decrease of sediment size to the north, which is the downstream

direction, is very obvious. The sediments exposed in the cliffs are in complete contrast to fine grained sandy bedload in the present day channel of the river. The section is reduced to ~6 m to the east of Jhura village where the cliff section gradually goes below the recent fan shaped sandy alluvium of the Kaila river further north.

To the west of Jhura, the Sonva nala stream also exposes Quaternary sediments along its 8-10 m high incised cliffy bank (Fig. 4.1, litholog 2). The river follows a N-S oriented gorge like incised course for about 2 km after emerging from the hilly terrain of eastern part of Jhura dome. The stratigraphic development is restricted as compare to Kaila River. Here the Quaternary deposits overlie the north dipping Mesozoic sediments which form about 4m of the basal part of the cliff section. The Mesozoic rocks are unconformably overlain by ~1 m of pebbly gravel. The gravel is matrix supported and consists of clasts of Mesozoic sandstone. The unorganized, structureless pebbles and abundant coarse matrix indicates the cohesive nature of depositing agent. As the lithofacies comprises of matrix rich gravel with absence of sedimentary structures it can be inferred that the sediments were deposited by cohesive, low strength turbulent or laminar flow with an inertial bedload. Absence of imbrication, sorting and sedimentary structures suggest rapid deposition by cohesive clast rich sediment gravity flows (Rust 1978, Miall, 1996 e.g. Blair and McPherson, 1992; Garzione et al. 2003; Dorsey and Roering, 2006; Pope et al. 2008). They are overlain by coarse gravel which shows clasts of cobble sized. The cobble gravel is 2 m thick and easily distinguishable from the lower pebbly gravel unit by its grain size. The unit consists of cobble size clasts embedded in matrix of medium to fine sand. The clasts comprise rock fragments of shales and laminated sandstone and are platy in nature with their flat bases giving the appearance of pseudostratification. The clasts show high angularity and are imbricated in the downstream direction. Although the lithofacies have been deposited by the same depositional process as the former one, the increased clast size indicates relatively increased strength of the flows. The top of the exposed section is marked by compacted valley fill miliolites. It consists of sand sized grains of miliolitic sand cemented by calcareous matrix. The valley-fill miliolites also contain clasts of Mesozoic rocks of varying sizes embedded within the compacted miliolites grains which points to fluvial deposition. The valley fill miliolites owe their origin to erosion of aeolian miliolites in the upstream area which were fluvially reworked, carrying the Mesozoic rock fragments along with them and redeposited. This horizon brackets the underlying deposits together with those exposed along the Kaila river as of pre-miliolite phase.

PART-B Kachchh Mainland Fault (KMF)

Further west of Sonva nala river, the Quaternary deposits continue to form a north sloping surface in front of KMF scarps up to Nirona river. The surface is extensively directed by several north flowing streams including the Badi river that arises from the core portion of the Jhura dome. Good exposures of the sediments are observed in an unnamed lower order stream to the west of it that exhibits an incised course exposing varied lithologies of the Quaternary sediments (Fig. 4.2c). Here the section starts with aeolian miliolite which forms the floor of the incised valley (Fig. 4.3d). The aeolian origin of the miliolite is evident by its laterally extensive and uniformly fine grained nature and well developed aeolian cross bedding (Fig. 4.2d). The deposits forms a part of the extensive obstacle dune that was formed in front of the KMF scarps, of which, a small part is exposed in the valley floor while the rest of it is covered by the younger Quaternary deposits. The aeolian miliolite is part of the regionally extensive and prolonged phase of miliolite deposits witnessed all over the Kachchh basin from Middle to Late Pleistocene (Baskaran et al. 1989). The aeolian miliolite is overlain by 3.2 m thick gravelly sand that contains dispersed angular clasts of Mesozoic rocks (Fig. 4.1, litholog 3). The massive texture of the sand with presence of isolated clast and the absence of sedimentary structures suggest the rapid deposition of gravelly sand (Miall, 1996). It is interpreted that the structureless fine to coarse pebbly sand was deposited as sheetflood sedimentation by sediment gravity flow (Miall 1996; Stokes and Mather, 2000; Coltorti et al. 2010). This is followed by ~1.7 m thick semi-compacted valley fill miliolite that characteristically shows stratification and angular pebbles of Mesozoic rocks.

A 0.7 m thick gravel overlies the valley fill miliolite. The clasts include cobbles as well as boulders of sandstones. The large angular clasts are clast supported while the smaller ones are matrix supported. The entire sediment succession horizon shows marked tilting towards the north (Fig. 4.2c). The clasts are weakly graded, poorly sorted, and does not show imbrications and sedimentary structures which are the characteristic properties of debris flow deposits (Miall, 1996). Further, the clast supported cobbles and pebbles indicate hyperconcentrated, low strength, clast rich pseudoplastic nature of the depositing fluid (Rust, 1978; Miall, 1996). Hence, it is inferred that the sediments were deposited by low strength pseudoplastic debris flow (e.g. Blair and McPherson, 1992; Aziz et al. 2003; Pope et al. 2008). The gravel is followed by ~1.0 m thick sand which is in turn overlain by 1 m thick gravelly sand marking the top of the succession. These both lithofacies have sheet like geometry, massive texture and the absence of sedimentary structures suggests the deposition by sediment gravity flow that could be related to the sheetflood

sedimentation (Miall, 1996; Coltorti et al. 2010). On the basis of miliolite deposits at the base, the overlying sediments are clearly the result of post-miliolite depositional phase. The tilting of the sediments provides strong evidence for reactivation of KMF in post-miliolite time.

KUNARIA- LODAI SEGMENT

This segment extends from Kunaria in the west to Lodai in the east and corresponds to the KMF zone to the north of the Habo dome (Fig. 3.1a and b). The Quaternary deposit occurs in a 2-3 km wide band to the north of the KMF scarp developed in the northern limb of the Habo dome (Fig. 3.1b; 4.3a). The major rivers are the Pur and Kaswali river that flow in the saddles to the west and east of the Habo dome respectively. Between them several unnamed streams arising from the hilly topography of the Habo dome flow northward incising through the Quaternary sediments before disappearing in the Banni Plain (Fig 3.1b). All rivers expose variable thickness of their deposits overlying the Mesozoic rocks. Maximum stratigraphic development of the deposits is seen in the Falay river (Fig. 4.4). Vertical cliff sections in the Falay river and a small tributary near Falay on its right bank reveals the heterogeneity of the dominantly coarse grained fluvial deposits (Fig. 4.4, litholog 4). The deposits unconformably overlie the vertically dipping Mesozoic strata (Fig. 4.4a). In the downstream side, several tens of meter wide zone of highly sheared Mesozoic rocks underlie the Quaternary deposits.

The dominantly coarse nature of the Quaternary deposits is very striking (Fig. 4.4). Overlying the Mesozoic rocks is clast supported bouldery gravel which shows a maximum thickness of ~6 m (Fig. 4.3b, c). The thickness varies along the river as it overlies the uneven topography of the underlying Mesozoic rocks. The unit shows several phases of deposition of very coarse gravel as separated by 0.3 - 0.5 m thick discontinuous lensoid sand bodies of variable thickness within the gravels. The bottommost sand body is massive in nature and shows extensive development of nodular calcretes. The clasts size is mostly cobbly but boulder size fragments also regularly occur. All clasts are highly angular and indicate very short transport. The general appearance is that of typically unsorted colluvium deposits, however fluvial reworking is indicated by distinct aggradation phases and intervening sandy layers. The extremely short transport is implicit from the geomorphic setting as the source area is less than a kilometre to the south in the hilly terrain of the Habo dome (Fig. 4.3a). We interpret these as debris flows deposit as they are weakly graded, poorly sorted, and does not show imbrications and sedimentary structures. The occurrence of bigger clasts in large amount and massive texture indicate

deposition by hyperconcentrated, low strength, clast rich pseudoplastic debris flows (Rust, 1978; Miall, 1996; e.g. Blair and McPherson, 1992; Aziz et al. 2003; Pope et al. 2008). A sand lens from this horizon has yielded an OSL age of 100±7 Ka.

Figure 4.3 **(a)** Panoramic view of the KMF zone showing the field setting of the Quaternary colluvio-fluvial deposits along the Falay River. Note the flat surface formed over the colluvio-fluvial deposits exposed along the incised cliff of the river. Also seen are the vertical to sub vertical sheared Mesozoic rocks in the river bed and the sharp unconformable contact with the overlying stratified colluvio-fluvial deposits. **(b)** Close view of the colluvio-fluvial deposits resting unconformably over the Mesozoic rocks in Falay river. **(c)** View of the clast supported gravel in Falay river. Note the coarse nature of the deposit and the angular nature of the clasts. **(d)** View of a knick point in Falay river showing the sedimentary succession. Note the valley-fill miliolite dividing the colluvio-fluvial deposits into two distinct phases. Location of the knick point is about half kilometer upstream of the photographs in (a), (b) and (c).

The thick colluvio-fluvial unit is overlain by 2-3 m thick valley fill miliolites (Fig. 4.3d). The miliolite contains dispersed clasts of pebbles to large boulder size pointing to

fluvial origin of the miliolite. The miliolite is again overlain by 2 m thick colluvio-fluvial deposit represented by matrix supported gravel (Fig. 4.3d). This unit shows finer clast size than the thick colluvio-fluvial deposits underlying the valley-fill miliolite. The presence of medium to coarse grained sandy matrix indicates cohesive nature of the depositing agent. The gravels unimbricated, poorly sorted and massive which suggests rapid deposition by sediment gravity flows (Rust, 1978; Miall, 1996). Overall, the presence of matrix and fabric suggest that the sediments deposited by cohesive, clast rich debris flow (e.g. Blair and McPherson, 1992; Garzione et al. 2003; Dorsey and Roering, 2006; Pope et al. 2008). This unit has yielded an OSL age of 41±6 Ka.

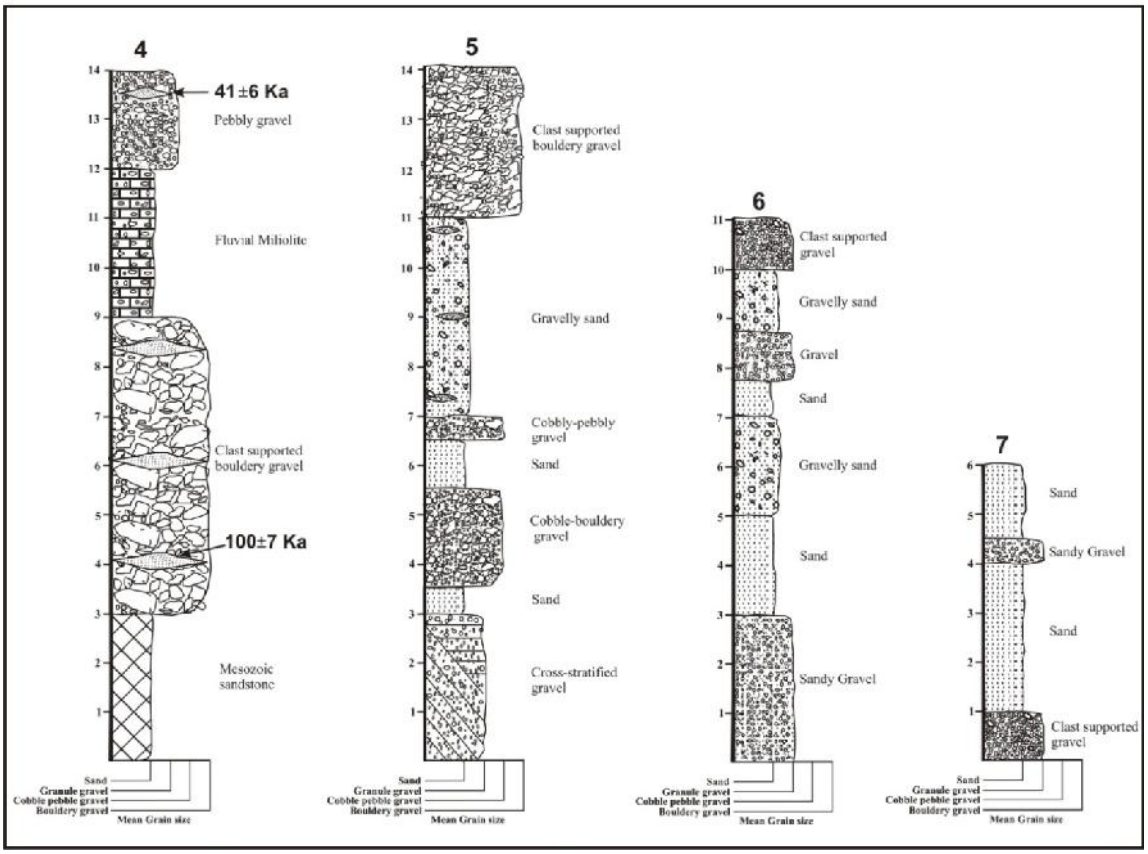

Figure 4.4 Lithologs of Quaternary sediments exposed in Falay river in Segment-II. Location of the lithologs is shown in Fig. 3.1b. The vertical scale is in meters.

About one km downstream, a 15 m thick section is exposed in a deeply entrenched meander (Fig. 4.4, litholog 5). The sediments are markedly finer than the above described section. A 3 m thick matrix supported gravel forms the base of sedimentary succession which shows large scale cross stratification. The clasts comprises pebble size rock fragment. The pebbles are supported by medium to coarse sand which indicates cohesive, viscous property of depositing medium whereas the presence of cross stratification indicates that the sediments could have been deposited as lag deposits (Miall, 1996). It

could be inferred that the sediments are lag deposits that were deposited by cohesive debris flow (Miall, 1996; Garzione et al. 2003; Dorsey and Roering, 2006). Overlying this is a 0.5 m thick sand followed by 2m thick cobbly gravel which shows sparsely distributed boulders as well. Above this unit lies 1 m thick sand followed by 0.5 m thick cobbly pebbly gravel. The sand facies is characterized by massive texture, lack of sedimentary structures and poor sorting which indicates deposition by sediment gravity flows (Miall, 1996; Stokes and Mather, 2000; Coltorti et al. 2010). The overlying cobbly pebbly gravel lithofacies comprises subangular to subrounded, poorly sorted, coarse matrix supported gravels. The absence of sedimentary structures, poor grading and lack of sorting suggest the deposition by clast rich debris flows (Miall, 1996; Blair and McPherson, 1992; Dorsey and Roering, 2006; Kallmeier et al. 2010). This is followed by 4 m thick horizontally stratified gravelly sand. The sand shows several gravel rich lensoid bodies. The gravels are of pebble size, subrounded and show horizontal stratification. On the basis of structure and sediment fabric we interpret that the lithofacies was deposited by clast rich laminated debris flow (Rust, 1978; Miall, 1996; Pope et al. 2008; Kallmeier et al. 2010; Coltorti et al. 2010).

The top of the succession is marked by 3 m thick clast supported bouldery gravel. The poor sorting and grading, massive texture and the absence of sedimentary structures indicate deposition by viscous, hyperconcentrated clast rich debris flow (Rust, 1978; Miall, 1996; Aziz et al. 2003; Pope et al. 2008; Kallmeier et al. 2010). The overall finer nature of the sediments is in conformity with the fact that the section is located downstream of the previously described section. Further downstream, a 11 m thick cliff section shows increasing content of sand and prominent decrease in clast size in the various gravelly layers (Fig. 4.4, litholog 6). However, the sediment succession is stratigraphically comparable. About a kilometre further downstream in the north, the cliff section is reduced to 6m. The section exposes 1 m thick clast supported gravel at the base followed by 3 m thick sand (Fig. 4.4, litholog 7). This is overlain by 0.5 m sandy gravel and 1.5 m thick sand at the top.

Over all, the Quaternary sediments of the Falay River typifies the occurrence of these deposits in the KMF zone. The sedimentary characteristic reveals that the deposits are reworked colluvial deposits. The colluvium was generated in the hilly region comprising Mesozoic sedimentary formation in response to neotectonic uplift of the hill range along the KMF. These were later reworked by fluvial agencies and redeposited in front (to the north) of the range front scarps.

PART-B Kachchh Mainland Fault (KMF)

Another notable section exposing Quaternary deposits is found in an unnamed stream between Dhrang and Lodai. The section is ~6 m in height is exposed on the left bank close to the scarp line (Fig. 4.5, litholog 8). The lower~2 m of the incised section exposes steeply dipping Mesozoic shale over which the Quaternary sediments were deposited with a distinct unconformity. The Quaternary deposits are divisible into distinct aggradation phases; however, internal stratification is obscure. Overall, the section shows ~5 m thick horizontal to sub-horizontal layers of gravelly to pebbly sediments with elongated lensoid bodies of sand. The bottom most matrix supported cobbly gravel unit is the coarsest with occasional clasts of boulder size. The matrix supported massive nature of cobbly-bouldary gravels indicate cohesive, viscous property of depositing medium whereas, the cross stratification structure suggests that may have been deposited in form of lag deposits (Miall, 1996). It is inferred that the sediments are lag deposits that may have been deposited by debris flows (Miall, 1996; Blair and McPherson, 1992; Garzione et al. 2003; Dorsey and Roering, 2006; Pope et al. 2008). This is followed by stratified sandy gravel which shows increased content of sand. The gravels are of pebble to cobble size, poorly sorted and graded, supported by sandy matrix suggest cohesive, viscous debris flow. It displays horizontal stratification indicating the deposition by laminated debris flow (Miall, 1996; Pope et al. 2008; Kallmeier et al. 2010; Coltorti et al. 2010). Towards the top, a distinct 0.5 m thick sandy body of massive nature is seen. The massive texture, lack of sedimentary structures and poor sorting indicate deposition by sediment gravity flows (Miall, 1996; Stokes and Mather, 2000; Coltorti et al. 2010). The top of the succession is marked by pebbly gravel that shows several boulders size clasts embedded in sandy matrix. The largest boulder measured is ~0.60 m. The presence of matrix indicate the cohesive nature of depositing agent, while absence of imbrication, poor sorting and sedimentary structures which suggest the rapid deposition of sediments by sediment gravity flow (Rust 1978, Miall, 1996). These sediments show a rapid fining of clasts within a short distance of less than a kilometre in the downstream direction. Near the Banni plain the stream show fine sandy alluvium exposed along the vertical cliffs of ~1 m height.

About 1 km south of Lodai, the sediments are exposed along a small stream that rises from the eastern flank of the Habo dome and meets the Kaswali river. The stream exposes 2 m of basement Mesozoic rocks (Fig. 4.5, litholog 9). The Quaternary section starts with a 0.7 m thick structureless clast supported bouldery gravel. The bigger angular clasts are encased in matrix of pebble size clasts. The facies exhibits bigger clasts in

noticeable amount, massive clast supported structure, poorly sorted fabric, absence of stratification, imbrications and weak grading suggests deposition by low strength hyperconcentrated clast rich debris flow (Rust, 1978; Miall, 1996; Aziz et al. 2003; Pope et al. 2008; Kallmeier et al. 2010). This is overlain by 1.7 m thick massive sand with thin lenses of fine gravel. The massive texture, lack of sedimentary structures and poor sorting indicate deposition by sediment gravity flows (Miall, 1996; Stokes and Mather, 2000; Coltorti et al. 2010). The top 3.5 m is composed of well stratified matrix supported gravel. The gravels are of pebble to cobble size and supported by fine to coarse sandy matrix; poorly sorted and weakly graded indicate sediment gravity flow; whereas, the presence of horizontal stratification, indicate the deposition by high strength, clast rich laminated debris flow deposits (Miall, 1996; Pope et al. 2008; Kallmeier et al. 2010; Coltorti et al. 2010).

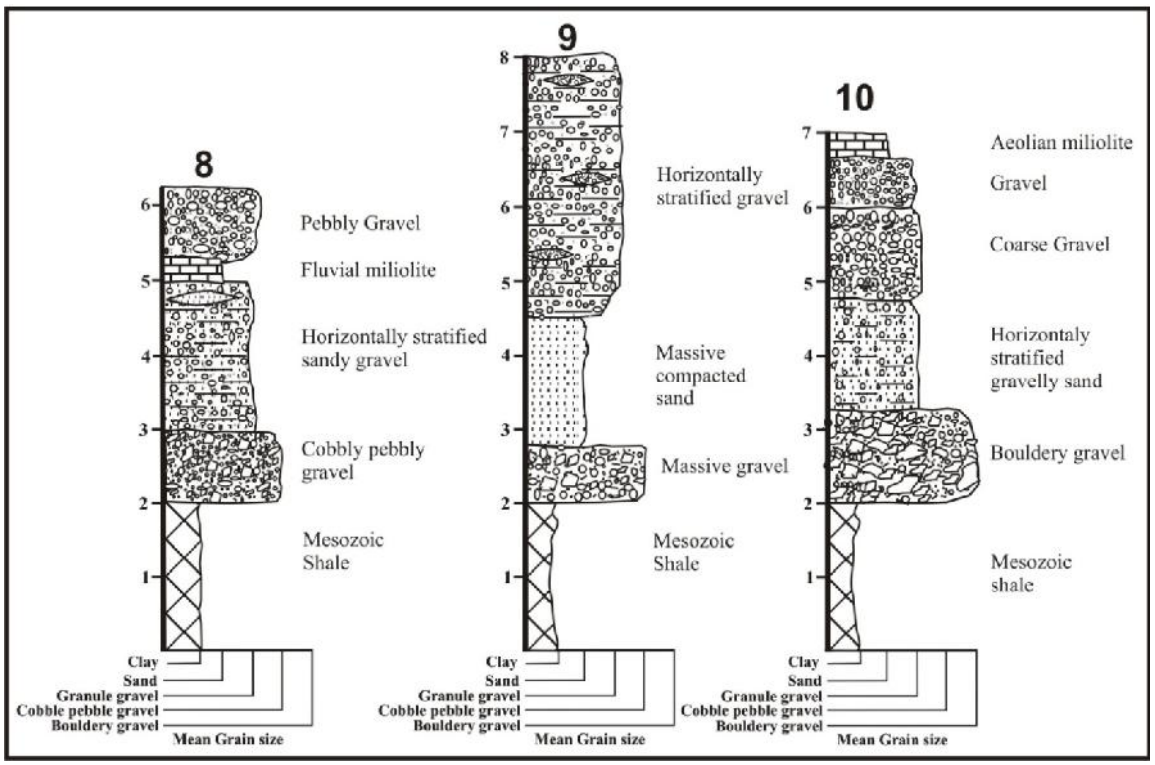

Figure 4.5 Lithologs of Quaternary sediments in Segment-II. Location of the lithologs is shown in Fig. 3.1b. The vertical scale is in meters.

Further south of this section, about one kilometre in the upstream direction of the Kaswali river, the Quaternary sediments are exposed in the long N-S trending cliff section on the left bank of the river. The deposits form a distinct terraced surface that is incised by >6 m (Fig. 4.5, litholog 10). The vertical section shows ~2 m of steeply dipping Mesozoic rocks that are part of the eastern flank of the Habo dome. Overlying it is a 1.5m thick boulder bed with a sharply erosional basal contact. The horizon shows large highly

angular boulder sized clasts which are crudely imbricated in the downstream direction. The matrix consists of finer clasts of Mesozoic rocks. The matrix supported texture indicates cohesive, viscous property of depositing medium whereas, the crude stratification indicate that the sediments could be deposited in form of large longitudinal bar deposited by debris flow (e.g. Miall, 1996; Garzione et al. 2003; Dorsey and Roering, 2006). This is followed by a horizontally stratified sandy horizon containing sparsely distributed gravel clasts. The horizontal stratification, occurrence of floating gravels and poor sorting indicate transverse bedform sedimentation by laminar sediment gravity flows (Miall, 1996; Stokes and Mather, 2000; Coltorti et al. 2010). The sand is overlain by a coarse gravel layer consisting of pebble sized clasts. This is capped by finer structureless gravel. The absence of sedimentary structures, weak grading, poor sorting and absence of imbrications suggest that gravels deposited by low strength, hyperconcentrated clast rich debris flow (Rust, 1978; Miall, 1996; Aziz et al. 2003; Pope et al. 2008; Kallmeier et al. 2010); whereas the decreased clast size of the overlying gravelly lithofacies may attributed to change in hydraulic properties of the depositing flows (Miall, 1996). The deposits are overlain by thin veneer of aeolian miliolite most part of which is eroded away. The exposed sediments are therefore bracketed as of pre-miliolite phase.

LODAI-JAWAHARNAGAR SEGMENT

This segment extends from the Lodai to the west and Jawaharnagar in the east. Here the scarps are developed in the Mesozoic rocks that form small domes forming a chain of small hills (Fig. 3.1a). South of these small hills is marked by the imposing presence of E-W trending Kas hill escarpment. The Kas escarpment is prominently visible up to Jawaharnagar (Fig. 3.1a). The north facing Kas escarpment is a scarp face of a large cuesta that is formed in the south limb of the large Kas anticline. Biswas (1993) describes the domes between the KMF and the Kas escarpment as small domal closure within the large Kas anticline. Prominent domes amongst these are the Wantra and Lotia domes.

The Quaternary sediments in this segment are lithologically very distinct from those of previously described sediments in segment-I and segment-II. East of Lodai to Wantra, the sediments form a continuous alluvial cover. At Wantra, a stream coming out of the Wantra dome exposes ~9 m of the Quaternary alluvial sediments on its right bank (Fig. 4.6, litholog 11). The base is marked by 1.5 m stratified sand. Overlying this is a 1 m thick semi compacted gravel. This is overlain by 1 m sand. Sand is further followed by 3.5 m thick sandy gravel which show several thin gravel rich layers. The gravel clasts are angular and unsorted. A 0.5 m structure less gravel overlies this. The top of the section is

marked by 1.0 m thick sandy gravel. The overall sediment nature is finer as compared to the dominantly coarse grained sediments in segment-I and II to the west. Further upstream, aeolian miliolites abutting against the scarps are found to occur along the river, though they do not form vertical cliffs and are covered by dense vegetation. The aeolian miliolite outcrops become more extensive eastward along the scarps and occurs discontinuously for few kilometres directly overlying the Mesozoic rocks. The geomorphological setting suggests that the deposition of miliolite took place as obstacle dunes against the scarps Mesozoic rocks. The alluvial sediments described above therefore belong to post-miliolite phase of fluvial deposition. Further east of Wantra, a tongue of flat Banni plain in found to extend up to the scarps.

The Lotia stream branches into two channels as it emerges from the hills. The western branch exposes continuous cliff section of Quaternary sediments overlying the Mesozoic rocks. It flows towards WNW and further towards NNW in the downstream before disappearing in the Banni plain (Fig. 3.1b). Mesozoic strata exposed in the river channel shows vertical dips. In the downstream the basement rocks are replaced by near horizontal Tertiary shales. The river exposes mainly fine sandy alluvium with gravel layer overlying the sheared Mesozoic and Tertiary rocks (Fig. 4.6, litholog 12). Overlying the basement rocks is a 1.5 m thick gravel with an erosional contact. This is overlain by 1.7 m fine to medium sand that passes upward into gravelly sand which is 1.3 m thick. A prominent 3 m thick sand horizon with indistinct stratification follows. Overlying this thick sand is 0.5 m sandy gravel that is capped by 2.5 m sand marking the top of the section. OSL date from the top of this unit suggests an age of 17±2 Ka. Though the gravels are relatively less, lithologically they appear to be similar to the gravel horizons in the Wantra section. The deposits represents post-miliolite phase of alluviation as revealed by extensive miliolite deposits overlying the Mesozoic rocks to the east of Wantra and near Jawaharnagar in the west.

To the west of Jawaharnagar, a north flowing stream bifurcates into two channels which flow further northward as independent streams to meet the Banni plain (Fig. 3.1b). The western channel follows a deeply incised channel exposing Quaternary sediments. The channel shows two major knick points within a distance of 1 km that show a vertical drop of 6 m and 5 m respectively away from the scarp. The Quaternary deposits exposed along the cliffy banks of the stream consists of 8 m thick aeolian miliolite, followed by ~2 m thick valley fill miliolite capped by discontinuous ~1 m thick fine alluvial sand (Fig. 4.6, litholog 13). The aeolian miliolite appears to have been deposited as a large obstacle

dune in front of the scarp line as evidenced by an extensive mound like morphology of the deposits. The western fringe of the dune is buried by alluvial deposits exposed in Lotia stream. The WNW orientation of the Lotia stream is possibly controlled by neotectonic uplift of the miliolites with dunal morphology. The eastern margin of the presumed obstacle dune is buried under thick alluvial deposits to the east of Jawaharnagar described later. Near the scarp line on to the left bank of the stream the miliolite strata in contact with the Mesozoic rock shows vertical dips. The youthful topography, several knick points and vertically inclined miliolites near the scarps indicates post-miliolite reactivation of the KMF.

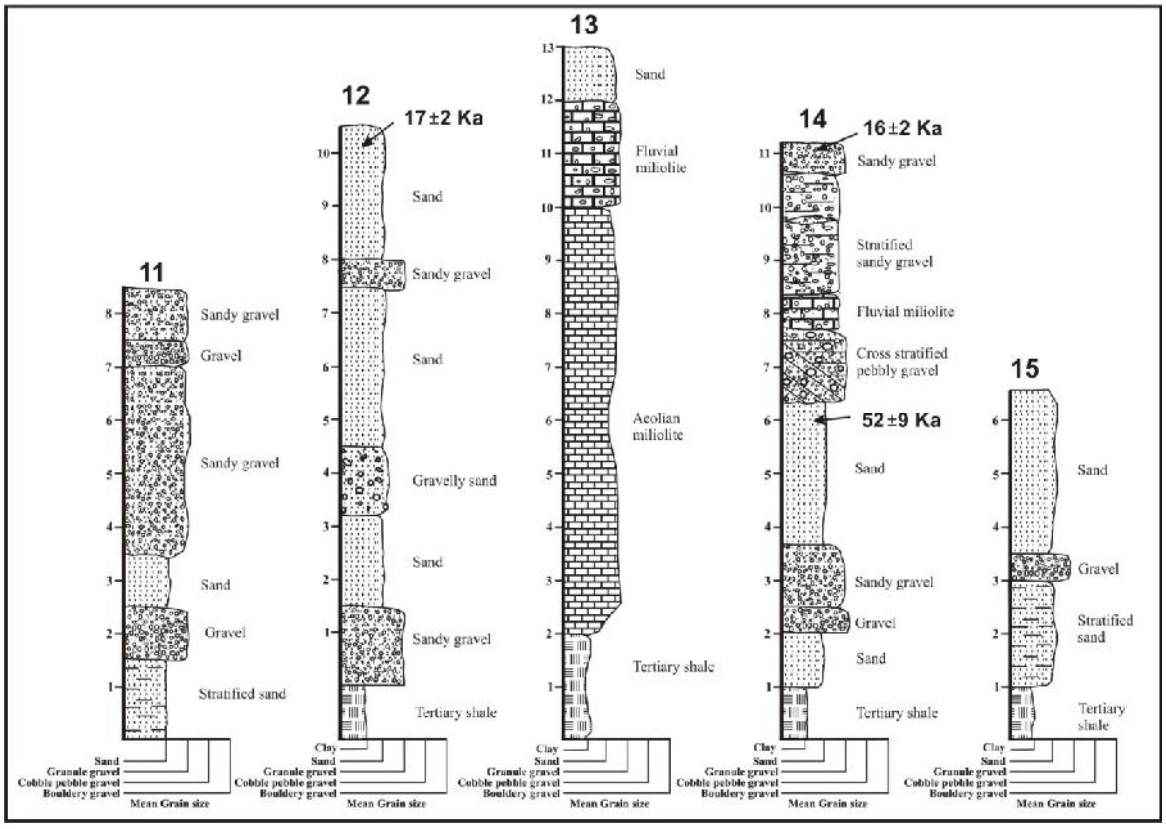

Figure 4.6 Lithologs of Quaternary sediments in Segments III and IV. Lithologs 11-13 are from Segment-III while lithologs 14-15 are from Segment-IV. The vertical scale is in meters.

The significance of the Quaternary sediments in segment-III is that they are comparatively finer and contain a higher amount of sand than that of segment-I and II. The sedimentary succession comprises multistoreyed bodies of gravel and sand. The constituent lithofacies are sandy gravel, sand and gravelly sand lithofacies. Thick sandy gravel facies comprises of well organized pebble clasts and fine to coarse grained sandy matrix. The lithofacies show moderate sorting and good lateral continuity. The alternating sand and gravelly sand lithofacies is composed of moderate to poorly sorted, massive and

weakly stratified sand and gravel. The matrix varies from fine to coarse grained sand wherein floating pebbles are embedded.

Because, the gravelly facies are well stratified and include clasts which are moderately imbricated, these can be interpreted as longitudinal bar deposits that filled up relatively shallow braided gravelly channels (Hein and Walker, 1977; Garzione et al. 2003). The sand may have been deposited on the top or flanks of bar during waning flow. In contrast to the alluvial fan lithofacies of segment I and II, these facies are finer and shows better sorting as well as increased sand content. Furthermore, facies bases tend to be sharp and exhibits sheet geometry. Overall the sediments represent deposits of infrequent sheet floods in shallow braided stream channels (Rust, 1972; Miall, 1977; 1996; Hein and Walker, 1977; Garzione et al. 2003; Kallmeier et al. 2010).

JAWAHARNAGAR-KHIRASARA SEGMENT

This segment lies between Jawaharnagar in the west to Khirsara in the east (Fig. 3.1a). The Quaternary sediment cover comprises mostly fine sandy alluvium that shows greatest thickness in the central part of the segment. The best exposure of Quaternary sediments is observed along a large entrenched meander of a stream flowing in the central part of the segment (Fig. 4.7a). The deeply incised meander is developed in alluvial sediments. The incision is however found to decrease rapidly to less than a metre near the Banni plain (Fig. 4.7b). The exposed sediments show a total thickness of ~11 m (Fig. 4.6, litholog 14). The sequence starts with a 1.0 m thick semi compacted massive sand. The compacted nature of sand is presumably because of the calcareous content derived from the older miliolite deposits well exposed near Jawaharnagar. This sand is overlain by 0.5 m thick semi-compacted clast supported lensoidal body of gravel. The gravel is followed by ~1 m thick sandy gravel which is overlain by 2.6 m massive and unconsolidated fine to medium fluvial sand. The unit has yielded an OSL age of 52±9 Ka.

Overlying this is a 1.2 m crudely cross stratified pebble gravel with sandy matrix and a scored base. This unit is overlain by 1 m thick fluvial miliolite. This is again overlain by 3.5m thick well stratified and unconsolidated sandy gravel with lenses of sand. The top is marked by 0.5 m thick sandy gravel. The unit has been dated to 16±2 Ka. Overall the coarser gravelly layers show lensoid nature while the sandy horizons are more consistent. Towards north in the upstream direction, a condensed section of ~10m is exposed in a small but tight meander. The sediments are similar but are notable for the increased size of the gravel clasts.

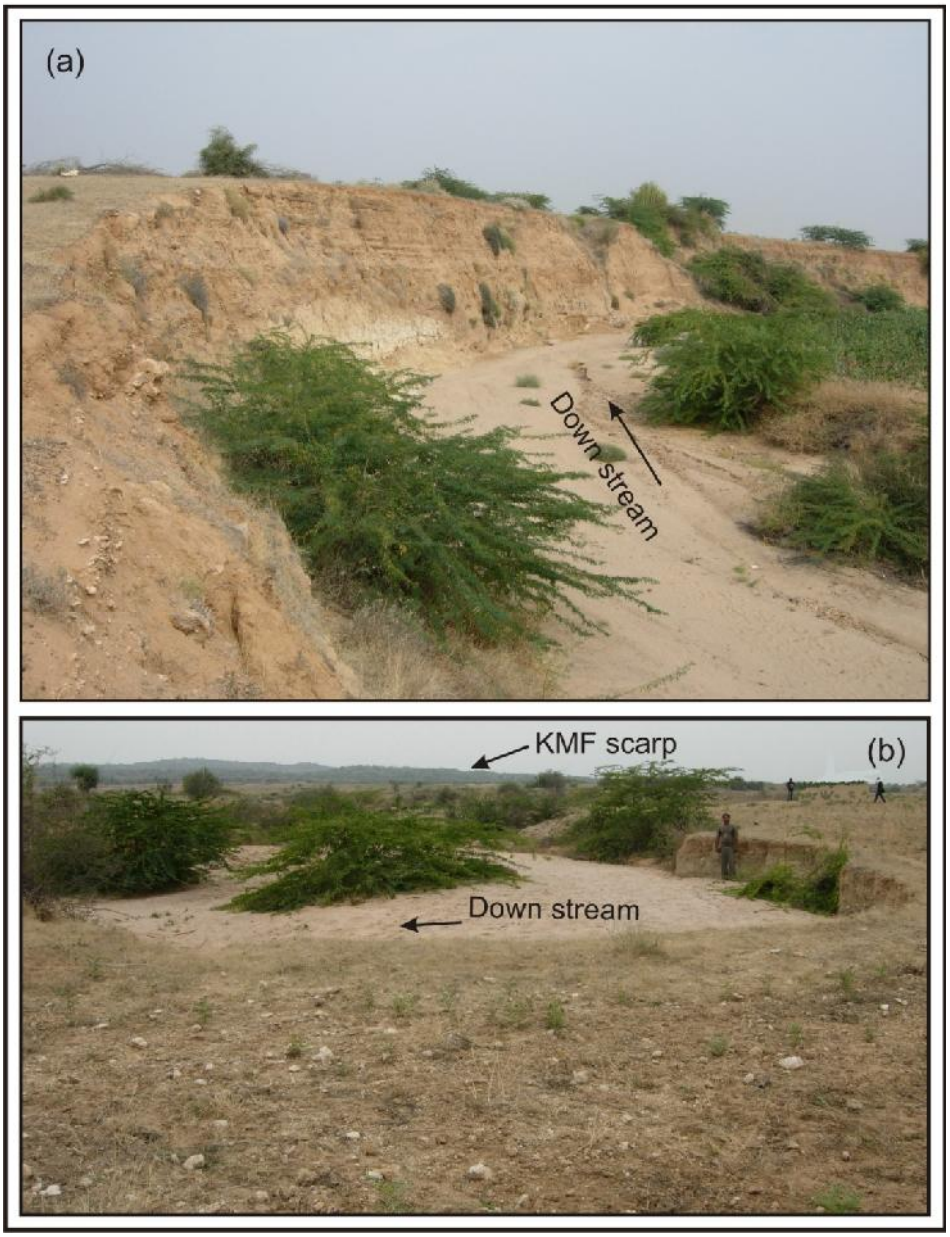

Figure 4.7 (a) Downstream view of large entrenched meander formed in Quaternary deposits to the north of the KMF scarp in Segment- IV. Note the deep incision and overall fine grained nature of the sediment succession exposed in the cliff which is in contrast to the sediments in segments to the west shown in earlier photographs. **(b)** View of a small incised meander in close to the Banni plain. The KMF scarp is seen in the background. Note the sharp decrease in incision as compared with the incision shown in a. Rapid decrease in depth of incision in less than two kilometers suggests that neotectonic movements along the KMF are responsible for the incision of Quaternary sediments.

Another stream in the east exposes a maximum thickness of ~6 m Quaternary sediments in an entrenched meander. The sequence overlies the uneven surface of the Mesozoic shale that forms the basal 1m of the vertical section (Fig. 4.6, litholog 15). The basement rocks are overlain by 2 m thick horizontally stratified sand followed by 0.5 m

thick fine basal gravel. This is overlain by 3 m thick massive sand followed by 1 m thick brown coloured sand. Further east the exposed alluvial thickness rapidly decreases, while at Khirsara the sediment cover is less than a one meter. Overall, the Quaternary sediments of this segment are sandy in nature and are in complete contrast to the coarse grained sediments exposed in other segments to the west. The unconsolidated nature and field relationship suggests that the sediments are younger than the miliolite depositional phase.

In this segment the sediments are composed of two lithofacies association, sand and sandy gravel. The sand lithofacies exhibit sheet like geometry, good lateral continuity, moderate sorting, massive or weakly horizontally stratified. Massive to moderately stratified structure of sand represent the deposits of sheet floods or highly concentrated flows (Rust, 1972; McPherson et al. 1987; Miall, 1977; Garzione et al. 2003). The thick sandy gravel comprises of well organized pebble clasts and fine to coarse grained sandy matrix. It shows cross to horizontal stratification and scoured base which are the indicators of confined channel deposits (Miall, 1977). Stratification, moderate sorting and organized gravel clasts in sandy gravel lithofacies indicate transport and deposition by sheet floods in braided stream channels (Rust, 1972; Miall, 1977; Aziz et al. 2003; Kallmeier et al. 2010).

KHIRSARA-DEVISAR SEGMENT

This segment includes the eastern most part of the KMF zone from Khirsara in the west to Devisar and further east. The general relief of the hill range in this segment is lower than other segments (Fig. 3.1a) but remains rugged as evidenced by the deeply incised river courses in the bedrock. The Quaternary sediment cover in front of the scarp is very thin. The Quaternary sediments forms a thin blanket of structureless and unconsolidated alluvial sands and fine gravels averaging 1-2 m in thickness covering the Mesozoic and Tertiary rocks. Major Quaternary aggradation phases evident in other segment are absent though the drainages appear to be of similar characteristics. It is surprising that this segment escaped significant Quaternary sedimentation in an identical geological setting where other segments to the west of it show stratigraphically well developed Quaternary sedimentary sequences. It can be inferred that this particular segment has had much lesser or subdued relief during much of the Quaternary period which did not provide sites for deposition and source area for generation of sediments as well. This also suggests that the segment-V attained the present relief later than other segments which can be attributed to eastward propagation of the KMF.

PART-B Kachchh Mainland Fault (KMF)

LITHOSTRATIGRAPHY

The Quaternary sediments occur in a thin band (1-3 km) in front of the north facing range front scarps marking the physiographic expression of the KMF. The scarp is an erosional remnant that owes it origin to faulting along the KMF. The Quaternary sediments form a northward sloping and highly dissected surface that gradually merges with the flat terrain of the Banni plain in the north. The sediments are obviously derived from the hilly terrain of the Northern Hill Range comprising deformed Mesozoic rocks and deposited by various streams in front of the scarps. The Quaternary sediment cover though thin, exhibits wide variation in lithology vertically as well as laterally along the KMF zone. All segments of the KMF zone investigated in the present study, show excellent stratigraphic development, except in the easternmost segment-V. OSL dating of the samples taken from selected horizons was also carried out (Table 4.1). The sediments are well exposed along the incised cliffs of north flowing small streams. In general, the maximum exposed thickness is found near to the scarps where the incision is also maximum which rapidly decreases towards north.

Table 4.1 OSL ages of the exposed Quatenary sediments. Sample PCH-1 is from the Pachham island while the rest are from the Quaternary sediment successions exposed in the KMF zone.

Field No.	Lab No.	U (ppm)	Th (ppm)	K %	Cosmic ray	Water content (%)	Wt. mean Ed	**Wt. mean Age(Ka)**	Dose Rate (Gy/a)
FAL-1	LD1203	1.5	10.4	0.6	150±30	15±5	65±9	**41±6**	1.6±0.1
FAL-2	LD 1204	1.6	13.6	1.0	150±30	15±5	75±13	**35±6**	2.1±0.1
FAL-3	LD 1205	1.6	12.1	0.7	150±30	15±5	180±7	**100±7**	1.8±0.1
PCH-1	LD 1209	1.4	8.1	1.1	150±30	15±5	68±10	**37±6**	1.8±0.1
JWN-1	LD 1210	1	6.5	0.3	150±30	15±5	16±2	**16±2**	1±0.1
JWN-2	LD 1211	1.4	11.8	0.45	150±30	15±5	80±12	**52±9**	1.5±0.1
KAI-1	LD 1212	2.2	17.4	0.94	150±30	15±5	10±1	**4±0.5**	2.4±0.2
KAI-2	LD 1213	1	4.1	0.4	150±30	15±5	32±4	**34±5**	0.9±0.1
LOT-1	LD 1215	1.3	9.4	0.4	150±30	15±5	22±2	**17±2**	1.3±0.1

The prominent development of the miliolite phase in the study area can be considered as a marker horizon which can be used in correlation of the underlying and overlying phases of the sedimentary record (Fig. 4.8). The Quaternary sediments of the KMF zone can be classified into three major aggradation phases (Fig. 4.9). The oldest

phase includes the sediments occurring below the miliolites. The second is the miliolite phase that includes the aeolian miliolites and valley-fill fluvial miliolites. The youngest phase is the post-miliolite phase that includes all deposits younger than miliolite. The deposits older than the miliolite phase are well exposed mainly in segment-I and segment-II to the north of Jhura and Habo domes respectively (Fig. 4.8). These deposits are dominantly coarse grained and are composed of clast supported to matrix supported gravels. The striking feature of these deposits is the large size of the clasts that ranges from boulder to pebbles (Fig. 4.8). The basal clast supported bouldery gravel seen in the cliff section of the Kaila and Kaswali rivers overlying the uneven surface of the underlying Mesozoic rock from the oldest Quaternary deposits of the KMF zone. This is overlain by several depositional phases of various kinds of gravel deposits. These deposits are unsorted and contain large angular clasts of Mesozoic rocks. The deposits underlying the miliolites imply short transport of the colluvial debris generated in the hilly region presumably due to uplift of the source area in response to neotectonic activity along the KMF. The pre-miliolite sediments can therefore be categorized in general as colluvio-fluvial deposits, which correspond to the pre-miliolite phase of neotectonic activity along the KMF. These deposits are in sharp contrast to the present day sandy bed load of the various streams and large rivers like the Kaila and Kaswali rivers.

The miliolite phase is the most characteristic Quaternary depositional phase of the region which includes both the aeolian as well as fluvial deposits. These comprise medium to coarse grained semi-compacted clastic limestones with higher lithic content than the comparable and more intensively studied miliolite rocks of Saurashtra (Biswas, 1971). These are described as originally carbonate rich sediments blown by wind from coastal area and deposited as scattered obstacle dunes along the rocky slopes within the hill ranges and in part of the scarps (Biswas, 1971). The miliolites are the only dated Quaternary sediments of Kachchh which have regional distribution. Since the lithologic and chronologic correlatability of the miliolites of Kachchh with their more well developed and more intensely investigated counterpart in Saurashtra is already well established and accepted (Baskaran et al. 1989; Chakrabarti et al. 1993; Somayajulu, 1993), they form important reference point for the interpretation of other Quaternary deposits in Kachchh especially in those occurring in the known active fault zones and for which no chronological data is available. (e.g. Patidar et al. 2007).

PART-B Kachchh Mainland Fault (KMF)

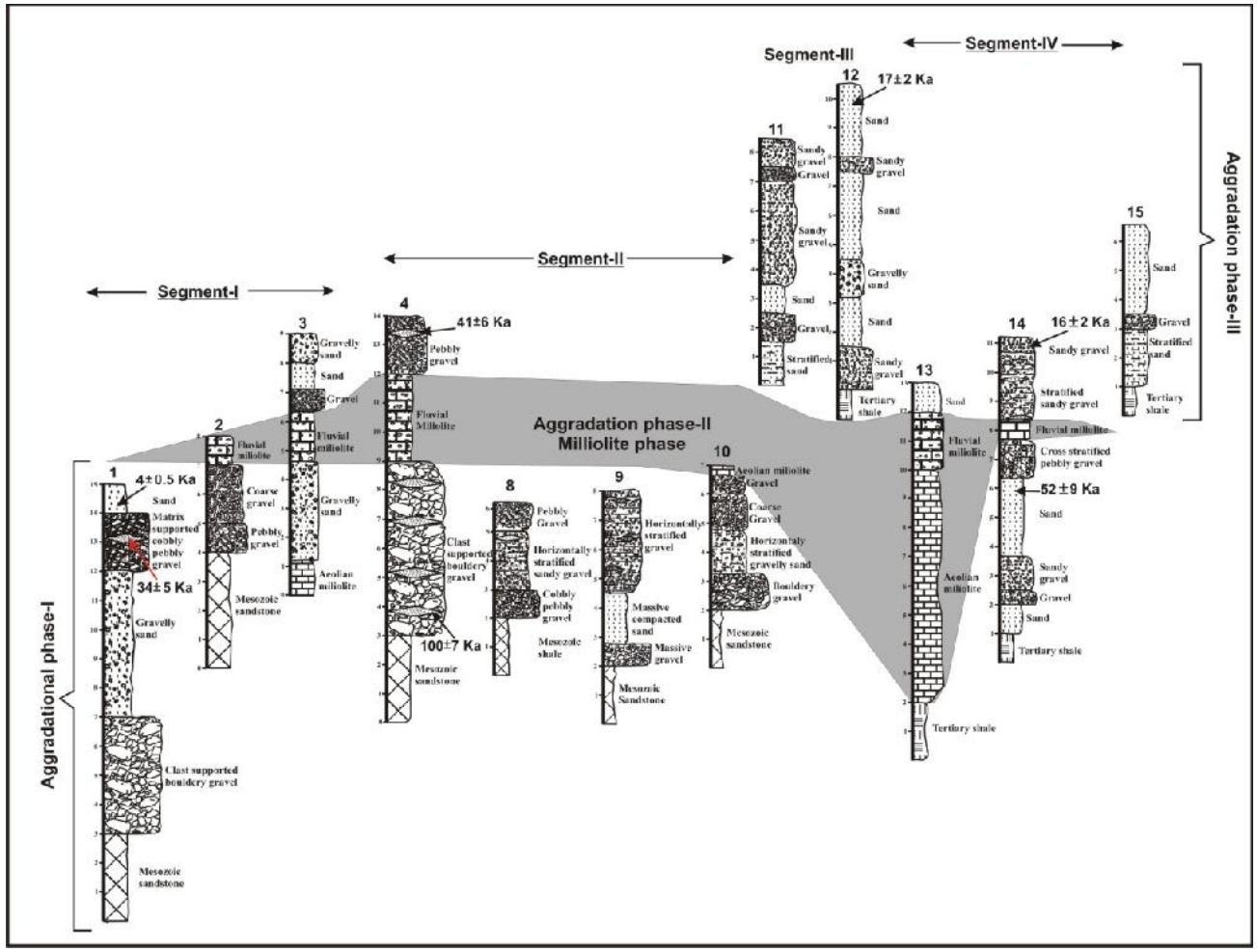

Fig. 4.8 Lateral correlation of the Quaternary sediments exposed in the KMF zone. Note the clear distinct three phases of aggradation. The vertical scale is in meters.

However, almost all dates of miliolites are reported from the central mainland Kachchh and none from the KMF zone. $^{230}TH/^{234}U$ ages of the Kachchh miliolite ranges from 30 to 130 ka (Baskaran et al. 1989; Chakrabarti et al. 1993; Somayajulu, 1993). The miliolite phase therefore represents an extensive depositional phase all over the Kachchh basin from middle Pleistocene to late Pleistocene. Aeolian miliolite comprises fine grained texture while in reworked fluvial miliolite, the presence of varying sizes of clasts of Mesozoic rocks and horizontal stratification is seen. The thickest aeolian miliolite deposit is seen in the Jawaharnagar stream where ~8 m thick deposit forms dunal morphology and abuts against the KMF scarp where it shows the vertical dip near the scarp. This suggests post-miliolite phase of neotectonic activity along the KMF. Reworking of the aeolian miliolite by fluvial agencies has resulted in the formation of valley-fill miliolite or fluvial miliolite (Biswas, 1971; Patidar et al. 2007). The maximum exposed thickness of the valley fill miliolite is seen in the Falay river where the maximum thickness of these deposits is ~3 m.

The post-miliolite phase is represented by the alluvial deposits overlying the miliolites. Typical exposures of the sediments younger than miliolite are found at Wantra and in large incised meanders to the east of Jawaharnagar. These sediments also show lithological heterogeneity along the length of the KMF zone. In segment-I these consist of cobbly-pebbly gravel with sands where they overlies the miliolite and are tilted. In segment-II this phase is separated by matrix supported gravel overlying the valley fill miliolite in Falay river. The clast size here is of pebble size. Further east in segment-III at Wantra, clast size is visibly reduced and the sand content is found to increase. The Wantra section exposes the post-miliolite deposit; the sediments are unconsolidated and characterized by relatively less amount of gravel deposits. Since the source area is the same, the relatively finer nature of the deposits could be indicative of comparatively less intense neotectonic activity along the KMF during the deposition of post-miliolite sediments. However, the tectonically controlled incision of the Quaternary deposits observed in all the segments indicates a post-depositional tectonic activity along the KMF.

The sedimentary characteristics and stratigraphic set up of the Quaternary sediments of the KMF zone described earlier are suggestive of very specific depositional processes. The geomorphic setting, proximity of the source area and the fact that the deposits overlap an active fault zone are further strong indicators of the nature of sedimentary processes that operated during the deposition of these sediments. The

deposits are in sharp contrast to the present day sedimentation that occurs by the seasonally active rivers and the resultant deposits are sandy.

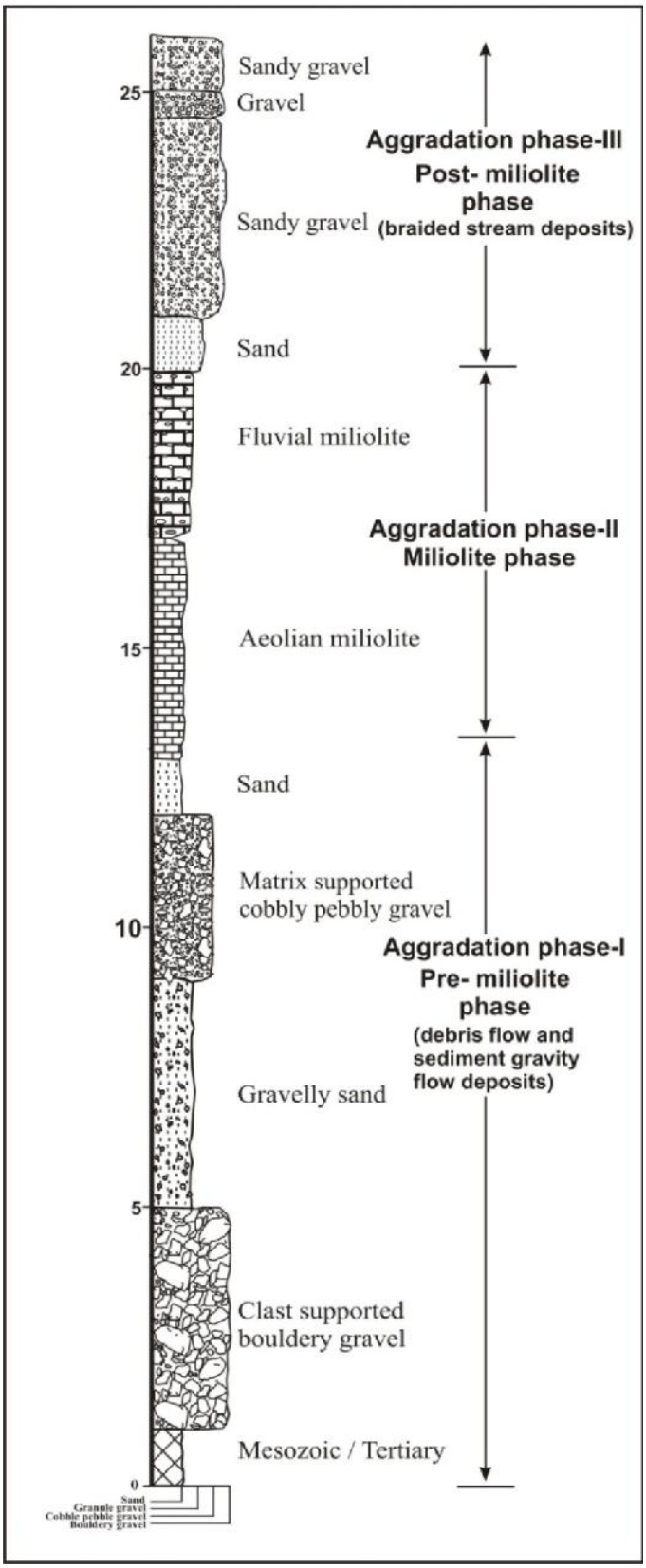

Figure 4.9 Composite lithostratigraphic log of the Quaternary sediments occurring along the KMF zone in the study area. The vertical scale is in meters.

PART-B Kachchh Mainland Fault (KMF)

NEOTECTONIC IMPLICATIONS

Neotectonics is the prime factor that governs the sedimentation pattern and geomorphic evolution in active fault zones. The Quaternary deposits occurring in the seismically active KMF zone provide important clues for neotectonic evolution. The lateral continuity and excellent stratigraphic development of the deposits in the KMF zone are in a way contrasting with the dominantly rugged rocky landscape of the Kachchh developed over Mesozoic rocks with negligible Quaternary sediment cover. The confinement and deposition of Quaternary sediments in front of the scarps along the KMF zone points to the primary control exerted by neotectonic activity in the generation and deposition of the Quaternary sediments. The rugged hilly terrain of the Northern Hill Range consisting of deformed Mesozoic rocks acted as the source area for the generation of sediments which were transported and deposited in front (north) of the scarps. Tectonic uplift of the hill ranges due to neotectonic activity along the KMF led to the generation of vast amounts of colluvial deposits which were reworked by fluvial agencies and transported northwards. The multistoreyed sedimentary architecture of the sediments indicate deposition in the form of small coalescing alluvial fans by multi-distributary channel systems in the backdrop of an active fault controlled range front. The dominantly coarse grained nature of the pre-miliolite deposits are particularly well developed in segments I and II, and the sedimentary characteristics indicate that deposition occurred in phases mainly by debris flows and sediment gravity flows as discussed in the previous section. Available chronological data suggests that the overlying miliolite deposits represent a prolonged period from middle to late Pleistocene (Baskaran et al. 1989) thus bracketing the neotectonic activity represented by the colluvio-fluvial deposits to early to middle Pleistocene.

Broadly, the overlying aeolian and fluvial miliolites are stratigraphically and lithologically comparable with their more extensively developed and studied counterpart in Saurashtra (Baskaran, 1989). The aeolian miliolites were deposited as scattered obstacle dunes within the Northern hill range and also in the KMF zone in front of the north facing scarps. These were fluvially reworked and deposited over the colluvio-fluvial deposits possibly during the early Holocene. Similar valley fill miliolites in the Katrol Hill Fault (KHF) zone in central part of the mainland Kachchh have been related with the humid phase of the early Holocene (Patidar et al. 2007). The nature of neotectonic activity during the deposition of miliolite is not clear as the deposits are scattered and fine grained by virtue of their aeolian origin. Moreover, no fluvial deposits within aeolian

miliolites are observed or reported from elsewhere in Kachchh by previous workers. However, vertically disposed aeolian miliolite near the scarps and tilted gravel layers overlying fluvial miliolites indicate post-miliolite tectonic activity along the KMF.

The interlayered sandy gravel and sand deposits overlying the miliolites are striking finer than the pre-miliolite colluvio-fluvial deposits. The finer nature of the deposits, well exposed in segments III and IV, is evidenced by the increased sand content and pebble sized clasts in the gravel. The sediments were deposited dominantly as sheet floods in shallow braided stream channels. Since the source area for the generation of sediments remained the same, the relatively finer nature of the deposits could be indicative of comparatively less intense neotectonic activity along the KMF in the post-miliolite time. Based on the sedimentary facies and multistoreyed architecture, we infer braided multi-distributary channel systems for the deposition of the post-miliolite Quaternary sediment succession along the KMF zone.

The present day setting of the KMF is in contrast to the one indicated by the exposed Quaternary sediments. Presently, the Quaternary deposits form a narrow 1-3 km wide highly dissected northward sloping surface along the length of the KMF zone. The drainages are deeply entrenched with narrow ephemeral sandy stream channels bound by vertical cliffs exposing the sediments. The depth of incision is maximum near the scarps which rapidly decreases northward as the streams disappear into the Banni plain. This suggests post-depositional tectonic activity along the KMF that resulted in tilting of the Quaternary sediment surface away from the scarps and tectonically controlled fluvial incision and dissection of the sediment sequences.

The variable geomorphic response to neotectonic activity along the KMF is interesting. Many studies exist which describe controls of tectonics and climate on sedimentation and incision but studies that discuss factors that trigger change from deposition to incision under tectonically active conditions are rare. It is difficult to determine the precise causes of change from deposition to incision in the study area even though the KMF continues to be tectonically active as evidenced by the tectonically controlled incision and occurrence of several earthquakes. The role of climate change is ruled out as Kachchh falls in the hyper-arid climatic belt of western India that includes the Thar Desert to the north as well. The scanty rainfall means that the present discharge and stream power alone cannot account for the amount of incision observed. Moreover arid conditions do not favour generation of large amount of sediments in source areas. The sand dominated floor of the present day rivers even within the hill ranges testify to the

low degree of sediment generation, stream power and sediment carrying capacity. We therefore believe that marked reduction in sediment supply could be the reason for transformation of rivers from depositional to erosional under uniformly tectonically active conditions. Modelling of changes in sediment flux and incision in tectonically active conditions show that reduction in supply of sediment leads to river incision and/or diversion (Humphrey and Konrad, 2000). This also shows that in tectonically active environment incision is favoured during phases of enhanced tectonic activity (Chen et al. 2011). It is inferred that, continued neotectonic activity along KMF that continues at the present time is the prime factor responsible for causing incision and dissection of the Quaternary sediments while climate may have played an indirect role in switching off the sediment supply. However, while the role of neotectonic activity is very obvious, the role of climate change needs to be substantiated by further studies.

The inferences of the present study are consistent with previous studies in active fault zones in Kachchh and other parts of the globe which identify variation in rates of tectonic activity as the first order influence on sedimentation and erosion. Tectonically controlled Quaternary deposition reported previously from Kachchh include the vast basin of the Ranns, the coastal plain along the Gulf of Kachchh in the south and the Katrol Hill Fault (KHF) zone in the central part of Mainland Kachchh (Biswas 1974; Thakkar et al. 1999; Maurya et al. 2003b; 2008; Patidar et al. 2007; 2008). These sediments were deposited in structurally controlled sites/basins and have provided vital stratigraphic and geomorphic evidences for reconstructing neotectonic evolution of the respective areas (Merh 2005; Maurya et al. 2008; Patidar et al. 2007; 2008). This indicates the significant role played by neotectonic activity along various active faults including the KMF in controlling the Quaternary sedimentation and geomorphic evolution in the Kachchh basin.

CHAPTER 5

GROUND PENETRATING RADAR (GPR) STUDIES

Ground Penetrating Radar (GPR) is now a widely used geophysical technique to explore shallow subsurface geology. Presently, it is a globally preferred and a very successfully applied geophysical technique to investigate the shallow subsurface structural properties of active faults (Smith and Jol, 1995; Benson, 1995; Meschede et al. 1997; Chow et al. 2001; Gross et al. 2004; Patidar et al. 2006; 2007; McClymont et al. 2008; 2010; Christie et al. 2009). GPR is capable of producing high-resolution images of near surface ranging from a few meters to tens of meters in depth (Davis and Annan, 1989). GPR It is analogous to seismic reflection methods as it gives a vertical subsurface cross-section of reflector geometry and amplitude. GPR is particularly advantageous for high resolution mapping of subsurface structures, and can thus image fault-offset layers or fault planes themselves (Cai et al. 1996). It can therefore be applied to determine the subsurface stratigraphy and tectonic landforms or features produced by coseismic deformation (Cai et al. 1996; Anderson et al. 2003).

IMPORTANCE OF GPR TECHNIQUE IN ACTIVE FAULT STUDIES

To understand the neotectonic behavior of active faults in recent past, accurate mapping of fault plane/zones is of fundamental importance (Green et al. 2003; Salvi et al. 2003). Geomorphic mapping of the fault zones help in delineating the landscape changes due to neotectonic activity along a fault. It is also essential to map the active fault strands accurately and delineate the shallow subsurface nature of the fault plane to fully comprehend the stress regime and neotectonic evolution of the faults. Precise mapping of fault lines have proved vital for future excavation based studies to reconstruct the palaeoseismic history. This is of fundamental importance in geomorphic settings where faults are buried or have been eroded since their last motion or absence of surface rupturing events.

GPR technique has been proved to be a powerful tool in fault studies around the globe. Faulted geological horizons are good radar reflectors. It is conceivable that a high angle fault could generate a diffraction which is more commonly produced by other discontinuities (Beres and Haeni, 1991; Sun and Young, 1995). If the lithologies change across the thrust plane, a change in reflection pattern may occur, this can be mapped as

distinct radar facies (Jol and Smith, 1991). It may also be possible to identify repeating patterns of reflections if thrusting has repeatedly stacked a geological sequence, which produces a number of distinct radar reflections (Busby and Merritt, 1999). The GPR technique can also be used as an important reconnaissance tool to assist selection of sites for geological excavations, and consequently, it may be helpful in accelerating the construction of the paleoseismological chronology. The geological trenching and excavation can only go to a depth of limited distance but the GPR is nondestructive technique that provide accurate image of the subsurface upto tens of meters depth.

GPR STUDIES ALONG KMF

The rugged landscape of Kachchh Mainland Fault (KMF) zone reveals imprints of multicyclic tectonic movements. The active nature of the fault during the pre-Quaternary and Quaternary time shows that KMF is a major seismogenic fault (Biswas and Khattri, 2002; Chowksey et al. 2011a). Delineation and characterization of shallow subsurface nature of associated active faults is essential for appreciating neotectonic activity and the prevailing stress regime in the area. The detailed GPR studies were carried out along KMF, an important intra-basinal fault of the Kachchh basin to understand its nature, potential for stress accumulation and to delineate the pattern of neotectonic activity. In the present study, GPR was used to precisely map the near surface trace of the KMF, image the subsurface geometry of the fault plane along its length and stratigraphic framework. Details of tectonic geomorphology and Quaternary sediments and their neotectonic implications have been described in previous chapters. The geomorphic setting of KMF is characterized by a dynamic range front environment with a complex interplay between deposition, erosion, and tectonic activity during the Quaternary (Chowksey et al. 2011b). Moreover, the neotectonic setting is complex owing to its segmented nature and the presence of thin but near consistent cover of Quaternary sediments. These attributes make the use of GPR technique very pertinent and necessary to map and unravel the near surface structural intricacies. During the present study, a Geophysical survey system Inc. (GSSI), USA manufactured SIR-20 GPR system with antenna frequencies in the range of 40-200 MHz was used. This system has been consistently and successfully used in the last almost one decade in mapping of active faults and Quaternary sediments in Kachchh (Maurya et al. 2005; 2006; 2013; Patidar et al. 2007; 2008; Mulchandani et al. 2007; Chowksey et al. 2011a).

PART-B Kachchh Mainland Fault (KMF)

GPR DATA ACQUISITION AND PROCESSING STRATEGY

The basic fundamentals and principles of the GPR technique and the method of recognizing faults in GPR data are described in Appendix. The profiles from KMF were obtained by shielded 200 MHz, and unshielded Multi-low frequency (MLF) antennas. Data generation by GPR involves moving the antennas or shifting it manually in continuous or point manner over predetermined and measured transects while the profiles are displayed and stored on laptop computer which controls the main GPR unit as well (Jol and Bristow, 2003). At the preliminary stage of surveying, several trial profiles were raised to determine the basic acquisition parameter and a set of most appropriate parameters were applied to obtain final GPR profiles. The time window of 140-150 ns, auto gain function with 5 points and the sampling rate of 512 sample/scan were found adequate for 200 MHz frequency monostatic antenna. The best data sets were subjected to post-survey processing using RADAN software. The file header parameters were edited to correct the horizontal scale and surface positions of the reflectors. The Distance normalization function was applied on all the profiles to establish constant horizontal scale. The power spectrum was calculated to select the filter values and then the vertical and horizontal filters were used to remove interference (noise) produced by extraneous objects. The identification of the unwanted signals and causes of their origin and their removal using appropriate filters is a difficult but important step of GPR data processing and interpretation (Neal, 2004). AGC (automatic gain control) was applied on some profiles to enhance the visibility of low frequency features. Surface normalization was applied to profiles those were obtained over undulating or sloping surfaces. The multiple offset reflection profiles (CMP) were also collected from the study area and the calculated velocity of 0.124m/ns was used for time-depth conversion.

Velocity analysis

To obtain accurate results and right interpretations, velocity analysis was performed at several locations using the bistatic Multiple Low Frequency (MLF) antenna. The calculated velocity values are used to convert two-way travel time into depth. The obtained values are applied on each GPR profiles, to calculate accurate depth of subsurface anomalies. The aim of the velocity estimations is obtain the minimize error in the final interpretations of the GPR profiles. The velocity analysis was carried out using Common mid-point (CMP) method. The velocity profiles were collected from every GPR survey locations using CMP method. Two representative CMP profiles are shown in Fig. 5.1. The profiles were obtained using 80 Mhz bistatic GPR antenna. The initial offset was

fixed on 1.25 m, while the transmitter and receiver were shifted in opposite directions by 25 cm step size up to the maximum distance. The final data was collected with two-way travel time window of 200 ns. The detailed methodology of CMP data acquisition is described in Appendix. The relative dielectric permittivity of 5.7 was found adequate for the sand rich lithologies of the study area.

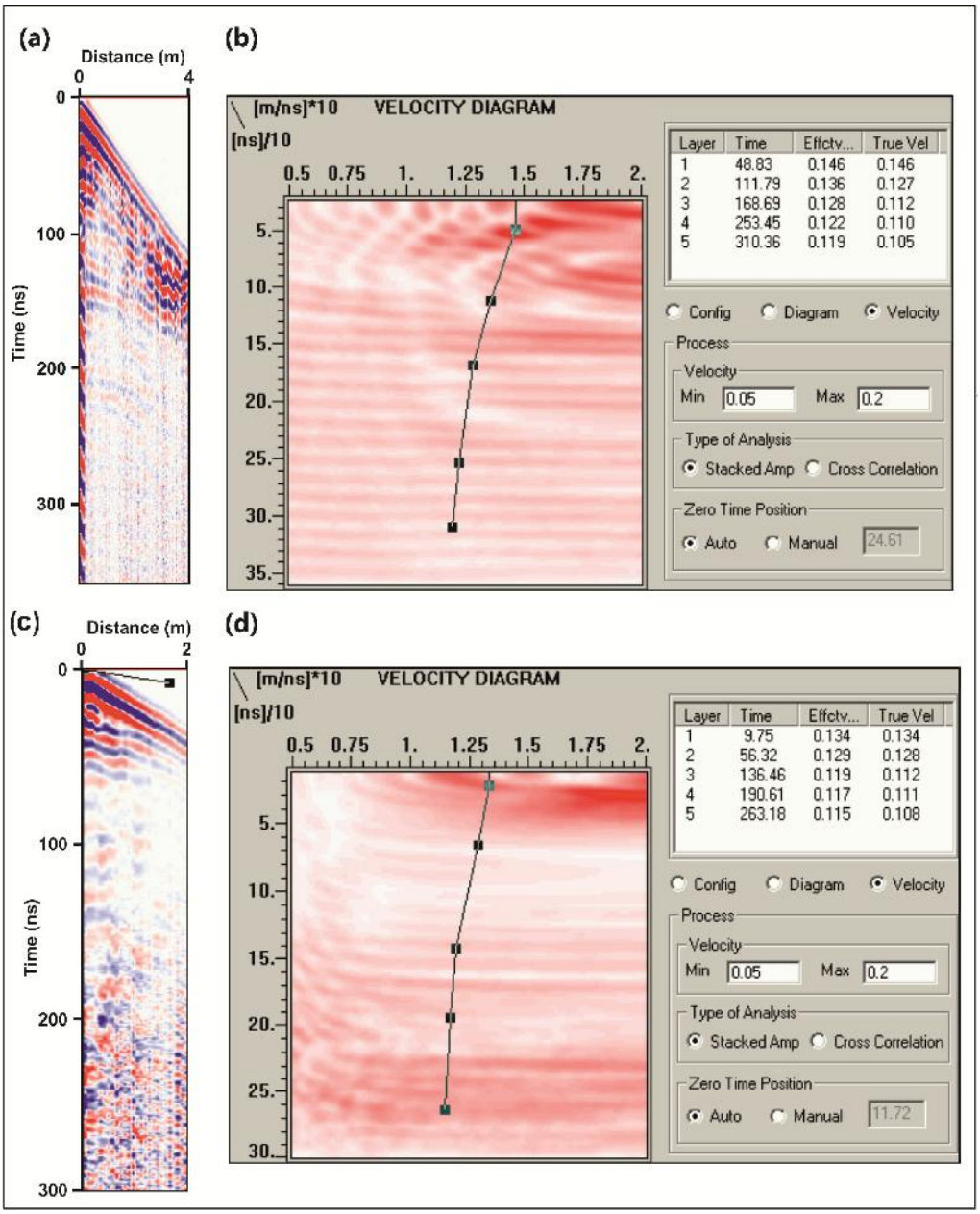

Figue 5.1 **(a)** Processed CMP profile taken over the cliff section of a stream near Dhrang. **(b)** Velocity diagram of the CMP profile shown in (a). **(c)** Processed CMP profile taken over the cliff section of Falay river. **(d)** Velocity diagram of the CMP profile shown in (b).

The velocity analysis was carried out by using GSSI RADAN software which computes the velocity by plotting the multi-offset data on a graph of velocity versus two-way zero-offset travel time. The frequency analysis was also performed in order to obtain

the loss factor and to check the filtering effects of the ground in the radar signals. The average velocity of the medium is calculated from the equation A given in the Appendix. Values obtained by the analysis of the CMP profiles at all locations were found to be similar because of similar lithological characteristics all along the KMF. For confirmation purposes, the CMP data was obtained separately over the Mesozoic and Tertiary rocks at few locations. The obtained true velocity values of Mesozoic and Tertiary rocks are 0.13 m/ns and 0.12 m/ns respectively. However, effective velocity values of Mesozoic and Tertiary rocks are same i.e. 0.13 m/ns (Fig.5.3). In general, when GPR survey is carried out along vertically displaced strata, the average velocity which shows good spatial correlation in the depth correction is used (McClymont et al. 2010; Pauselli et al. 2010; Denith et.al., 2010). Therefore, the average velocity of 0.12 m/ns was used for time/depth conversion.

RADAR CHARACTERISATION OF QUATERNARY SEDIMENTS

Since the KMF is buried under a thin cover of Quaternary sediments, it was found necessary to identify and characterise the radar characteristics of these sediments. In this section, the radar characteristics of the on the colluvio-fluvial deposits from the Kunaria-Lodai segment (Segment-II) which lies to the north of the Habo dome are described (Fig. 5.2a). This segment shows the most complete stratigraphic development and maximum vertical heterogeneity (sand to coarse grained colluvio-fluvial) in terms of the nature of sediments as discussed in the previous chapter. Here, the geophysical signatures of the various sedimentary facies associated with the colluvio-fluvial deposits occurring in the KMF zone are discussed (Fig. 5.2a). The Quaternary deposits have extensively developed along a 2-3 km wide narrow strip to the north of the KMF scarps formed in the northern limb of the Habo dome. The deposits form a distinct geomorphic surface that abuts against the KMF scarps in the south (Fig. 5.2a). Towards north the surface shows a transitional to abrupt contact with the flat surface of the Banni plains. As mentioned earlier, the colluvio-fluvial surface shows a gentle slope towards north. Near the scarps the surface shows an elevation of ~40 m and merges with the Banni plain surface which is about 4-6 m amsl. The colluvio-fluvial surface is dissected by several lower order streams that arise from the KMF scarp line (Fig. 5.2b, c). The streams flow towards north, incising through these deposits, thereby exposing the colluvio-fluvial deposits along the cliff sections (Fig. 5.2c). The depth of incision is found to be maximum (~10 m) near the scarps which rapidly decreases towards north. The decrease in the depth of incision is consistent with the northward gradient of the surface.

PART-B Kachchh Mainland Fault (KMF)

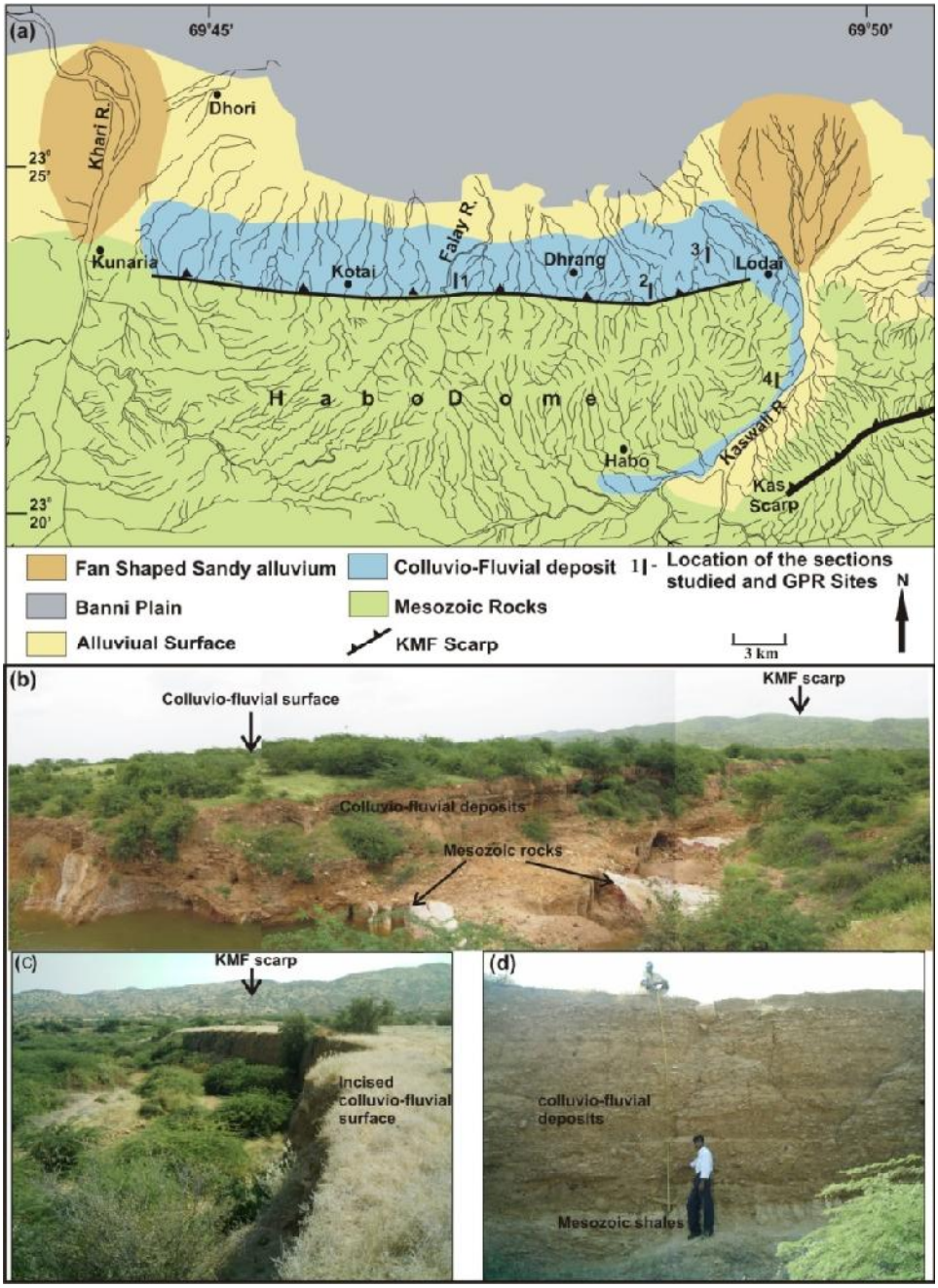

Figure 5.2 **(a)** Geomorphological map of KMF zone to the north of Habo dome. Locations of the sections studied and GPR sites are also shown. **(b)** Panoramic view of the KMF zone showing the field setting of the Quaternary colluvio-fluvial deposits along the Falay River. Note the flat surface in the front of the KMF scarps formed over the colluvio-fluvial deposits exposed along the incised cliffs of the river. Also seen are the vertical to sub vertical highly sheared Mesozoic rocks marking the KMF and the sharp unconformable contact with the overlying stratified colluvio-fluvial deposits. GPR survey (site 1) was carried out at the left hand corner of the photograph. **(c)** View of the incision of colluvio-fluvial surface by a stream to the east of Dhrang. **(d)** View of the exposed section in the incised cliff shown in b. Note the Mesozoic shales at the base and the distinct depositional phases. Height of the person in the picture is 170 cms.

PART-B Kachchh Mainland Fault (KMF)

Closer to the scarps the deposits are found to overlie the steeply dipping and at places sheared Mesozoic rocks (Fig. 5.2b). The eroded surface of the Mesozoic rocks marks a distinct unconformity over which the colluvio-fluvial sediments were deposited. The colluvio-fluvial deposits indicate deposition in well marked phases and are at places well stratified (Fig. 5.2d). Overall, the deposits comprise horizontal to sub-horizontal layers of gravelly to pebbly colluvio-fluvial material with elongated lensoid bodies of sand. The coarser layers mostly matrix supported gravels and pebbles are devoid of internal stratification. In some sections, large clasts comprising subrounded cobbles and boulders form distinct bouldery gravel beds while they may also be randomly distributed within finer gravels. The size of the large clasts may vary from 0.5 m to more than a meter.

The N-S transects were preferred for GPR surveys to allow for correlation with the exposed cliff sections. Several trial profiles were obtained to determine appropriate acquisition parameters to obtain final GPR profiles. Post-survey processing steps applied include simple trace editing, band pass filtering, static correction, stacking and amplification of weak signals using gain function. All profiles were time-zero corrected and finalised in wiggle trace format. The GPR data generated were interpreted in conjunction with the exposed sediment in cliff sections. Four sites are discussed here.

Site 1 is located north of the scarps along the Falay River that arises from the central part of the Habo dome and flows northward incising through Quaternary colluvio-fluvial deposits (Fig. 5.2a). At this site, the deposits unconformably overlie the highly sheared Mesozoic rocks (Fig. 5.2b). The exposed section shows ~4.5 m of crudely stratified colluvio-fluvial deposits with the basal part of the section consisting of sheared Mesozoic rocks (Fig. 5.3, litholog 1) The GPR survey was carried out on top of the cliff section using 200 MHz antenna along the N-S transect. The processed profile is shown in (Fig. 5.4a). The profile depicts three major radar facies- the upper part comprising discontinuous inclined reflectors, followed by continuous and parallel high amplitude reflectors, and low amplitude parallel discontinuous reflector. The lower part showed high attenuation of radar energy due to the fine grained and sheared lithologies of the Mesozoic rocks. The inclined reflectors observed in the upper part are usually produced by cross-bedded strata (Kostic and Aigner, 2007; Overmeeren, 1998). However, here it is on account of coarse pebbly-cobbly deposits that were laid down on a scoured erosional palaeo-surface. The colluvio-fluvial layers in the deposits attained low dips in conformity with the unevenness of the available surface. The underlying parallel continuous

reflectors were produced by the crude horizontal stratification of the colluvio-fluvial deposits (Kostic and Aigner, 2007). The reflectors appear to have been formed due to the clast rich layers alternating with relatively clast poor layers. The low amplitude parallel discontinuous reflections are attributed to the presence of sand with finer gravels (Kostic and Aigner, 2007).

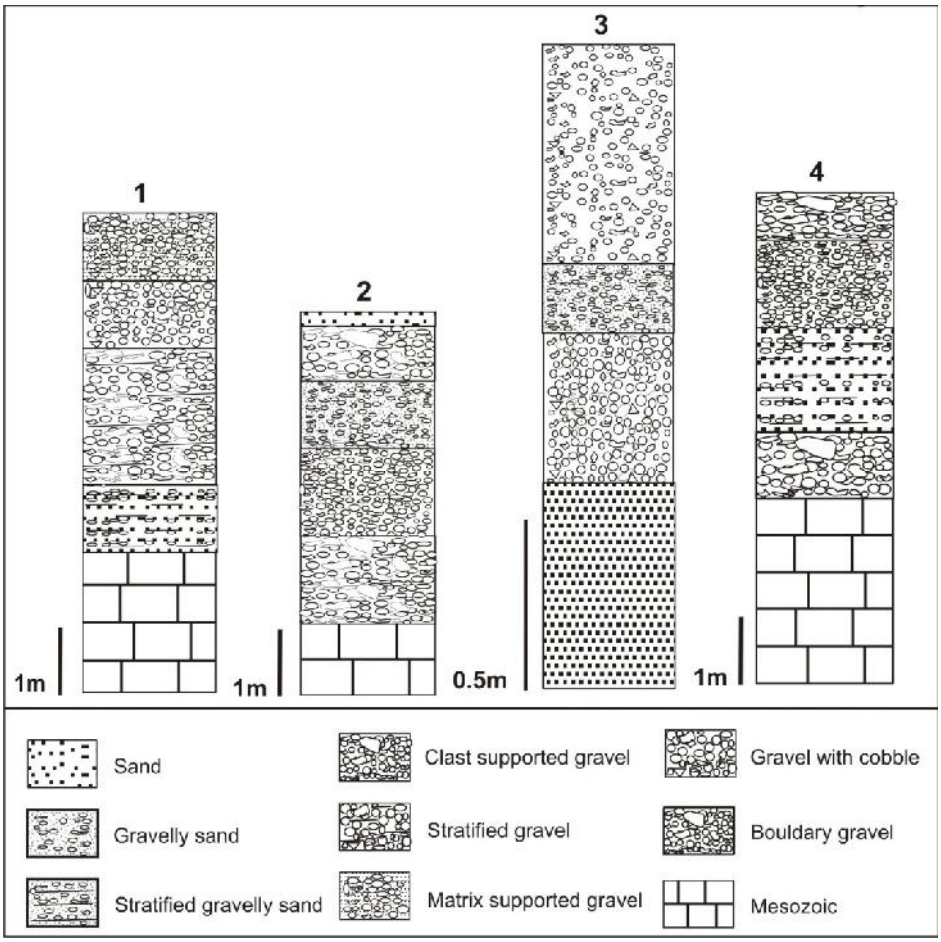

Figure 5.3 Lithologs of exposed sections of Quaternary colluvio-fluvial deposits at sites 1 to 4. Site 1, 2 and 4 are of river cliff sections while 3 is from a pit section. Location of lithologs is shown in Fig. 5.2a.

Site 2 is located between the scarp line and the KMF zone that lies further north (Fig. 5.2a). The incised cliff section here is about 6 m high that exposes 4 m of Quaternary colluvio-fluvial deposits unconformably overlying the Mesozoic shales. The colluvio-fluvial deposits consist of well stratified gravels and sandy gravel layers. The gravels are mostly of pebble size, however, some of the layers contain isolated boulder size clasts of Mesozoic sandstones (Fig. 5.3, litholog 2). The GPR data was obtained by moving the 200 MHz antenna along N-S transects on top of the cliff section. The GPR profile (Fig. 5.4b) shows data up to the depth of 7 m. The GPR profile is divisible in two distinct parts. In the lower part of the profile up to 4.5 m depth, low amplitude signals

with reflections not showing any particular pattern are observed. The attenuation of the radar signal is generally observed in the clay rich sediments (Overmeeren, 1998). Here it is on account of the northward dipping Mesozoic shale. The upper part of profile corresponding to the colluvio-fluvial deposits shows three major radar facies. The upper part of the profile up to 1.5 m shows subparallel to wavy reflections with distinct hyperbolas. The reflections correspond to the matrix poor pebbly gravels with an erosional base (Fiore et al. 2002; Kostic and Aigner, 2007). The hyperbolas are on account of isolated subrounded to angular boulders of Mesozoic sandstones. Below this, a zone of (1.5-3.5 m depth) high amplitude parallel reflectors is observed. These correlate with the alternate layers of horizontally stratified gravel and sandy gravel (Beres et al. 1999). The contacts of these layers are sharp resulting in distinct parallel reflections. Small hyperbolas within this zone are attributed to the floating boulder size clasts in the gravel layers.

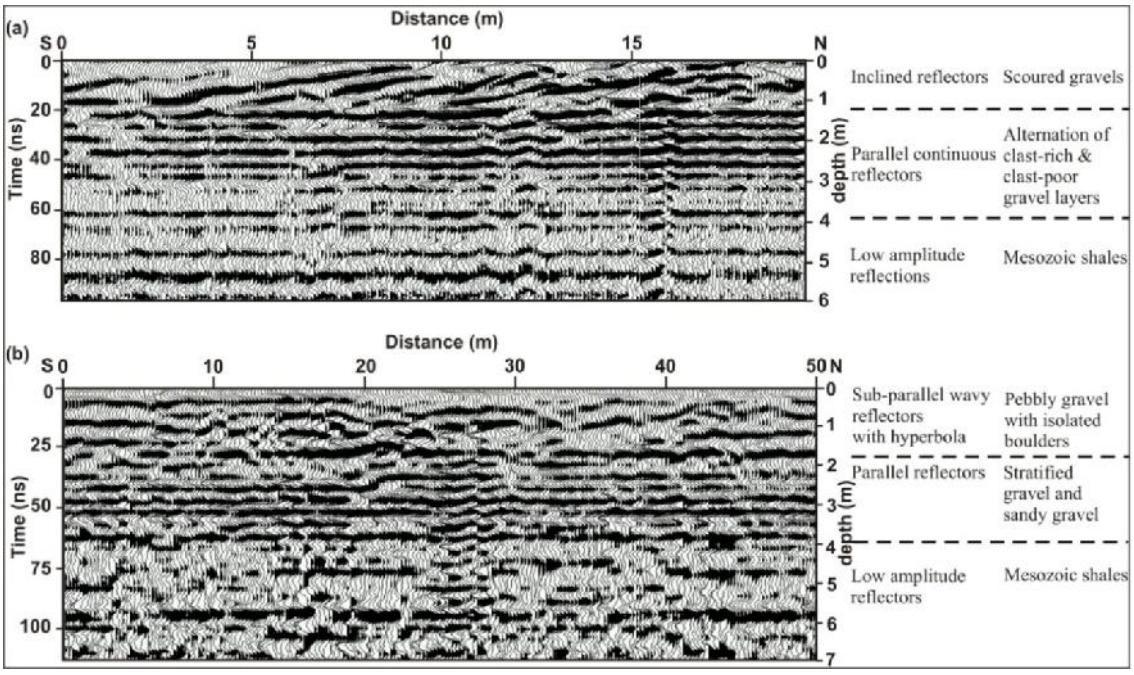

Figure 5.4 200 MHz monostatic antenna GPR profiles in wiggle mode. Various radar facies and corresponding lithologies are indicated against each profile. Location of sites is shown in Fig. 5.1a. **(a)** S-N profile from site 1 near the Falay River showing three distinct radar facies. **(b)** S-N profile from site 2 showing three distinct radar facies.

Site 3 is located to the west of Lodai (Fig. 5.2a). The GPR survey was carried out above a pit section dug by local people. The pit was 2 m deep and the section exposed in pit wall was 14 m long. Since the site is the farthest from the scarp line as compared to other sites, the colluvio-fluvial deposits here were found to be of finer gravels (Fig. 5.3, litholog 3). The 200 MHz antenna was dragged over the pit wall and the data obtained

were compared with the exposed section. The GPR radar profile (Fig. 5.5a) shows good correlation with the exposed pit section. The entire profile shows two distinct types of reflections. The upper part up to 3.5 m depth exhibits high amplitude returns interpreted as the total thickness of colluvio-fluvial deposits at the site. In this part, three major radar facies are identified which comprise high amplitude discontinuous parallel reflectors, relatively low amplitude discontinuous parallel reflectors and high amplitude continuous parallel reflectors. The parallel discontinuous high amplitude reflections correspond to the matrix supported stratified gravels that form the top part of the exposed pit section. The high amplitude parallel continuous radar facies is found to grade laterally into discontinuous parallel reflections of low amplitude. Comparison of GPR data with the exposed section in the pit indicates the grading of the radar facies closely relates with the lateral variation of the clast rich gravels into matrix rich gravel. Thickening and thinning of the individual strata are also observed in the exposed section. In general, high amplitude parallel continuous radar facies is found to have been produced by the clast rich gravels (less matrix) while the discontinuous parallel reflections of low amplitude are attributable to gravels with more amount of matrix (Kostic and Aigner, 2007). Collectively, the three radar facies suggests that the thickness of colluvio-fluvial deposits at the site is about 3.5 m of which, the upper 2 m are exposed in the pit section. Reflections below 3.5 m depth are found to be of low amplitude and highly attenuated which is interpreted as the fine grained lithology, possibly shales forming the basement of the colluvio-fluvial deposits. This is further supported by the fact that the Mesozoic rocks are exposed on the surface very close to the south and east of the site.

Site 4 is located behind (south) the scarp line along the left bank of the Kaswali River at the eastern fringe of the Habo dome (Fig. 5.2a). The studied section is located along the incised cliff section of the Kaswali River (Fig. 5.3, litholog 4). Here, the 6.5 m section exhibits colluvio-fluvial deposits underlain by Mesozoic rocks (Fig. 5.5b). The GPR data were obtained by dragging the 200 MHz antenna on top of the cliff section. As seen at other sites, the GPR data (Fig. 5.5b) of this site is also characterized by attenuation of radar waves below 4.5 m which is attributable to the Mesozoic rocks forming the base of the exposed section. However, attenuation is of less magnitude as compared to other sites mainly because the Mesozoic rocks here consist of alternations of thinly bedded sandstones and shales. The overlying group of reflectors (1.5-4.5 m) comprises parallel and consistent reflections. In the exposed section, the corresponding lithology consists of the basal bouldery gravel (1 m thick), followed by unconsolidated matrix rich gravel (1.5

m thick) and indurated matrix rich gravel (1.5 m thick). The lithology of the later two horizons is similar, though; both are readily distinguished in the section owing to the variation in the degree of induration. However, both are represented by the same radar facies because of the similarity in gross lithology. The basal bouldery horizon is also not clearly picked in the profile which could be due to the laterally discontinuous and dispersed nature of the boulders. Also, we cannot rule out the possibility of the absence of boulders at this depth along the profile line which was about 1.5 m away from the vertical cliff face. The uppermost part of the profile shows reflections marked by several partial and incomplete formation of hyperbolas and few inclined reflectors as well. These correlate with the uppermost horizon consisting of clast supported gravel with randomly distributed cobbles, possibly, responsible for the indistinct hyperbolas (Sass and Krautblatter, 2007).

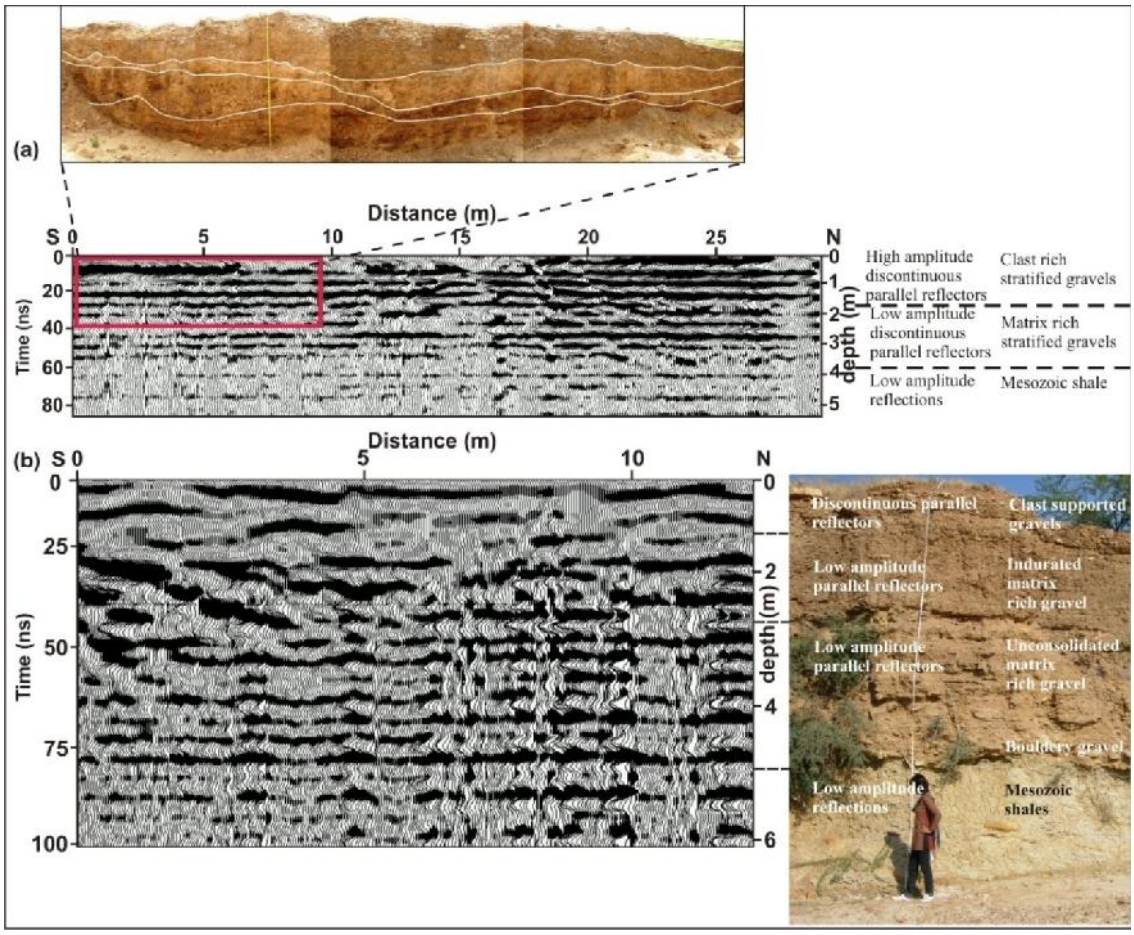

Figure 5.5 200 MHz monostatic antenna GPR profiles in wiggle mode. Various radar facies and corresponding lithologies are indicated against each profile. Location of sites is shown in Fig. 5.1a. **(a)** S-N profile from site 3. Photograph shows the exposed pit section. The rectangular box in the profile corresponds to the exposed pit section. **(b)** S-N profile from site 4 with photograph of the river section. Height of the person in the picture is 1.58 m.

PART-B Kachchh Mainland Fault (KMF)

The radar characteristics of the Quaternary sediments delineated proved useful for interpreting the GPR data on the KMF described later. The sedimentary facies observed comprise, bouldery layers, semi-compacted to compacted clast-rich to matrix-rich gravels and sandy gravels. In general, it was found that the radar facies correlated well with the sedimentary facies seen in exposed sections. Three major radar facies have been identified which are easily distinguished from the adjacent radar reflections. The discontinuous inclined to wavy reflections with indistinct hyperbolas relate to coarse gravel deposits with floating boulders. The discontinuous wavy reflections are produced by the interfaces between the cross-bedded fine sandy layers and gravel layers (Kostic et al. 2005). Formation of hyperbolas is attributed due to scattering radar waves from large clasts (>30 cms) (Sass and Krautblatter, 2007). The second radar facies comprising parallel discontinuous reflections are found to be produced by sandy gravels or matrix rich gravels (Kostic and Aigner, 2007). Well stratified gravel was found responsible for the third radar facies consisting of parallel and continuous radar reflections. The basement rocks comprising Mesozoic shales were clearly visible in the GPR data as a zone of attenuation of radar waves below the high amplitude reflections representing the colluvio-fluvial deposits. In such cases, the bedrock interface may not necessarily produce a strong reflector, instead fading of radar signals can be observed corresponding to basement rocks consisting of fine grained and sheared lithologies (Sass and Krautblatter, 2007).

MAPPING THE KMF USING GPR

GPR data were collected using a PC-based digital pulse SIR-20 system manufactured by GSSI Inc., USA. Fig. 5.6 shows the locations and directions of the acquired GPR profile. GPR data was collected by using both monostatic as well as bistatic antennas depending upon the requirement. The GPR surveys using a 200 MHz antenna were carried out in continuous mode. While GPR surveys using bistatic antenna (80 MHz & 40 MHz) were carried out by the common offset (CO) method in point mode. After setting the desired parameters during the acquisition, data were collected in the N–S direction, i.e. across the fault (Fig. 5.6). Precautions were taken during the acquisition to minimize the reflections from above-ground objects which can mask subsurface targets (Sun and Young, 1995).

Data processing was done using GSSI RADAN processing software (RADAN for Windows 2000). The basic processing was kept simple in order to avoid introducing any artefacts into the data. The processing steps involved file header editing, followed by horizontal scale normalization to correct for differences in the movement speed of the

antennas during data collection (monostatic antenna). The data were then band pass filtered to cut out very high and very low frequencies. Lastly, an automatic gain control function was applied to compensate for the loss in amplitude at depth due to spherical convergence, scattering and dielectric loss, as well as amplitude loss occurring during some data processing steps. Before the final layout, required static correction was incorporated into the processed profiles.

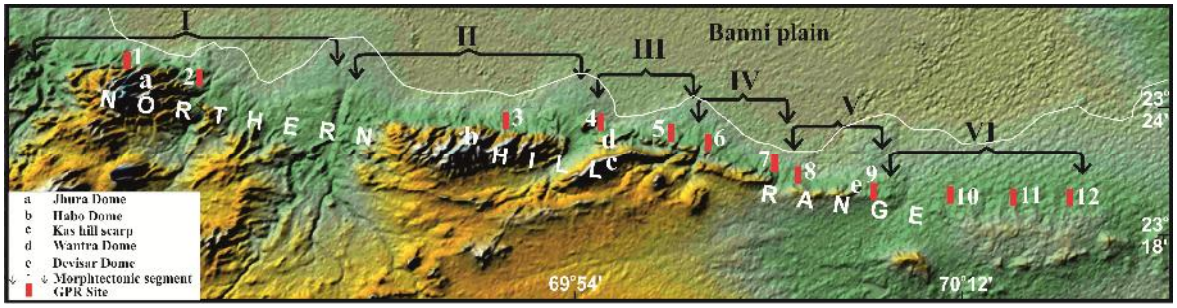

Figure 5.6 Digital Elevation Model (DEM) of the study area prepared from Aster data highlighting the geomorphic set up of the KMF zone along with various morphotectonic segments of Kachchh Mainland Fault (KMF). 1-12 are the locations of the GPR survey transects.

RECOGNITION OF KMF IN GPR DATA

In the present study, the GPR survey was carried out at selected sites along the KMF zone to characterize the shallow subsurface nature of the fault to provide evidence for the type of stress conditions responsible for differential uplift and ongoing seismic activities. The present study has been able to precisely map the near surface location of the fault plane and its nature in the shallow subsurface. The process of selection of sites for GPR surveys included DEM modelling and detailed geomorphic studies. Each of the sites was narrowed down after attempting several unsuccessful surveys starting from the base of the scarp, gradually moving away towards north until the fault was picked up in the profile. In the initial phase of the GPR studies, several long transects were taken up by GPR at these sites with a view to precisely locate the fault plane/zone. As it is the usual practice and requirement of the GPR data acquisition, the process was repeated several times until good quality data were obtained. The GPR profiles were obtained by manually towing the antenna along measured survey lines across the fault trace inferred from geomorphic mapping. A critical field input for narrowing down the fault zones was obtained by undertaking traverses along several north flowing streams for observing the sporadic rocky outcrops in the river bed.

Since the general trend of the KMF is E-W, all the GPR surveys were carried out along the N-S oriented transects located at the different segments of the KMF with a view

to precisely locate the fault plane/zone and to determine the near surface characteristics of the fault. GPR data from a total of nine sites covering the five segments of KMF zone from Nirona to Amrapar in the east are presented in this chapter. Using the present GPR and field studies, the KMF has been mapped further eastward up to Sikra village which is recognized as sixth segment (Amrapar-Sikra segment). This is a significant outcome of the study which has resulted in the providing critical evidence for eastward extension and propagation of the KMF at least upto the epicentral area of the 2001 Bhuj earthquake. The GPR profiles and field data of the newly identified segment of the KMF are included in the next chapter.

A usual way of interpreting GPR data is by correlating the characteristics of reflections with subsurface lithology as shown in the previous section of this chapter. The most common way of interpreting GPR data is through identification of radar facies. A radar facies is defined as a group of reflections or reflectors whose parameters differ from adjacent units and usually define lithological units, sediment packages or mappable three-dimensional sedimentary units (Bristow, 1995; Jol and Bristow, 2003; Maurya et al. 2006). However, recognition and interpretation of faults in GPR data is more complex than simple lithological interpretation (Meschede et al. 2007). The interpretation of faults in seismic profiles is based on apparent offsetting of stratigraphic reflections rather than direct reflections from fault whereas in GPR profiles the direct reflections from fault plane are also observed (Cai et al. 1996; Slater and Niemi, 2003). Faults are identified in GPR profiles on the basis of the termination of laterally continuous reflections along a plane, presence of diffraction hyperbolas around the fault plane, drastic decrease of amplitude along the fault plane and the offsetting of reflections from either side of the fault strand with varying intensities and the changes in dip angle and the thickness of reflected signals across the fault plane.

Reflection terminations and offsetting in GPR data are direct indicators of faulting. However, faults demarcating contrasting lithologies like the KMF are easier to interpret as they show distinct radar facies owing to strong dielectric contrasts. In the present study, this criteria is found to be the most suitable for interpreting the fault trace in the GPR data. This is due to the fact that the near surface trace of the KMF is marked by the lithotectonic contact between the compact sandstone rich lithologies of Mesozoic formations and the fine grained shale rich lithology of the Neogene sediments as discussed above. This lithological distinction, marking the KMF is clearly observed as a sharp amplitude contrast in all the GPR profiles presented. In general, the Mesozoic rocks

are characterized by consistent reflections of high amplitude while the Neogene sediments are characterized by inconsistent low amplitude reflections. The amplitude contrast mainly account of the attenuation of radar waves attributed to the shale rich finer grained lithology of the Neogene rocks. The GPR data obtained along the KMF in various morphotectonic segments is described in the following paragraphs.

NIRONA-JHURA SEGMENT (SEGMENT-I)

Site-I

In the Nirona-Jhura segment, the KMF zone to the north of the range front scarps comprises a north sloping Quaternary surface which has effectively buried the near surface trace of the fault. The site 1 is located in the central part of the segment close to a northward flowing stream to the east of Palanpur village (Fig. 5.6). The incised stream section exposes Quaternary sediments overlying Mesozoic rocks steeply dipping towards north which formed the main criteria for selecting this site for GPR survey. The Mesozoic rocks strike N105^0 with a dip of 61^0 due north. The exposed Quaternary sediments include the aeolian miliolite, valley fill miliolite, gravel-pebble. The sediments show a strong tilting towards the north consistent with the slope of the surface. The processed GPR is shown is shown in Fig. 5.7a.

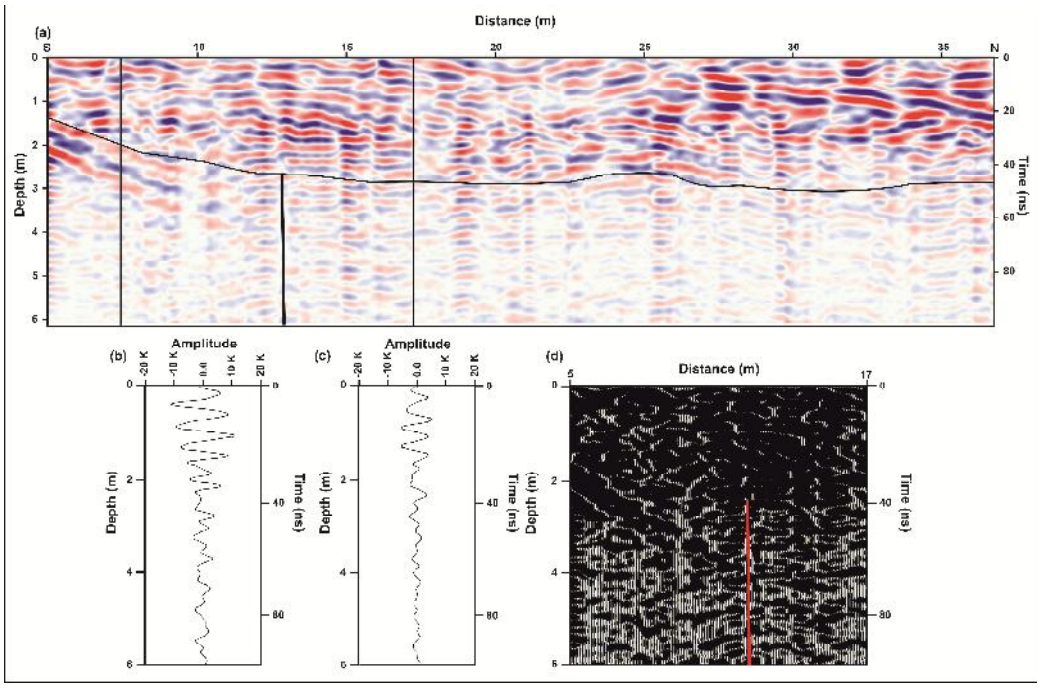

Figure 5.7 (a) GPR profile taken from the northward flowing stream to the east of Palanpur village with 200 MHz antenna, location of site is shown in Fig. 5.5. Note the strong reflections emanating from the fault plane. **(b)** Oscilloscope of a single scan emanating from of the Mesozoic rocks **(c)** Oscilloscope of a single scan emanating from of the Tertiary rocks. **(d)** The boxed portion of (a) is shown in a Wiggle mode.

PART-B Kachchh Mainland Fault (KMF)

The 48m long S-N GPR profile was obtained using a 200 MHz monostatic antenna in continuous mode over a relatively smooth but northward sloping surface. The profile depicts strong high amplitude reflections in the upper 2-3 m part of the profile. As per the field setting the high amplitude reflections in the upper part is on account of radar reflection of lithologically variable Quaternary sediments. A sharp discontinuity in the reflection pattern can be seen below the Quaternary sediments which reflect the unconformable contact of Quaternary sediments with the basement rocks. The basement in the profile shows two distinctly different reflection patterns of high amplitude and low amplitude. The high amplitude reflections are seen in the southern side of the profile while low amplitude reflections are seen in the northern margin of the profile. The high amplitude reflections in the northern part of the profile are on account of the compact Mesozoic sandstones while the low amplitude reflection in the northern part of the profile indicates the relatively softer and finer grained Tertiary rocks, which is dominantly clayey in nature (Fig. 5.7b, c). Sharp contact between the high amplitude and low amplitude signals which is interpreted as the fault plane is seen around ~13 m which is steeply inclined towards north (Fig. 5.7a, d). It is therefore interpreted that the KMF is expressed as a steep northward dipping fault in this segment.

Site-II

This site is located to the SW of Jhura village. The site is located on flat gently sloping ground. Sheared steeply dipping Mesozoic rocks striking $N130^0$ are exposed in a small mound further west of the transect. The GPR survey was carried out over a gently northward sloping surface in order to delineate the sub surface behaviour of the KMF. The ~40 m long S-N profile was taken with the help of 200 MHz monostatic antenna. The data was acquired in the continuous mode. The best profiles were later processed and required surface correction was applied. A 10 m part of the acquired profile is shown in Fig. 5.8a. The top 2-3 m portion in the profile shows horizontal reflections which accounts for the scree material overlying the basement rock. The basement reflection is characterized by both high and low amplitude radar reflections. The southern portion in the profile has high amplitude reflection while the northern portion is characterized by low amplitude reflection. This reflection pattern is on account of variation in lithology viz. high amplitude reflection represents relatively good propagation of wave in a non-conducting media in which the much of radar energy during transmission is not lost while low amplitude is on account highly conductive lithology (media) where energy is lost as it is transmitted downward. Comparison of the GPR data with the field setting it can be said

that the Mesozoic sandstones are represented by the high amplitude reflections while the Tertiary rocks which are clayey in nature are represented by low amplitude reflections (Fig. 5.8b, c) A sharp almost vertical truncation of radar reflection is noticed around ~7 m in the GPR profile (Fig. 5.8a, d). This truncation represents the faulted litho-tectonic contact between the Mesozoic and Tertiary rocks representing the KMF. Thus, KMF in this segment is represented by steep southward dipping fault plane. This indicates reverse nature of the KMF in this segment. This contrasts with the GPR data at site 1 in the same segment which KMF as a steep northward dipping fault plane. The reverse nature of the KMF can be attributed to change in the strike of the KMF as it swerves southwards due to the effect of strike slip movement along transverse faults further east. Presence of transverse faults in close vicinity caused increased level of compressive stresses leading to the reverse nature of the KMF.

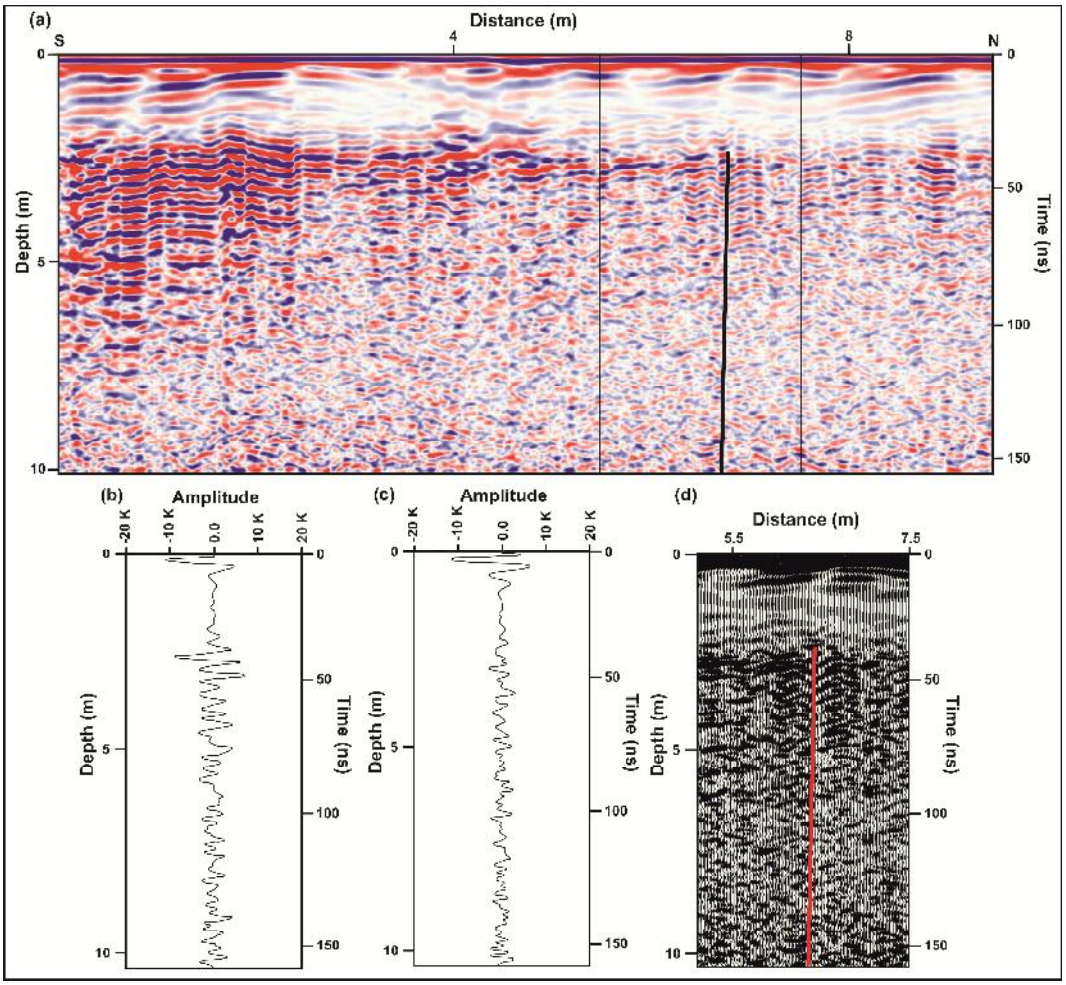

Figure 5.8 (a) GPR profile taken from South of Jhura village with 200 MHz antenna, location of site is shown in Fig. 5.5. Note the strong reflections emanating from the fault plane. **(b)** Oscilloscope of a single scan emanating from of the Mesozoic rocks **(c)** Oscilloscope of a single scan emanating from of the Tertiary rocks. **(d)** The boxed portion of (a) is shown in a Wiggle mode.

PART-B Kachchh Mainland Fault (KMF)

KUNARIA-LODAI SEGMENT (SEGMENT-II)

Site-III

The KMF zone in this segment lies north of the Habo dome and is characterised by an extensively dissected and northward sloping surface developed over the Quaternary sediments. The Quaternary sediment succession exposed along the vertical incised cliff section of the Falay river near Falay village can be considered as the best section along the entire KMF zone. The site typifies the neotectonic setting of the KMF in contemporary stress regime. The present GPR profile shown in the Fig. 5.9a is acquired over the Falay river cliff section. The fault is buried under a thick sedimentary succession of Quaternary sediments as revealed by the vertically dipping sheared Mesozoic rocks in the river bed. Around ~36 m long processed GPR profile acquired by a 200 MHz monostatic antenna in continuous mode over a relatively flat surface is shown in Fig. 5.9a. The profile shows strong high amplitude radar reflections in the upper 2-3 m portion of the profile. The radar reflection pattern varies from high amplitude continuous reflection, wavy reflection to inclined reflections pattern. This type of reflection pattern is attributed to the dominantly clast rich colluvio-fluvial sediments (Chowksey et al. 2011a). A distinct change can be seen at the contact of Quaternary sediments and the basement rocks. The radar reflection in the basal part of the profile clearly shows high amplitude reflection and low amplitude reflection. The northern side of the profile is characterised by low amplitude reflections while the southern side is characterised by the high amplitude reflections. This variation accounts for lithological variation within the basement (Fig. 5.9b, c). This abrupt variation in the radar reflection from high to low amplitude is on account of fault plane of the KMF marked by the tectonic contact between compacted Mesozoic sandstone and clayey Tertiary sediments respectively. The sharp contact is seen near ~5 m distance (Fig. 5.9a, d). This sharp vertical contact is inferred as KMF. Thus KMF in this segment is inferred as a vertical fault.

LODAI-JAWAHARNAGAR SEGMENT (SEGMENT-III)

Site-IV

The segment III is characterised by the small domes lying between the KMF scarp north of the Kas hill scarp in the south. These small domes in the north are bounded by the KMF. The selective GPR profile is described in this text. A GPR profiles were acquired in a S-N transect behind the Khengarpar village. The profile was acquired across the strike of the near vertically dipping Mesozoic rock.

PART-B Kachchh Mainland Fault (KMF)

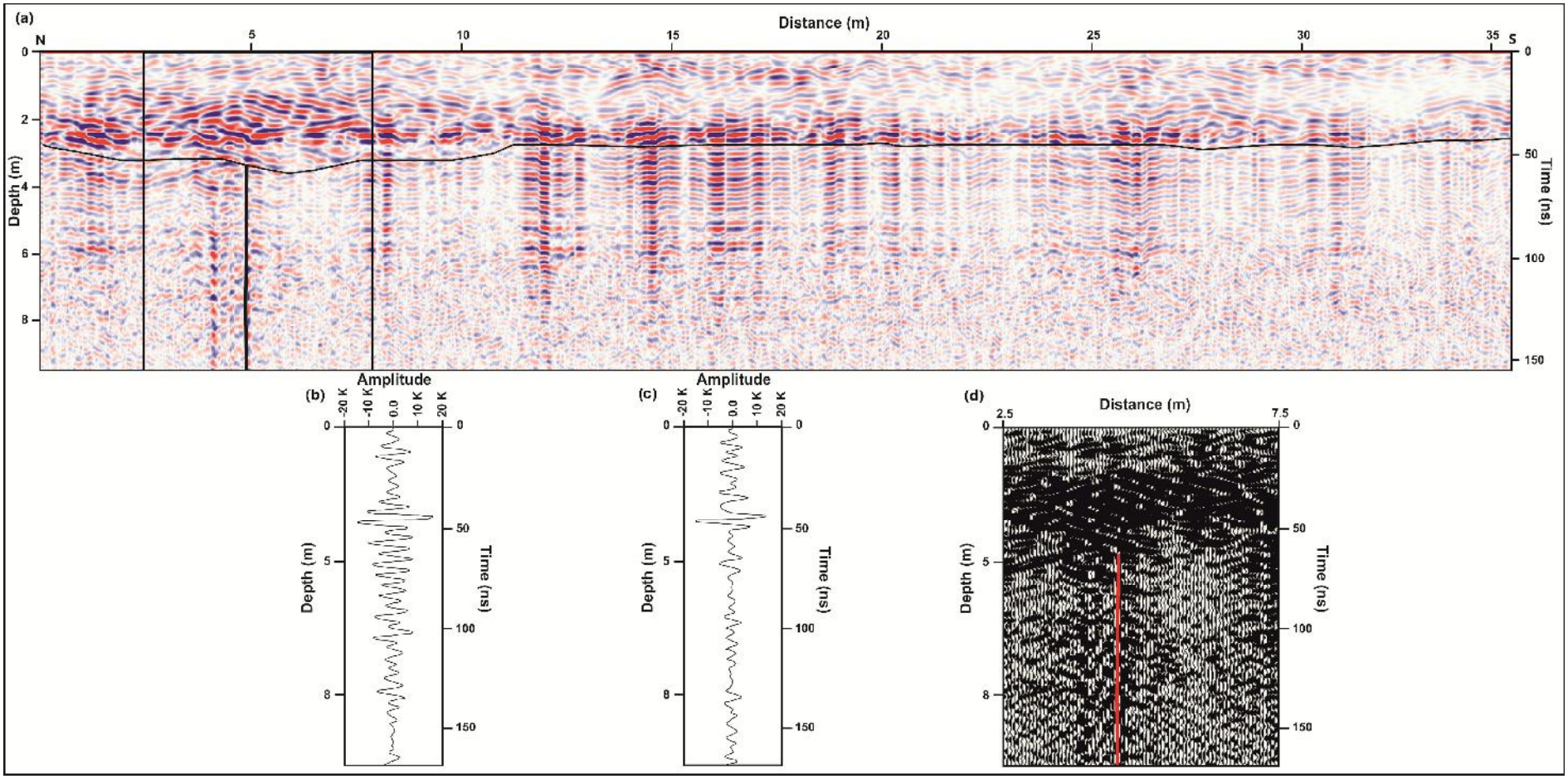

Figure 5.9 (a) GPR profile taken from cliff section of the Falay river with 200 MHz antenna, location of site is shown in Fig. 5.5. Note the strong reflections emanating from the fault plane. **(b)** Oscilloscope of a single scan emanating from of the Mesozoic rocks **(c)** Oscilloscope of a single scan emanating from of the Tertiary rocks. **(d)** The boxed portion of (a) is shown in a Wiggle mode.

PART-B Kachchh Mainland Fault (KMF)

A 50 m long S-N profile was acquired by a 200 MHz monostatic antenna in a continuous mode over an undulating surface formed over the vertically dipping Mesozoic rock north of the scarp. Only 18m part of the acquired profile is shown after the final processing (Fig. 5.10a). The top ~1m part in the profile represents the scree material developed over the basement rocks. The profile is characterized by the high amplitude reflections at the southern side of the profile while the northern side is characterised by the low amplitude reflections. This variation is on account of variable lithology of the basement rocks. The high amplitude reflection pattern is on account of less conductive medium which according to our field setting represents the compacted Mesozoic sandstone (Fig. 5.10b). While the low amplitude radar reflection is because of conductive medium this is in conformity with the clayey nature of Tertiary rock (Fig. 5.10c). A sharp truncation of the radar reflection can be seen at a distance of ~14 m in the profile which marks the faulted contact of the Mesozoic and Tertiary rocks (Fig. 5.10a, d). The KMF in this segment is represented by a near vertical plane with a steep northward dip.

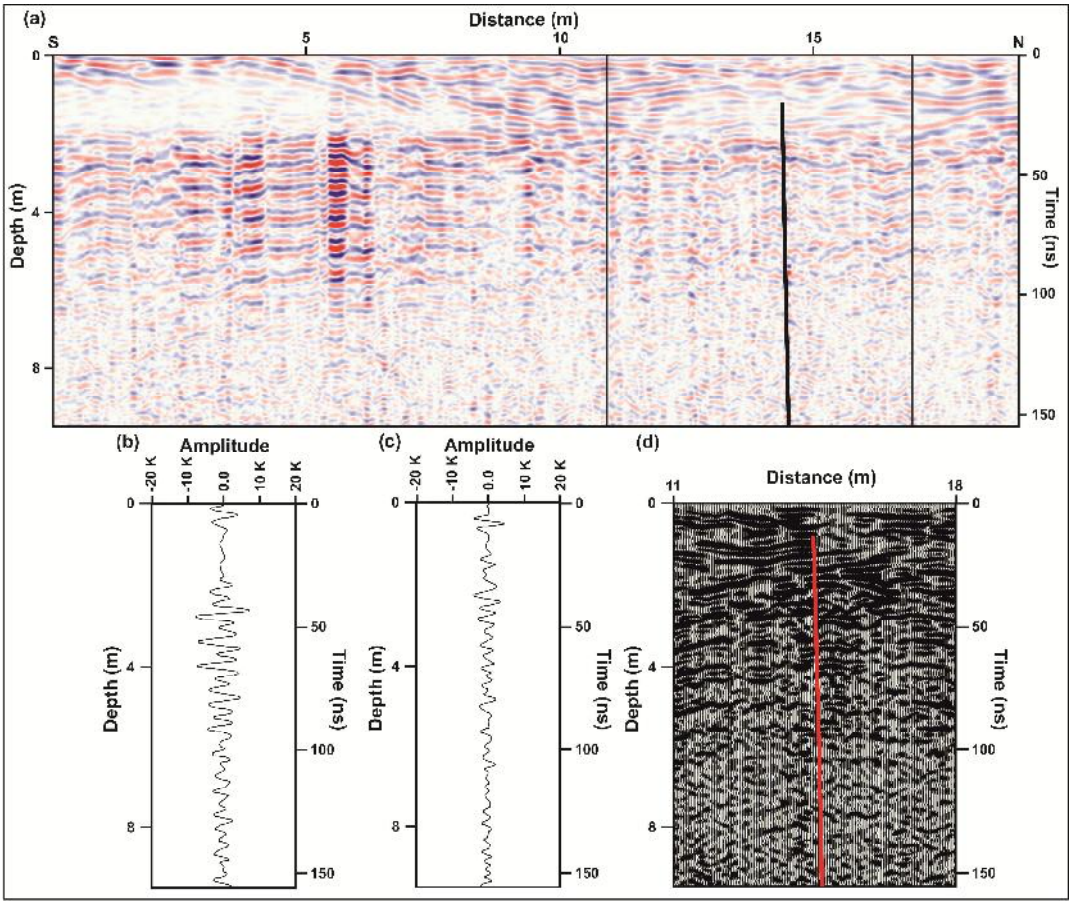

Figure 5.10 **(a)** GPR profile taken from south of Khengarpar with 200 MHz antenna, location of site is shown in Fig. 5.5. Note the strong reflections emanating from the fault plane. **(b)** Oscilloscope of a single scan emanating from of the Mesozoic rocks **(c)** Oscilloscope of a single scan emanating from of the Tertiary rocks. **(d)** The boxed portion of (a) is shown in a Wiggle mode.

PART-B Kachchh Mainland Fault (KMF)

Site-V

A S-N profile is collected from a cliff section of a distributary of the Dharampur stream near the Lotia dam. A ~20 m long S-N profile was collected by a 35 MHz bistatic antenna in a point mode across the sheared E-W striking Mesozoic rock over the right bank cliff section of the stream.

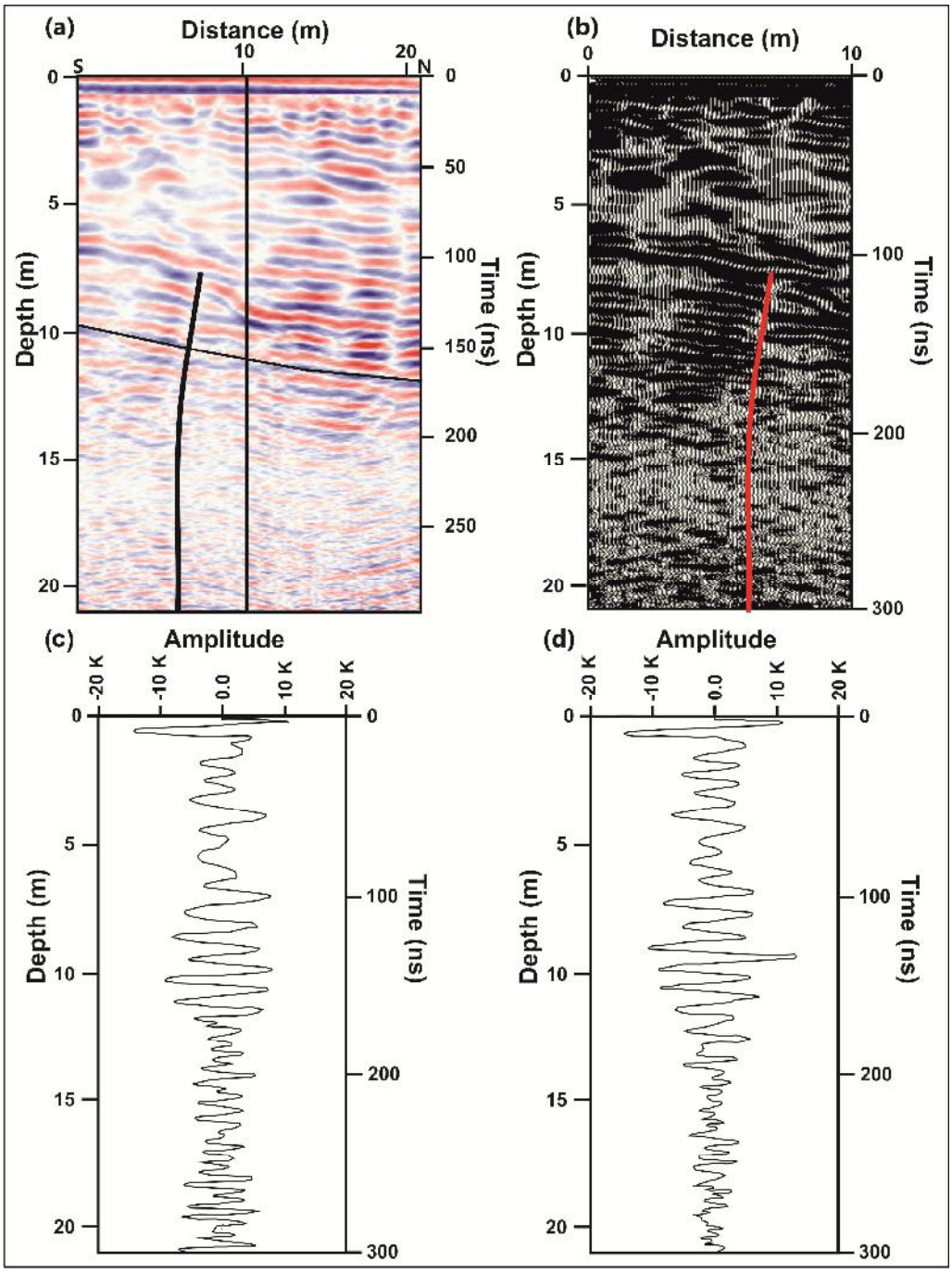

Figure 5.11 **(a)** GPR profile taken from a cliff section of a distributary of the Dharampur stream near the Lotia dam with 35 MHz bistatic antenna in a point mode, location of site is shown in Fig. 5.5. Note the strong reflections emanating from the fault plane. **(b)** The boxed portion of (a) is shown in a Wiggle mode. **(c)** Oscilloscope of a single scan emanating from of the Mesozoic rocks **(d)** Oscilloscope of a single scan emanating from of the Tertiary rocks.

PART-B Kachchh Mainland Fault (KMF)

The profile is characterised by high amplitude reflections which varies from horizontal continuous to wavy reflection pattern (Fig. 5.11a). These reflections correlate with the exposed Quaternary sediments in the cliff section. The basement rocks are characterised by low and high amplitude reflections. The low amplitude radar reflections are seen on the southern side of the profile while the northern side is represented by high amplitude reflections. The field setting suggests that the high amplitude reflections are on account of the well compacted Mesozoic sandstones while the low amplitude reflections are on account of clayey rich Tertiary rocks (Fig. 5.11c, d). The reflections of the basement attenuate with depth due to weakening of the radar energy. A sharp truncation of the radar reflections in seen at a distance of ~7 m (Fig. 5.11a, b). This truncation is seen to extend upward in the lower most Quaternary sediment unit. This line of truncation marked in the profile represents the KMF fault plane that has offset the Quaternary sediments as well. The KMF appears as a steep southward dipping fault which becomes vertical at depth. This change in the fault behaviour is attributed to the accumulation of compressive stresses along the KMF during the Quaternary.

JAWAHARNAGAR-KHIRSARA SEGMENT (SEGMENT IV)

Site VI

This site is located in the central part of the Jawaharnagar-Khirsara segment. The site is located downstream of the Quaternary sediments section of this segment described in the previous chapter. The Quaternary sediment cover is negligible at the site. The surface along the transect is gently with rocks fragments strewn around owing to the presence of basement rocks below the thin alluvial cover. The deformed Mesozoic rocks striking N 120^{o} with steep northward dips were observed in the low incised cliff section of the nearest stream to the east of the transect.

A 48 m long processed S-N profile of 80 MHz bistatic antenna is presented (Fig. 5.12a). The upper part of the profile up to the depth of ~3 m is characterised by high amplitude horizontal to wavy reflections are interpreted as Quaternary gravelly sand deposits. The unconformable contact of Quaternary sediments with the basement is distinctly identifiable in the GPR profile. The basement is characterised by high and low amplitude reflections. The high amplitude reflection is seen in the southern part of the profile while the low amplitude reflection is seen in the northern part. The variation in the amplitude of the radar reflection from high to low is on account of increased percentage of conducting media in the lithology (Fig. 5.12 b, c). The higher amplitude reflection represents the compacted Mesozoic sediments while the lower amplitude reflection in the

northern part of the profile represents the clay rich Tertiary sediments. At a distance of around 27 m a sharp truncation of the radar reflections is seen (Fig. 5.12 a, d). This truncation marks the faulted contact of the Mesozoic and Tertiary rock which is identified as the fault plane of the KMF. Thus, the KMF in this segment is characterised by almost vertical fault plane.

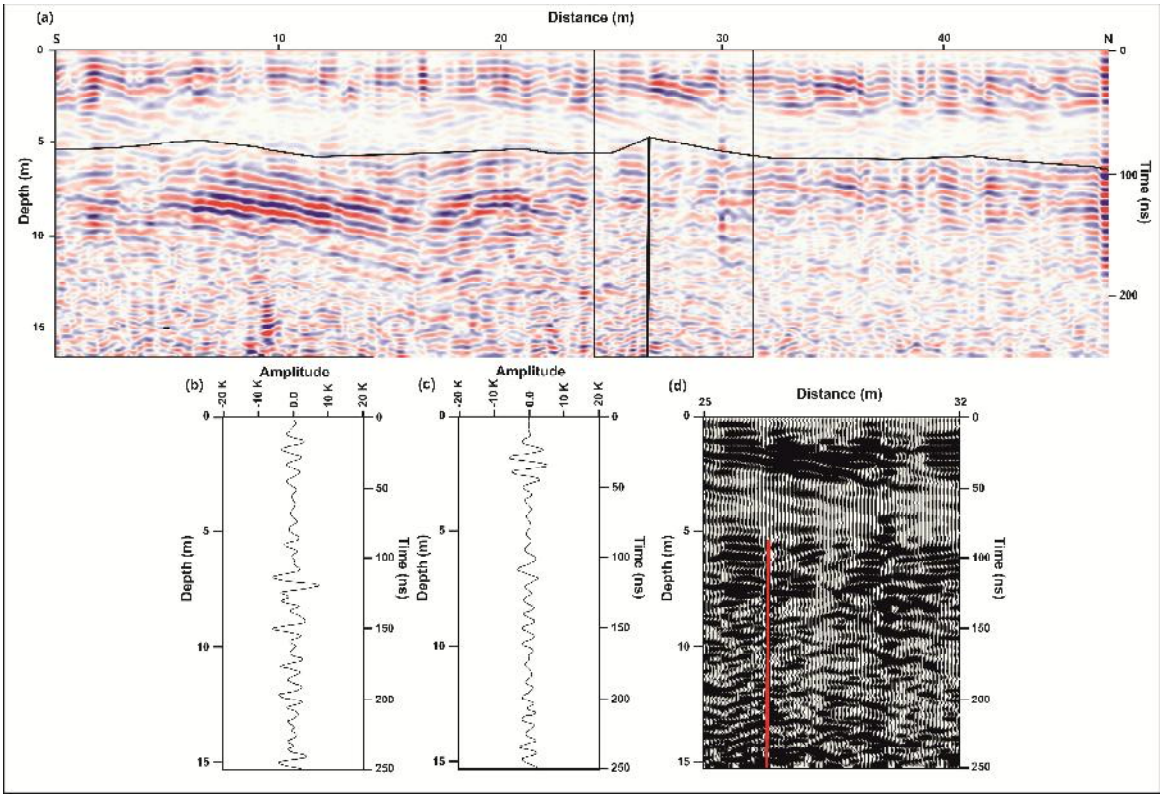

Figure 5.12 **(a)** GPR profile taken from a cliff section of a north flowing stream near Jawaharnagar, location of site is shown in Fig. 5.5 with 80 MHz bistatic antenna in a point mode. Note the strong reflections emanating from the fault plane. **(b)** Oscilloscope of a single scan emanating from of the Mesozoic rocks **(c)** Oscilloscope of a single scan emanating from of the Tertiary rocks. **(d)** The boxed portion of (a) is shown in a Wiggle mode.

Site-VII

This site is located to the north of Khirsara village. A 30 long S-N profile was acquired by 200 MHz monostatic antenna in continuous mode and only a part of acquired profile is shown in Fig 5.13a. The top 2-3 m part of the GPR profile is characterized by the high amplitude reflections which on the basis of our field observation represents the Quaternary sediments. The thickness of the sediments is found to increases northward in the profile. Unconformable contact of the Quaternary sediments with the basement is clearly distinguishable in the GPR profile. The basement is characterised by the high and low amplitude reflections (Fig. 5.13b, c). The radar reflection directly depends upon the conductivity of the medium i.e. highly conductive material will results in the low

amplitude reflection due to loss of wave energy during transmission. While high amplitude reflection can be directly related to low conductive medium. On the basis of the field setting the high amplitude reflections are attributed to compacted Mesozoic sandstones while the low amplitude reflection represents the Tertiary rocks. A sharp truncation of the radar reflection is seen at a distance of around ~ 3m (Fig. 5.13a, d). This truncation represents the faulted contact of Mesozoic and Tertiary rock. This faulted contact represents the KMF fault plane. The KMF in this profile represents a nearly vertical north dipping fault.

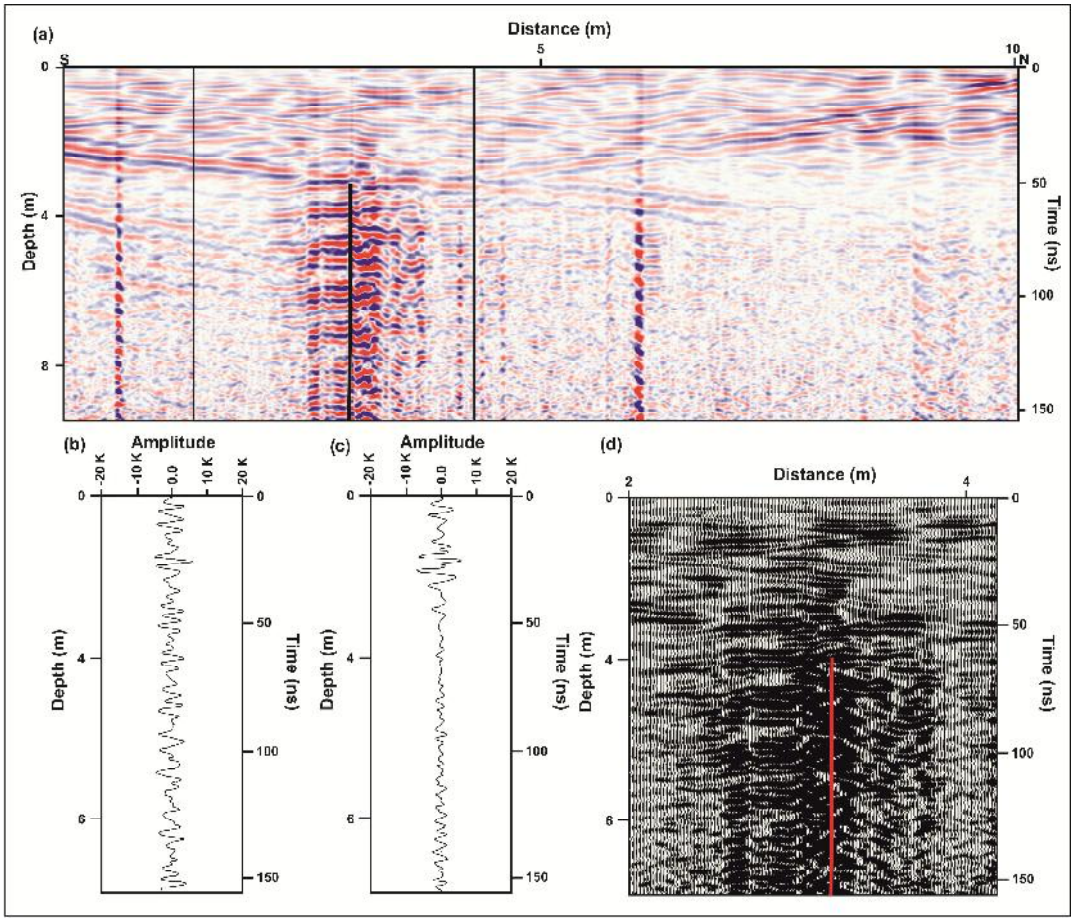

Figure 5.13 (a) GPR profile taken from north of Khirsara with 200 MHz antenna, location of site is shown in Fig. 5.5. Note the strong reflections emanating from the fault plane. **(b)** Oscilloscope of a single scan emanating from of the Mesozoic rocks **(c)** Oscilloscope of a single scan emanating from of the Tertiary rocks. **(d)** The boxed portion of (a) is shown in a Wiggle mode.

KHIRSARA-DEVISAR SEGMENT (SEGMENT V)

The KMF is well exposed in this segment along the cliff sections of small streams as described in Chapter 3. However, the fault is covered by alluvium in the margins of the segments. The GPR surveys were carried out to confirm the extension of the KMF throughout the segment.

PART-B Kachchh Mainland Fault (KMF)

Site-VIII

This GPR site is located an unmetalled road from Khirsara to Morwandh village located at the fringe of Banni plain. The GPR survey was carried out along the eastern side of the road as it crosses the KMF scarp. Nearly vertical Mesozoic rock with a strike of N 135^{o} was seen in a nearby first order stream. Several N-S profiles were collected by 80 MHz bistatic antenna in a point mode and one of the best profile was selected for processing and later used for interpretation (Fig. 5.14a).

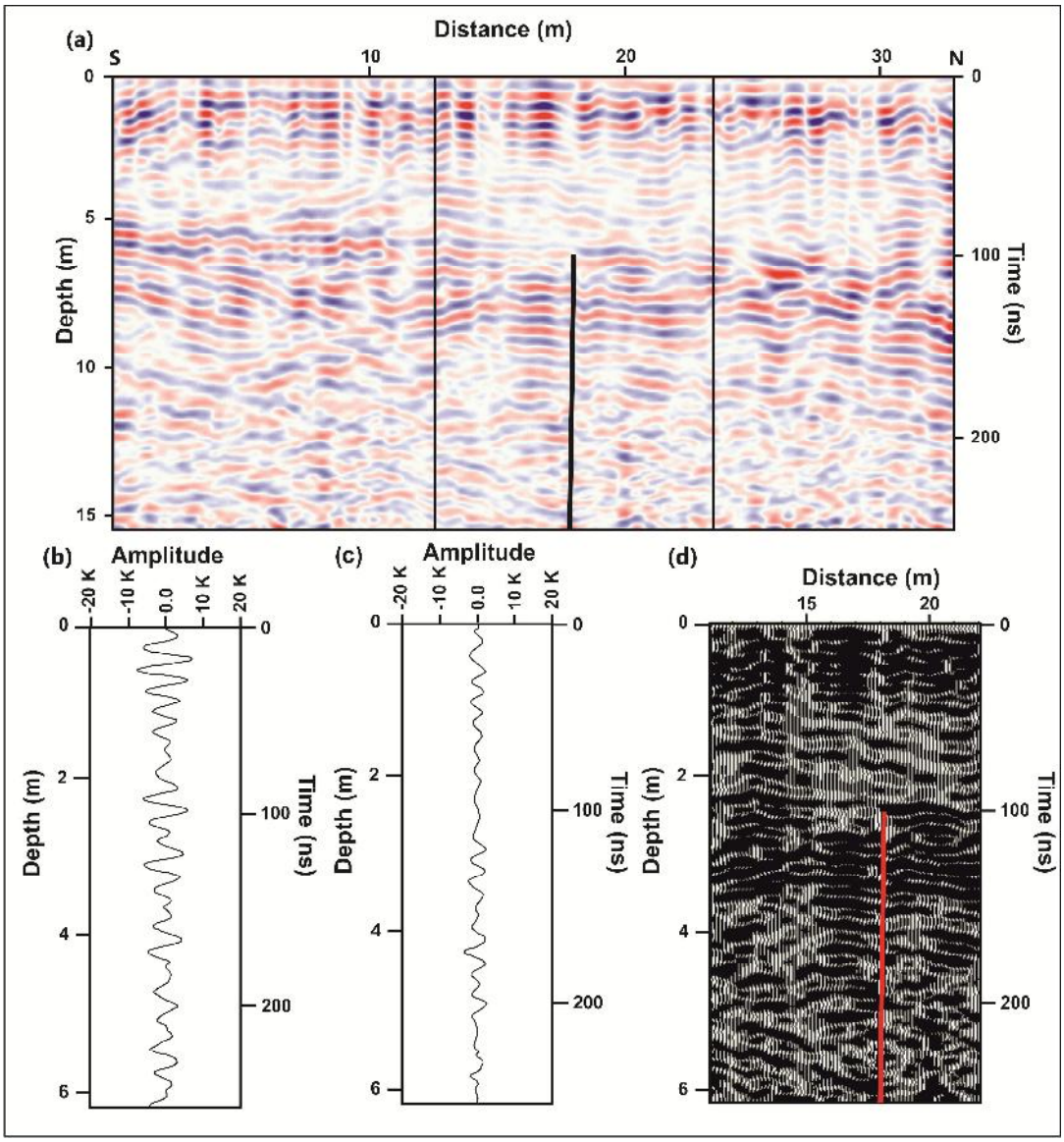

Figure 5.14 (a) GPR profile taken from south of Morwan village with 80 MHz bistatic antenna in a point mode, location of site is shown in Fig. 5.5. Note the strong reflections emanating from the fault plane. **(b)** Oscilloscope of a single scan emanating from of the Mesozoic rocks **(c)** Oscilloscope of a single scan emanating from of the Tertiary rocks. **(d)** The boxed portion of (a) is shown in a Wiggle mode.

PART-B Kachchh Mainland Fault (KMF)

The profile was acquired in an agricultural field with relatively horizontal surface. The upper ~5m part of the GPR profile represents the alternating horizontal continuous, wavy and inclined radar reflection of high to low amplitude. This is attributed to the vertical lithological variations in the Quaternary alluvial sediments. The Quaternary sediments overlie the basement rocks with a sharp unconformity. The basement rock is characterised by high amplitude and low amplitude radar reflection (Fig. 5.14b, c). This variation is on account of conductive and non-conducting media. Field observations described earlier in the chapter have indicated that the Mesozoic rocks comprise sandstone while the Tertiary rocks are clayey rich. Clays are generally conductive in comparison to sand. Thus it can be interpreted that the high amplitude reflection is on account of Mesozoic sandstone while the low amplitude radar reflection represents the Tertiary clays. A sudden truncation of the reflection in the basement is seen at a distance of ~19m (Fig. 5.14a, d). The truncation of the reflection generally represents the faulted contact that marks the near surface trace of the KMF. The truncation of the reflection is also seen in the basal unit of the Quaternary deposits. Thus it can be presumed that KMF is a vertical fault in this part and has propagated upwards during the Quaternary time.

Site IX

This site is located near a check dam of small north flowing stream south of Amrapar village (Fig. 5.15a). The S-N 25m long profile was collected in a dry channel of the river with the help of 80 MHz bistatic antenna in point mode. The top 2-3 m part of the GPR profile is characterised by high amplitude horizontal to wavy reflectors. These radar reflection patterns characterises the thick Quaternary alluvium overlying the basement rock. The radar reflection of Quaternary sediments can be easily distinguished from the radar reflection of the basement rock. The basement rock is characterised by radar reflections of high to low amplitudes (Fig. 5.15b, c). The high amplitude reflections form the southern part of the profile while the northern part of the radar profile is characterised by low amplitude reflections. This variation in the amplitude of the radar reflection is similar to the earlier described profiles where high amplitude reflections define the Mesozoic sandstones while the low amplitude reflections are characterised by clayey Tertiary rocks. The truncation of the reflectors is seen in the basement at a distance of 17 m (Fig. 5.15a, d). This truncation defines the KMF fault plane which is interpreted as a northward dipping near vertical fault. Thus, the GPR profile confirms the continuation of the near surface trace of the KMF up to easternmost extremity of the KMF scarps.

PART-B Kachchh Mainland Fault (KMF)

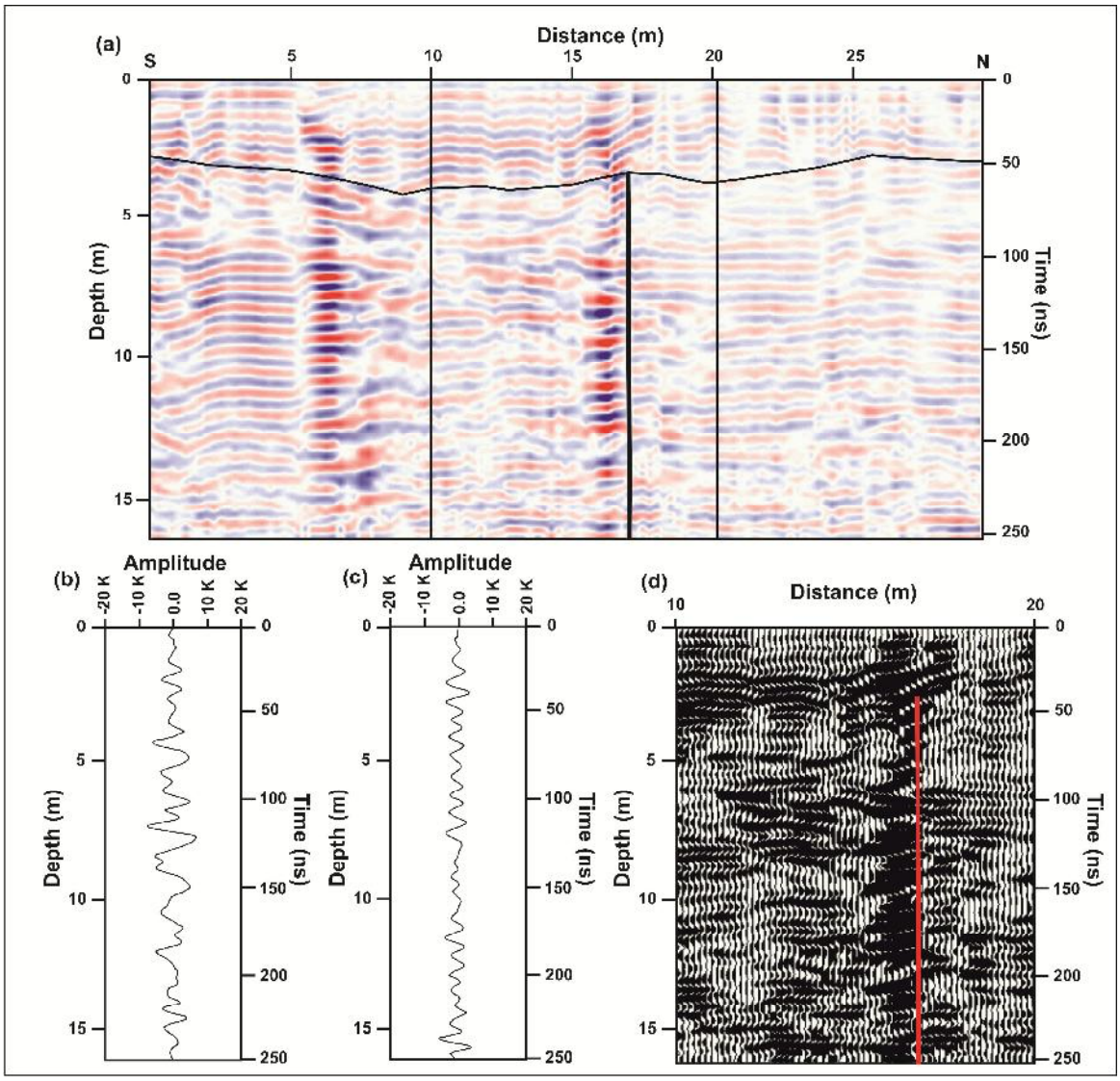

Figure 5.15 (a) GPR profile taken from a north flowing stream south of Amrapar village with 80 MHz bistatic antenna in a point mode, location of site is shown in Fig. 5.5. Note the strong reflections emanating from the fault plane. **(b)** Oscilloscope of a single scan emanating from of the Mesozoic rocks **(c)** Oscilloscope of a single scan emanating from of the Tertiary rocks. **(d)** The boxed portion of (a) is shown in a Wiggle mode.

CHAPTER 6

EVIDENCE FOR EASTWARD EXTENSION AND PROPAGATION OF THE KMF

The field and GPR data generated during the present course of study along the KMF and described in the previous chapters suggest a rather complex neotectonic setting and Quaternary evolutionary history. The fault typically displays the characteristics of an ideal large and active range bounding segmented fault. The fault has a prominent geomorphic expression up to the area to the east of Devisar where the KMF scarp line finally dies out. Further eastward the fault loses its geomorphic expression as the rugged mountain front geomorphic set up of the KMF zone is replaced by an almost flat topography with gentle northward gradient that merges with the Samakhiali plain. Significantly, the epicentre of the 2001 Bhuj earthquake lies in this zone. Moreover, several coseismic secondary features associated with the 2001 event were documented from this region that included extensive lateral spreading to the north of Budharmora village. Subsequent seismic monitoring have revealed that low to moderate intensity earthquakes have continued to occur in this part. Therefore in the present study, efforts were made to ascertain and map the eastward continuity of the KMF using field and GPR studies. The details of these investigations included in the present chapter, provide field and shallow subsurface geophysical evidence in support of the eastward lateral extension and propagation of the KMF up to the epicentral area of the 2001 earthquake. As a result of the studies carried out, the traceable length of the KMF has been extended eastward by ~20 kms. This extended part is recognised as an additional easternmost segment (Segment-VI) of the KMF and identified as the Amrapar-Sikra segment. The description here includes geomorphological studies followed by the results of shallow subsurface geophysical studies using GPR.

TECTONIC GEOMORPHOLOGY-SEGMENT VI:

As mentioned above the general topography in this segment is nearly flat to gently undulating with a gentle but distinct gradient towards the north. Further northward, lies the saline terrain of the Great Rann while towards the south the terrain shows a relatively uneven rocky topography with several mounds and low hills trending in a general E-W direction up to Bhachau (Fig. 6.1). The landscape of this segment comprises mostly

gently undulating rocky with a narrow zone of sandy alluvial sediments that slope northward to merge with the salt encrusted surface of the Great Rann. A general E-W trending narrow zone passing through Budharmora, Morgar, Amardi, Krishnanagar and Sikra was observed along which the outcrops of Mesozoic rocks appeared to terminate. However, extensive field work all along this presumed zone of the fault did not reveal any scarp or scarplet or any other geomorphic indicator throughout this segment. In view of this, a detailed topographic analysis of the landscape in segment-VI was attempted.

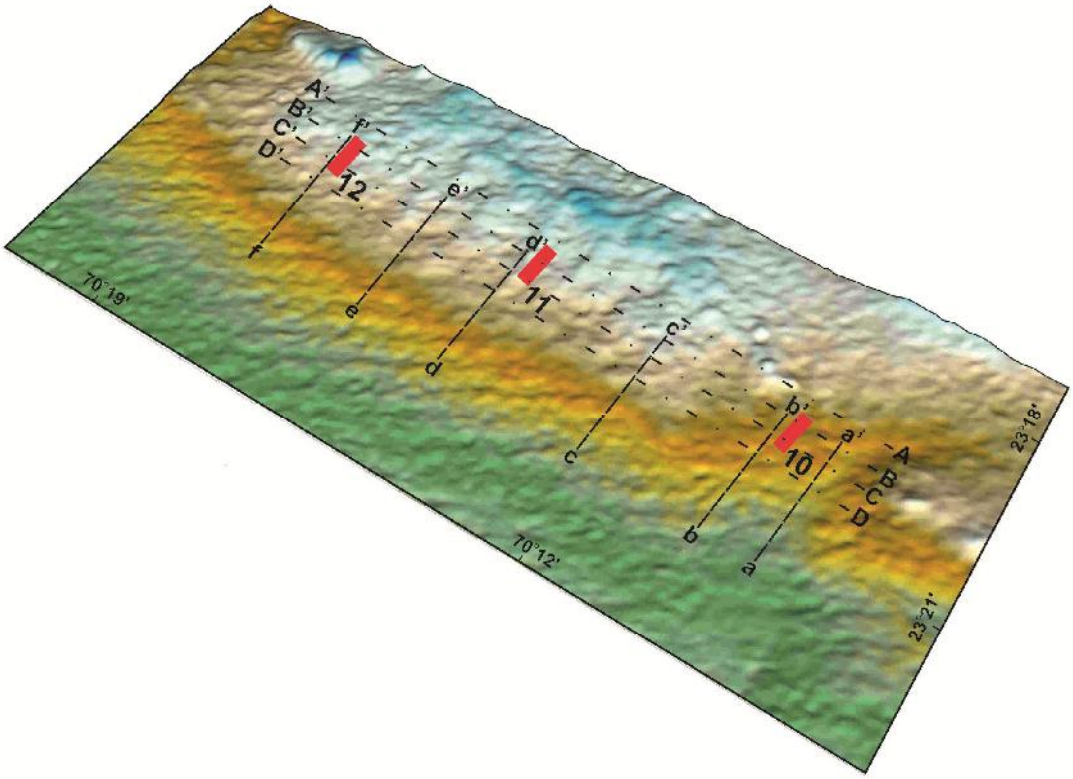

Figure 6.1 Digital Elevation Model (DEM) of Segment VI. The lines aa'-ff' are the location of the N-S topographic profiles shown in Fig. 6.2 while AA'-DD' are the location of E-W topographic profiles shown in Fig. 6.3. The thick red lines (10-12) denote the sites of GPR surveys described in this chapter.

GEOMORPHIC ANALYSIS

Geomorphic analysis of Segment-VI was done using DEM studies and elevation data from the topographical maps and Google earth data. Qualitative interpretation of the landscape was done from the topographic data. For interpretation, it is assumed that the geological setting of the KMF should be similar to the other five segments described in the previous chapters. The main reason for this assumption is that the rocks exposed in Segment-VI comprise compacted sandstones of the Bhuj Formation of late Cretaceous

age, while the Chhasra Formation and Sandhan Formation of Tertiary age occupies the Samakhiali plain (Biswas, 1993). The structure of the Samakhiali plain is interpreted as a graben structure bounded by the KMF in the south and the South Wagad Fault (SWF) in the north (Biswas and Khattri, 2002).

Several topographic profiles were drawn in E-W and N-S directions covering the Segment-VI from Amrapar in the west to Sikra in the west. The N-S topographic sections are shown in Fig. 6.2. The cross sections show a gentle but prominent northward slope towards the Great Rann. The slope is uniform and do not show the presence of any scarp of sharp topographic breaks that can be indicative of the presence of the fault. The field studies showed that the gentle northward slope is occupied by sandy alluvium that varies in thickness from 1-3 m and is used for agriculture. The cross sections also show that the northward slope in general begin at 40 m elevation. The southern reach beyond this elevation shows a undulating topography corresponding to the presence of Mesozoic rocks. The northward slope starting from the 40 m elevation was interpreted as the possible fault zone of the KMF and therefore identified as the area of focus for GPR studies in this segment.

E-W trending topographic profile were also constructed to delineate the subtle elevation along strike differences of the KMF zone in this segment. The Fig. 6.3 shows the E-W trending topographic sections drawn across segment-VI. Of these, one profile is drawn over the alluvial sediments comprising the northern gently sloping part of the segment. The other three profiles are drawn of the rocky surface forming the southern part of the segment. The three profiles drawn over the gently undulating rocky surface shows a prominent depression in the westernmost part of the Segment-VI. This topographic depression is interpreted as the saddle part controlled by the structural pattern of the Mesozoic rocks. This is consistent with the geomorphic set up of the other segments to the west where the Northern hill range consists of a linear chain of several domes which are separated by prominent saddles between them. As described in the previous chapters, all saddles reaches are occupied by a major river e.g. the Kaila river, the Kaswali river, the Khirsara stream and few others. All these rivers are characterised by broad shallow sandy channels in contrast to the smaller streams cutting through the KMF scarps that show deeply incised narrow channels. Conforming this geomorphic set up, a stream with an anomalously broad and shallow channel is found to occupy the saddle interpreted in the westernmost part of the Segment-VI. The presence of the saddle appears to a structural continuation of the KMF scarp that gradually disappears in the subsurface at the

western margin of this segment. The presence of this topographic low corresponding to a structurally controlled saddle is also clearly seen in the DEM of Segment-VI (Fig. 6.3). Further eastward along the same trend the topography rises to an elevation of >40 m and continues in the same way up to Sikra.

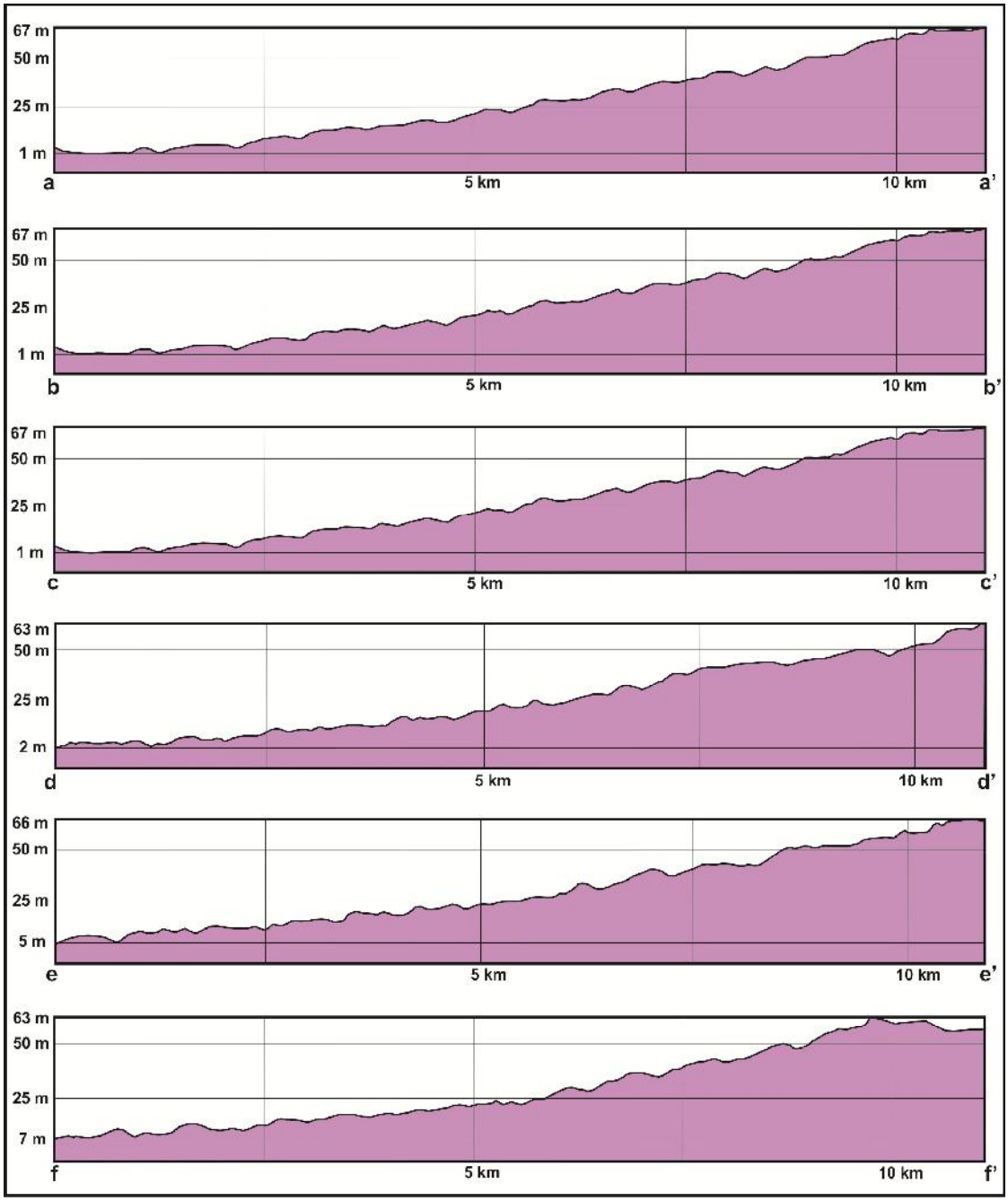

Figure 6.2 N-S topographic profiles showing the prominent northward slope. Note the absence of surface indication of the KMF. The highest part of the slope consists of Mesozoic rocks with thin alluvial cover. The location of profiles is shown in Fig. 6.1.

The topographically high part continuing up to Sikra corresponds to an undulating rocky ground. This suggests that though the KMF scarp dies out, the Northern hill range

continues to extend eastwards in the shallow subsurface as evidenced by the outcropping Mesozoic rocks. The convex up shape of the topographic profiles indicates the region to the east of the saddle up to Sikra corresponds to a positive structural feature i.e. an anticline or a dome. This inference matches with the general structure of the Northern hill range which is basically a E-W trending chain of domes separated by saddles. Overall, the topographic analysis of Segment-VI provides strong evidence for the eastward extension of the Northern hill range up to Sikra with the development a prominent saddle at the western extremity and a positive structural high possibly in the form a dome in the central and eastern part of the segment.

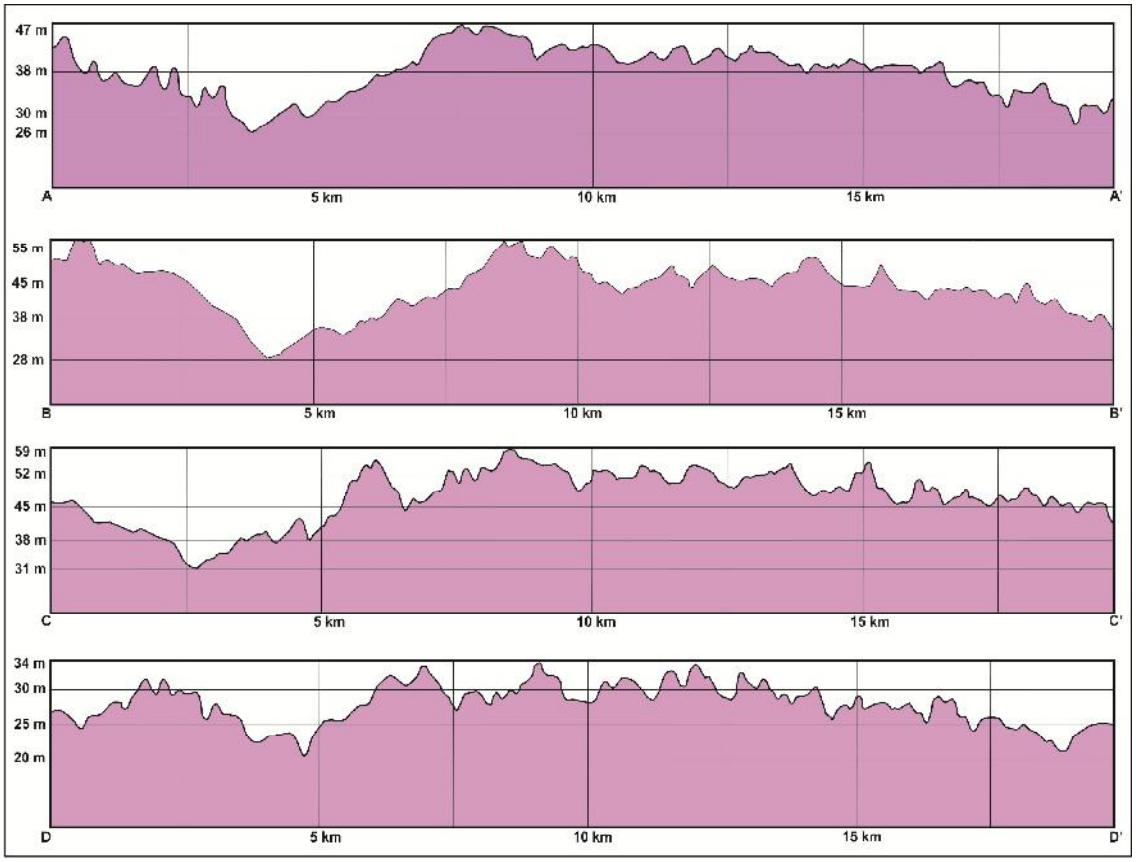

Figure 6.3 E-W topographic profiles along the length of segment VI. location of the profile is shown in the Fig. 6.1. Note a prominent topographic low in the western part of the segment interpreted as a saddle. The topographically high central and eastern parts of the segment correspond to Mesozoic rocks in shallow depth and is interpreted as a structural high in the buried Northern Hill Range.

DRAINAGE CHARACTERISTICS

The nature of the drainages of the Segment-VI is markedly different from the normally well entrenched drainages of the other segments of the KMF in the west. The drainage shows several anomalies which are conspicuous and unique to this segment. In general, the drainage consists of parallel to sub-parallel north flowing lower order streams

that merge into the Great Rann surface (Fig. 6.4). The streams are very short and arise from the rocky terrain in the southern part of the segment. Though short in length, several streams show narrow gorge-like channels that have incised into the bedrock by 1-3 m (Fig. 6.5a). However, some channels, most prominently the stream located in the westernmost part of the segment which is interpreted as a saddle from the topographic analysis described in the previous section of this chapter. This river is characterised by an anomalously broad shallow channel exposes Mesozoic sandstones in the low cliffs of 1-1.5 m height. The cliffs quickly die out northward as the channel progressively becomes wider up to ~ 2 kms and finally merging with low flat terrain of the Banni plain in the north. The other rivers Northern hill range that flow through saddle part separating the domes like the Kaila river, Kaswali river and others show similar development of broad sandy channels. The presence of this stream with anomalous broad channel is therefore consistent with the structurally controlled saddle in this part of Segment-VI as evidenced by the topographic analysis.

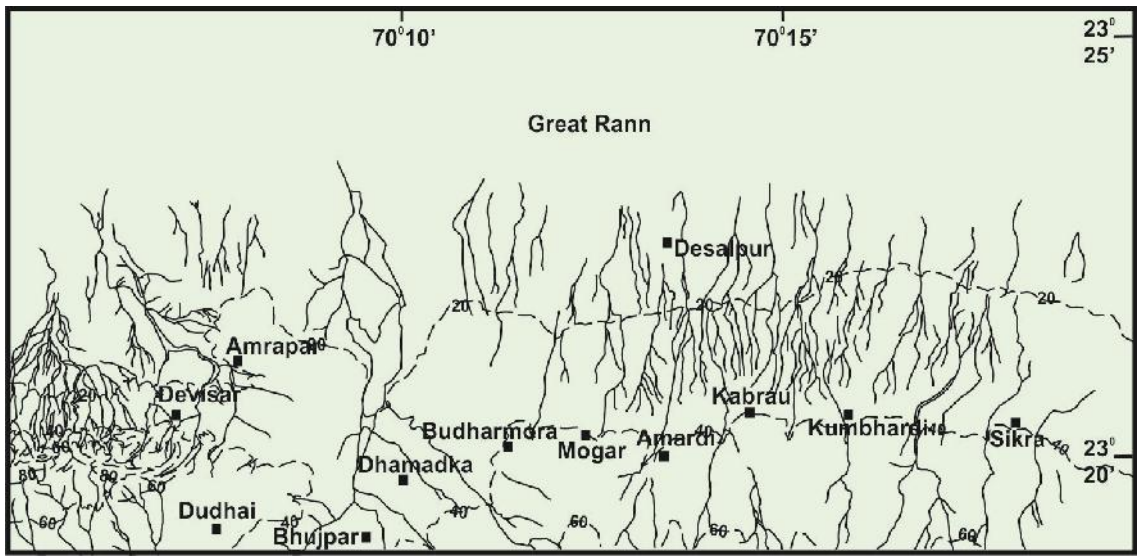

Figure 6.4 Drainage map of the segment-VI. Note the parallel north flowing streams consistent with the slope direction. The streams emerge from the nearly flat suggesting recent uplift along the KMF buried at shallow depth.

The drainage to the further east up to Sikra village show narrow incised channels of the lower order streams that corresponds to the topographic high revealed in the topographic analysis and interpreted as indicative of a positive structural feature, possibly a dome. The drainage also appear to confirm this inference as most of the streams are short and appear to originate along this narrow E-W trending topographically high area. The origin of a large number of north flowing streams from this subtle topographic high,

markedly parallel drainage pattern and their strongly incising nature suggest neotectonic uplift of the Northern hill range.

Figure 6.5 Photographs showing the geomorphic characteristics of a small north flowing stream near Krishnanagar (east of Amardi) in segment-VI. **(a)** Upstream view of the narrow gorge like channel formed by the stream in compact Mesozoic bedrock. **(b)** Visibly broadened channel of the same stream further north after it emerges from the Mesozoic rocks. The stream bed in the foreground shows patchy exposures of Tertiary rocks. GPR survey was carried out in this reach (site 2) for demarcating the near surface trace of the KMF. **(c)** E-W trending extensional ground cracks developed on alluvial surface in the vicinity of the GPR site 3 at Sikra. **(d)** Close view of the cracks **(e)** E-W trending cracks stream bed near the GPR site 2 shown in b **(f)** Close view of the crack in the stream bed.

Overall, the drainage characteristics together with the topographic analysis confirm the eastward extension of the structurally complex Northern hill range up to Sikra village which marks the eastern limit of the Segment-VI of the KMF zone identified in the present study. The dominantly lower order streams suggest that the drainage is formed due to neotectonic uplift and are much younger than the drainages in the other segments to the west. The continuing rising up of the Northern Hill range from the shallow subsurface is testified by the 2001 Bhuj earthquake and associated secondary deformation that occurred in this segment. During the course of present study, several E-W trending ground cracks were observed in the agricultural fields at several places. The fissures extended for several tens of metres with shorter and less numerous N-S trending fissures (Fig. 6.5c, d, e, f). Significantly, all the fissures were found to be located immediately to the north of the KMF traced through GPR studies described later in the chapter. The localisation of the fissures in the fault zone and the preferential E-W trend points to continued tectonic activity along the KMF in this segment.

GPR STUDIES

The GPR studies were carried out in Amrapar-Sikra segment (Segment-VI) primarily to confirm the lateral eastward extension of the KMF. As described above, there are no geomorphic indicators of the precise trace of the KMF as seen in other morphotectonic segments in the west where it is morphologically expressed as a steep range front scarp. However, the geomorphic described above clearly point to the continuity of the Northern hill range along with its typical structural pattern with a very subdued topographic expression. The sites for GPR survey were constrained on the result of geomorphic studies and extensive field observations all along the length of the Segment-VI. The field studies included traverses along the stream channels and observing the extension and indications of fault induced deformation. Special attention was paid to the stream reaches where the Mesozoic outcrops ceased to occur further north. A few streams showed poorly exposed Tertiary rocks in the channel bed which suggested that the near surface trace of the KMF is marked by the sharp lithotectonic contact between the Mesozoic and Tertiary rocks. This is in conformity with the geologic setting of the KMF as delineated in the other morphotectonic segments described in the previous chapter. The field observations were utilised to interpret the GPR profiles collected in Segment-VI. GPR data from three sites are presented here which conclusively establish the continuation of the KMF up to the epicentral area of the 2001 earthquake.

PART-B Kachchh Mainland Fault (KMF)
Site X

This site is located about one kilometre to the north of Budharmora village. The site was selected on the basis of topographic and field studies described earlier. Incidentally, the selected site is located in an agricultural field that was affected by large scale lateral spreading during the 2001 Bhuj earthquake (Rajendran et al. 2001; 2008; McCalpin and Thakkar, 2003). Lateral spreading is produced by liquefaction, generally on very gentle slopes (most commonly between 1^0 and 3^0) and move down slope toward a free face. Flows may consist of completely liquefied soils or blocks of intact material, riding on layers of liquefied soil, the whole process causing deformation of the soil layers, often leading to ground failure (Obermeier, 1996).

At Budharmora, and at many other locations in the epicentral area, lateral spreads had given rise to a series of ground cracks showing step-like displacements and compressional features at the toe of the mass movement (Rajendran et al. 2001). Subsequent trench studies however, did not reveal any fault plane that might have been activated during the 2001 earthquake, though a small slip plane towards the top is recorded (Rajendran et al. 2008). The stratigraphy of the 3-m-deep trench 1 at Budharmora (Fig. 6.6), excavated at the across the 2001 lateral spread, showed sequence of black silty clay, yellowish fine sand and brownish gritty sand (Rajendran et al. 2008). From the calibrated age of 10,151 cal years B.P. obtained for the top part of the two stratigraphic units, it is estimated that the earliest event that produced the first generation sand dikes occurred between ca. 10.1 Ka and 13.8 Ka (Rajendran et al. 2008).

During the present study, the GPR survey was done close (~10 m) to the east of the trench location of Rajendran et al. 2008. The distance was deliberately maintained to avoid the excavated material and later filling of the trench itself so as to encounter original in situ conditions. Since the trench did not extend downward to the basement to the basement rocks, the GPR data provided the opportunity to gain insight into the geological setting at greater depth. The GPR survey line was oriented precisely along the N-S trend.

A 13 m long S-N profile was acquired by 200 MHz monostatic antenna in a continuous mode shown in Fig. 6.7a. The top 2.5 m in the profile depicts high amplitude horizontal radar reflection which generally represents a stratified alluvium and can be roughly correlated with the sediments in the nearby trench excavated by Rajendran et al. (2008). A sharp unconformable contact of Quaternary and basement rock can be easily identified in the profile.

PART-B Kachchh Mainland Fault (KMF)

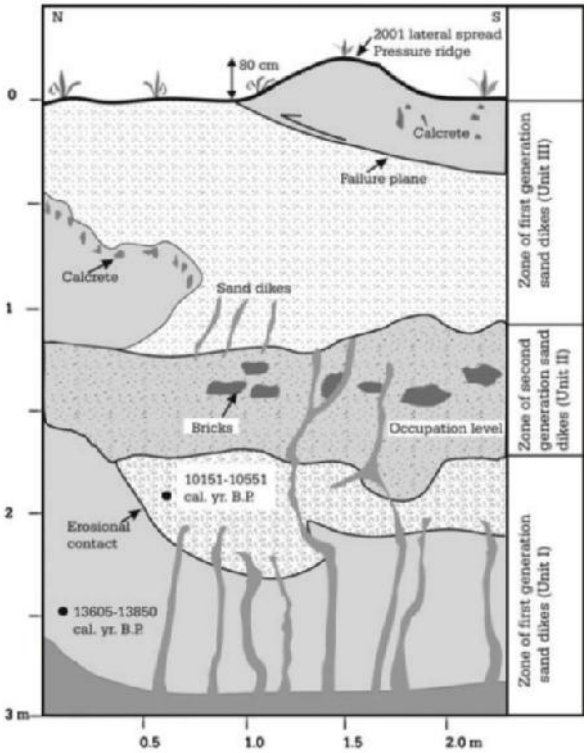

Figure 6.6 Log of Trench 1 excavated by Rajendran et al. 2008 across the lateral spread during 2001 earthquake near Budharmora.

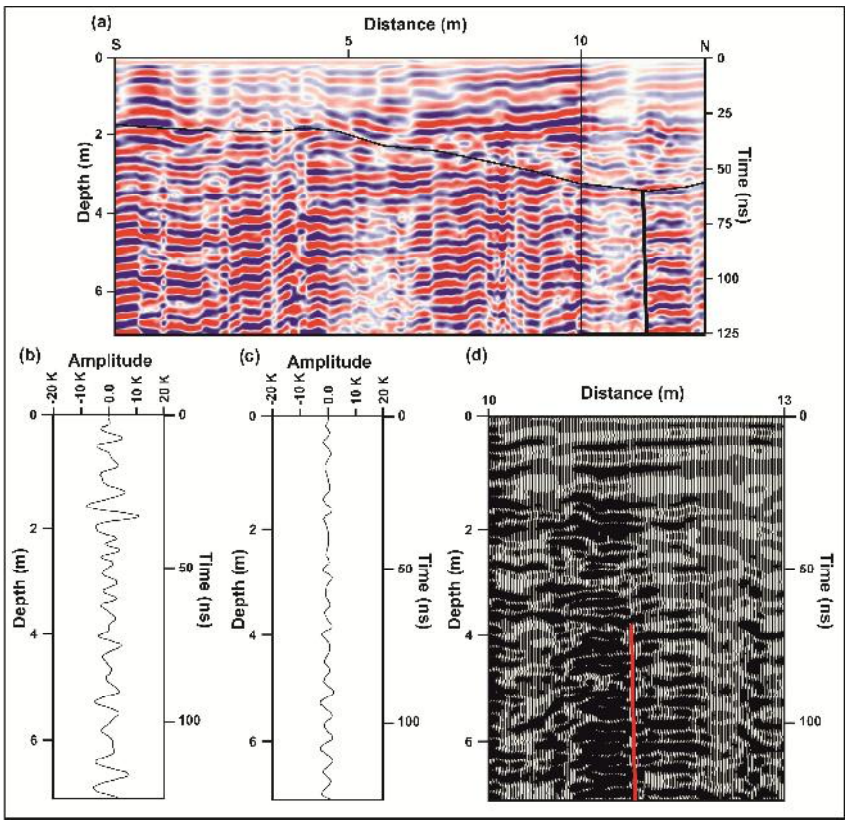

Figure 6.7 (a) GPR profile obtained north of Budharmora. The profile was collected with 200 MHz antenna over close to the trench section shown in Fig. 6.5. Location of site is shown in Fig. 6.1. **(b)** Oscilloscope of a single scan emanating from of the Mesozoic rocks **(c)** Oscilloscope of a single scan emanating from of the Tertiary rocks. **(d)** The boxed portion of (a) is shown in wiggle mode.

PART-B Kachchh Mainland Fault (KMF)

The basement here is characterised by high and low amplitude radar reflection. The high amplitude reflection is seen in the southern part of the profile while the low amplitude reflection is seen in the northern part. The variation in the radar reflection is interpreted as indicative of a abrupt lithological contrast (Fig. 6.7b, c). Generally, the conductive material like clays shows a low amplitude radar reflection because of loss of energy during wave transmission in a conducting media. Thus, based on the GPR surveys across KMF in other segments and described in the previous chapter, it is inferred that the low amplitude radar reflection is on account of conducting material which in conformity with field setting represents the Tertiary rock. The field setting around the KMF region also suggests that the high amplitude radar reflections to be the result of the Mesozoic sandstones. The abrupt contact of the two distinctly different lithologies is seen at a distance of ~11 m in the GPR profile (Fig. 6.7a, d). The contact region is interpreted as the fault plane of the KMF that is near vertical. The results of the present GPR study demonstrates that the extensive lateral spreading along a E-W trending zone to the north of Budharmora village is directly linked to the presence of the KMF in the shallow subsurface. McCalpin and Thakkar (2003), based on their detailed study of the epicentral zone of the 2001 event had earlier suggested that the lateral spread at this area indicates a possible influence of an overall structural control of the KMF.

Site-XI

This site is located in the central part of Segment-VI to the east of Amardi and the north-western vicinity of the post-2001 earthquake rehabilitated site named as Krishnanagar. The site is located in the bed of a small stream that in the upstream shows a narrow gorge-like channel incised into the bedrock comprising the sandstones of the Bhuj Formation (Fig. 6.5a). The river banks showed a consistent blanket of 1-2 m sandy alluvium over the bedrock (Fig. 6.5b). Downstream of the GPR survey transect, few patches of fine grained Tertiary rocks could be recognised on the sandy river bed of the broad shallow channel of the stream. The site was selected in view of the abrupt change in channel morphology and the possible presence of contrasting lithology. Of the several GPR profiles taken, a 15 m long S-N profile acquired by 80 MHz bistatic antenna in point mode is shown in the Fig. 6.8a. The profile reflects a very thin Quaternary cover and basement is characterised by high amplitude reflections and low amplitude reflections. The high amplitude reflections are seen in the southern side of the profile which are interpreted as compacted Mesozoic rocks based on the exposed sections in the stream channel (Fig. 6.8b). While, the low amplitude reflections in the profile is due to the loss

of energy during transmission of radar waves (Fig. 6.8c). A sharp and abrupt transition in the nature of radar reflections is seen at a distance of ~6.5m (Fig. 6.8a, d). This is the interpreted as the faulted lithotectonic contact representing the KMF. The KMF is reflected as a vertical fault at the site.

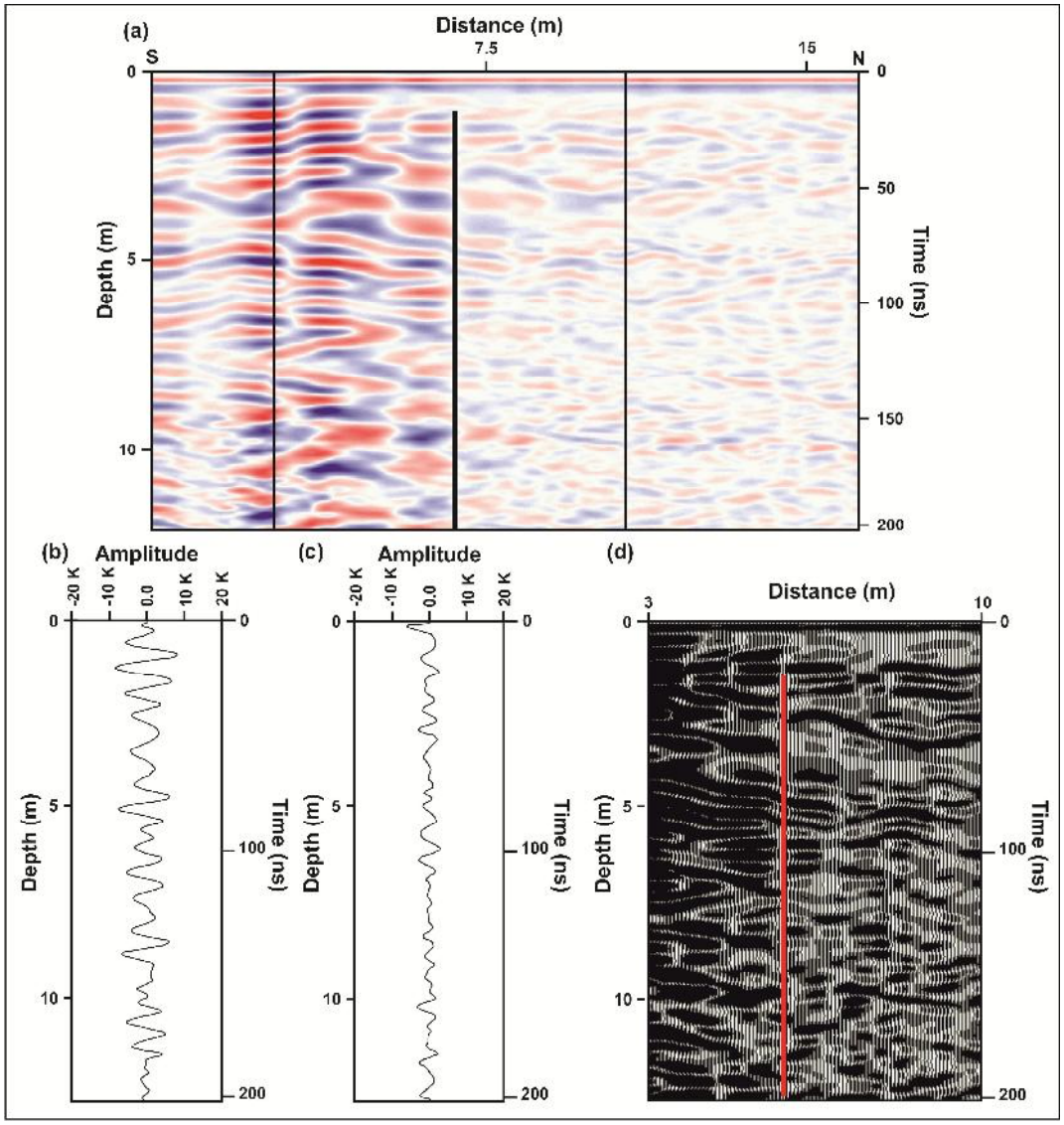

Figure 6.8 (a) GPR profile taken east of Amardi. The profile is collected with 80 MHz bistatic antenna. Location of site is shown in Fig. 6.1. **(b)** Oscilloscope of a single scan emanating from of the Mesozoic rocks **(c)** Oscilloscope of a single scan emanating from of the Tertiary rocks. **(d)** The boxed portion of (a) is shown in wiggle mode.

Site-XII

This site is located along close to the stream to the west of Sikra village. The GPR transect is located to the north of the Bhuj-Bhachau road and on the left bank of the stream. The stream shows a transition from a narrow channel incising the Mesozoic rocks to a broad shallow sandy channel. Fig. 6.9a shows a 34 m long S-N profile was acquired

by 200 MHz monostatic antenna in a continuous mode. Another 15m long S-N profile was acquired by 80 MHz bistatic antenna in a point mode (Fig. 6.9c).

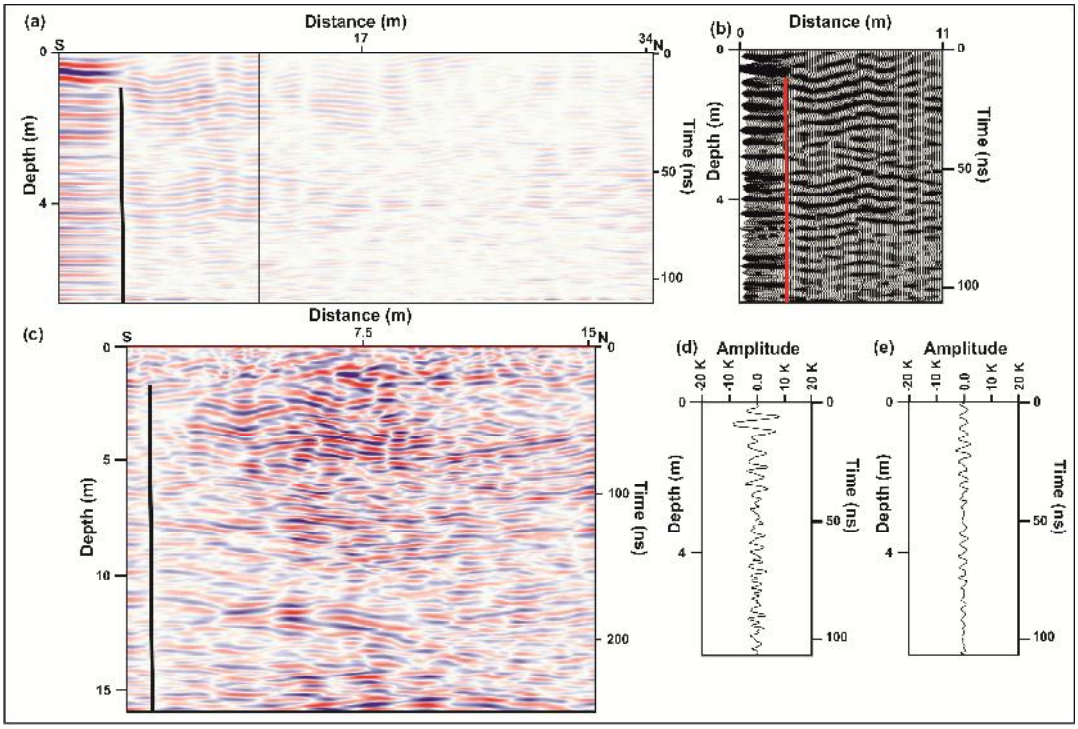

Figure 6.9 (a) GPR profile taken to the west of Sikra village. The profile was collected with 200 MHz antenna. Location of site is shown in Fig. 6.1. **(b)** The boxed portion of (a) is shown in wiggle mode. **(c)** A 80 MHz bistatic antenna profile collected in a point mode **(d)** Oscilloscope of a single scan emanating from of the Mesozoic rocks **(e)** Oscilloscope of a single scan emanating from of the Tertiary rocks.

The upper 2 m part of the profile depicts horizontal continuous reflection is interpreted as sandy alluvium deposited over the basement. The basement is characterised by the high and low amplitude radar reflection. Considering the interpretation of the other GPR profiles of KMF described earlier, it is inferred that this variation is on account of sharp lithological contrast that is typical of the neotectonic setting of the KMF. The high amplitude radar reflection lying on the southern part of the profile represents the Mesozoic sandstones while the low amplitude reflections are on account of clay rich Tertiary rocks (Fig. 6.9d, e). The abrupt contact of the contrasting radar reflections is seen at a distance of 5 m in the GPR profile (Fig. 6.9a, b). This represents the KMF fault plane which appears as a steep north dipping fault. The present field and GPR based study has been able establish the continuity and shallow subsurface nature of the KMF up to Sikra village which located to the south of the actual epicentre of the 2001 Bhuj earthquake.

CHAPTER 7

FIELD AND GPR STUDIES ALONG SOUTH WAGAD FAULT (SWF)

The Wagad Highland is the second largest uplift of the Kachchh basin after the mainland uplift. It occurs to the east of the Banni basin separating it from the depression of the Little Rann of Kachchh. It is surrounded by the Rav Basin to the north and to the east and south by the residual depression of the Little Rann of Kachchh (Fig. 7.1). The Rav Basin separates it from the Bela uplift. Only a narrow stretch of Little Rann which is a very shallow depression separates it from the Radhanpur-Barmer Arch. The uplift is thus close to the marginal High of the Kachchh Basin towards the east.

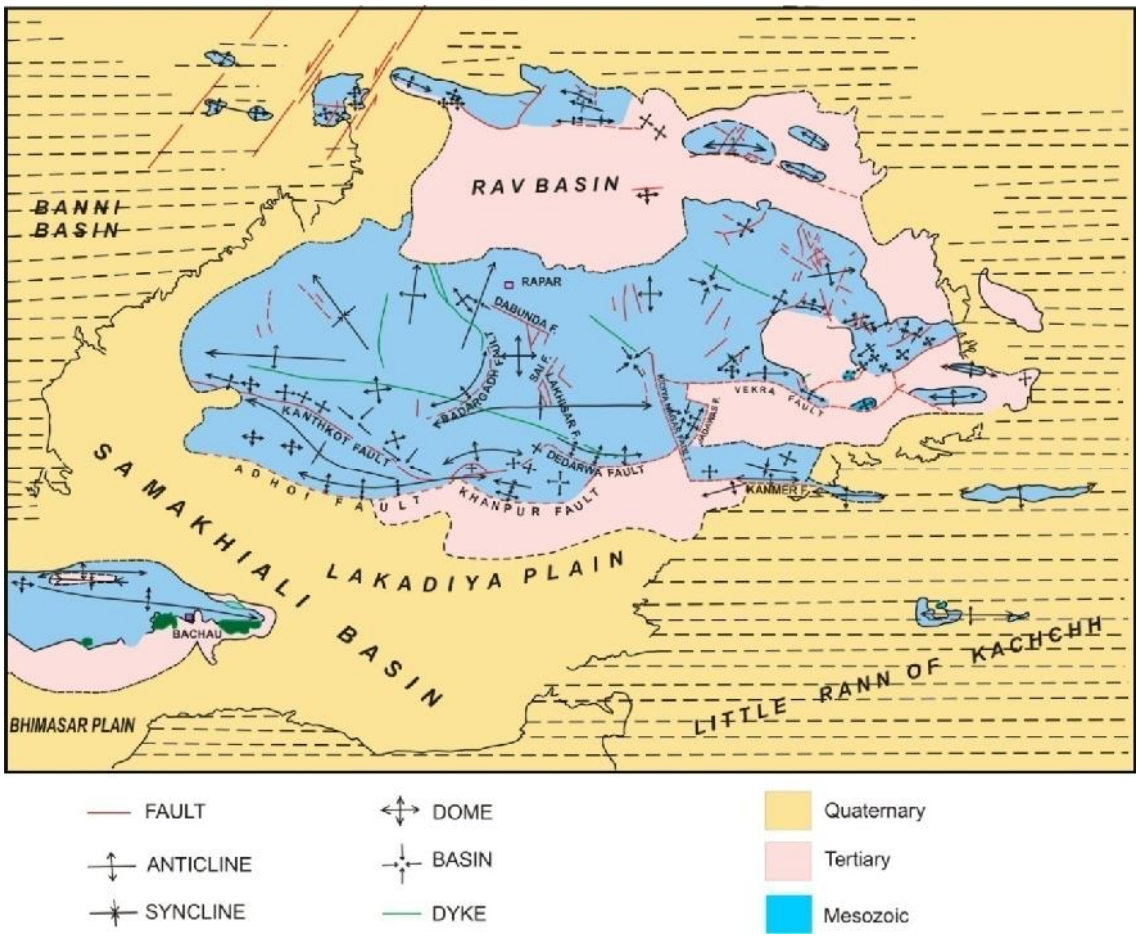

Figure 7.1 Geological map of Wagad region (after Biswas, 1993)

Structurally, the Wagad is a large oval uplift with a central dome and a highly faulted southern part (Fig. 7.1). Unlike the other uplifts which are bounded by one marginal fault accompanied by a flexure, this uplift is not bounded by a single fault or a

marginal monocline. Several concentric, mutually converging, peripheral faults, each accompanied by a flexure parallel to it, present a complicated structural pattern of its southern part which has been uplifted with a northerly tilt. The northern part has been down thrown against the Gedi Fault which separates it from the Bela uplift. This northerly tilt has given rise to the structural low of the Rav Basin. The northerly tilt of Wagad is just opposite of the southerly tilt of the other uplifts. Each individual fault block is similarly oriented giving rise to a series of steps to the north with folds bordering the faulted up edges. Even the smallest fault is accompanied by a fold. All these faults are shattered in the southern half of the uplift and are collectively called as the South Wagad Fault System. The crestal part of the uplift has its own peculiarity. The central Wagad Hills represent the highest elevated part of the domal uplifts bounded by faults. Complementary structural lows are lacking, the domes are juxtaposed by faults. Thus the Wagad uplift is mainly divided into three zones – The Northern Zone, The central Zone and The Southern Zone.

Along the southern margin of Wagad occurs a long narrow hill range running from Mae village in the West, through Adhoi, to Gaun at the eastern tip of the area. This southern marginal range is broken at places by valleys and lowlands to form separate hills, e.g. Wamka Hill, Adhoi Hill, Chitrod Hill, Mewasa Hill, Gagodar Hill and Kanmer-Gon Ridge, form west to east. Further east in the Little Rann, the narrow east-west ridge of Mardak Bet is the eastward extension of this southern range of Wagad. Chitrod Hill shows the highest elevation in this entire range.

THE SOUTH WAGAD FAULT

A complex of idiomorphic folds, mainly domes and brachy anticlines, occurs on the southern part of the Wagad uplift, associated with a system of coalescing and ramifying faults. Several wedges, blocks, horses and troughs have been formed by the intersecting faults within the system (Biswas, 1993). Each of them is featured by a number of folds. The folds are elongated parallel or sub-parallel to the local strike of the accompanying fault. The folds are lined up along a fault on its up throw side even though individually they are variously oriented.

The faults of this zone together comprise the South Wagad Fault system (Fig. 7.1). The fault system consists of peripheral faults having sinuous trends (Biswas, 1993). Though many faults have been described by local names, in general they are parts of two continuous faults which describe broad concentric arcs on the map. The inner arc is represented by Kanthkot, Kharol, Dedarwa and Jadawas faults from the west to the east

(Biswas, 1993). The outer arc of faulting which defines the southern margin of the Wagad uplift, is represented by Adhoi and Khanpar faults. In the central and eastern part of this structural zone, both arcs of faulting converge and bifurcate at different points to give rise to wedge shaped fault blocks. They meet near Wastawa in the middle Wamka in the south-western Wagad and the other between Wastawa and Chitrod in the southern central Wagad. The Chitrod Fault wedge is divided again by a cross fault which bifurcates from the Kanthkot fault of the inner arc near Ghantodia and joins the Khanpar fault of the outer arc with an arcuate trend. This part which is bounded by the Khanpar and Kanthkot faults and Ghantodia cross- fault can be referred to as Wastawa-Ghantodia fault-wedge (Biswas, 1993). The part, to the east of the cross fault, may be referred to as the Chitrod fault block. To the east of Mewasa the two arcs converge finally and only the inner arc continues eastward as Dedarwa fault till it meets the Kidiyanagar cross fault. It continues beyond the Kidiyanagar fault after being off-set by the latter and finally dies off in the Ghanithal low (Biswas, 1993). This part of the fault has been named as the Jadawas fault. Besides these another semicircular fault block occurs to the east of the Wastawa dome. It seems to be a horse of the Kanthkot fault. The sense of movement along all the faults of the South Wagad Fault (SWF) system is the same. Both the peripheral faults have upthrow in the north like pair of step faults. The folds have been produced on the edges of the steps as is the general rule of the region.

A series of small domes and anticlines are seen along the two semi-concentric peripheral faults described above. The folds are closures within the fault flexures like the folds in the flexure zones of the Mainland uplift but they are much narrower and smaller in size, being restricted within one mile wide zones of folding along the bounding faults. Two long flexure zones along the two mutually converging peripheral faults are the main features of this structural zone. The Kanthkot-Dedarwa flexure zone occurs along the inner fault and the Adhoi-Chitrod flexure zone along the outer or marginal fault (Biswas, 1993). As the faults converge and bifurcates the two flexure zones also tend to coalesce and branch off. This has given rise to the intricate fold pattern and peculiar irregular outline to the intervening low. It may be mentioned here that these flexures, like all other flexures, are fault flexures and the flexures and faults mutually replace each other through the continuity of the faults.

The Kharol fault occurs to the northwestern margin of the Chitrod dome. Kharol fault strikes NE-SW with 70^0 dip towards northwest. This fault separates the Chitrod and Wastawa uplifts. Dedarwa fault starts from south of Dedarwa where the Kharol fault ends

and it marks the northern margin of the Chitrod block and to the northeast of the Mewasa it becomes a marginal fault of the Wagad uplift (Biswas, 1993). It is typically an upthrust with steep marginal flexure along the edge of the upthrown block. Vekra fault occurs to the north of the Kanmer fault and trends parallel to it. The strike of this fault is E-W but takes swing to the WNW in the western extremity.

GEOMORPHOLOGY AND QUATERNARY SEDIMENTS

The geomorphic set up of the SWF zone is marked by a comparatively subdued south facing scarp (Fig. 7.2) and, a prominent southward slope developed over the Quaternary sediments in front of the scarps that further merges with the Samakhiali-Lakadia plain. In general, the tectonogeomorphic set up of the SWF zone is a miniaturized version of the KMF zone explained earlier. The south facing scarp is formed over the south facing Mesozoic rocks comprising the steeper southern limbs of the domes that make up the flexure zone on the northern upthrown side of the fault (Biswas, 1993). The scarp is dissected by the streams which originate from the southern limbs and also by streams that flow along the inter-domal saddles and originate on the northern sides of the flexure zone. As mentioned, the scarps show a subdued geomorphic expression. This is mainly because of the Quaternary sediments which show maximum thickness of 8-10 m that overlap the SWF zone and abut against the scarp faces.

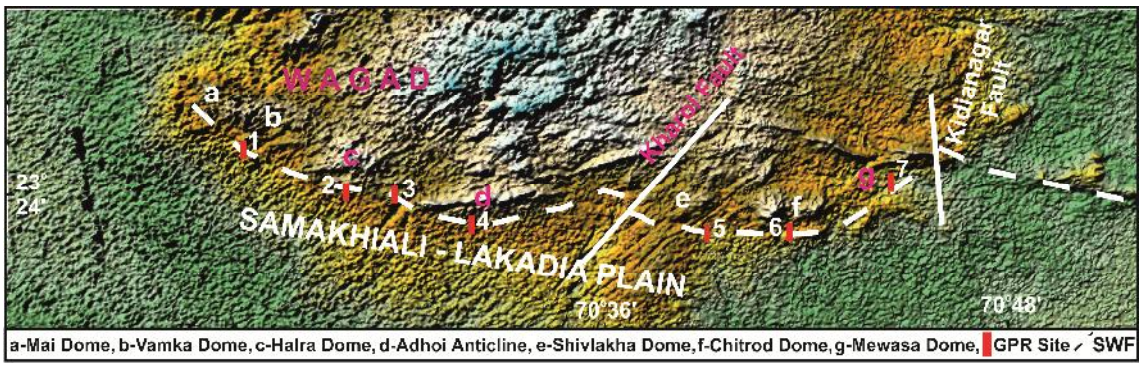

Figure 7.2 DEM of the SWF zone showing the sharp physiographic contrast along the fault. The sites of GPR survey are also shown.

The Quaternary sediments occurring in the SWF zone (Fig. 7.3) consists of mainly miliolites and sandy to gravelly alluvial sediments. All miliolites deposits occurring in the SWF zone are of aeolian origin. The aeolian nature of the deposits is easily recognized owing to the uniform grain size and the prominent south sloping surface developed over them. They show typical morphology of obstacle dunes. The deposition of aeolian miliolites correlates with the rather prolonged regional phase of miliolite deposition documented from various places including the fault zones in Kachchh (Baskaran et al.

1989; Patidar et al. 2007; Chowksey et al. 2011b). However, the deposition of aeolian miliolites is much more extensive in the SWF in comparison to the KHF and KMF zones where they occur in patches. In the SWF zone, the 8-10 m thick obstacle dunes of miliolites are found to continuously occur in front of the scarps from Mae in the west to Chitrod in the east.

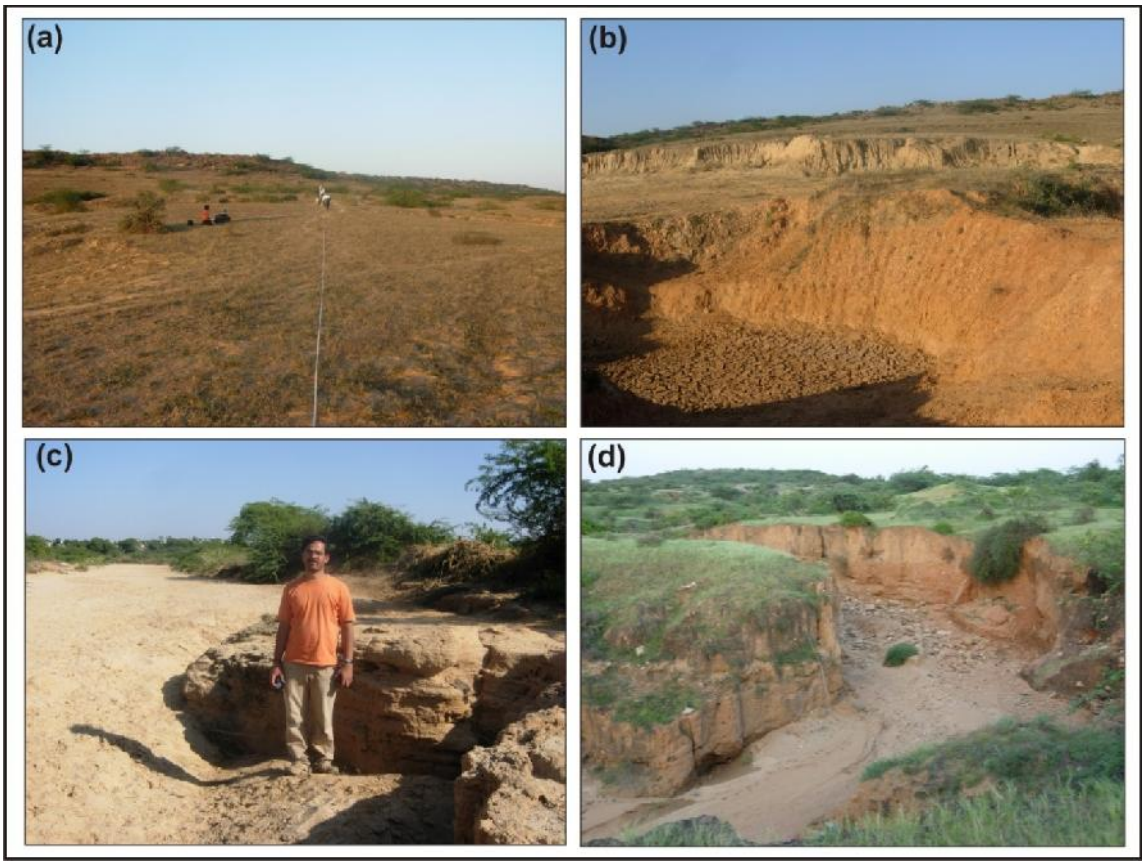

Figure 7.3 (a) North facing view of the surface developed over the Quaternary sediments in the SWF zone to the east of Adhoi. The low ridge at the far end marks the SWF scarp which exposes steeply dipping Mesozoic rocks. **(b)** View of the SWF zone near Adhoi village showing the Tertiary rocks overlain by Quaternary sediments as exposed in a pit in the foreground. The prominent surface abuts upslope with the SWF scarp seen as a low ridge at the far end. **(c)** Upstream view of Adhoi river showing semi-compacted aeolian miliolite exposed in the river bed. **(d)** Upstream view of the incised channel of Kara Vokra river near Halra village in SWF zone exposing Quaternary alluvial deposits. The linear ridge at the far end marks the SWF scarp.

The more extensive deposition of aeolian miliolites in the SWF zone is possibly because of the south facing nature of the scarps which provided the most effective obstruction and site for the miliolite sediments brought by the winds blowing from the south. In contrast, the KHF and the KMF scarps are north facing and therefore received much less aeolian miliolite sediments. The dunal nature of the miliolites appears to have almost overwhelmed the rugged topography and the fault scarps of the SWF zone (Fig.

7.3a, b, c, d). Due to this, the SWF is almost completely buried below the miliolite and alluvial sandy deposits up to the eastern margin of the Chitrod dome near Khanpar. Further east the SWF is exposed in small patches along the incised south flowing streams (Fig. 7.4a, b). The fault is also expressed on the surface as vertical sheared Mesozoic rocks that mark the fault zone (Fig. 7.4c). Prominent knickpoints are also developed along the courses of small streams as they flow across the SWF zone (Fig. 7.4d, e).

Figure 7.4 **(a)** Exposure of the SWF along a stream at the SE margin of the Chitrod dome. Note the almost vertical sheared Mesozoic rocks and the Tertiary rocks exposed in the cliff section on the downstream side. **(b)** Southward view of the dissected topography. The SWF is seen in the foreground. **(c)** Vertical sheared Mesozoic rocks marking the SWF zone. Wamka village is seen in the background. **(d)** Upstream view of the knick point formed along the SWF by a small south flowing stream near Shivlakha **(e)** Narrow chasm carved out by the stream across the knick point shown in d.

PART-C South Wagad Fault (SWF)

The miliolites at places are overlain by unconsolidated alluvial sediments. These sediments are seen in several incised sections of the streams that cut through the SWF zone. Prominent sections exposing the alluvial sediments are observed along the Mae stream and the Kara Vokra river cutting through the southern part of the Halra dome (Fig. 7.3d). The alluvial sediments comprise mostly sands with layers of stratified to massive stream gravels. The alluvial sediments are also found to abut against the scarps comprising Mesozoic rocks.

The drainages arise from the hilly terrain of the South Wagad hills (Fig. 7.5). The Kanthkot hills, Kharoi ridge, Adhoi anticline, various domes such as Mae, Wamka, Halra strongly controls the drainage pattern in the region. The low lying areas such as Gamdau valley, Samakhiali-Lakadia plains also plays significant role in the drainage development in the region. The overall drainage pattern shows a remarkable correspondence with the lows and highs of the South Wagad Flexure zone suggesting a strong structural control.

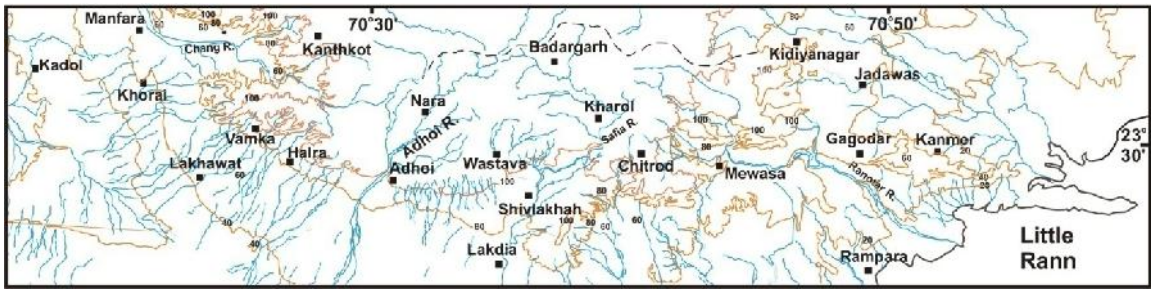

Figure 7.5 Drainage map of the SWF zone.

The major stream flow direction is southward and majority of them debouch into the Gulf of Kachchh. The radial drainage pattern is observed along the domal structures of the region such as Mae, Wamka, Halra etc. To the north of these domes the Chang River flows between two major east-west trending highlands, namely Kanthkot flexure zone to the northern and Southern flexure zone to southern side. The river flows through roughly ESE-WSW and E-W trending highlands which are structurally complex zones. Most of the streams form 2-8 m deep and narrow incised channels in the SWF and broad branching channels in the Samakhiali-Lakadia plain. The drainages in these plains show several drainage anomalies which are described in the next chapter. The drainages arising from the Mae dome take westward swing to meet the westward flowing Khari Vokra river in the Samakhiali-Lakadia plain. The southern limb of the Adhoi anticline shows several parallel streams which abruptly disappear in the Samakhiali-Lakadia plain.

PART-C South Wagad Fault (SWF)

GPR DATA ACQUISITION

The principle and methodology used during the acquisition of the GPR data are explained in details in the Appendix. The importance of GPR studies in active fault zones and interpretation of faults in GPR data is described in Part-A. The main purpose of the GPR surveys in the SWF zone was to identify the near surface trace and delineate the shallow subsurface nature of the SWF. The profiles during the present study were collected by both shielded (monostatic) and unshielded (bistatic) antennas. The shielded antenna used during the present study comprises of a monostatic antenna with a central frequency of 200 MHz on the other hand unshielded antennas used during the present study had a central frequency of 40 and 80 MHz. Data was acquired in a continuous mode by using a monostatic antenna while point mode method of acquisition was used for bistatic antennas. Profiles were recorded in a laptop computer which is connected to the main unit. Initial several profiles were acquired to set the desired parameters. The time window of 140-150 ns was found sufficient to serve the purpose of our study while using 200 MHz monostatic antenna. And for bistatic antenna a time window of 250 ns for 80 MHz antenna and a time window of 500 ns for 40 MHz antenna were used. Auto gain with 5 was used during acquisition. It is followed by post acquisition processing of raw data which includes the distance normalization, noise filtering, surface correction followed by gain. The multiple offset profiles were collected at several sites in order to calculate the precise depth of our investigation. Common Mid Point (CMP) analysis was used to calculate the velocity of wave during its propagation in the ground which helps in calculating the dielectric constant of the ground. Velocity of 0.12 m/ns was calculated from the CMP analysis which is used for time- depth conversion.

Velocity Analysis

The velocity analysis was carried out by using MLF antennas at several locations. This type of analysis generally helps in determining the depth of investigation. The detailed methodology used is described in the Appendix part. The obtained value of velocity from the survey was then applied on each profile to calculate the precise depth of subsurface anomalies. Velocity profiles were collected at different locations in order to calculate the average velocity. The representative profile is shown in Fig. 7.6 which is acquired by 80 MHz bistatic antenna near Mewasa. The initial separation between the two antennas was 1.25 m and a step size of 0.25 m was used. The velocity analysis was carried out with the help of RADAN software which computes the velocity by plotting the multi offset data on graph of velocity verses two way zero offset travel time. The

value of the velocity was later used to calculate the dielectric constant by using the formula given in the Appendix. Average velocity obtained from the velocity analysis is 0.12 which gives a relative dielectric permittivity of 5.76.

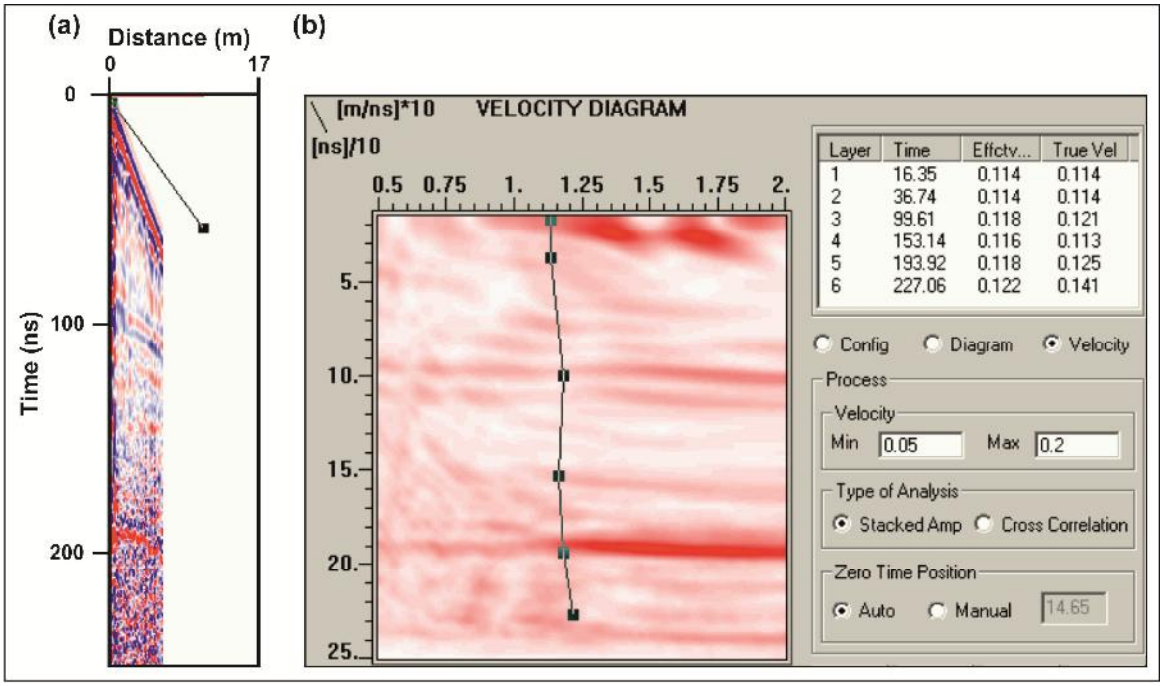

Figure 7.6 (a) Processed CMP profile recorded near Mewasa **(b)** Velocity diagram of the CMP profile shown in (a).

Near surface trace of SWF

The structural set up and neotectonic setting of the SWF is given at the beginning of this chapter. The fault is exposed in patches in the eastern part while in the western and central parts it is buried under a thick apron of Quaternary sediments (Fig. 7.4a, b). Field observations were made during traverses along the south flowing streams to narrow down the fault zone based on the rocks and sediments exposed in the cliff sections. However, since the fault zone is almost completely buried, the interpretation of GPR data was based on the nature of SWF as exposed in the eastern part. It was found that the SWF marked a faulted lithotectonic contact between the Mesozoic rocks to the north and the Tertiary (Neogene) rocks to the south (Fig. 7.4a, b). The Mesozoic rocks assumed vertical to steep southward dips in the fault zone. The setting was found to be similar to the KMF with reversed directions of down throw. The Mesozoic rock are compacted sandstone mostly belonging to the Wagad Formation while the Tertiary rock consist of Chhasra Formation and are softer in nature as they are dominated by clays. The Tertiary rocks show steep to vertical dips near the fault zone while they are almost horizontal in the Samakhiali-Lakadia plain in the south.

PART-C South Wagad Fault (SWF)

GPR studies

The GPR surveys were concentrated in the central and western part where the fault zone of the SWF is buried under thick Quaternary miliolite and alluvial deposits. The GPR profiles included here were acquired at seven sites. All sites were selected after intensive field studies. The interpretations are based on the observations made during the field studies.

Site I

This site is located to the east of Wamka village at the southern fringe of the Wamka dome (Fig. 7.2). The site is located close to a stream that dissects the central part of the dome and flows southward. The site was selected as the possible fault zone of the SWF based on the small outcrops of the steeply dipping Mesozoic rocks jutting out of the gently undulating ground. Several N-S profiles were acquired across the general E-W trend of the fault. The best of the profile after the processing were considered for interpretation (Fig. 7.7a). The profile was taken with the help of 200 MHz monostatic antenna in a continuous mode.

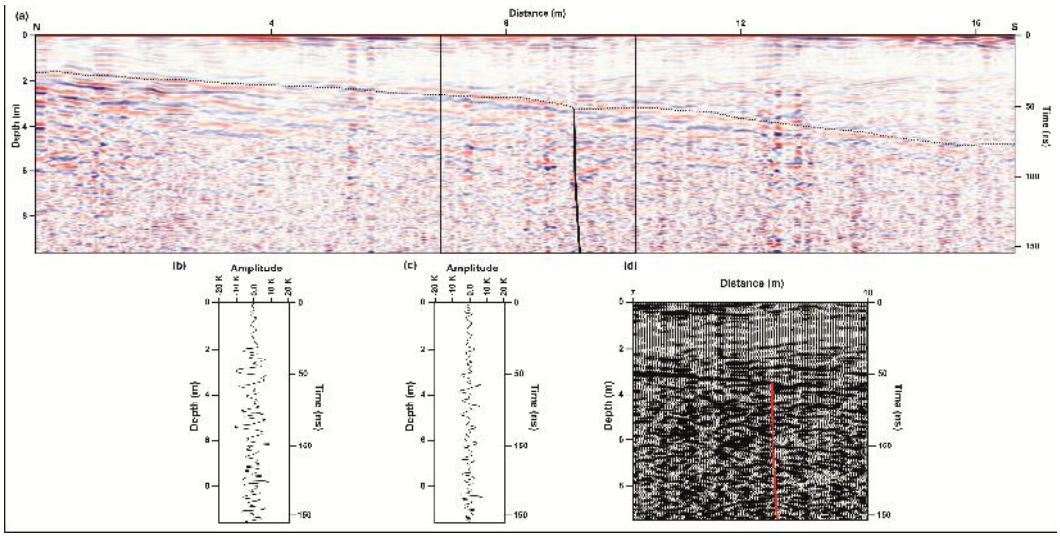

Figure 7.7 (a) GPR profile obtained from east of Wamka village with 200 MHz antenna, location of site is shown in Fig. 7.2. Note the strong reflections emanating from the fault plane. **(b)** Oscilloscope of a single scan emanating from of the Mesozoic rocks **(c)** Oscilloscope of a single scan emanating from of the Tertiary rocks. **(d)** The boxed portion of (a) is shown in a Wiggle mode.

The profile shown is a 17 m part of a long GPR profile. The top portion of the profile is characterized by high amplitude continuous to wavy reflection which denotes the Quaternary sediments deposited by the nearby channel. The thickness of the Quaternary sediments is found to increase southward and it attains a thickness of around ~4m at the southern margin of the profile. The Quaternary sediments are easily

distinguishable with the underlying radar reflections. A distinguishable radar reflection is seen at the base of Quaternary sediments. The basement is characterized by high amplitude, broader radar reflection and low amplitude radar reflections which are thin and chaotic. The variation in the amplitude of high amplitude and low amplitude reflection is clear from the amplitude traces (Fig. 7.7b and c). Based on the field setting of the SWF zone, the high amplitude radar reflection are interpreted as indicating the compacted Mesozoic rocks in which the high amplitude reflection is on account of less energy loss during its propagation while the low amplitude reflection is on account of the clayey rich Tertiary rock which acts as a highly conductive medium resulting in the attenuation of the energy during transmission. The truncation of the two distinct radar reflections is seen at a distance of ~9m which characterizes the faulted contact of Mesozoic and Tertiary rocks (Fig. 7.5a and d). The South Wagad Fault (SWF) from the profile can be characterized as a south dipping near vertical reverse fault.

Site II

This site is located at the southern margin of the Halra dome at about 2 kms east of Halra village (Fig. 7.2). The southern limb of the Halra dome is steep and forms prominent geomorphic expression of the SWF in the form of south facing scarps. Several N-S profiles were acquired with the help of 40 MHz bistatic antenna (Fig. 7.8). The separation between the two antenna during the acquisition were kept 2.25 m with a step size of 25 cms.

The top portion in the profile in the central part of the profile is characterized by a thin continuous horizontal reflectors which is on account of scree material generally deposits over slope (Fig. 7.8a). Below it the reflection in the northern margin is characterized by the broader and continuous of relatively higher amplitude. On the contrary, the southern margin in the profile shows chaotic reflections which generally occur due to presence of conducting material in the subsurface. The higher amplitude radar reflections are formed on account of the compacted Mesozoic rocks while the chaotic reflections are on account of energy loss due to clayey rich Tertiary rocks. The variation in the amplitudes of radar reflections from the Mesozoic and Tertiary rock is shown in Fig. 7.8b and c. Abrupt truncation of the two different types of radar reflections is noticed at a distance of 34 m in the profile (Fig. 7.8a, and d). The GPR profile shows that the SWF is near vertical fault near the surface that shows marked decrease in the amount of dip at depth with a southward dipping fault plane.

PART-C South Wagad Fault (SWF)

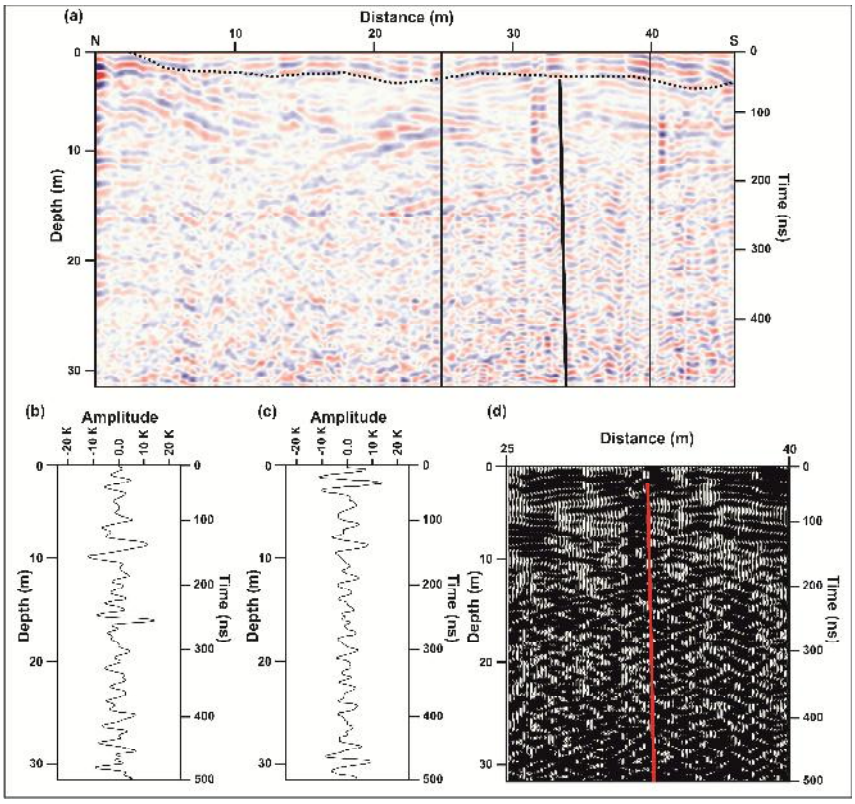

Figure 7.8 (a) GPR profile taken from south of Halra dome with 40 MHz bistatic antenna, location of site is shown in Fig. 7.2. Note the strong reflections emanating from the fault plane. **(b)** Oscilloscope of a single scan emanating from of the Mesozoic rocks **(c)** Oscilloscope of a single scan emanating from of the Tertiary rocks. **(d)** The boxed portion of (a) is shown in a Wiggle mode.

Site-III

The Adhoi anticline is the longest flexure in the entire South Wagad Flexure zone. The Adhoi anticline is characterized by the steeper southern margin which is due to the existence of the SWF in the southern margin. The fault is well exposed near the Adhoi village. Considering that fact we have taken a profile near the bank of Adhoi river lying west of Adhoi town (Fig. 7.2). The profile was acquired by 80 MHz bistatic antenna in point mode along S-N direction.

The upper ~3 m part of the profile is characterized by very high amplitude continuous radar reflections which is generally on account of good low conducting material like sand (Fig. 7. 9a). As the profile is acquired near the right bank of Adhoi river it can be said that the high amplitude reflectors is representing the Quaternary alluvium deposited by the Adhoi river. Below the Quaternary sediments two different radar reflection phases can be identified. The southern margin is characterized by low amplitude reflections and the northern margin is characterized by the high amplitude reflections. Considering the field setting of the region the variation amplitudes of the radar reflections below the Quaternary cover is attributed to lithological contrast. The low

amplitude reflections generally represent the Tertiary rock which is in conformity with the field setting and the high amplitude radar reflection represents the compacted Mesozoic rock (Fig. 7.9b, and c). The truncation of the high amplitude and low amplitude radar reflection is seen at a distance of ~20 m (Fig 7.9a and d). The present GPR study near the Adhoi suggests that the South Wagad Fault is a near vertical fault in the shallow subsurface.

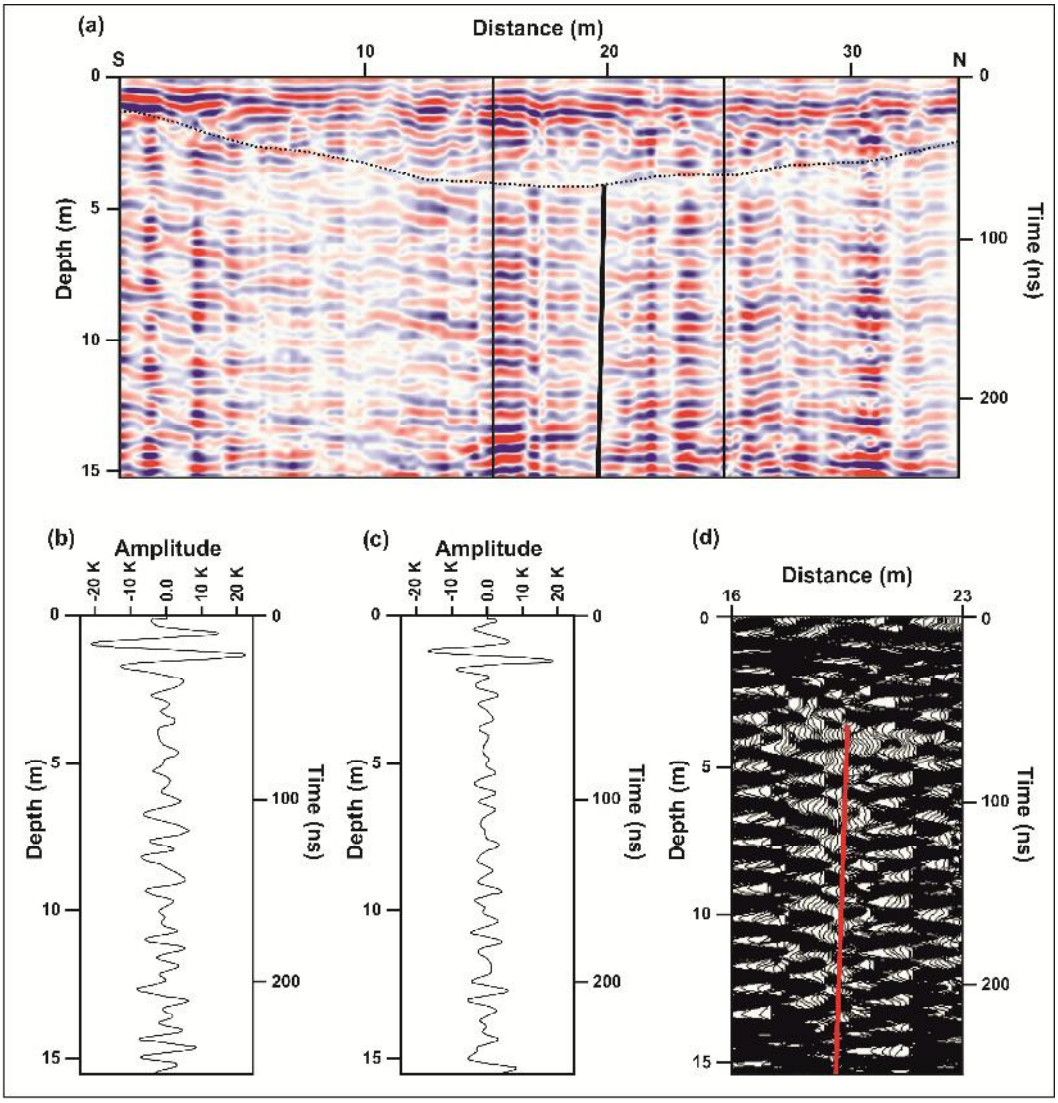

Figure 7.9 (a) GPR profile taken near the bank of Adhoi river with 80 MHz bistatic antenna, location of site is shown in Fig. 7.2. Note the strong reflections emanating from the fault plane. **(b)** Oscilloscope of a single scan emanating from of the Mesozoic rocks **(c)** Oscilloscope of a single scan emanating from of the Tertiary rocks. **(d)** The boxed portion of (a) is shown in a wiggle mode.

Site IV

This site is located about 2 kms to the east of Adhoi town where thick Quaternary deposits abut against the scarp face which comprises steep southward dipping Mesozoic rocks (Fig. 7.2). At the southern edge of the prominent southward sloping surface over the

PART-C South Wagad Fault (SWF)

Quaternary deposits, several man-made pits expose Tertiary rocks which consists of mostly shales and marls. The fault trace is therefore buried below the Quaternary sediments. The N-S profile acquired over the southward sloping surface over the Quaternary sediments with the help of 40 MHz bistatic antenna in point mode is shown in Fig. 7.10a.

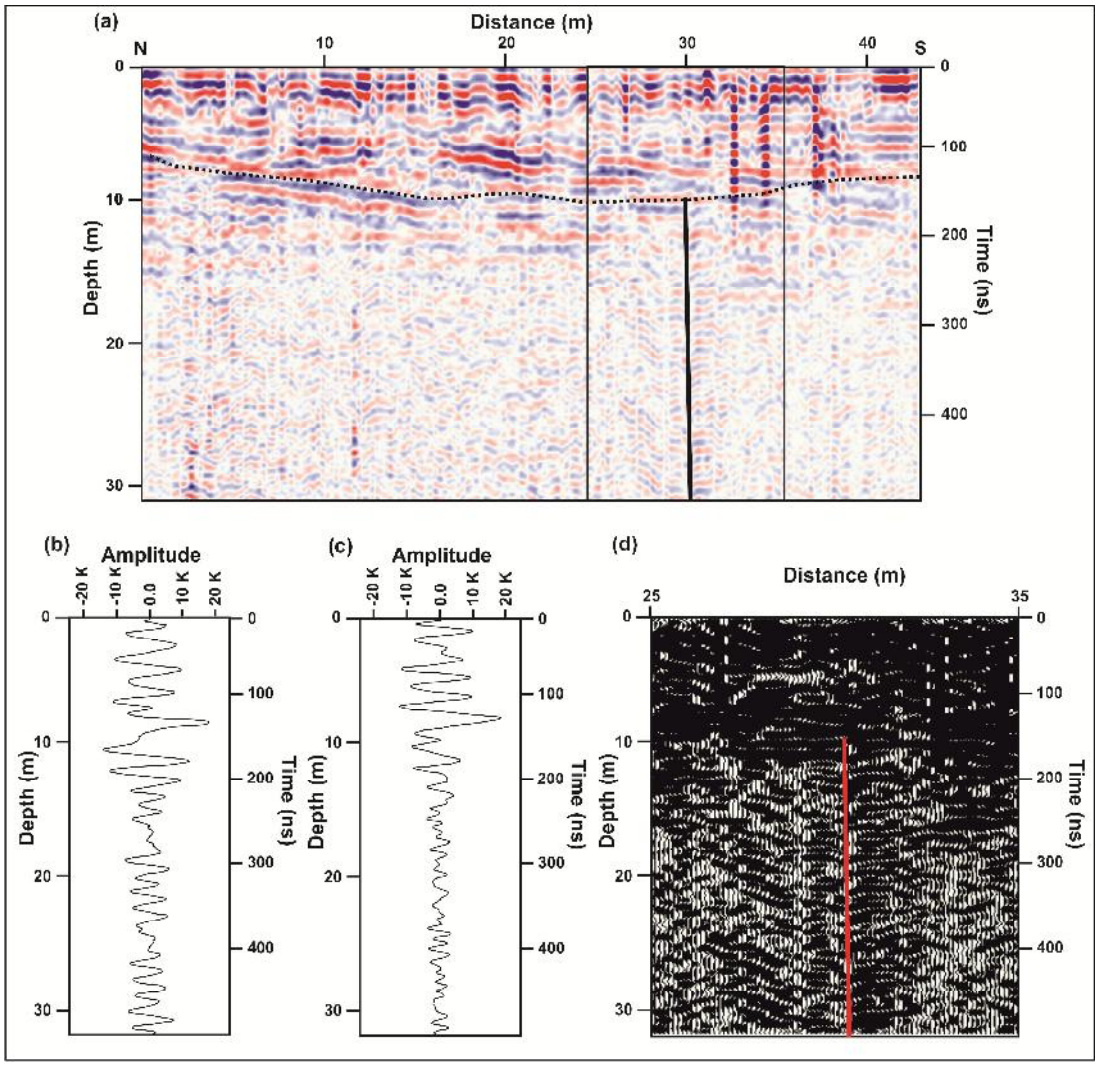

Figure 7.10 (a) GPR profile taken from east of Adhoi town with 40 MHz bistatic antenna, location of site is shown in Fig. 7.2. Note the strong reflections emanating from the fault plane. **(b)** Oscilloscope of a single scan emanating from of the Mesozoic rocks **(c)** Oscilloscope of a single scan emanating from of the Tertiary rocks. **(d)** The boxed portion of (a) is shown in a Wiggle mode.

The initial separation distance between the antenna was kept 2.25 m with the step size of 25 cm. The upper part of the profile is characterized by the high amplitude continuous to high amplitude inclined reflections represent the Miliolite sedimentary cover as observed in the field whose thickness increases upto 7-8 m towards the south. The inclined reflections are attributed to the foresets of the aeolian cross bedding developed in the miliolite deposits. The basal reflections in the profile can be easily

separated out on the basis of variation in the nature of radar reflections. The northern margin below the Quaternary cover is characterized by the high amplitude radar reflection on the contrary the southern margin is characterized by the low amplitude radar reflection pattern. The variation in the amplitude of both reflection is depicted in the Fig. 7.8b and c. The variation in the amplitude from high amplitude to low amplitude in the radar reflection is only possible with the contrasting media property through which the radar wave propagates. Correlating the GPR data with the field observations, the high amplitude reflections are interpreted as the compacted Mesozoic rock while the low amplitude radar reflections are interpreted as the clay rich Tertiary rock. Truncation of high amplitude and low amplitude radar reflections is seen at a distance of ~ 30 m (Fig.7.10a and d). This marks the faulted contact of the Mesozoic and Tertiary which defines the SWF. The shallow subsurface nature of the SWF at this site as reflected in the GPR data is inferred as a nearly vertical fault.

Site V

This site is located at the south of the Shivlakha dome (Fig. 7.2). The transect was located along a south flowing stream that arises nearby but exhibits a spectacular knick point as it flows across the SWF zone. The knick point height is ~4 m and is developed over last outcrop of well compacted Mesozoic sandstones, south of which river enters and incises the Quaternary alluvium of the flat terrain of the Samakhiali-Lakadia plain. The GPR survey was carried out in a barren agricultural field located on the left bank of the stream. The GPR survey was carried out with the help of 80 MHz bistatic antenna in point mode.

The prominent characteristic of the GPR profile is the presence of the high amplitude radar reflection whose thickness increases southward (Fig. 7.11a). This presence of the high amplitude continuous and wavy reflection is in conformity with the presence of Quaternary alluvium at the site. The basement rocks further below are characterized by the presence of thicker continuous reflections along with thin irregular or chaotic radar reflections. As the thicker continuous reflections are located on the northern side of the transect and therefore correspond to compacted Mesozoic rock while the irregular and chaotic reflections in the southern part are on account of Tertiary rocks. The amplitude of Tertiary appears to be relatively more at this site which may be due to the presence of water (Fig.7.11b, and c). The presence of a shallow pool of water at the base of the knick point in the stream confirms this inference. The truncation of the radar

reflections marking the SWF is seen at a distance of ~ 19 m (Fig. 7.11a, d). The fault plane of the SWF at this site is inferred as vertical.

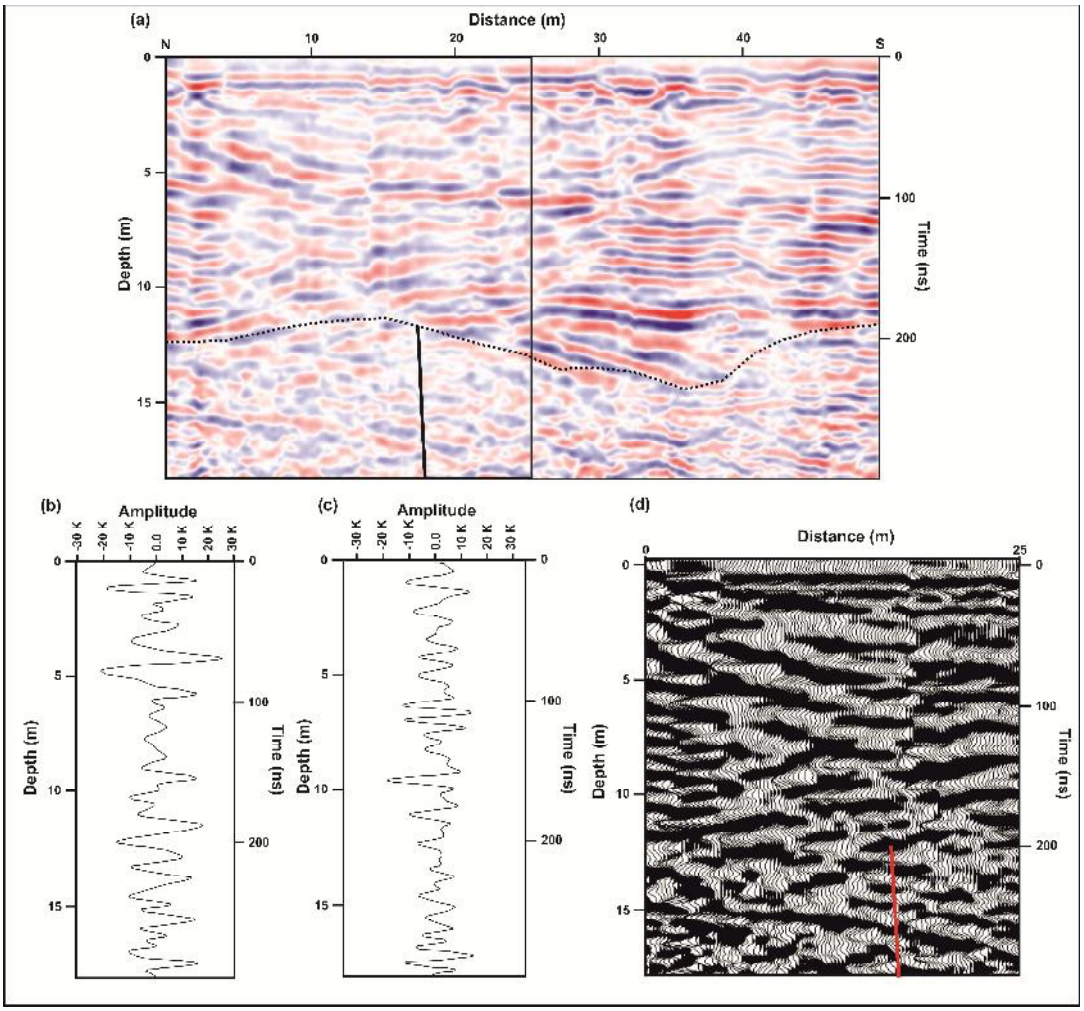

Figure 7.11 (a) GPR profile taken from south of Shivlakha dome with 80 MHz bistatic antenna, location of site is shown in Fig. 7.2. Note the strong reflections emanating from the fault plane. **(b)** Oscilloscope of a single scan emanating from of the Mesozoic rocks **(c)** Oscilloscope of a single scan emanating from of the Tertiary rocks. **(d)** The boxed portion of (a) is shown in a Wiggle mode.

Site VI

This site is located to the south of Chitrod dome. The Chitrod dome is largest of all the domal structures developed along the SWF. The geomorphic setting of the SWF scarp is similar to that at the previous site in the sense that a major part of the scarp face is covered by aeolian miliolite deposits. A prominent southward slope is developed over the surface of the miliolite deposits that is deeply dissected by gullies that further extend southward as steams into the Samakhiali-Lakadia plain. The SWF zone is therefore effectively buried by the Quaternary miliolite deposits. At the southern edge of the slope, Khanpar village is located where the Tertiary rocks are exposed in the ~7 m high vertical

incised cliffs along a sharp entrenched meander of a stream that arises from the scarp face. The N-S profile was acquired with the help of 80 MHz bistatic antenna in a point mode.

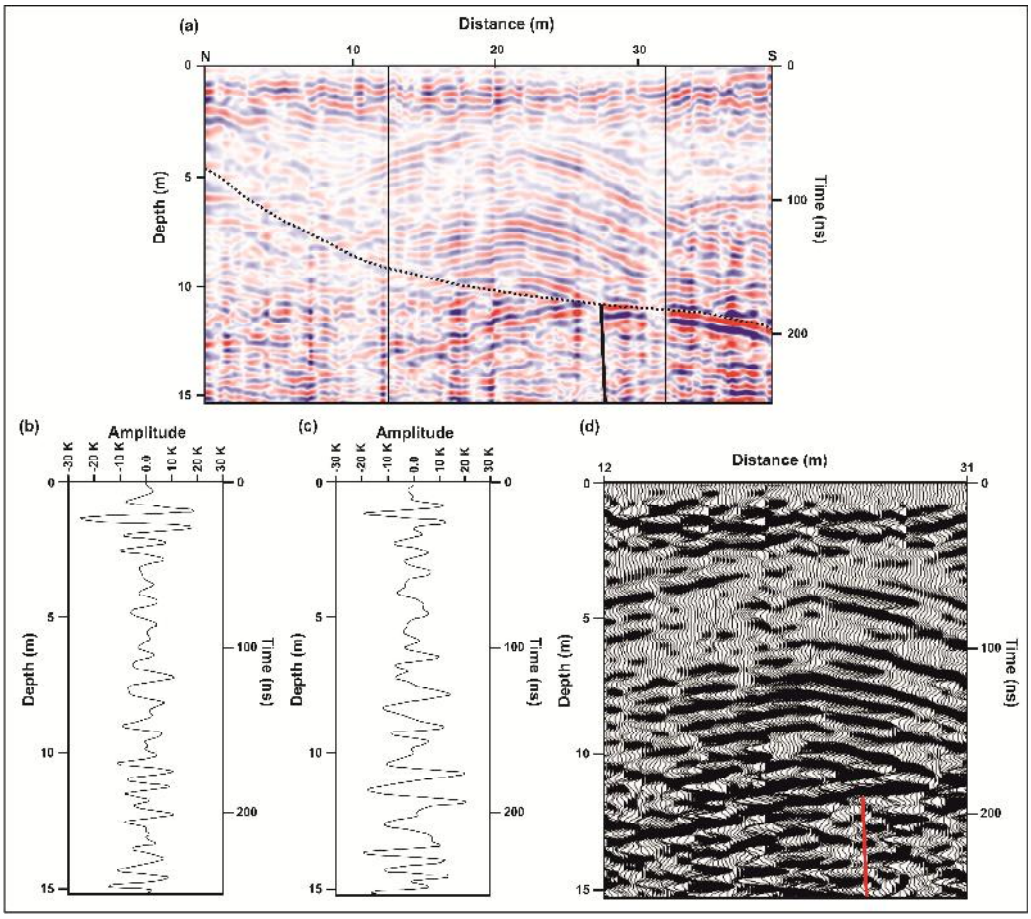

Figure 7.12 (a) GPR profile taken from south of Chitrod dome near Khanpar village with 200 MHz antenna, location of site is shown in Fig. 7.2. Note the strong reflections emanating from the fault plane. **(b)** Oscilloscope of a single scan emanating from of the Mesozoic rocks **(c)** Oscilloscope of a single scan emanating from of the Tertiary rocks. **(d)** The boxed portion of (a) is shown in wiggle mode.

The profile is 40 m long and depicts high amplitude radar reflection (Fig. 7.12a). The northern part in the profile is characterized by 2-3 m thick miliolite deposit over the basement which increased upto 10 m southward. A prominent hyperbolic surface in the upper part is on account of miliolite dune and the radar reflection marks the dunal topography over it lies the horizontal reflections over which the horizontal surface have been developed over which we acquired GPR profile. The upper part reflects the several phase of dunal activity which the area has undergone. The basement in the profile is easily recognized by the amplitude variations Fig. 7.12b and c. The northern part in the profile is characterized by the presence of continuous high to medium amplitude reflectors which is in contrast to the southern lying chaotic reflection. The amplitude variation is on account of lithological contrast. The high amplitude reflection represents the Mesozoic rock while the low amplitude reflection represents the Tertiary rock (Fig. 7.12b and

c). Truncation of the radar reflection is seen at a distance of ~28m (Fig. 7.12a and d). SWF in this segment is characterized by near vertical reverse fault.

Site VII

This site is located in a agricultural field in front of the scarp face of the SWF near Mewasa (Fig. 7.2). The profile was taken perpendicular to the trend of the scarp face. The profile shown in the Fig. 7.13a was acquired with 80 MHz bistatic antenna in point mode.

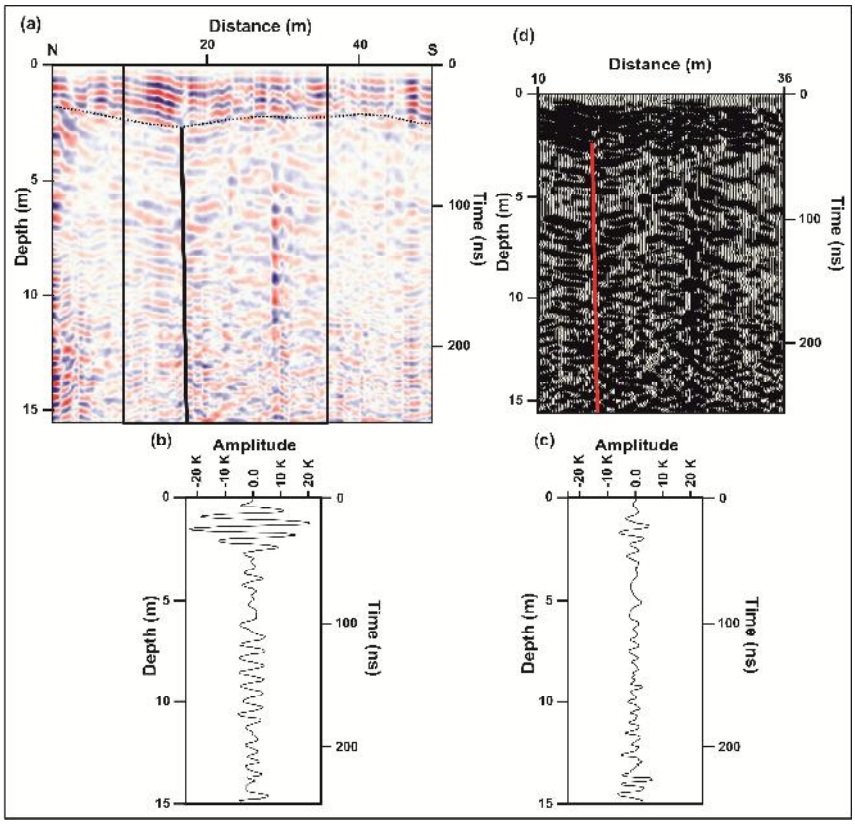

Figure 7.13 (a) GPR profile taken near Mewasa with 80 MHz monostatic antenna, location of site is shown in Fig. 7.2. Note the strong reflections emanating from the fault plane. **(b)** Oscilloscope of a single scan emanating from of the Mesozoic rocks **(c)** Oscilloscope of a single scan emanating from of the Tertiary rocks. **(d)** The boxed portion of (a) is shown in a Wiggle mode.

The profile in the upper part comprises of continuous high amplitude reflections whose thickness varies from 2 to 3m. These high amplitude reflections are from the alluvium cover over basement rocks in the shallow subsurface. The basement rocks are represented by high amplitude and low amplitude radar reflections. The high amplitude reflections lie close to the proximity of the Mesozoic ridge lying in the north thus represents the Mesozoic rocks. The contrasting low amplitude radar reflections in the southern part of the profile represent the clay rich Tertiary rocks (Fig. 7.13b and c). A sharp truncation in the reflection pattern is seen at a distance of ~19 m (Fig. 7.13a and d. This truncation of the radar reflection represents the SWF fault plane which is interpreted as a vertical fault at this site.

CHAPTER 8

TECTONIC GEOMORPHOLOGY OF THE SAMAKHIALI-LAKADIA PLAIN

The post-2001 seismotectonic studies in Kachchh have concluded that the region between the Samakhiali-Lakadia plain bounded by the E-W trending Kachchh Mainland Fault (KMF) and South Wagad Fault (SWF) is the most stressed part of the basin as the epicenter lies in this region (Biswas and Khattri, 2002). The area to the east of KMF and to the south of SWF and extending up to the Gulf of Kachchh and Little Rann comprises a gently undulating plain termed as the Samakhiali-Lakadia plain. Geologically, the area of the Samakhiali-Lakadia plain is composed of Tertiary sediments with a thin cover of Quaternary sediments. The plains abut against the Southern Wagad hills and the rocky terrain of the mainland to the east, both of which expose Mesozoic rocks. The southeastern and southern boundaries of the plains are marked by the Little Rann and Gulf of Kachchh respectively. In the present study a detailed geomorphic characterization of the Samakhiali-Lakadia plain was carried to delineate the neotectonic deformation as a consequence of the compressive stresses accumulation and its periodic release along two faults i.e. the KMF and the SWF. Since the Samakhiali-Lakadia plain comprises a south sloping plain visible geomorphic effects neotectonic activity are not readily visible. In view this, a detailed qualitative and quantitative geomorphic analysis of the Samakhiali-Lakadia plain was done using remote sensing and GIS technique to delineate the pattern of ongoing neotectonic deformation in the context of contemporary seismotectonic setting. The studies included detailed field observations, particularly of the drainages, and documentation of exposed Quaternary sediments. The study compliments the field and GPR based investigations along the causative faults, the KMF and SWF described in previous chapters. In the present chapter, the data generated on tectonic geomorphology of the Samakhiali-Lakadia plain is discussed while the quantitative geomorphic analysis using remote sensing and GIS analysis is included in the next chapter.

LANDSCAPE CHARACTERISTICS

Overall the Samakhiali-Lakadia plain is a gently undulating terrain with a general southward slope. The contour map clearly brings out the salient terrain characteristics of the plains (Fig. 8.1). In general, the slope of the western part of the plain is gentle while

the slope in the eastern part if steeper. This can be observed by the closely spaced contours in the eastern part. Moreover, anomalous slopes are also observed in the plains. For descriptive purpose, the study area is divided into two parts- the western part is termed as the Samakhiali plain while the eastern part is termed as the Lakadia plain.

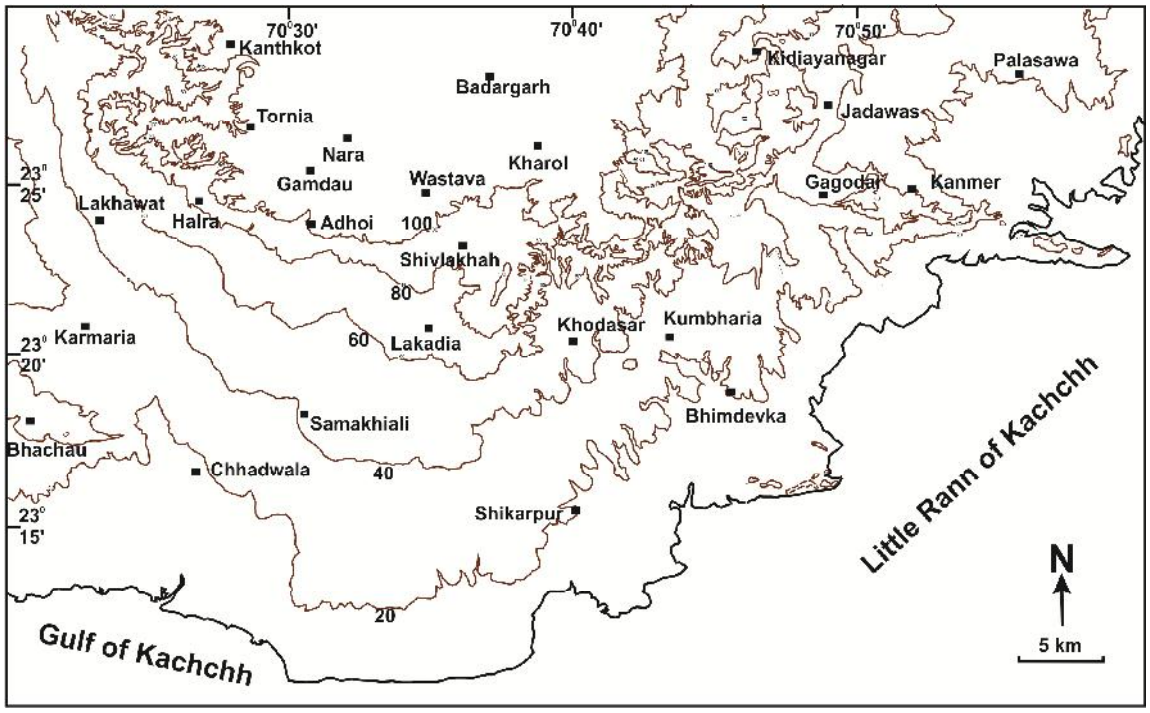

Figure 8.1 Contour map of Samakhiali-Lakadia plain. Note the wider spacing of contours in the eastern part (Samakhiali plain) indicating gentle slope and relatively closely spaced contours in the western part (Lakadia plain) indicating steeper slope.

The Samakhiali plain

The Samakhiali plain extends from the edge of the mainland Kachchh in the west to the Lakadia in the east. The northern portion of the Samakhiali plain is marked by the series of domes viz. Mae to the westernmost part and Vamka, Halra dome to the east and also Adhoi anticlinal ridge to the easternmost side of the plain. The structure of the northern part of the Samakhiali plain is controlled by the SWF and the KMF. In this part, it forms a graben structure between the SWF in the north and KMF in the south. The graben is believed to be under a state of high stress as evidenced by the 2001 Bhuj earthquake which occurred in this region and the aftershocks that followed the main shock. The KMF ridge abruptly ends to the east of Devisar. However, it appears that the ridge continues in the subsurface further eastward. The topographic profiles across the Samakhiali plain clearly bring out the topographic high indicating the continuation of KMF ridge in the subsurface (Fig. 8.2). Seismic activity suggests that the ridge may be rising up in response to the compressive stresses accumulating in the region. Further

westward the Samakhiali plain is characterized by long gentle slopes upto the coastline in the south. However, anomalous slopes are seen in the central part of the plain where the drainages appear to get disrupted. This is clearly seen in the Kara Vokra basin and the Adhoi basin and is described later in the chapter. This suggested a zone of gentle upwarping of the surface trending in E-W direction. This zone is in continuity of the KMF ridge. This suggests rise of KMF ridge in the subsurface. In the field this zone appears as a broad and gentle convex up E-W trending linear topographic high.

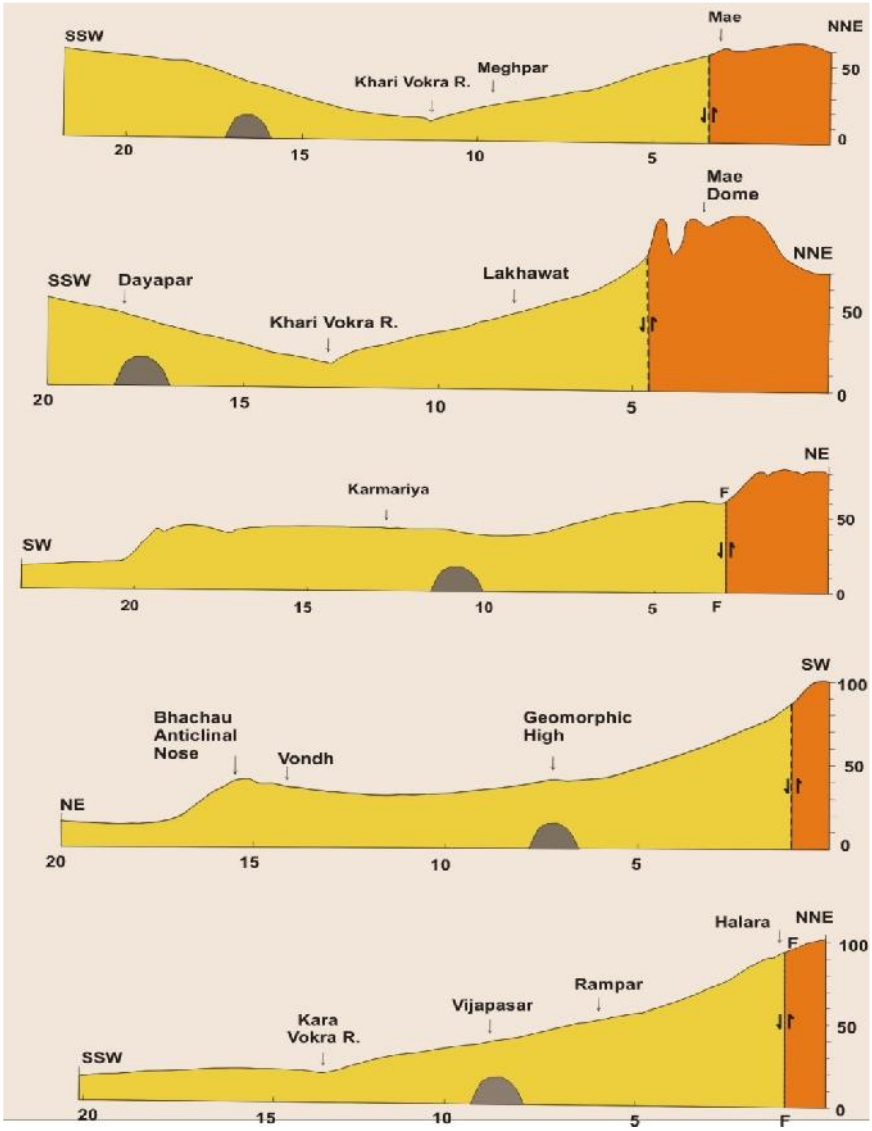

Figure 8.2 N-S topographic sections across Samakhiali plain showing the subtle geomorphic high in response to the rising KMF ridge in the subsurface.

The Lakadia plain

The eastern part of the study area is termed as the Lakadia plain. The general slope of the area is towards south and southeast. The slope of the Lakadia plain is steeper than the Samakhiali plain as observed in the closely spaced nature of the contours. The

topographic sections of Lakadia plain show a E-W trending zone of geomorphic high (Fig. 8.3) which is in continuation of similar feature observed in Samakhiali plain.

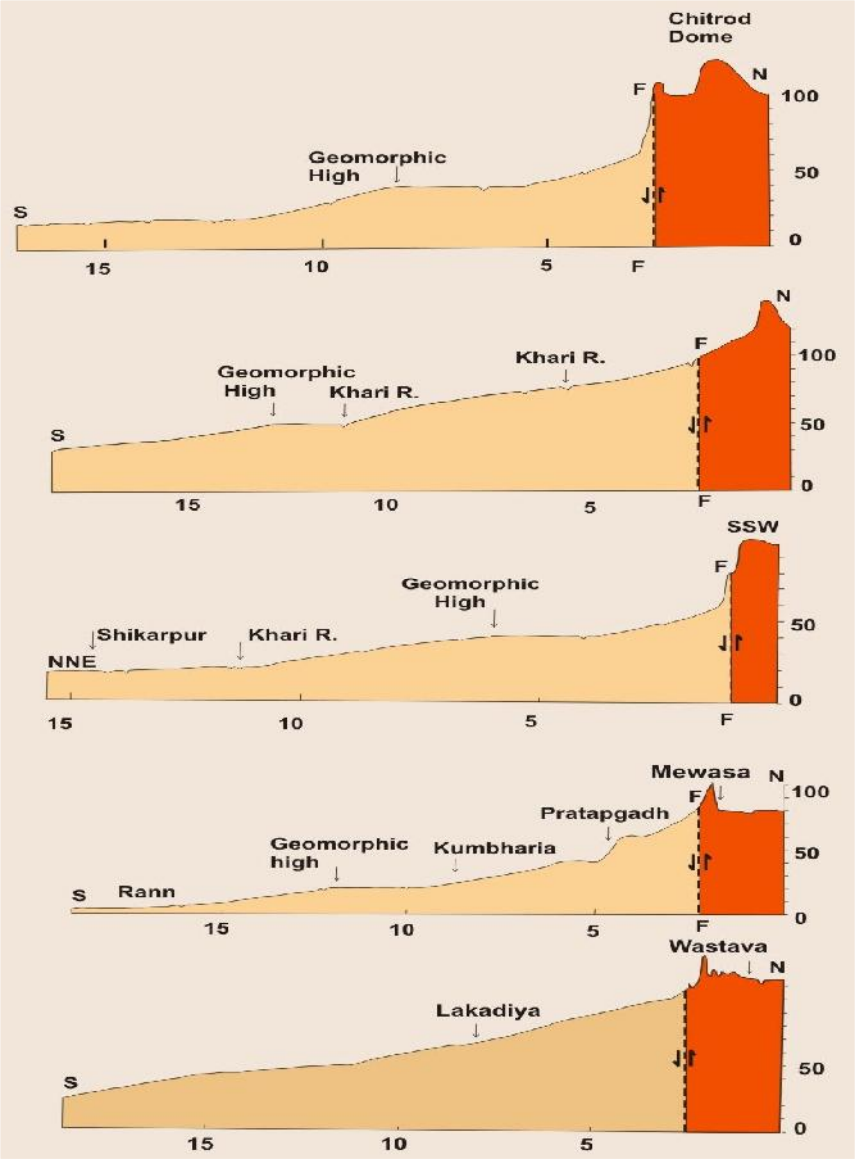

Figure 8.3 N-S topographic profiles across the Lakadia Plain.

A significant characteristic of the Lakadia plain is the existence of a well entrenched deeply incised drainage which is in contrast with the Samakhiali plain where the drainage lines are disrupted and show shallow channels. The topography of this part is also more than rugged especially the northern part adjacent to the SWF. A conspicuous NNE-SSW trending geomorphic high is present to the east of the Khari river in the northern part of the plain. The geomorphic high consists of upper Tertiary rocks and attains an elevation of more than 80 amsl. This geomorphic high controls the channel of Khari river near Lakadia. The geomorphic high has resulted in the development of radial drainage locally. The trend of the geomorphic high correlates with the transverse Kharol

fault mapped in the Mesozoic rocks in south Wagad hills. The southward extension of this fault appears to match with the western fringe of the geomorphic high. The geomorphic high therefore suggests that the Kharol fault possibly extends into the Lakadia plain below the Tertiary rocks and neotectonic movement along this fault may have resulted in the formation of this geomorphic high.

DRAINAGE CHARACTERISTICS

The Samakhiali-Lakadia plain in general comprises south flowing drainages (Fig. 8.4). All the rivers of Samakhiali-Lakadia plain are ephemeral, as runoff is dependent upon the precipitation, which is controlled by the present hyper arid climate. The rivers are mostly southward flowing and debouching into the Gulf of Kachchh and Little Rann of Kachchh in the Eastern part, and into the Great Rann in the NW part (Fig. 8.5). The various rivers arise in the south Wagad hills and flow southwards to meet the Gulf of Kachchh and the Little Rann in the south east. In the Wagad hills the drainage is dendritic to radial and is dominantly controlled by the domal and anticlinal flexures. However, the drainage pattern in the Samakhiali-Lakadia plain is characterized by parallel drainage.

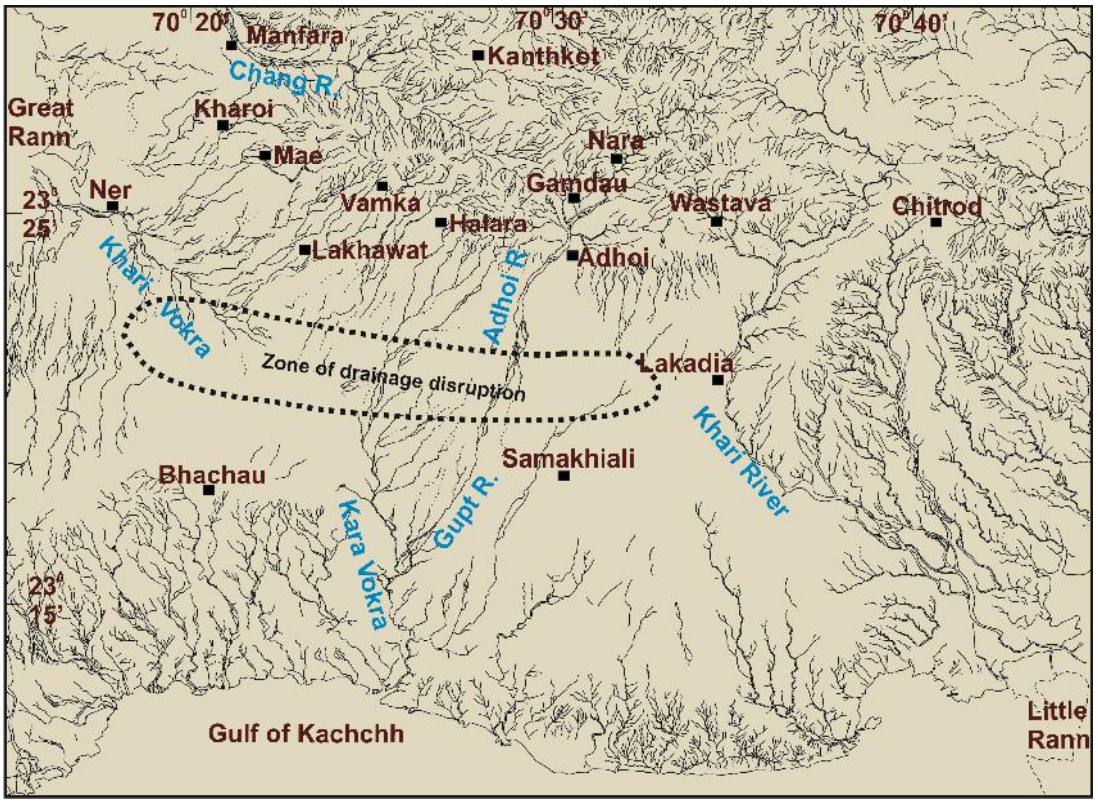

Figure 8.4 Drainage map of Samakhiali-Lakadia plain. The E-W trending zone of drainage disruption in Samakhiali plain is also shown.

The drainage in the Samakhiali-Lakadia plain is divisible into several distinct basins which show great diversity in terms of fluvial geomorphology and pattern. Major

drainage basins of the area include the Adhoi, Khari, Kara Vokra and Khari Vokra basins (Fig. 8.4). The area is divisible into two distinct morphotectonic domains- the western Samakhiali plain and the eastern Lakadia plain. The drainages of both these domain show several characteristics that are in complete contrast with each other. The rivers of Samakhiali plain are characterized by discontinuous shallow channels with low incision and a distinct zone of disruption (Fig. 8.4). However, the rivers of Lakadia plain exhibit well entrenched incised and consistent channels (Fig. 8.4). In addition, several other drainage anomalies are present which are unique to each of these morphotectonic domains.

The Samakhiali plain

The Samakhiali plain shows typical parallel drainage with dendritic pattern in some parts. Most of the drainages after arising from the south Wagad hills meet the Gulf of Kachchh in the south. Some drainage arise from the Bhachau anticlinal ridge and flow south wards while some drainages arise from the central part of the plain and flow southwards. The Khari Vokra river arises from the western part of the Wagad hills and flows westward to meet the Banni-Great Rann basin (Fig. 8.4). Apart from these there are several isolated areas of no drainage in the plain (Fig. 8.4).

Geomorphologically, the northwestern part of the plain between the SWF and the KMF is an area with low relief. Moderately steep southward slope is observed from the SWF ridge in the north while a similar moderately steep northward slope as a consequence of the KMF ridge is observed. These two slopes converge forming a local E-W trending depression at the centre of the graben near Kunjisar (Fig. 8.2). Small drainages from the KMF ridge and the SWF ridge flow towards the centre of the graben which is occupied by the he Khari Vokra river that flows westward to meet the Banni-Great Rann basin (Fig. 8.4a, and b). The river exposes Tertiary rocks with a thin cover of alluvium that thickens towards north and south. The Khari Vokra river is an exception in the sense that it arises from the south Wagad hills and flows westward whereas the other drainages of Samakhiali plain also arise from the south Wagad hills but these flow southwards to meet the Gulf of Kachchh (Fig. 8.4). The anomalous drainage of the Khari Vokra river is attributed to the graben structure between the KMF and SWF.

Further eastward lies the Kara Vokra and Adhoi river basins. These arise in the south Wagad hills and flow southward to meet the Gulf of Kachchh. Both rivers show a consistent channel with 3-5 m deep incised channel in the northern part of the plain. The Kara Vokra river shows anabranching pattern in the central part. However, both rivers

almost disappear in the central part of the plain. The channels become broad and shallow which are almost indistinguishable from the surrounding plain (Fig. 8.4c). However, further south, the channels again reappear and continue up to the Gulf of Kachchh forming estuarine mouths. The disappearance of the river channels and their reappearance with consistent 2-3 m incised channels with same orientation and alignment clearly indicates that the drainages get disrupted in the central part of the Samakhiali plain (Fig. 8.4). The reappeared Adhoi river channel in the southern part of the channel is known as the Gupt river (Fig. 8.6d, e, f). The Kara Vokra river after its reappearance joins the Gupt river. Several drainages originate from the Bhachau ridge and flow in south direction giving rise to parallel drainage pattern. However, the area to the north of the ridge is an area of no drainage.

The disruption of the drainage and its reestablishment strongly points towards the presence of an E-W trending geomorphic high in the central part of the Samakhiali plain. The geomorphic high appears to have formed due to the upwarping of the Tertiary rocks due to the rise of the KMF in the subsurface in response to prevailing compressive stresses in the region. The presence of a geomorphic high in the central part of the plain is further evidenced by the several streams which arise suddenly and flow southward. Moreover, the area to the west of Kara Vokra basin and the Adhoi basin is an area which totally devoid of drainage lines. Several streams arise from the SWF zone between Adhoi and Wastawa which get disrupted before they reach the central part of the Samakhiali plain (Fig. 8.4).

All these evidences clearly point to neotectonic upwarping of Tertiary rocks in E-W direction in the central part of the Samakhiali plain. The upwarped region passes through Sikra, Karmariya, Vondhada, Vijapasar, and east of Gharana. The geomorphic high lies in continuity of the KMF ridge to the west of the Samakhiali plain. This suggests that the KMF ridge may be extending below the plain whose active nature may be responsible for the upwarping of the surface and the attendant drainage disruption. The upwarping is also responsible for the westward oriented course of the Khari Vokra river which meets the Banni-Great Rann basin to the northwest of the Samakhiali plain.

The Lakadia plain

The Lakadia plain is in complete contrast with that of the Samakhiali plain as they show consistent and deeply incised channels (Fig. 8.6). The Khari river is the largest river in the plain with several others viz. the Khodasar and Khanpar streams to the east of it. All rivers originate in the south Wagad hills flow in S to SSE direction to meet the Little

Rann. The various rivers show prominent knick points as they cut across the SWF and flow south into the plain. In general, the rivers of the Lakadia plain show parallel drainage pattern and are deeply incised (Fig. 8.4).

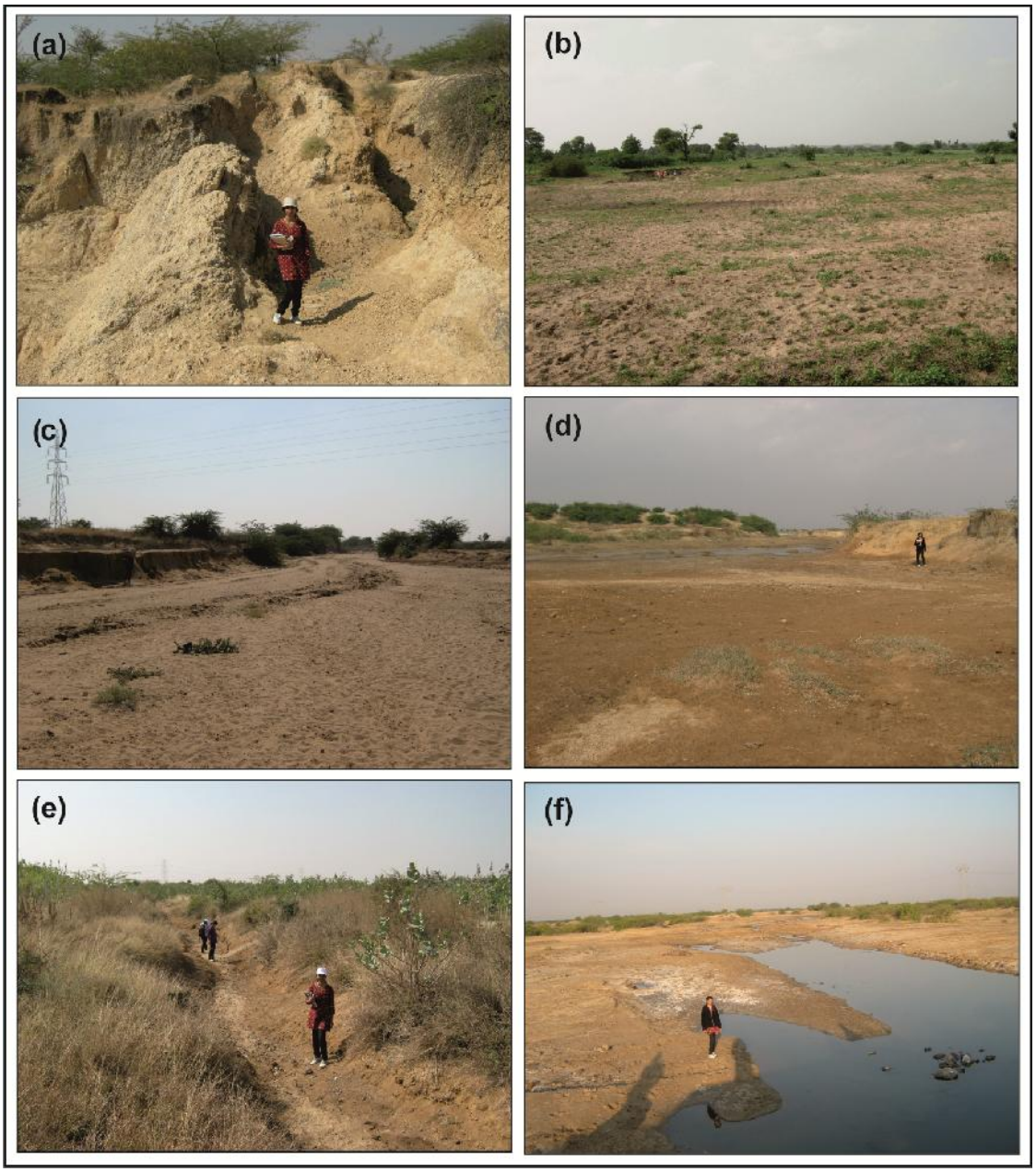

Figure 8.5 (a) View of the steeply dipping Mesozoic rocks in the SWF zone. **(b)** View of broad indistinct channel of the Adhoi river in the zone of disruption. **(c)** Upstream view of the well defined channel with incised cliffs of the Adhoi river in the upstream part. **(d)** Upstream view of the channel of Adhoi river (Gupt river) near Chhadwala to the south of zone of disruption where the channel is again reappears. **(e)** View of the straight and narrow channel of the Kara Vokra river in the zone of disruption. **(f)** View of the shallow broad channel of the Khari Vokra river which flows westward through the central part of the Samakhiali graben.

PART-D Surface deformation related to KMF-SWF interaction

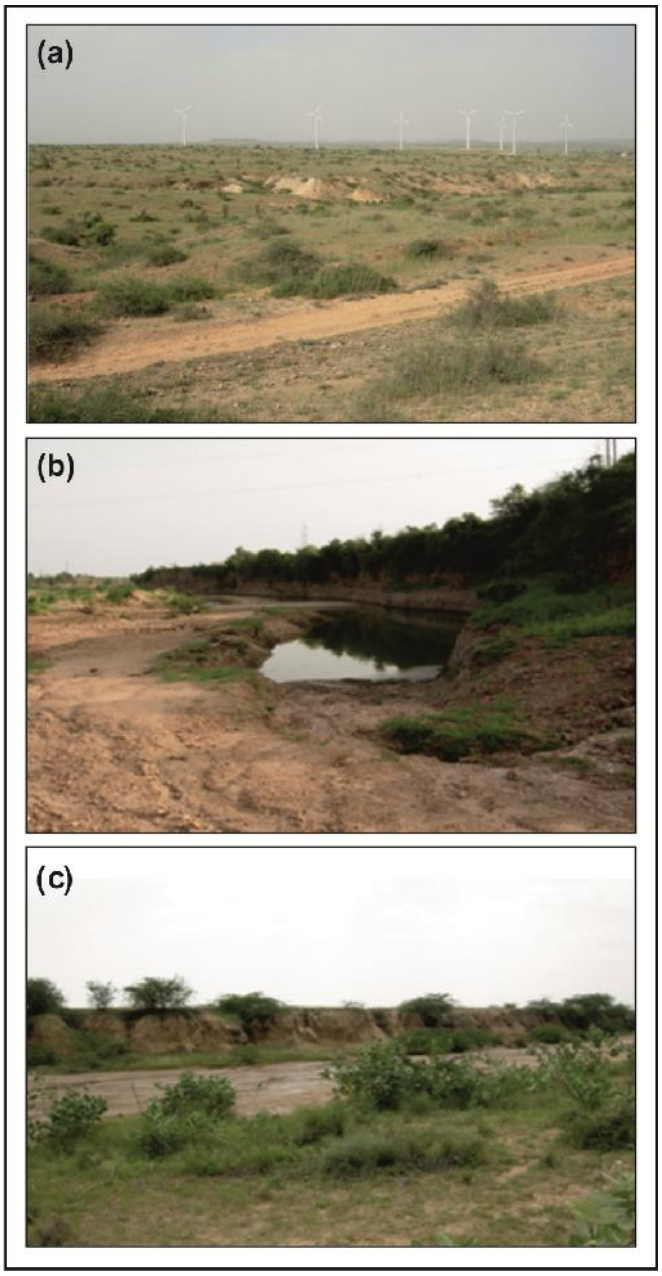

Figure 8.6 (a) View of the geomorphic high to the east of Lakadia with erosional gullies exposing Tertiary rocks. **(b)** Downstream view of the Khari river incising through Tertiary rocks near Lakadia. **(c)** View of the incised cliff section exposing Quaternary alluvial sediments along a stream to the south of Khanpar.

In the southernmost part of the plain, the rivers, especially the Khari river and its tributaries show anabranching pattern. The Khari basin in the northern part of the plain show a NNE-SSW trending elongated geomorphic high that consists of Tertiary rocks. The geomorphic high rises to more than 80 m and has resulted in radial drainage pattern with the tributaries arising from its eastern southern and western flanks. The geomorphic high is the result of the Kharol fault, a major transverse fault that displaces the SWF. The fault appears to continue to the south below the Tertiary sediments and possibly

responsible for the tectonic segmentation of the plains into the Samakhiali plain and the Lakadia plain.

A prominent feature of the rivers of the Lakadia plain which distinguishes it from the rivers of Samakhiali plain is their deeply incised channels (Fig. 8.6). The river courses are consistent as opposed to the rivers of Samakhiali plain which get disrupted. The incision varies from 2m to 12 m. The Quaternary sediment cover though thin is also found to be incised. A significant pattern in the variation in the depth of incision in Lakadia plain is noted. It is observed the depth of incision is maximum in the central part of the plain i.e. in the middle reaches of the various river. The zone of maximum incision extends E-W direction across the central part of the Lakadia plain. The increased incision in the central part of the plain suggests upwarping of the Tertiary rocks in E-W direction. The upwarping is in continuity of the similar feature inferred in the Samakhiali plain as described earlier.

Overall the Lakadia plain consists of Tertiary rocks which are consistently exposed along the incised cliffs of various rivers (Fig. 8.6a). However, a thin blanket of Quaternary fluvial sediments overlies the Tertiary rocks (Fig. 8.6b). The Tertiary rocks however exposed on the surface in the northern part of the plain where they are upthrusted over the Mesozoic along the SWF (Biswas, 1993). The Tertiary rocks here show extensive development of erosional gullies which have developed in response to neotectonic uplift of the Tertiary rocks along the SWF. Near Khanpar aeolian miliolite is seen to overlie the Tertiary rocks whose surface is also deeply gullied. In the central part of the plain, a distinct increase in the depth of incision in various rivers is observed which suggests upwarping of the Tertiary rocks along E-W trend.

LONGITUDINAL RIVER PROFILES

The longitudinal river profiles were drawn for three major rivers each from Samakhiali and Lakadia plains (Fig. 8.7and 8.8). The longitudinal river profiles show the distinct contrast for the rivers of the Samakhiali and Lakadia plains. The long profiles of Samakhiali plain show convex up nature in their middle reach (Fig. 8.7). The convex up part of the profiles correlates with the E-W trending zone of upwarp causing disruption of the drainage as described in the earlier chapter. This indicates the inability of the river to adjust to the upwarping occurring in response to compressive stresses. The rivers have therefore responded by disruption in the Samakhiali plain.

PART-D Surface deformation related to KMF-SWF interaction

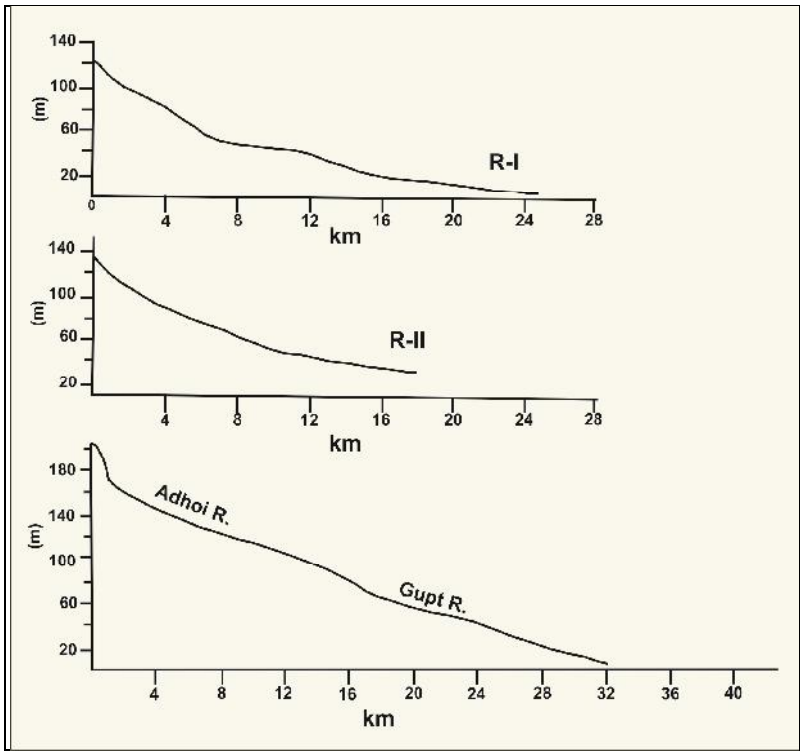

Figure 8.7 Longitudinal profiles of the rivers in Samakhiali plain

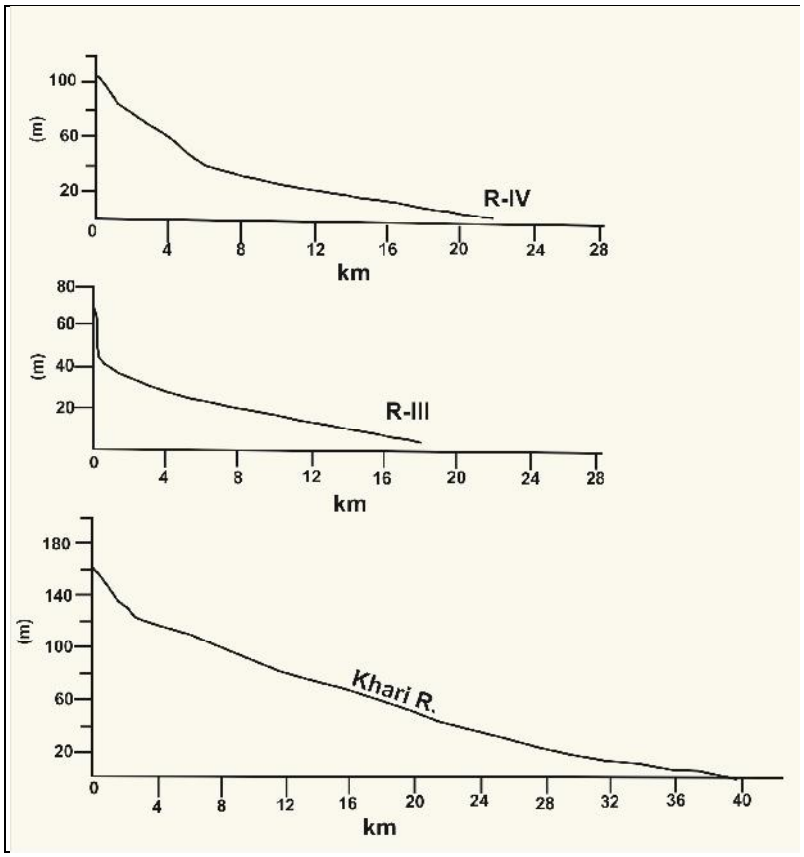

Figure 8.8 Longitudinal profiles of the rivers in Lakadia plain

The long profiles of the rivers of the Lakadia plain are in complete contrast with those from the Samakhiali plain (Fig. 8.8). The profiles show distinct concave up shapes

suggesting down cutting by the various rivers. This is in agreement with the field observation which show that the rivers of Lakadia plain show consistent deeply incised channels. Field observations have shown increased incision in the zone of upwarping. Since the rivers have responded to upwarping by incision, the nature of their long profiles consistently even and concave up. The upwarping therefore does not appear in the long profiles of the Lakadia plain. Since the climatic setting and the source area is the same for the entire study area, the incising nature of the rivers of the Lakadia plain can be attributed to the steeper slope of the plain. The long profiles clearly bring out the varying response of the rivers to neotectonic deformation in the Samakhiali-Lakadia plain.

CHAPTER 9

LANDSCAPE ANALYSIS OF SAMAKHIALI-LAKADIA PLAIN USING REMOTE SENSING AND GIS

Geomorphological studies in the Samakhiali-Lakadia plain described in the previous chapter reveal evidence of active surface deformation in response to the stresses accumulating in the region. In this chapter, a detailed landscape analysis using remote sensing and GIS technique is presented. The analysis includes calculation of basic morphometric parameters and evaluation of landscape parameters sensitive to tectonics. The drainage basin morphometric analysis was done using the GIS software. Drainage parameters sensitive to tectonics have been given special attention. For qualitative and quantitative geomorphic analysis, the USGS SRTM (*Shuttle Radar Topography Mission)* Digital Elevation Model of 90 m resolution and topographic maps were used as basic data. The data were analyzed using GIS software. Detailed terrain analysis was done by generating DEM and their derivatives. Various maps like Slope map, Aspect map and Hill shade map analysis by the ArcGIS software. Landscape parameters sensitive to tectonics like drainage asymmetry, stream gradient index and others were analyzed in detail using GIS technique.

MORPHOMETRIC ANALYSIS

The basic morphometric parameters were calculated for the all three drainage basins of the Samakhiali-Lakadia plain (Table 9.1). The Bifurcation ratios of the Khari Vokra basin, the Adhoi basin and the Khari basin are 2, 2.5 and 3.5 respectively (Table 9.2) which indicates that the geological structures are more disturbing the drainage pattern (Strahler, 1957). The drainage density values of the Khari Vokra basin, the Adhoi basin and the Khari basin are 0.0017, 0.0018 and 0.0025 respectively which indicates the coarse drainage texture and high resistant of highly permeable subsoil material under dense vegetative cover (Horton, 1932). The stream frequency of Khari Vokra basin is 1.5, Adhoi basin is 1.75 and Khari basin is 2.37 (Table 9.2). The value of stream frequency for the basin exhibits positive correlation with the drainage density value of the area indicating the increase in stream population with respect to increase in drainage density.

PART-D Surface deformation related to KMF-SWF interaction

The form factor value of the Khari Vokra basin, the Adhoi basin and the Khari basin are 0.0341, 0.1306 and 0.2007 respectively (Table 9.2) indicates elongated shape of the basins (Horton, 1932).

Table 9.1 Morphometric parameters, their mathematical expressions and references**.**

S.No.	Morphometric parameters	Formula	Description	Reference
1	Stream order	Hierarchical rank	-	Strahler, 1964
2	Bifurcation ratio (Rb)	Rb=Nu/(Nu + 1)	Rb=Bifurcation ratio, Nμ= No. of stream segments of a given order and Nμ +1= No. of stream segments of next higher order.	Schumm, 1956
3	Drainage density (Dd)	Dd = ∑L/A	Dd=Drainage density, ∑L= Sum of all stream lengths and A=Basin area.	Horton, 1932
4	Stream frequency (Fs)	Fs = Nμ/A	Fs=Drainage frequency, Nμ =Total no. of streams of all orders and A = Area of the basin.	Horton, 1932
5	Form factor (R_f)	$R_f = A/(L)^2$	F=Form factor, A=Area of the basin and L=Length of the basin.	Horton, 1932
6	Elongation ratio (Re)	$El = 2\pi\sqrt{A}/L$	El=Elongation ratio, A= Basin area, L=Basin length and π=Constant.	Schumm, 1956
7	Circularity Ratio (R_C)	Rc = 4πA/2	Rc=Circulatoryratio, A= Basin area and π = Constant	Miller, 1953

Table 9.2 Morphometric parameters for the rivers studied.

S.No.	Morphometric parameters	Khari Vokra	Adhoi	Khari
1	Total basin area (A) sq.km	119.35	226.76	227.85
2	Drainage order	4^{th}	6^{th}	6th
3	Maximum basin length (L) km	18.71	41.66	33.69
4	Bifurcation ratio (Rb)	2	2.5	3.5
5	Drainage Density (Dd)	0.0017	0.0018	0.0025
6	Stream Frequency (Fs)	1.52	1.75	2.37
7	Form factor (RF)	0.0341	0.1306	0.2007
8	Circularity Ratio (Rc)	0.54	0.32	0.36
9	Elongation Ratio (Re)	0.66	0.41	0.50

PART-D Surface deformation related to KMF-SWF interaction

Drainages of the Samakhiali plain

The Samakhiali plain includes two main river basins viz. Khari Vokra River basin and Adhoi River basin (Fig. 8.5). The rivers are characterized by discontinuous shallow channels with low incision and a distinct zone of disruption. The Khari Vokra is the 4th order smallest drainage basin of the study area occupying area of 119.35 km^2 (Fig. 9.1). The Khari Vokra River arises from the western part of the Wagad hills and flows westward to meet the Banni-Great Rann. There are several isolated areas of no drainage in the plain. Geomorphologically, the northwestern part of the plain between the SWF and the KMF is an area with low relief. The Khari Vokra River flows through a depression and flows westward to meet the Banni-Great Rann basin. The river exposes Tertiary rocks with a thin cover of alluvium that thickens towards north and south. The Khari Vokra River is an exception in the sense that it arises from the south Wagad hills and flows westward whereas the other drainages of Samakhiali plain also arise from the south Wagad hills but these flow southwards to meet the Gulf of Kachchh. The anomalous drainage of the Khari Vokra River is attributed to the graben structure between the KMF and SWF. The Adhoi River basin is the 6th order drainage basin occupying 226.76 km^2 (Fig. 9.2).

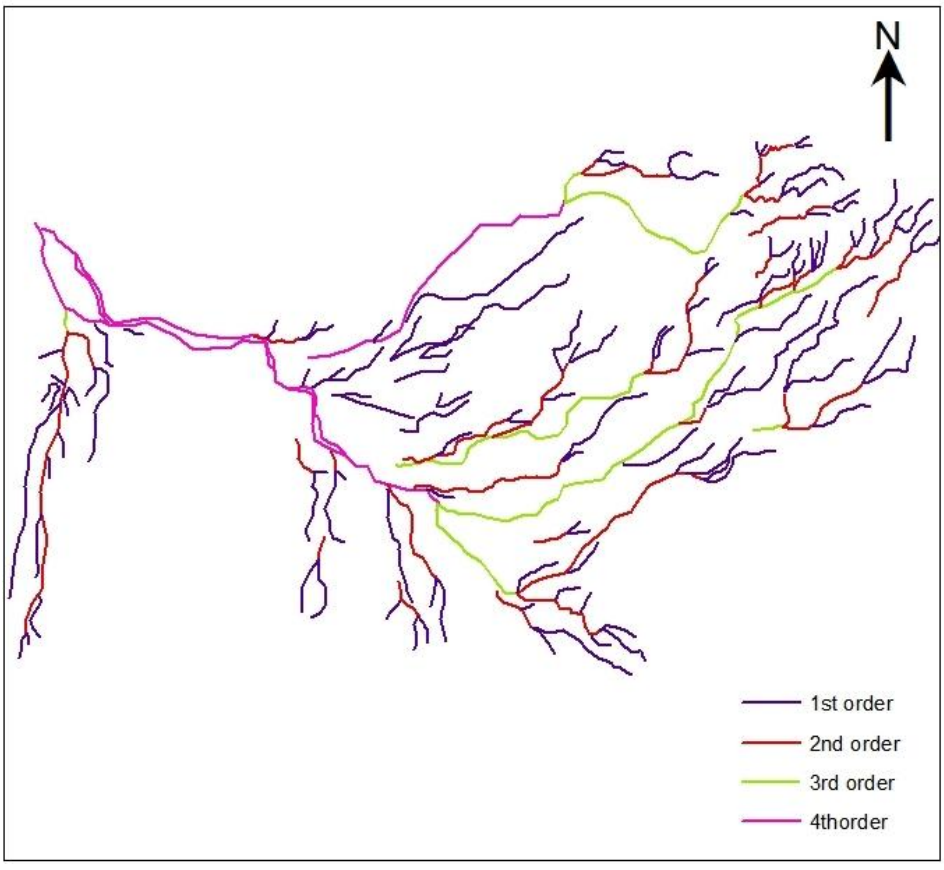

Figure 9.1 Drainage map of the Khari Vokra basin.

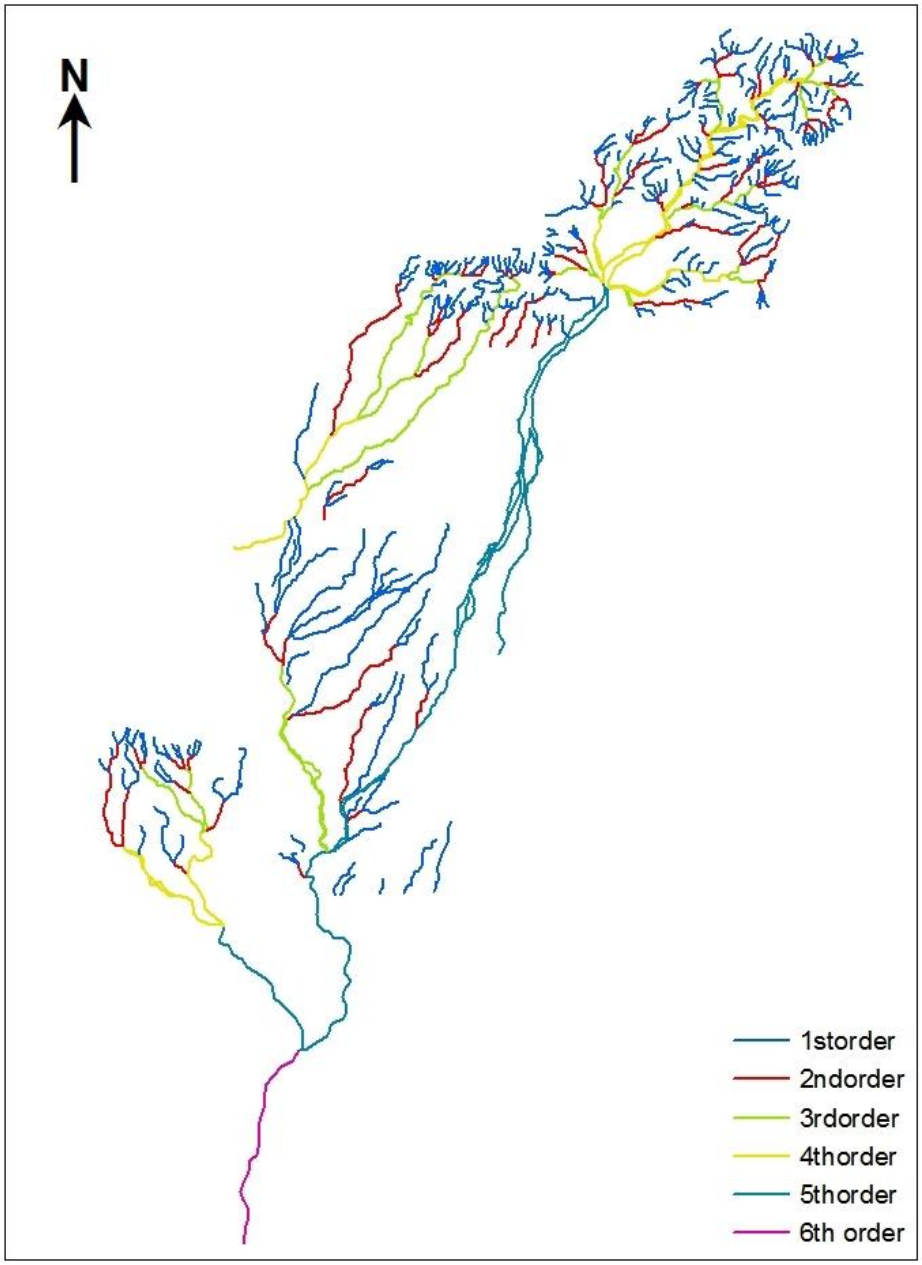

Figure 9.2 Drainage map of the Adhoi basin.

Drainages of the Lakadia plain

The Lakadia Plain is characterized by the long continuous drainages as compare to the Samakhiali drainage basin and also by the incision pattern as compare to Samakhiali Plain. The Khari River is the largest river in the plain with several others viz. the Khodasar and Khanpar streams to the east of it. All rivers originate in the south Wagad hills flow in S to SSE direction to meet the Little Rann. Khari River is the 6th order drainage basin occupying area of 227 km^2 (Table 9.1 and 9.2). The radial drainage pattern is observed in the northern part of the Khari River which is because of the geomorphic high and has resulted in the radial drainage pattern with the tributaries arising from its eastern, southern and western flanks (Fig. 9.3).

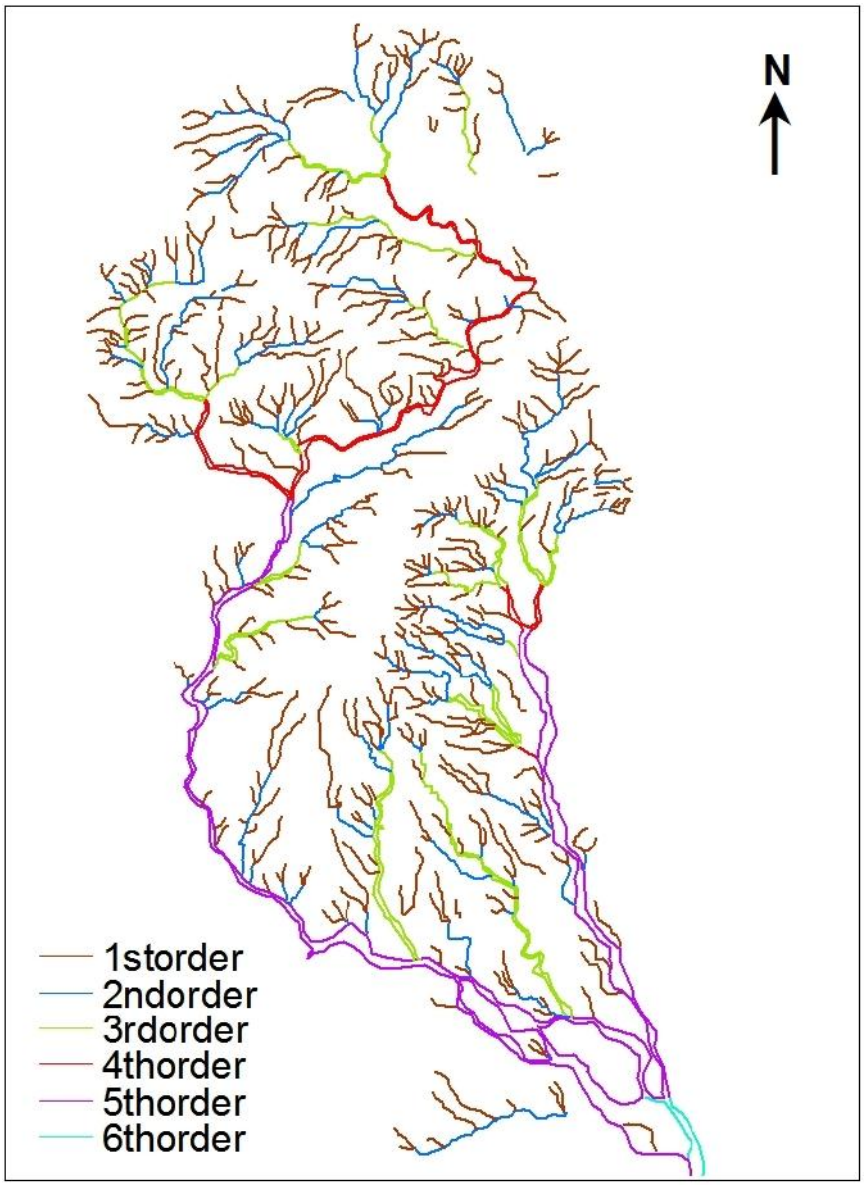

Figure 9.3 Drainage map of the Khari basin.

TERRAIN ANALYSIS

Terrain analysis was carried out by preparing DEM and its derivatives viz. slope map, aspect map and shaded relief map. DEM records the topographic expression of an area which can be extracted from different computer algorithms like slope, aspect and shaded relief. The tonal variation property of the DEM map is useful to study the topography and structural features of a region. Various geomorphic features have been observed from sharp changes in tone which related to corresponding changes in topographic relief.

Methodology

The USGS SRTM (*Shuttle Radar Topography Mission)* Digital Elevation Model of 90 m resolution and topographic maps were used as basic data. The data were analyzed

using GIS software, which is a precise, fast and inexpensive way for calculating morphometric parameters (Farr and Kobrick, 2000; Grohmann, 2004). The detailed methodology followed in the present study is illustrated in the flow chart given in Fig. 9.4 The first step of the analysis was the georeferencing which was done in ERDAS Imagine (v. 9.1). The common projection type, Universal Transverse Mercator (UTM), WGS 1984 zone 42 N was applied. For further analysis, ArcGIS (v.9.3) has been used. In ArcGIS, contour map, slope map, aspect map and hillshade map were generated using 3D Analyst module of Arc Toolbox. This was followed by the extraction and hydrological analysis of drainage basin of study area using Spatial Analyst module of Arc Toolbox. These data were used for the terrain analysis and the calculation of the geomorphic indices. The results were analyzed and interpreted with complementary fieldwork.

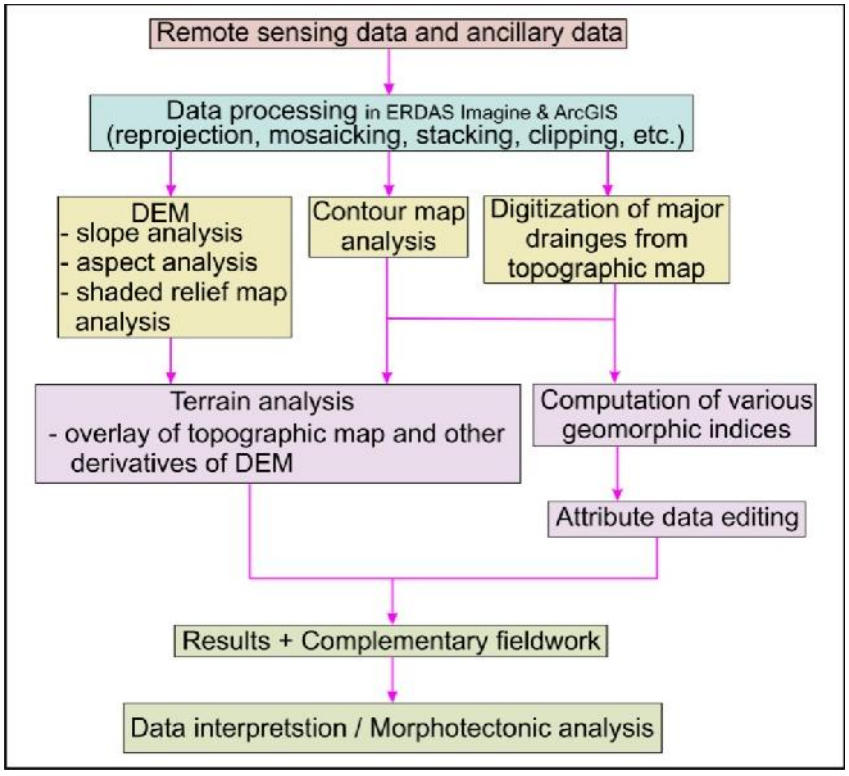

Figure 9.4 Flow chart showing the methodology adopted in the present study.

DEM analysis

In the DEM of study area rugged nature of the terrain is easily observed by geomorphological characteristics of surface determined systematic distribution of spectral brightness from dark blue to pale green tone distributed according to terrain relief (Fig. 9.6). In the DEM of the Samakhiali-Lakadia plain, KMF and SWF are expressed as continuous E-W trending dark yellowish brown to blue colored linear scarps (Fig. 9.4). The transverse Kharol Fault is seen as brown colored linear ridge displacing the South Wagad hills. The geomorphic high in the vicinity of the Kharol Fault is also seen. In front

of the scarps, the highly rugged surface is visible expressed as orange-yellow to dark green color (Fig. 9.5).

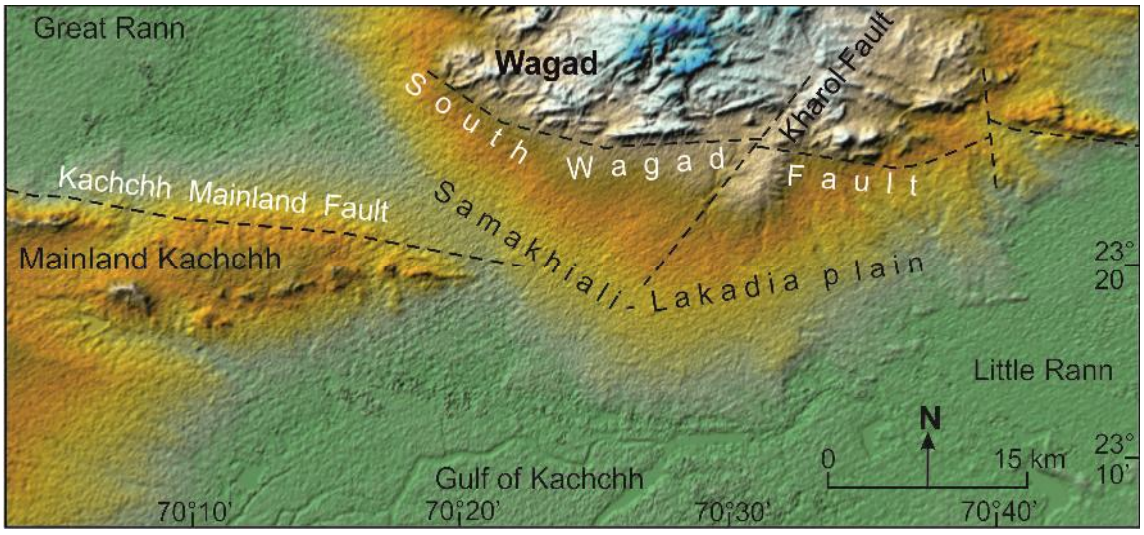

Figure 9.5 Digital Elevation Model (DEM) of the Samakhiali-Lakadia plain.

Slope analysis

Slope map is the first derivative of the DEM generated by 3D analyst tool of Arc toolbox in ArcGIS. The Slope function calculates the maximum rate of elevation change between each cell and its neighbors. The output slope raster can be calculated as percent of slope or degree of slope. Every cell in the output raster has a slope value. Abrupt change in slope across the landscape are indication of active faulting (Sanders and Selmmons, 1996; Hooper et al. 2003) and lineaments seen in the slope maps may represent fault scarp localities (Ganas et al. 2005). Higher degree slopes (5.61°-14.92°) are observed in front of the KMF and SWF (Fig. 9.6). The other significance is the high degree slope change (3-4 degrees) across the channel reach in the eastern part around Kharol Fault.

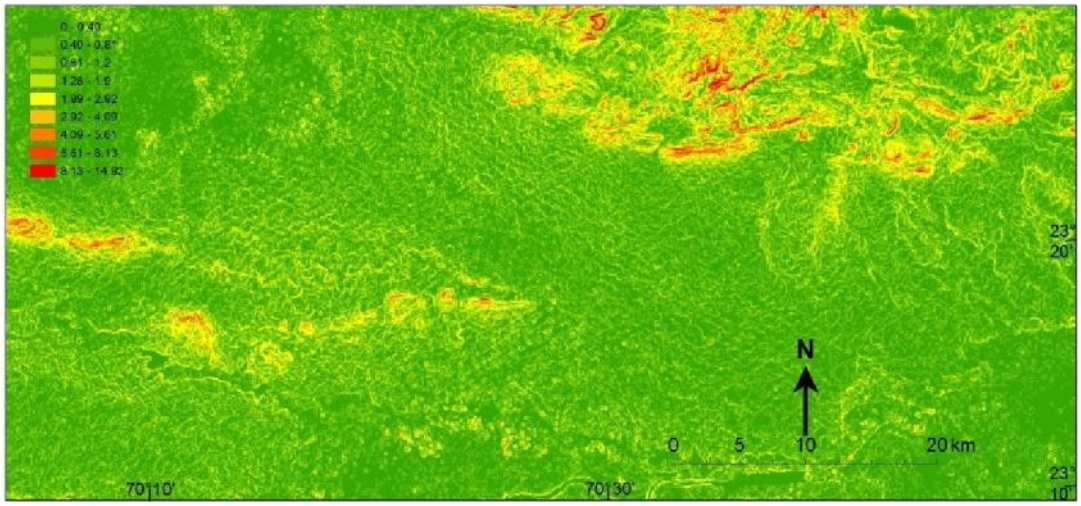

Figure 9.6 Slope map of the Samakhiali-Lakadia plain.

PART-D Surface deformation related to KMF-SWF interaction

Aspect analysis

Aspect map is the second derivative of the elevation data as it uses slope data to calculate aspect of the given pixels which is generated through 3D Analyst tool in ArcGIS. Aspect identifies the steepest down slope direction from each cell to its neighbors for an entire region. Aspect is measured clockwise in degrees from 0 to 360 due north. Flat area having no down slope direction is given a value of -1. In the western part of the study area dominant occurrence of pink and red colored pixels indicating a steep North-Northwest aspect of slope. Whereas in the eastern part dominance of light blue pixel suggesting southward aspect of slope. There is a significant radial aspect pattern formed in the eastern part around the Kharol Fault (Fig. 9.7). It is expressed by pink, green, light blue, yellow pixels arranged appropriate order and making a radial aspect surface around the Kharol geomorphic high.

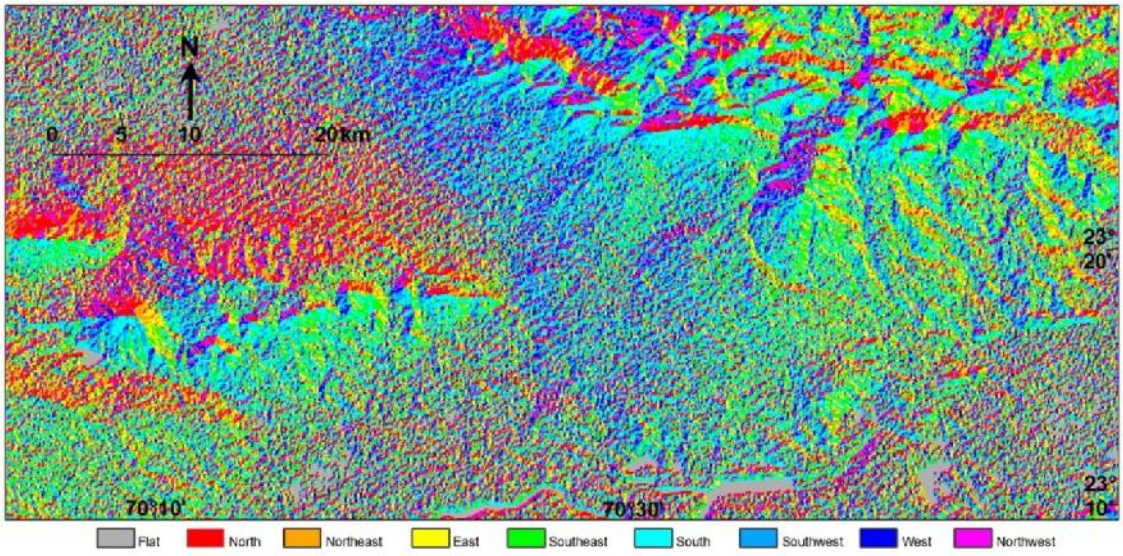

Figure 9.7 Aspect map of the Samakhiali-Lakadia plain.

Shaded relief

Shaded relief maps are useful to infer the geometry of footwall block along the strike of the major faults and to extract and study drainage patterns. In this algorithm, the illumination value for each cell is calculated by setting a position for hypothetical source of illumination (in degrees, 0-360) and calculating illumination value for each cell in relation neighboring cell. These values ranges from 0–255 (dark to light shades in gray scale), the 0 value is assigned to the cell which is not illuminated and it increases according to illumination conditions. Different views of illumination source can be decided on the basis of DEM resolution and tectonic setting of the area. It greatly enhances the visualization of topography. Also shaded relief map can be used as

background to overlay other vector or raster layers. The shaded relief map was generated from 3D analyst tool of ArcGIS with 170^0 azimuth angle of light source and 30^0 altitude angle above the horizon. Steep range front scarps of KMF and SWF are clearly visualized. In the eastern part, existence of incised parallel river valleys are also seen (Fig. 9.8). Maximum steepness with lower hillshade value is seen in front of the South Wagad hills. The hillshade was used as a base map for the overlay of various maps prepared during the analysis.

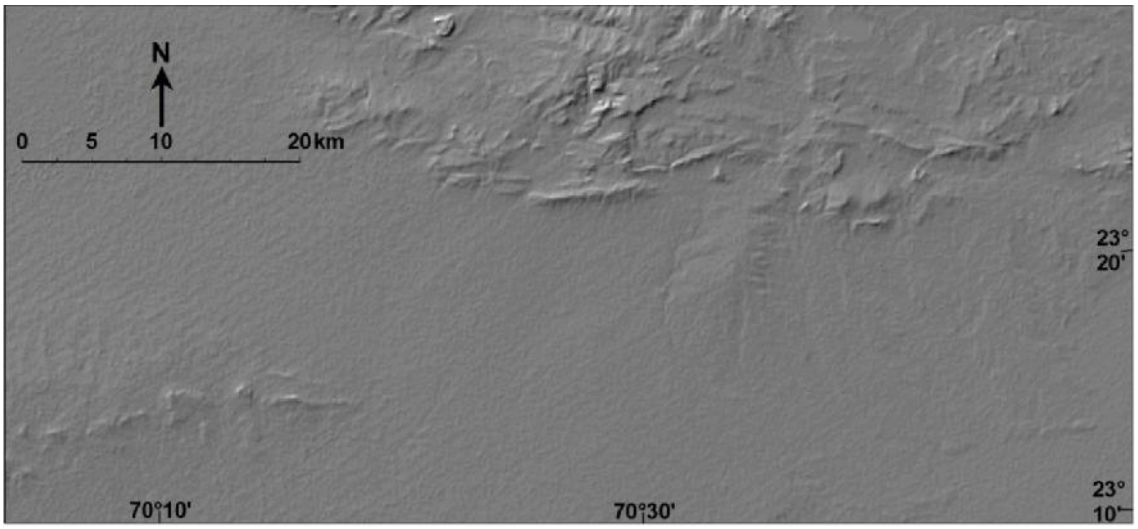

Figure 9.8 Hillshade map of the Samakhiali-Lakadia plain.

GEOMORPHIC INDICES

Four geomorphic indices which are reliable indicators of active tectonics (Keller and Pinter, 2002) were calculated including hypsometric curves and hypsometric integral (HI), drainage basin asymmetry (AF), transverse topographic symmetry factor (T) and stream length gradient index, (SL index). Basic principles of calculating each index is illustrated in schematic diagram (Fig. 9.10).

Hypsometric curve and Hypsometric integral (HI)

The hypsometric curve describes the distribution of elevations across an area of land, from one drainage basin to the entire planet. The curve is created by plotting proportion of total basin height (H/h) against the proportion of total basin area (A/a) (Strahler, 1952). A useful attribute of the Hypsometric curve is that drainage basins of different sizes can be compared with each other because area and elevation are plotted as function of total area and total elevation. The value of relative area (a/A) always varies from 1.0 at the lowest point in the basin (h/H=0.0) to 0.0 at the highest point in the basin (h/H=1.0). The calculated values for the three drainage basins studied are shown in Table 9.3, 9.4 and 9.5.

PART-D Surface deformation related to KMF-SWF interaction

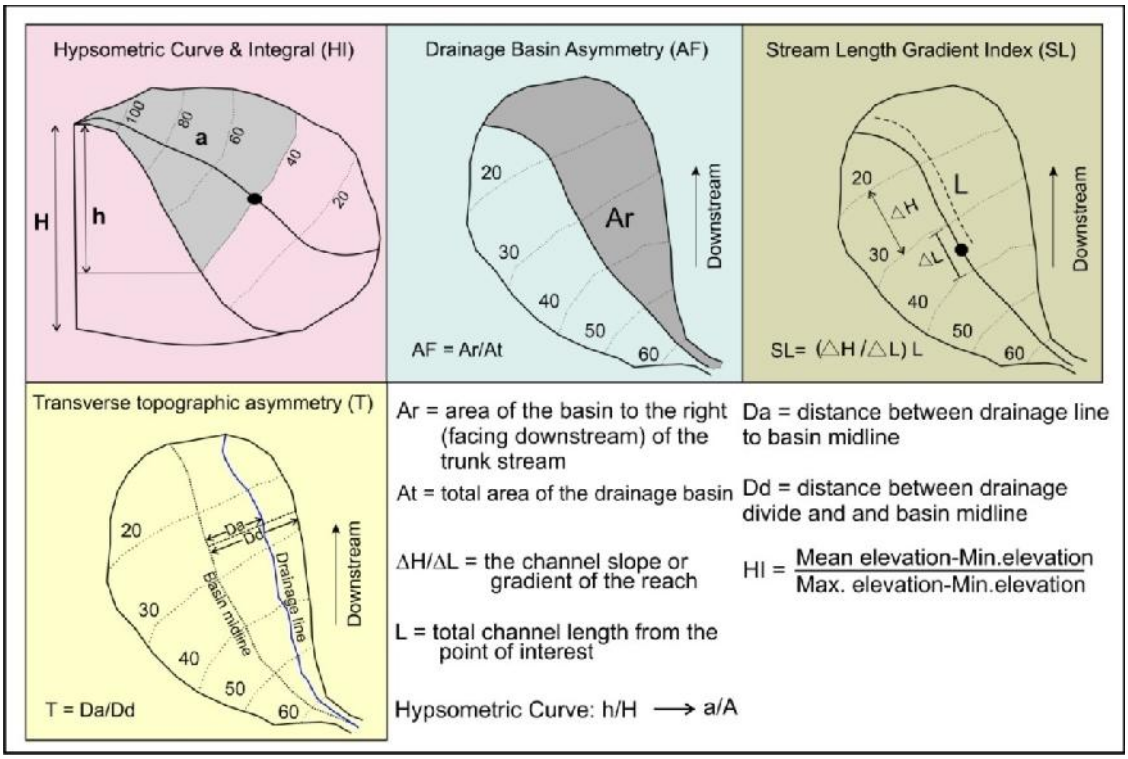

Figure 9.9 Schematic diagrams elaborating the method used for calculation of various geomorphic indices included in the present study.

Table 9.3 Calculated values of parameters for hypsometric curve of the Adhoi basin.

h (m)	a (m^2)	a/A	h/H
200	171613.64	0.00076	0.9524
190	2022906.37	0.0089	0.9048
180	6161252.66	0.0272	0.8571
170	10052768.08	0.0443	0.8095
160	13238526.75	0.0583	0.7619
150	16029494.65	0.0707	0.7143
140	20096981.43	0.0886	0.6667
130	25462225.05	0.1123	0.619
120	33614901.39	0.1482	0.5714
110	41144973.37	0.1814	0.5238
100	49426046.63	0.218	0.4762
90	53999761.66	0.2381	0.4286
80	58975178.89	0.2601	0.381
70	67411243.41	0.2973	0.3333
60	77619157.8	0.3423	0.2857
50	90056914.26	0.3971	0.2381
40	104054775.6	0.4589	0.1905
30	125212767.7	0.5522	0.1429
20	153881684.9	0.6786	0.0952
10	182562967.2	0.8051	0.0476
0	226765816.66	1	0

PART-D Surface deformation related to KMF-SWF interaction

The hypsometric curves prepared for three drainage basins of the study area are showing gradual change in the concavity of curve (Fig. 9.10). The hypsometric curves of the Khari Vokra and Adhoi drainage basins are concave up in the upper part and convex in the lower basin area. Whereas, the hypsometric curve of the Khari drainage basin is prominently convex.

The hypsometric integral is defined as the area under the hypsometric curve. The mathematical equation of hypsometric integral is as follow (Pike and Wilson, 1971; Mayer, 1990; Keller and Pinter, 2002):

$$\frac{\text{Mean elevation} - \text{Minimum elevation}}{\text{Maximum elevation} - \text{Minimum elevation}}$$

The relationship between the hypsometric integral and degree of dissection permits its use as an indicator of landscape's stage in the cycle of erosion. A high hypsometric integral indicates a youthful topography. The hypsometric integral of the Khari Vokra, Adhoi and Kari drainage basins are 0.48, 0.47 and 0.48 respectively.

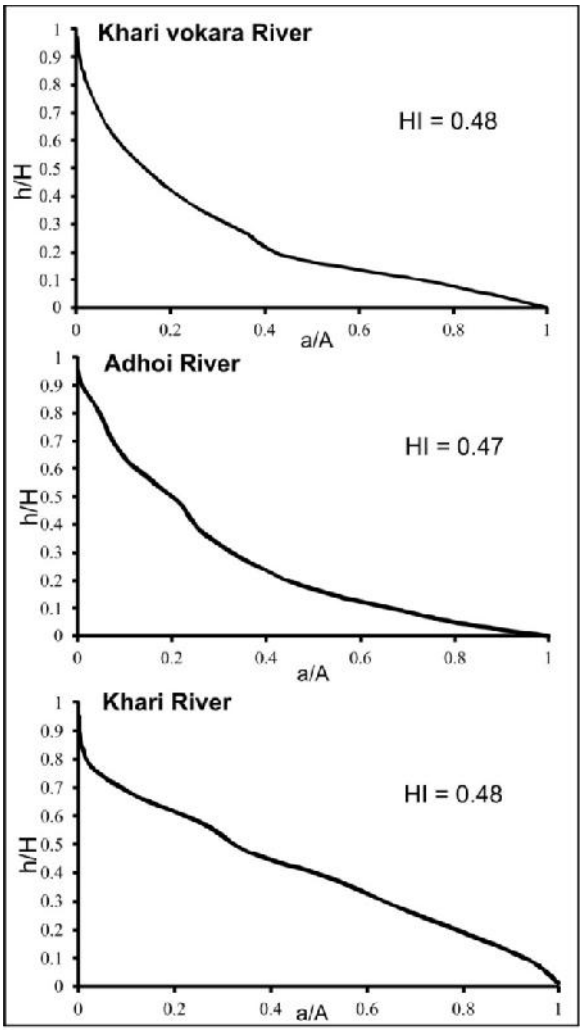

Fig. 9.10 Hypsometric curves of the drainage basins of Samakhiali-Lakadia plain.

PART-D Surface deformation related to KMF-SWF interaction

Table 9.4 Calculated values of parameters for hypsometric curve of the Khari Vokra basin.

h (m)	**a (m^2)**	**a/A**	**h/H**
110	99159.84	0.00083	0.97
100	1059469.8	0.0088	0.88
90	2806045.55	0.0235	0.8
80	5561985.6	0.0466	0.71
70	9265433.99	0.0776	0.62
60	15081266.71	0.1263	0.53
50	22187925.88	0.1859	0.44
40	31326208.1	0.2625	0.35
30	42550683.51	0.3565	0.27
20	53959912.07	0.4521	0.18
10	90368227.03	0.7571	0.09
0	119357136.2	1	0

Table 9.5 Calculated values of parameters for hypsometric curve of the Khari basin.

h (m)	a (m^2)	a/A	h/H
200	36442.77	0.00016	0.95
190	413096.41	0.00018	0.9
180	1674882.68	0.0073	0.85
170	3950520.76	0.017	0.81
160	7944716.73	0.035	0.76
150	14725331.56	0.065	0.71
140	30118634.99	0.132	0.66
130	42693573.18	0.187	0.62
120	59704826.11	0.262	0.57
110	71902877.46	0.316	0.52
100	81205426.43	0.356	0.47
90	102004013.6	0.448	0.43
80	119414366.7	0.524	0.38
70	133978098	0.588	0.33
60	150408708	0.66	0.28
50	166750962.9	0.731	0.24
40	181820630.7	0.798	0.19
30	196560844.9	0.863	0.14
20	213948751.6	0.939	0.09
10	222603035.5	0.977	0.05
2	227854228.2	1	0.0094

PART-D Surface deformation related to KMF-SWF interaction

Drainage basin asymmetry (AF)

The asymmetry factor (AF) is a rapid technique to evaluate the active ground tilting produced by tectonic activity or strong lithological control at drainage basin scale (Hare and Gardner, 1985; Keller and Pinter, 2002). It is calculated as:

$$AF = 100\ (A_r / A_t)$$

Where A_r is the area of the basin to the right (facing downstream) of the trunk stream, and A_t is the total area of the drainage basin.

In tectonically stable settings, AF should equal about 50. The AF is sensitive to tilting perpendicular to the trend of the trunk stream. Values of greater or less than 50 may suggest tilt. The AF values calculated for all three basins of study area are shown in (Fig. 9.11). The Khari River basin has AF value of 46.58 which is indicating a minor tilt in the right direction. The Adhoi River basin has AF value of 71.30 which is indicating tilting in the left direction. The Khari Vokra River basin has AF value of 36.30 which is indicating tilting of the basin in right direction.

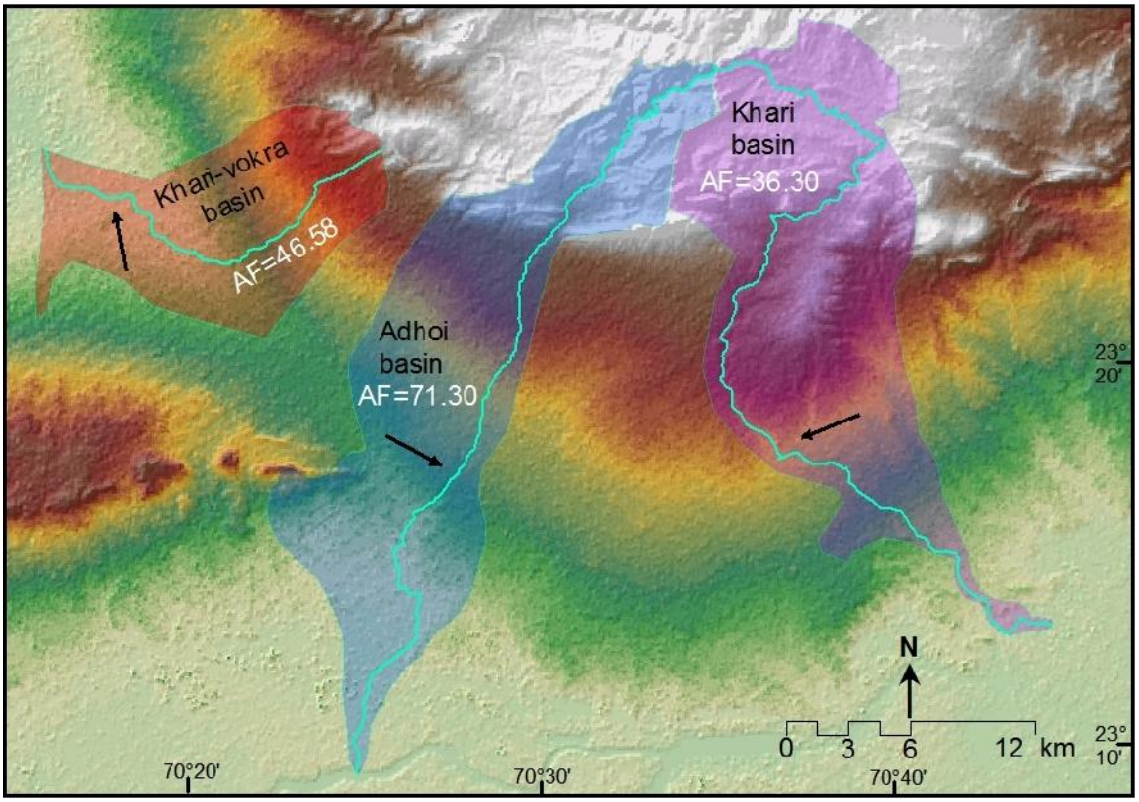

Figure 9.11 Map of drainage basins showing AF values.

Transverse topographic symmetry factor (T)

Another quantitative index to evaluate basin asymmetry is the transverse topographic symmetry factor (T) which is calculated by following equation (Keller and Pinter, 2002).

PART-D Surface deformation related to KMF-SWF interaction

$$T = D_a / D_d$$

where D_a is the distance between active drainage line and drainage basin midline and D_d is the distance from the basin midline to the basin divide.

For a perfectly symmetric basin, T = 0. As the asymmetry increases, T increases and approaches a value of 1. This method, as with AF does not provide direct evidence of ground tilting, but like AF, it is a method for rapidly identifying possible tilt (Keller and Pinter, 2002).The calculated values for the T are shown in the (Fig. 9.12). In the Khari Vokra basin and the Khari basin values of T are higher in the alluvial surface far southward from the scarpline, while in the Adhoi basin it is higher in the SWF zone.

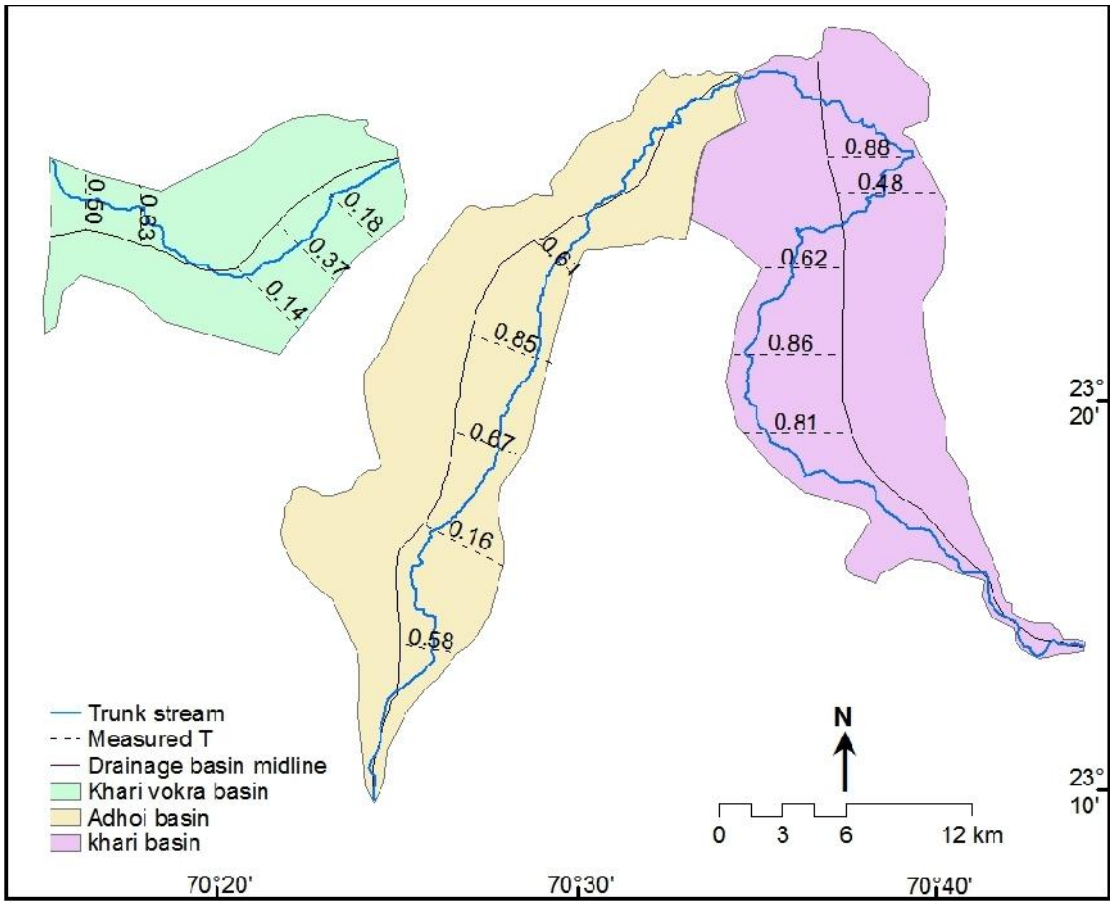

Fig. 9.12 Map of drainage basins showing locations and values of T.

Stream length-Gradient index (SL)

The stream length-gradient index (SL) is calculated for a particular reach of interest and defined as (Hack, 1973; Keller and Pinter, 2002).

$$SL = (\Delta H / \Delta L)\, L$$

Where SL is the stream length-gradient index, $\Delta H/\Delta L$ is the channel slope or gradient of the reach and L is the total channel length from the point of interest where the index is being calculated upstream to the highest point on the channel. The SL index is

very sensitive to changes in channel slope, and this sensitivity allows the evaluation of relationship among possible tectonic activity, rock resistance, and topography (Keller and Pinter, 2002). In landscape evolution, the adjustment of stream profiles to rock resistance is assumed to occur fairly quickly. Therefore, the SL index is used to identify recent tectonic activity by looking for anomalously high SL values on a particular rock type (Keller and Pinter, 2002; Merritts and Vincent, 1989, Brookfield, 1998).

The contour map with 10 m interval generated. Where these contours cross the mapped streams, locations are marked for each stream. Along each stream, measured the distance, ΔL, between successive contours along the streams as well as the total upstream stream length. The SL index for each small stream segment was calculated (Table 9.6), and marked the value at the midpoint between contours (Fig. 9.13).

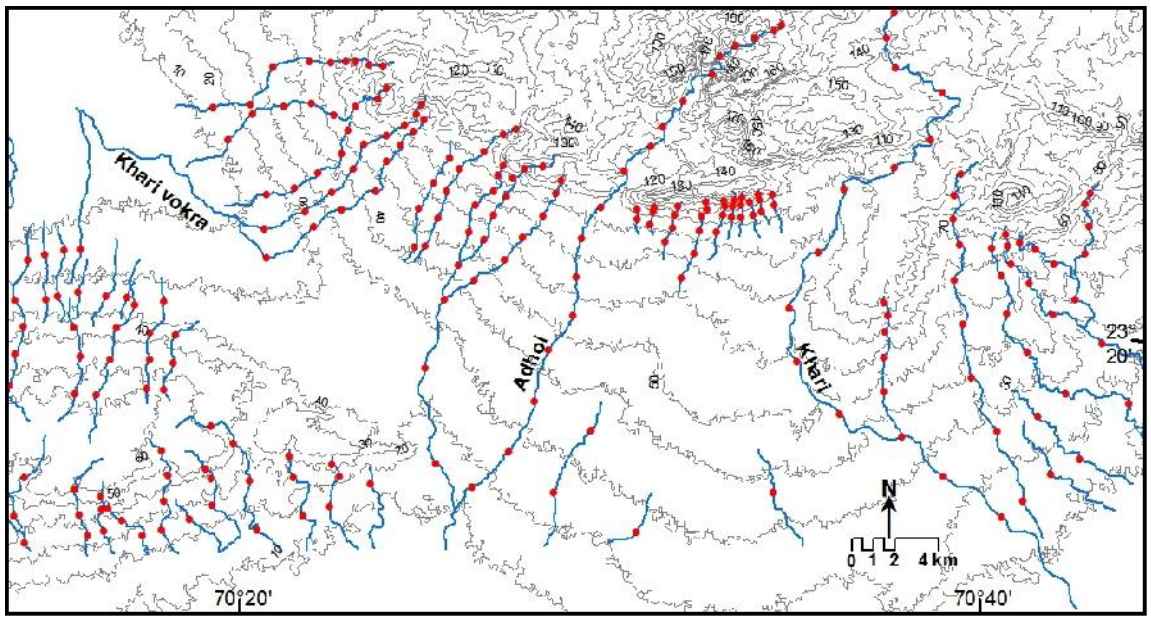

Fig. 9.13 Contour map showing drainages and midpoints for which SL index calculated.

With help of midpoint value two SL maps were prepared for the study area. SL values were divided in 7 classes and accordingly different color assigned to different drainage segments (Fig. 9.14). In the figure, rivers emerging from the South Wagad hills in the western part are showing relatively high SL index of class 3, 4, 5 and 6 in the SWF zone, while in the eastern part of the study area, rivers have high SL index values in SWF zone as well as in the alluvial plain area. In the SWF zone, rivers have SL index value of class 3 to 7 and in the alluvial plain area rivers have SL index value of class 3 and 4.

Also, the interpolation map was prepared using Kringing method in ArcGIS (Fig. 9.15). In the interpolation map SL index values divided into the 10 classes. In this map, it is seen that the zone of high SL index value is mainly in the KMF zone and SWF zone in

the western part of the study area, while in the eastern part it is significantly extended into the alluvial plain area also. This attributes to the relatively high degree of tectonic activity along the Kharol Fault in the eastern part.

Table 9.6 SL index values for the drainages of Samakhiali-Lakadia plain.

Drainage no.	Contour interval	SL index values	Drainage no.	Contour interval	SL index values
1	80-70	85.74		80-70	133.51
	70-60	44.68		70-60	68.44
	60-50	22.35		60-50	42.61
	50-40	13.91		50-40	27.23
2	70-60	119.76		40-30	19.52
	60-50	39.06		30-20	15.79
	50-40	23.87		20-10	11.90
3	80-70	150.36	30	100-90	533.40
	70-60	210.31		90-80	220.40
	60-50	96.04		80-70	120.27
	50-40	57.62		70-60	77.27
	40-30	34.42		60-50	55.27
	30-20	22.26		50-40	42.28
	20-10	15.08		40-30	32.48
4	70-60	246.19		30-20	26.71
	60-50	82.52		20-10	20.99
	50-40	43.37	31	60-50	183.26
	40-30	27.30		50-40	49.59
	30-20	17.18		40-30	25.33
	20-10	12.53		30-20	18.07
5	30-20	40.78		20-10	13.70
	20-10	15.18	32	90-80	573.51
6	20-10	24.55		80-70	145.19
7	100-90	205.05		70-60	54.71
	90-80	87.26		60-50	48.20
	80-70	54.84		50-40	35.05
	70-60	40.92		40-30	26.76
	60-50	29.86		30-20	18.44
	50-40	22.41		20-10	12.90
	40-30	17.55	33	100-90	236.86
	30-20	13.76		90-80	106.51
	20-10	11.01		80-70	62.30
8	90-80	238.19		70-60	48.89
	80-70	72.25		60-50	37.67
	70-60	40.13		50-40	28.79
	60-50	22.71		40-30	19.77
	50-40	14.27		30-20	14.61
9	100-90	31.96		20-10	12.00
	90-80	26.56	34	20-10	62.95
	80-70	21.95	35	40-30	152.29

PART-D Surface deformation related to KMF-SWF interaction

	70-60	19.27		30-20	50.37
	60-50	17.22		20-10	20.37
	50-40	15.27	36	40-30	228.43
	40-30	13.64		30-20	44.13
	30-20	12.61		20-10	15.77
	20-10	11.51	37	50-40	54.56
10	40-30	24.15		40-30	29.39
11	110-100	132.60		30-20	18.33
	100-90	29.23		20-10	11.58
12	120-110	111.96	38	50-40	46.71
	110-100	42.54		40-30	32.88
	100-90	16.57		30-20	19.64
13	110-100	114.68	39	30-20	28.69
	100-90	26.88	40	60-50	76.97
				50-40	28.79
14	120-110	73.69		40-30	18.14
	110-100	35.15		30-20	12.48
	100-90	17.68	41	50-40	114.57
15	120-110	53.49		40-30	30.33
	110-100	31.97		30-20	13.21
	100-90	17.75	42	60-50	57.54
16	120-110	290.46		50-40	27.69
	110-100	97.05		40-30	14.91
	100-90	40.14	43	70-60	63.42
	90-80	19.03		60-50	25.66
17	120-110	202.16		50-40	16.16
	110-100	91.35		40-30	12.13
	100-90	50.96	44	60-50	23.88
	90-80	29.18		50-40	11.44
	80-70	17.38	45	50-40	27.28
	70-60	11.73		40-30	11.90
18	110-100	126.78	46	60-50	84.22
	100-90	44.46		50-40	25.71
	90-80	23.49		40-30	16.08
	80-70	13.79	47	60-50	31.33
19	110-100	89.83		50-40	19.22
	100-90	38.32		40-30	14.52
	90-80	15.46		30-20	11.49
20	100-90	87.61	48	60-50	78.24
	90-80	21.48		50-40	24.17
21	30-20	16.63		40-30	13.85
22	40-30	55.16	49	60-50	90.81
	30-20	15.39		50-40	30.52
23	30-20	22.62		40-30	18.38
	20-10	13.59		30-20	12.26
24	100-90	324.68	50	70-60	99.06
	90-80	84.32		60-50	34.75
	80-70	35.78		50-40	19.26
	70-60	22.34		40-30	14.26

	60-50	16.76		30-20	11.60
	50-40	12.35	51	30-20	26.33
25	110-100	90.04	52	30-20	27.17
	100-90	45.06	53	30-20	21.91
	90-80	31.36	54	20-10	49.19
	80-70	21.74	55	60-50	39.78
	70-60	16.64		50-40	17.80
	60-50	12.97		40-30	12.87
26	100-90	597.80	56	30-20	36.85
	90-80	232.90		20-10	13.40
	80-70	118.89	57	30-20	44.42
	70-60	71.38		20-10	14.62
	60-50	48.20	58	60-50	151.99
	50-40	35.05		50-40	40.95
	40-30	26.76		40-30	24.55
	30-20	18.44		30-20	17.80
	20-10	12.90		20-10	12.19
27	110-100	351.52	59	40-30	28.00
	100-90	99.99		30-20	16.02
	90-80	39.37	60	30-20	29.52
	80-70	23.74	61	40-30	226.85
	70-60	17.82		30-20	83.42
	60-50	13.81		20-10	47.47
	50-40	11.23	62	40-30	222.45
28	80-70	80.34		30-20	65.29
	70-60	29.13		20-10	28.81
	60-50	17.97	63	20-10	18.28
29	90-80	657.26	64	20-10	26.23

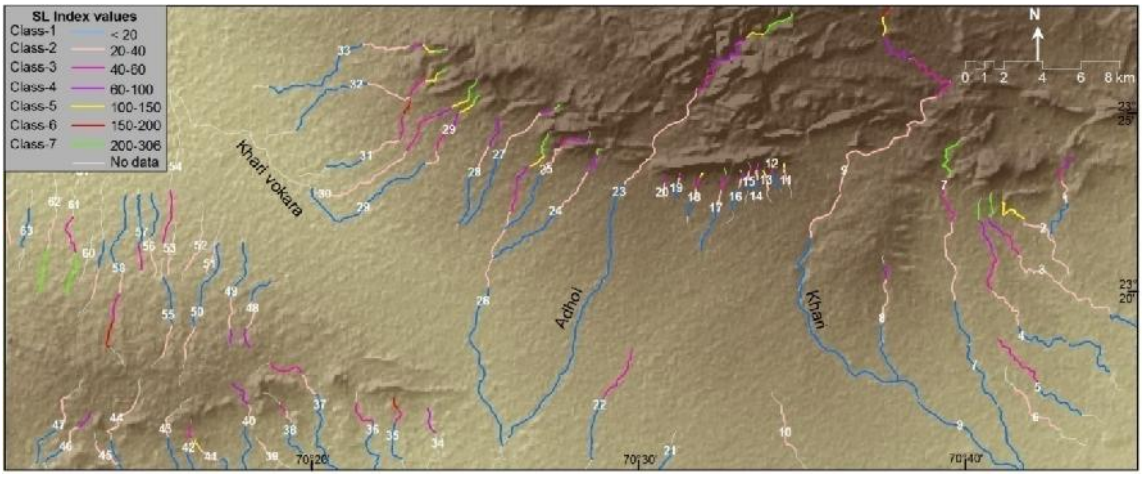

Figure 9.14 SL index map for the 64 drainages of the Samakhiali-Lakadia plain.

PART-D Surface deformation related to KMF-SWF interaction

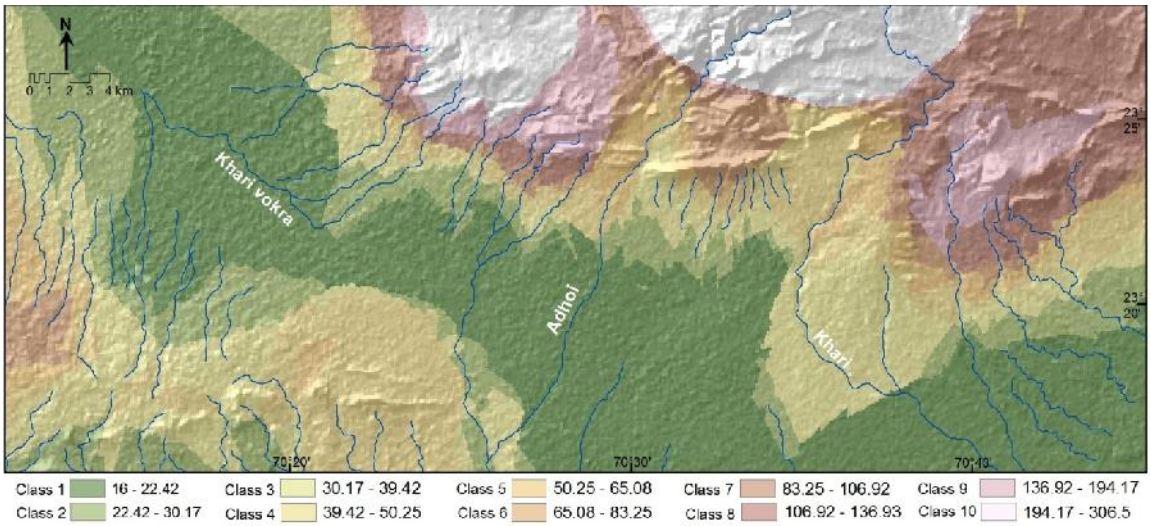

Figure 9.15 Interpolated SL index map of Samakhiali-Lakadia plain.

RESULTS AND INTERPRETATION

The Samakhiali graben is believed to be under a state of high stress as evidenced by the 2001 Bhuj earthquake which occurred in this region (Biswas and Khattri, 2002). Seismic activity suggests that the KMF ridge may be rising up in response to the compressive stresses accumulating in the region (Biswas, 2005). The rivers of the Lakadia plain are continuous, whereas the rivers of Samakhiali plain are discontinuous drainage. However anomalous slopes are seen in the central part of the plain where the drainages appear to get disrupted. This suggested a zone of gentle up warping of the surface trending in E-W direction. This E-W trending zone acts as a zone of drainage disruption throughout the Samakhiali Plain. The drainage of Samakhiali plain suddenly starts to disappear against this E-W trending geomorphic high and reappears almost on the same trend after crossing this high. This may indicates the reactivation of the old subsurface structure with slow rate of uplift as the drainages are survived and reappears on the same trend. Another high is the Bhachau ridge which forms the area of no drainage to its north and new drainages originates to its south which ultimately meets the Gulf of Kachchh.

In the Lakadia Plain the incision in various streams is two to three times to that of Samakhiali Plain. All the streams drain the area very well without any disruption. Occurrence of several faults in north of the Samakhiali-Lakadia plain and differential movement along these faults have played significant role in the segmentation of Samakhiali-Lakadia plain. The erosional cycles have shaped the present landscape to the region. The geomorphic highs are responsible for the disruption of the drainages of Samakhiali Plain. These highs are E-W trending and NE-SW trending. These geomorphic

highs are the expressions of the subsurface structures which is controlling the geomorphic set-up of the area. For this reason the detail drainage analysis and morphometric analysis has been done.

The Samakhiali-Lakadia plain is geomorphologically expressed by undulating alluvial surface which deposited in the front of tectonically active KMF and SWF. The terrain analysis done by DEM, slope map, aspect map and hillshade suggest higher degree of slope in the vicinity of the faults which is indicating active faulting along the KMF and SWF. The longitudinal profiles of the drainages show pronounced steep gradient in the downstream and knick-points in the upland reaches. The longitudinal profile of the Khari River is the steepest and convex than that of other two drainages of the study area. This confirms the higher depth of incision seen in the Khari River.

The hypsometric curves of the study area show defining pattern of change in the concavity of curve. The concavity of the curve decreases and convexity increases as move from west to east. The hypsometric curve of the Khari Vokra drainage basin shows concave profile in the upstream area and relatively convex curve in the downstream area fall in the alluvial plain. The convexity of hypsometric curve of the Adhoi basin is relatively higher than the Khari basin. The Khari basin shows the highest degree of convexity than the Adhoi basin and the Khari Vokra basin. The gradual change in the shape of the curves may be produced by spatial difference in the magnitude of tectonic activity. The shape of the hypsometric curves and values of hypsometric integral indicating the area is moderately eroded.

The AF value of the Khari Vokra basin indicates that basin is tilted towards right. The T values of the existing active river belt suggest that the deviation of the existing drainage from the basin midline is the maximum in its alluvial reach. The AF value of the Adhoi basin indicates tilting towards left side. The T values suggest maximum deviation of the existing active river belt from the basin midline in the SWF zone. The AF value of the Khari basin indicates that basin is tilted towards right. The T values indicates that the active river belt is maximum deviated from the basin midline in its alluvial course.

In the south-west part of the study area some drainage are showing high SL index values in the KMF zone which is far northward from the existing Mesozoic hills. In the north-west part drainages having higher SL index values in the SWF zone than that of south-west part of KMF zone. In the eastern part of the study area the zone of high SL index valued moved far south southward that the drainage having high SL index values

even in their alluvial courses. The anomalies occur in the SL index values indicate spatial difference in the magnitude of the controlling tectonic activity.

The disruption of the drainage and its reestablishment strongly points towards the presence of an E-W trending geomorphic high in the central part of the Samakhiali plain. The geomorphic high appears to have formed due to the upwarping of the Tertiary rocks due to the rise of the KMF in the subsurface in response to prevailing compressive stresses in the region. The presence of a geomorphic high in the central part of the plain is further evidenced by the several streams which arise suddenly and flow southward. The upwarped region passes through Sikra, Karmaria, Vondhada, Vijpasar, and east of Gharana. The geomorphic high lies in continuity of the KMF ridge to the west of the Samakhiali plain. This suggests that the KMF ridge may be extending below the plain whose active nature is responsible for the upwarping of the surface and the attendant drainage disruption. The upwarping is also responsible for the westward oriented course of the Khari Vokra river which meets the Banni-Great Rann basin to the northwest of the Samakhiali plain. The main reason of the surface deformation in Samakhiali-Lakadia plain is due to the tectonic upliftment. The present study provides strong evidence which shows that the deformation is caused by the lateral propagation of KMF eastward into the Samakhiali-Lakadia plain.

CHAPTER 10

FIELD AND GPR STUDIES ALONG GEDI FAULT

The present chapter describes the results of detailed field and GPR studies along the seismically active Gedi Fault (GF) located in the currently inverting Kachchh palaeorift basin in western India. The results of the study are significant in view of the poorly exposed fault trace and the heightened level of seismic activity along the Gedi Fault (GF) after the 2001 Bhuj earthquake (Mw 7.7) that occurred on another fault, the Kachchh Mainland Fault (KMF) located in the south (Mandal, 2009). Use of GPR is specifically very useful in mapping of buried faults. However, in case of partially exposed or poorly exposed faults also, the GPR has been proved extremely useful for mapping the continuity and shallow subsurface nature of faults (Demanet et al. 2001; Pauselli et al. 2010; Wallace et al. 2010). In the present study, field and GPR based studies along the Gedi Fault at the southern margin of the Desalpar uplift was carried out with a view to precisely map its near surface and shallow subsurface nature. The basic aim of the study is to understand the neotectonic setting and its seismic potential in the light of the ongoing seismic activity tentatively attributed to the stress perturbations following the 2001 Bhuj earthquake (Mandal and Chadha, 2008).

TECTONIC GEOMORPHOLOGY

The Desalpar uplift is a narrow E-W trending flexure zone occurring between two larger uplift zones- the Wagad uplift in the south and the Island Belt uplift (Bela and Khadir) in the north (Fig. 10.1). The Desalpar uplift forms a narrow E-W trending low elevated (~30 m amsl) but rugged rocky terrain exposing Mesozoic rocks forming E-W trending chain of asymmetrical domes and anticlines (Fig. 10.1, 2a). The flexure zone is bordered by the corresponding Balasar synclinal low in the north and the Rav basin in the south (Fig. 10.2a).

The Balasar syncline is occupied by the flat salt encrusted surface of the Great Rann which occurs few meters above mean sea level. The Rann locally means the saline wasteland and is considered to be the uplifted floor of an extensive former gulf (Glennie and Evans, 1976; Maurya et al. 2008). Historical accounts along with the archaeological evidences suggest that it was a navigable sea up to ~2000 yrs BP (Oldham, 1926). To the south of the flexure zone lies the Rav basin which exposes marine rocks belonging to the

Khari Series of Miocene age (Biswas, 1987). The Rann surface occurs in small patches along the southern margin of the flexure zone. Towards the west, the Gangta bet forms the extension of the flexure zone and is separated by a narrow patch of the salt encrusted surface of the Great Rann (Fig. 10.2a). The Gangta bet exposes Mesozoic rocks forming a dome in the central part with Miocene and Quaternary Rann sediments around it.

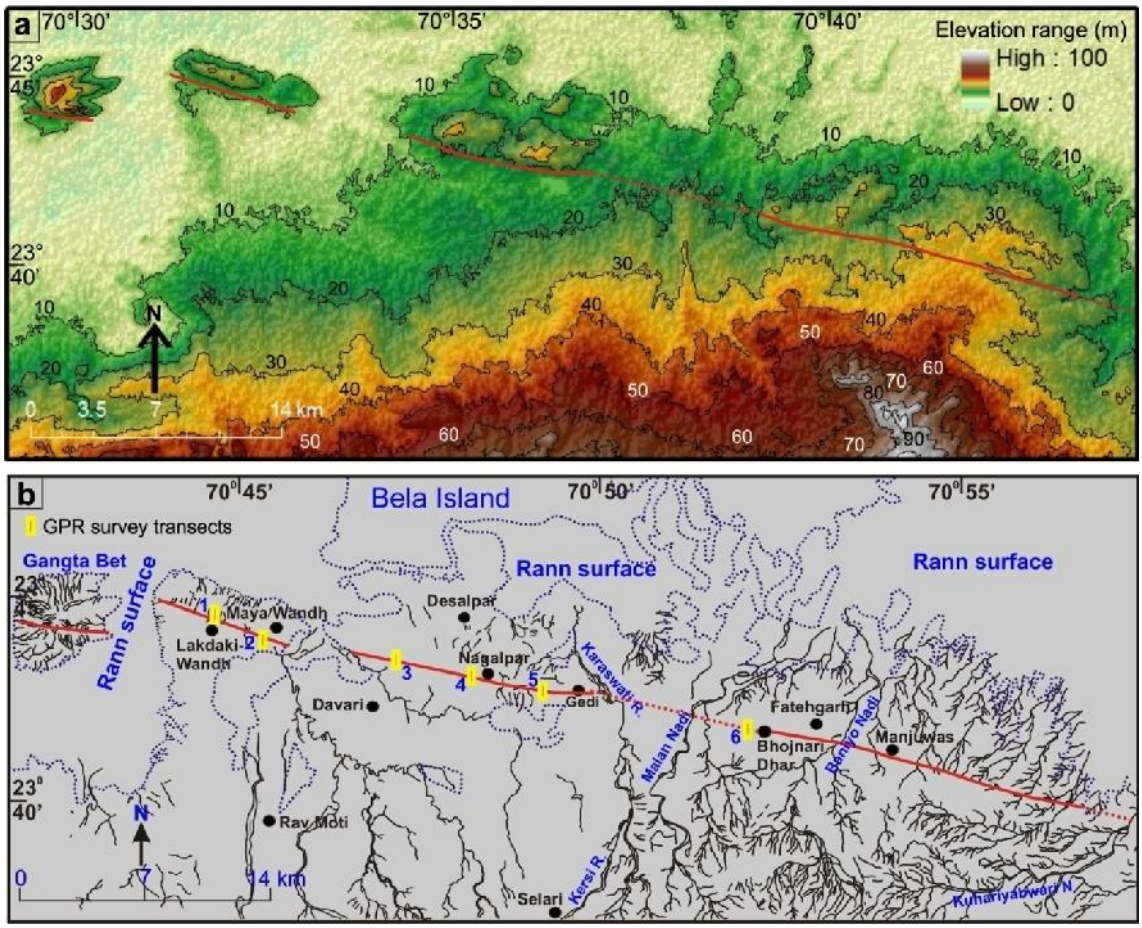

Figure 10.1 (a) DEM of the study area. The E-W trending low relief terrain of the Desalpar flexure zone is seen**. (b)** Drainage map of study area. Note the poorly developed drainage in the central part in contrast to the eastern part. Also note the radial drainage in Gangta bet in the extreme west. 1-6 are the locations of the GPR survey transects.

The Desalpar flexure zone shows poorly developed drainage lines, which is in conformity with its low relief (Fig. 10.1b). The drainages are more numerous in the eastern part. However, all drainage lines in the flexure zone, including the Gangta bet, are strongly controlled by the domes and anticlines (Fig. 10.1b). The Malan river and Karaswali river arise in the Wagad region in the south and flow northward across the Rav basin and Gedi Fault to debouch in to the Rann surface to the north of the flexure zone.

The Quaternary sediments form a thin E-W trending linear cover at the southern margin of the flexure zone and overlapping the trace of Gedi Fault (Fig. 10.2). These

consist of miliolite (semi-compacted aeolian carbonate sands), clayey Rann sediments and fluvial sands. The aeolian miliolites are described as originally carbonate rich sediments blown by wind from coastal areas and deposited as scattered obstacle dunes along the rocky slopes (Biswas, 1971). The Quaternary sediment thickness varies from less than a meter to ~8 meters.

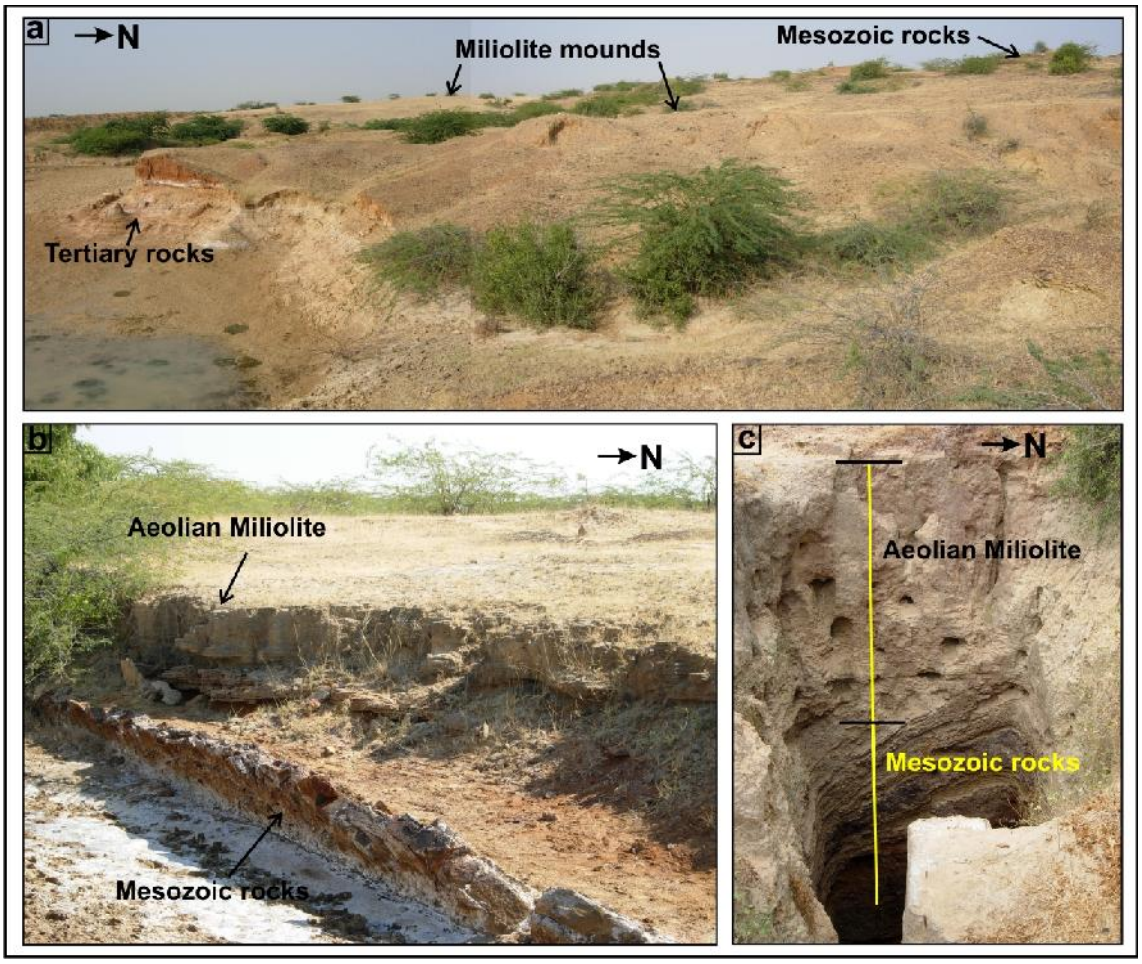

Figure 10.2 (a) Photomosaic showing the general geomorphology of the Gedi Fault zone. The mound like topography of the Quaternary miliolite deposits almost completely overwhelms the low relief fault scarp. The exposure of the Tertiary rocks shown is exposed due to the excavation done for the construction of a pond. (Loc. between Nagalpar and Gedi). (b) View of the north dipping strata of the overturned southern limb of the flexure. Also seen is the overlying thin sheet of aeolian miliolite deposits. (c) View of a well section showing the semi compacted aeolian miliolite deposits overlying the Mesozoic rocks. Note the southward steepening of dips of the Mesozoic strata due to the effect of the Gedi Fault which is located further left of the photograph. (Loc. west of Gedi).

Though the Gedi Fault may be described as a poorly exposed fault, the presence of the fault all along the southern margin of the Desalpar flexure zone is very obvious due to the physiographic contrast. The physiographic contrast is diluted by the presence of Quaternary sediments especially the aeolian miliolite deposits of middle to late

Pleistocene age which form large south sloping mounds abutting against the Mesozoic rocks and overlapping the fault line (Fig. 10.2a). The most extensive cover of the miliolite occurs from the west of Gedi to the region to the north of Davari (Fig. 10.2b and c). Stratigraphically, the miliolites are the oldest Quaternary sediments of the Gedi Fault zone followed by the Rann sediments and recent channel sands occurring in various streams.

The Gedi Fault

The northern limb of the Desalpar flexure zone show gentle dips and form the southern limb of the Balasar syncline. In contrast, the southern limbs are steeply dipping to vertical due to the effect of the Gedi Fault. The Miocene marine sediments also show vertical to steep dips in the vicinity of the fault and become horizontal in a short distance away from the fault. The Gedi Fault is therefore identified as the lithotectonic contact between the Mesozoic rocks forming the upthrown block and the Miocene sediments forming the downthrown block (Fig. 10.3a, b and c). However, the faulted contact is for the most part buried under thin Quaternary sediment cover. The Gedi Fault is, however, exposed in scattered outcrops starting from south of Fatehgarh to further east. The fault is also well exposed in Gangta bet island in the west. The fault here is characterized by a E-W striking reverse fault that show a steep dip towards north. The fault is expressed as a sharp contact between steep northward dipping Mesozoic sandstones and Miocene shales (Fig. 10.3c). There is a slight lateral dislocation in the fault when compared with the Gedi fault in the mainland which indicates the possible presence of a transverse fault buried beneath the sedimentary cover of the Rann surface at the eastern margin of the Gangta bet island. Another transverse fault is located to the east of Maya Wandh which is also similarly buried under Rann sediments.

GPR STUDIES

The GPR surveys using 200 MHz antenna were carried out in continuous mode and GPR surveys using 80 MHz antenna were carried out by Common Offset (CO) method in point mode. After setting the desired parameters during the acquisition, data were collected in N-S direction i.e. across the fault. Precautions were taken during the acquisition to minimise the reflections from above ground objects which can mask subsurface targets (Sun and Young, 1995).

Data processing was conducted using the GSSI RADAN processing software (RADAN for Windows, 2000). The basic processing was kept simple in order to avoid introducing any artifacts into the data. Processing step involved file header editing,

followed by horizontal scale normalization to correct for differences in the movement speed of the antennas during data collection (monostatic antenna). The data were then band pass filtered to cut out very high and very low frequencies. Lastly, automatic gain control (AGC) function was applied to compensate for the loss in amplitude at depth due to spherical convergence, scattering and dielectric loss, as well as amplitude loss occurring during some data processing steps. Before the final layout, the required static correction was incorporated to the processed profiles.

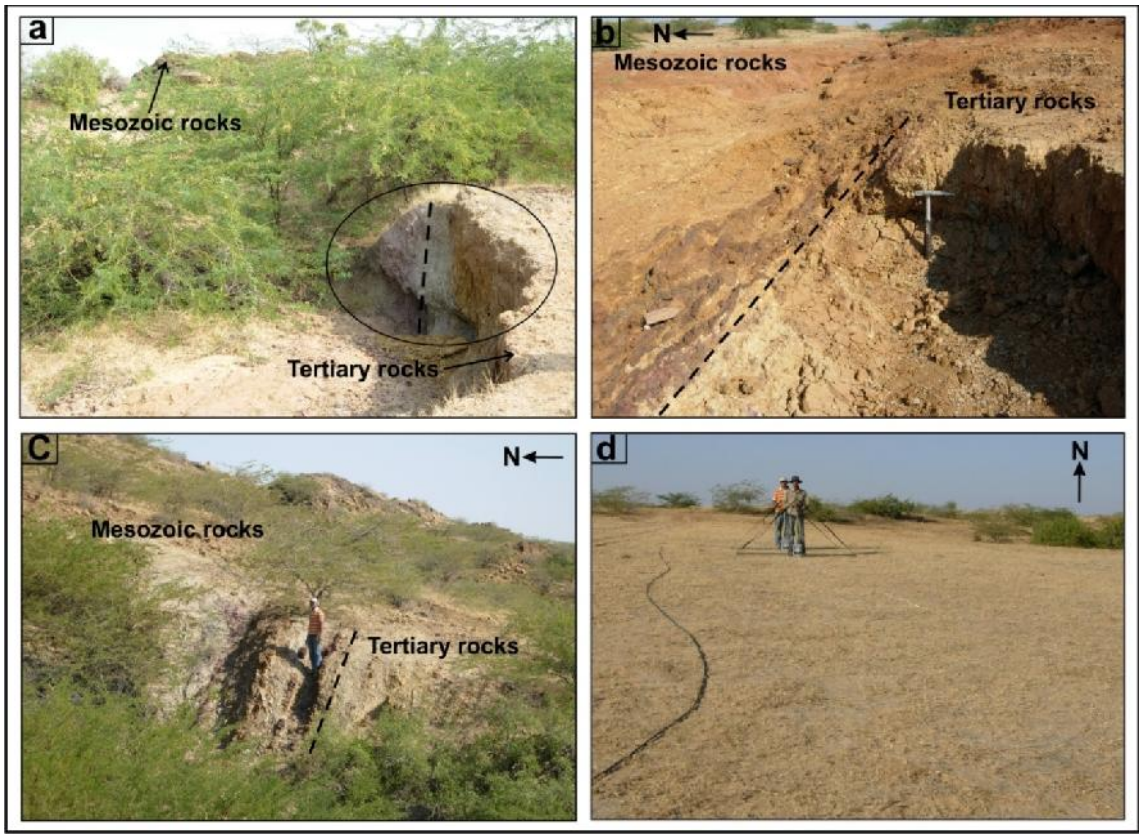

Figure 10.3. **(a)** Exposure of the Gedi Fault in a shallow stream to the south of Nagalpar. Note the subvertical contact between the Mesozoic rocks and the Tertiary rocks marking the Gedi Fault. **(b)** View of the Gedi Fault exposed in an artificial excavation between Nagalpar and Gedi. Note the steep northward dipping fault plane and the Mesozoic rocks riding over the Tertiary sediments. **(c)** Photograph showing the reverse nature of the Gedi Fault in Gangta bet. Note the steep northward dip of the compact Mesozoic strata and the softer Tertiary sediments. **(d)** View of the GPR survey using Multi Low Frequency (MLF) antenna over the miliolite deposits.

Velocity analysis

The CMP (Common Midpoint) profiles were used to determine the subsurface velocities, which were used for time/depth conversion. The velocity analysis was carried out by using GSSI RADAN software which computes the velocity by plotting the multi-offset data on a graph of velocity versus two-way zero-offset travel time. The CMP data

was obtained separately over the Mesozoic and Tertiary rocks. The obtained true velocity values of Mesozoic and Tertiary rocks are 0.13 m/ns and 0.12 m/ns respectively (Fig. 10.4). However, effective velocity values of Mesozoic and Tertiary rocks are same i.e. 0.13 m/ns (Fig. 10.4). In general, when GPR survey is carried out along vertically displaced strata, the average velocity which shows good spatial correlation in the depth correction is used (McClymont et al. 2010; Pauselli et al. 2010; Denith et.al. 2010). Therefore, we used the average velocity of 0.13 m/ns for time/depth conversion.

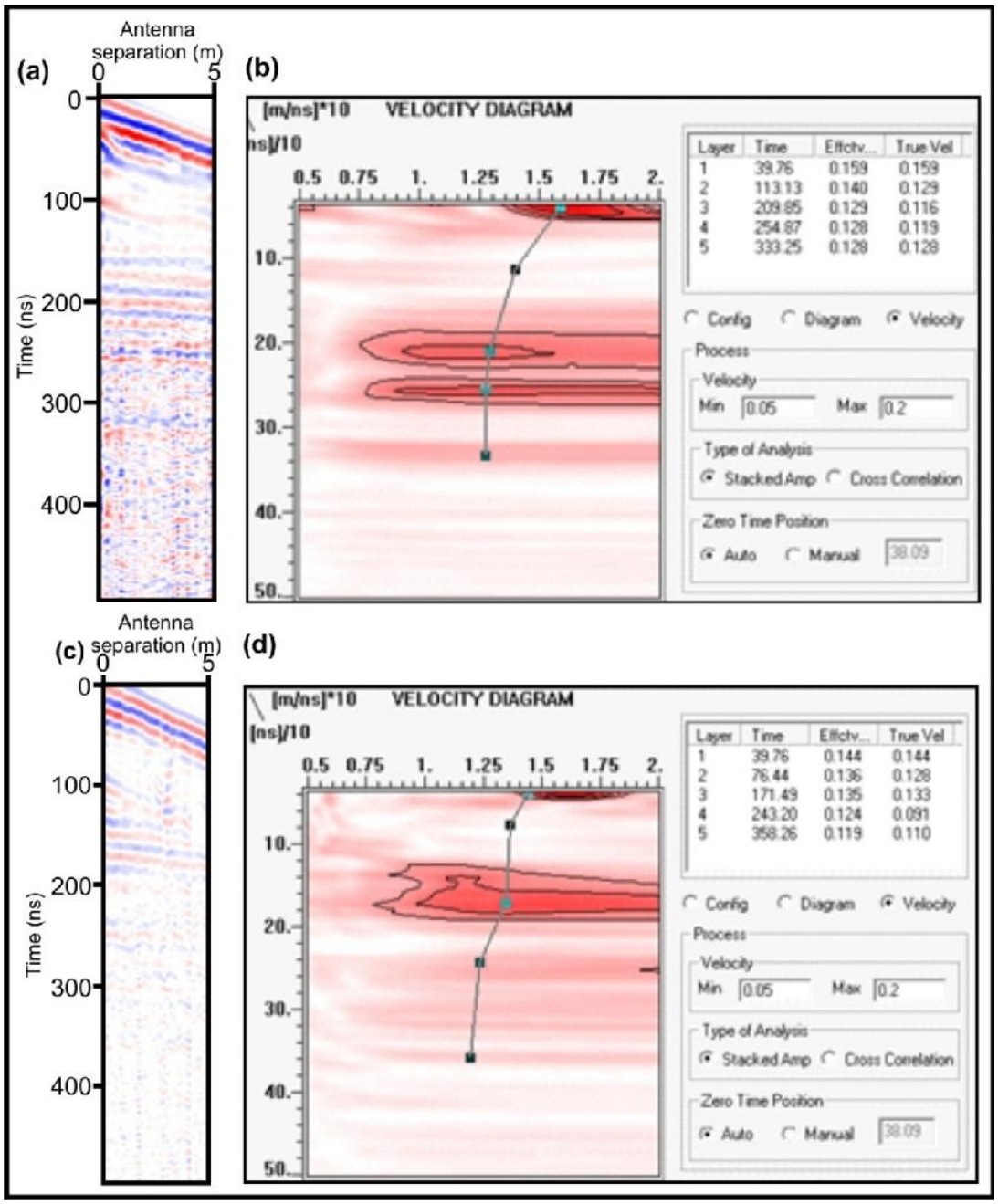

Figure 10.4 (a) Processed CMP profile taken over the Mesozoic rocks at Mayawandh. **(b)** Velocity diagram of the CMP profile shown in a. **(c)** Processed CMP profile taken over the Tertiary rocks at Mayawandh. **(d)** Velocity diagram of the CMP profile shown in b.

PART-E Gedi Fault (GF)

NATURE OF GEDI FAULT AND NEOTECTONIC IMPLICATION

The results of GPR surveys carried out across the Gedi Fault at six sites located to the north of Lakdaki Wandh south of Maya Wandh, northeast of Davari, south of Nagalpar, west of Gedi and southwest of Bhojnari Dhar are presented (Fig. 10.1b). As the fault strikes E-W, the GPR transects at all sites are oriented in N-S direction. All sites were selected after intensive field studies. As mentioned earlier, the fault trace exposed in the Gangta bet in the west and in the eastern part is manifested as the sharp lithotectonic contact between Mesozoic sandstones and Tertiary shales. This criteria was used to determine the possible fault location and precisely constrain the sites for GPR studies by examining the Mesozoic outcrops and scanty exposures of Tertiary sediments.

In general, the fault trace is identified in GPR profiles mainly on the basis of three criteria; displacement or truncation of reflection on either side of the possible fault strand, change in reflection pattern or drastic decrease of amplitude, and occurrence of a strong hyperbola (Meschede et al. 1997; Rashed et al. 2003; Ferry et al. 2004, Pauselli et al. 2010; Carpentier et al. 2012). The sharp and distinct lithological contrast proved to be advantageous in GPR investigations of the Gedi Fault. Thus, GPR data of the contact between two different lithologies with different electrical properties will result in the distinct pattern of reflections on either side of the contact plane. In our GPR profiles, Mesozoic rocks yielded relatively high amplitude reflections, whereas Tertiary rocks were represented by low amplitude returns because of the fine grained nature of Tertiary shales. The low amplitude of reflections is because of the attenuation of the radar waves attributed to the clayey nature of Tertiary shales. Thus, at some sites, fault is identified by an abrupt change in the amplitude and pattern of reflectors. However, at some sites, the subsurface location of fault plane is also represented by hyperbolic reflections in the GPR profiles.

Site 1

This site is located near Lakdaki Wandh village at the eastern margin of the Desalpar flexure zone. The GPR transect is located to the south of the ridge marking the flexure zone and comprising Mesozoic rocks. The Mesozoic rocks attain a near vertical dip at the base of the ridge. The GPR survey was carried out from the base of the ridge which extended southwards over a nearly flat surface. The data was acquired using a 40 MHz bistatic antenna in point mode with an initial separation of 2.25 m and a step size of 0.25 m. A part of the 48m long processed profile is shown in the Fig. 10.5a. The upper part in the profile shows high amplitude continuous to wavy reflection whose thickness

increases further southward. On basis of the observations at the site, these high amplitude reflections are attributed to alluvium cover whose thickness increases southward. A sharp transition in the reflections is seen below the radar reflections of soil cover. The basement for the soil cover is characterized by high amplitude reflection in the northern part of the profile while towards the south the amplitude of the reflections decreases abruptly. High amplitude reflections in the radar profile points towards the existence of low conductive medium through which the wave propagates. The close proximity of ridge in the north which exposes the compacted Mesozoic sandstone points towards the existence of the Mesozoic rock dominated by sandstone in the subsurface which is acting as a low conducting media (Fig. 10.5a). The low amplitude reflections in the radar profile accounts for highly conductive material like clays. Regional setting of the study area suggest it to be representing the Tertiary rocks which are rich in clay content as they are mostly shales (Fig. 10.6). This was confirmed in the shallow artificial pits about 1 km to the south of the site. The abrupt truncation of high amplitude and low amplitude reflections is seen at a distance of around ~ 16m (Fig. 10.5b). The truncation of radar reflections is interpreted as the fault plane of the Gedi Fault. The radar data shows that the Gedi fault is a vertical fault which shows a tendency to become a high angle reverse fault near the surface.

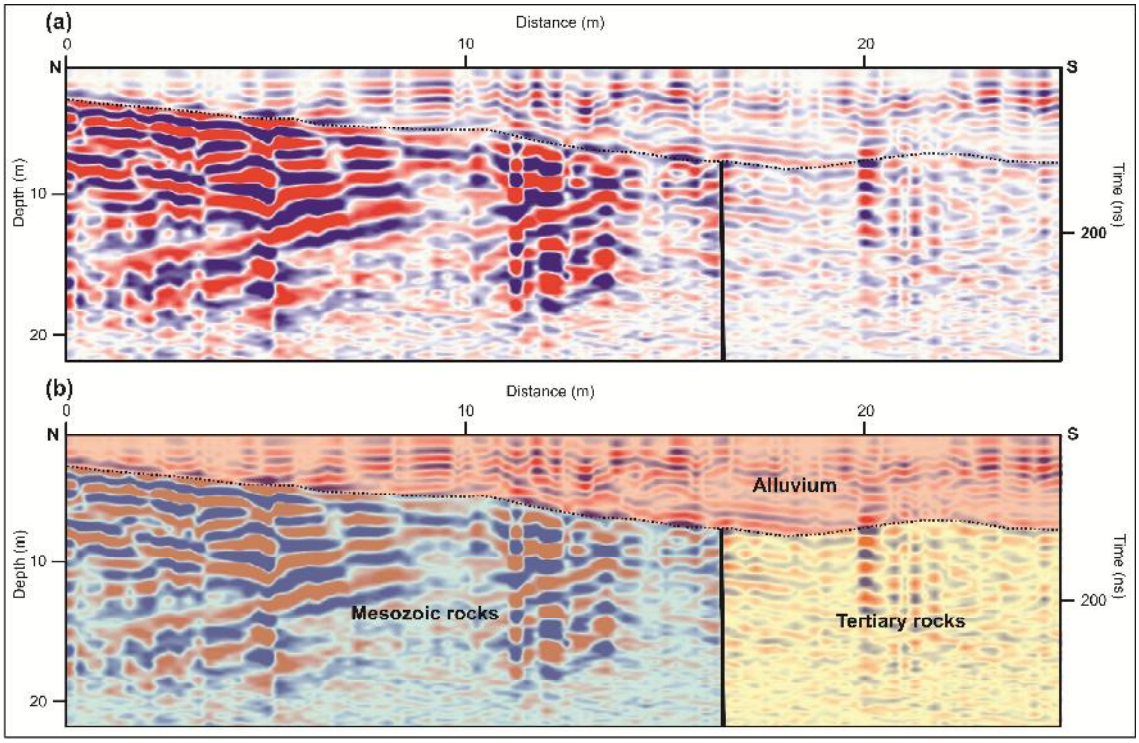

Figure 10.5 (a) GPR profile taken to the north of Lakdaki Wandh using 40 MHz bistatic antenna. Note the strong reflections emanating from the fault plane. **(b)** Interpreted section of the profile shown in a.

PART-E Gedi Fault (GF)

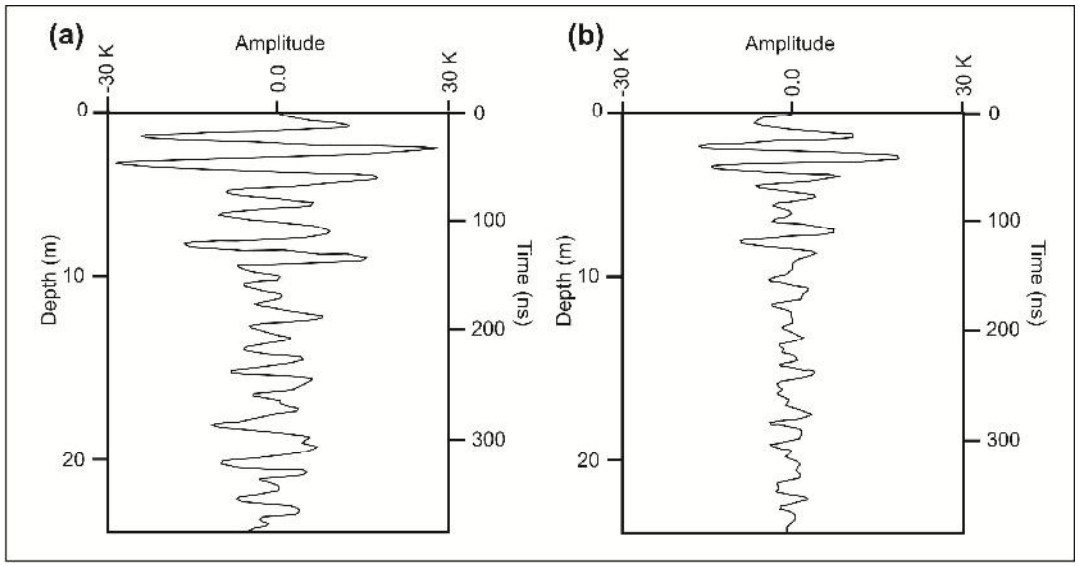

Figure 10.6 (a) Oscilloscope of a single scan emanating from of the Mesozoic rocks at site 2. **(b)** Oscilloscope of a single scan emanating from of the Tertiary rocks at site 1.

Site 2

Site 2 is located south of the Maya Wandh village. The Mesozoic and Tertiary rocks are covered by a thin veneer of loose Quaternary sediments that overlap the fault line. The GPR survey was carried out over a 25 m long N-S trending transect line using 80 MHz antenna in a common offset mode (Fig. 10.7a). The data was processed as described earlier. Topography correction was not required as the data was obtained over flat horizontal ground.

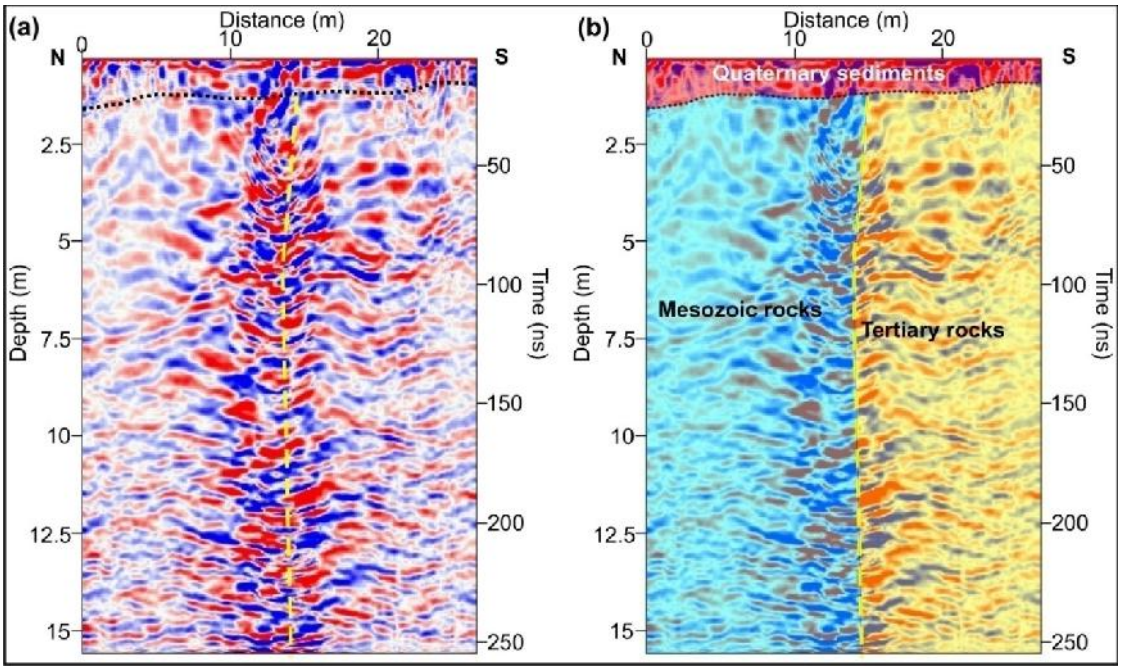

Figure 10.7. **(a)** GPR profile taken to the south of Mayawandh using 80 MHz antenna. Note the strong reflections emanating from the fault plane. **(b)** Interpreted section of the profile shown in a.

PART-E Gedi Fault (GF)

In the processed profile, a strong hyperbolic diffraction is seen at the distance of ~15 m (Fig. 11.4a). The occurrence of hyperbola could be because of the boulders or fault related structure (Ferry et al. 2004; Pauselli et al. 2010). The hyperbola is produced due to diffraction of radar waves from the steep fault plane. The well compacted Mesozoic sandstones and the semi compacted Tertiary rocks are characterized by high amplitude and low amplitude returns respectively on either sides of the fault (Fig. 10.8). The GPR data shows that the Gedi Fault is a steep northward dipping reverse fault (Fig. 11.4b). This is verified by the field measurements on the exposed Mesozoic strata exposed nearby.

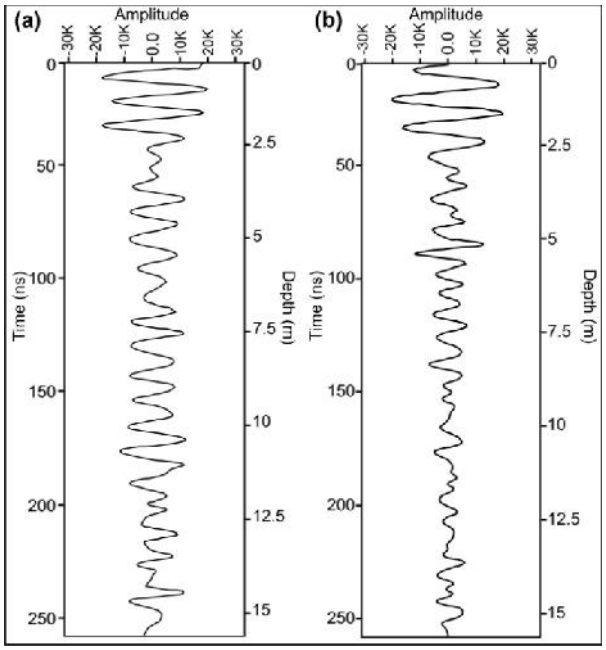

Figure 10.8 (a) Oscilloscope of a single scan emanating from of the Mesozoic rocks at site 2. **(b)** Oscilloscope of a single scan emanating from of the Tertiary rocks at site 1.

Site 3

Site 3 is located to the northeast of the Davari village. At this site, the Mesozoic and Tertiary rocks are overlain by 2-3 m thick semi compacted aeolian miliolite deposits that form small mounds. The GPR survey was carried out over a mound of miliolite dune along the N-S transect. The site was selected based on the exposures of Mesozoic rocks to the north of the mound and the Tertiary shales in the shallow E-W trending stream channel in the south. A 13 m long profile was collected by 80 MHz bistatic antenna at this site is shown in Fig. 10.9a. In the processed profile, the high amplitude continuous horizontal reflections from the surface to ~3 m depth are interpreted as representing the well stratified miliolite deposits (Fig. 10.9b). The part of the profile below ~3 m

constitutes the reflections from the Mesozoic and Tertiary rocks. The high amplitude signals in the northern side of the profile correspond to the Mesozoic rocks while the low amplitude reflections in the south correlate with the dominantly fine grained Tertiary sediments (Fig. 10.10a and b). The low amplitude returns are attributed to attenuation of radar waves as they propagate downward through the fine grained sediments. The abrupt change in the amplitude of the radar waves along the almost vertical line is interpreted as representing the fault plane. The GPR data shows that the Gedi Fault is reflected as a vertical fault at this site (Fig. 10.9b). However, the fault plane truncates at the contact with the overlying miliolite sediments suggesting that the fault has not propagated upward during Quaternary time.

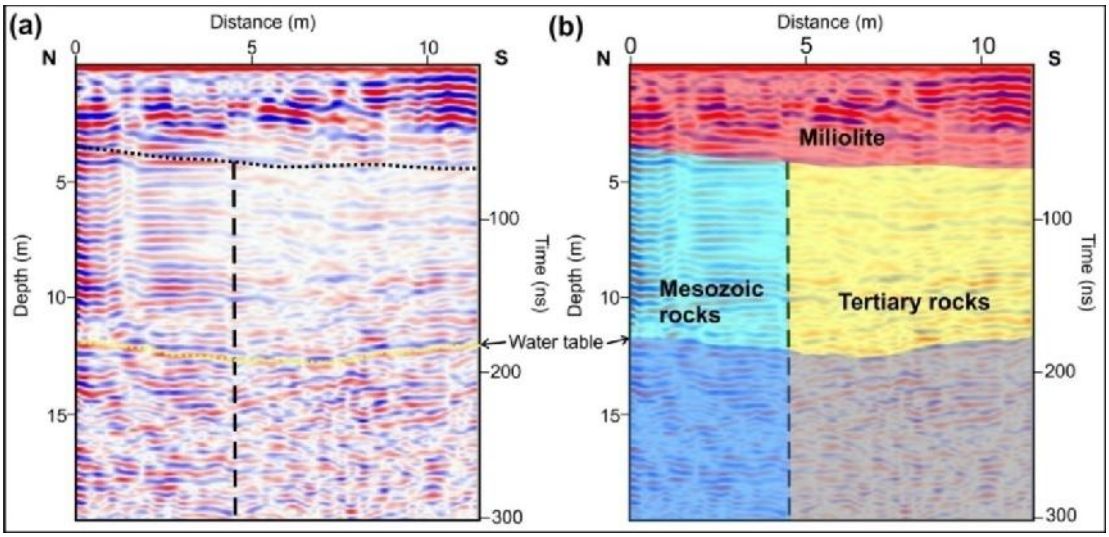

Figure 10.9 (a) GPR profile taken to the north of Davari using 80 MHz antenna. Note the sharp amplitude contrast marking the trace of the Gedi Fault. Also seen is the tendency of the fault to become reverse near the surface. **(b)** Interpreted section of the profile shown in a.

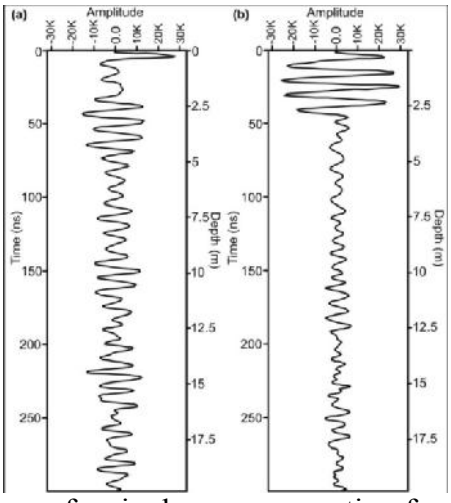

Figure 10.10 (a) Oscilloscope of a single scan emanating from of the Mesozoic rocks at site 3. **(b)** Oscilloscope of a single scan emanating from of the Tertiary rocks at site 2.

PART-E Gedi Fault (GF)

Site 4

This site 4 is located to the south of the Nagalpar. The Mesozoic and Tertiary rocks are found to be covered by a thin Quaternary alluvial sediment cover that is less than 0.5 m thick. The GPR data was obtained along the N-S trending survey line. Fig. 10.11a shows a processed profile obtained using monostatic 200 MHz antenna in a continuous mode. The thin Quaternary sediments are characterized by high amplitude parallel reflections in the upper 0.5 m in the processed profile (Fig. 10.11b). The profile shows relatively high amplitude reflections from the distance of 0 to 13 m corresponding to the Mesozoic rocks (Fig. 10.12a). Further southward from 13 m, there is a remarkable change in the pattern and amplitude of reflections (Fig. 10.11a and Fig. 10.12b). The reflections become significantly of low amplitude and also show the change in the pattern. It is interpreted that the change in the amplitude and pattern of reflection at the distance of 13 m is due to the tectonic contact between Mesozoic and Tertiary rocks (Fig. 10.11). Here, the Gedi Fault is interpreted as a normal vertical fault in this segment.

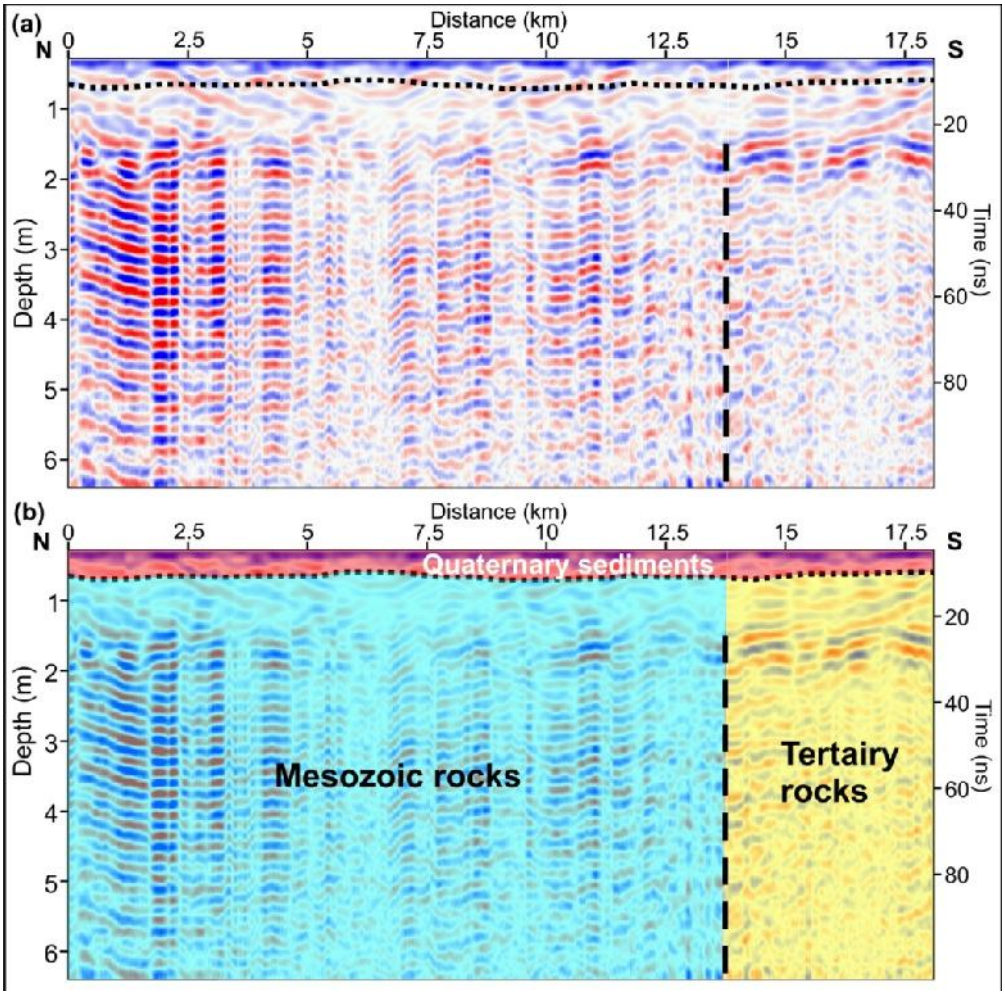

Figure 10.11 **(a)** 200 MHz profile obtained to the south of Nagalpar. Note the thin Quaternary sediment cover and the vertical nature of the fault. **(b)** Interpreted section of the profile shown in a.

PART-E Gedi Fault (GF)

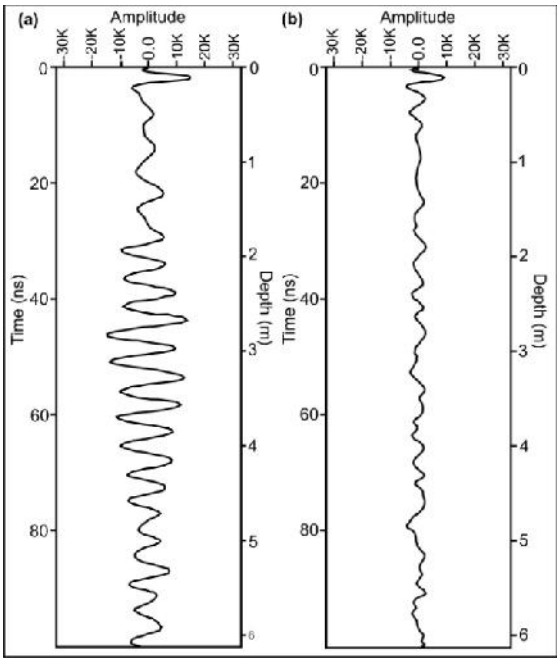

Figure 10.12 (a) Oscilloscope of a single scan emanating from of the Mesozoic rocks at site 4. **(b)** Oscilloscope of a single scan emanating from of the Tertiary rocks at site 3.

Site 5

Site 5 is located near the Gedi village. Field studies revealed that the trace of the Gedi fault is concealed below miliolite cover. The GPR survey carried out over a 45 m long S-N profile using 200 MHz antenna in a continuous mode (Fig. 10.13a).

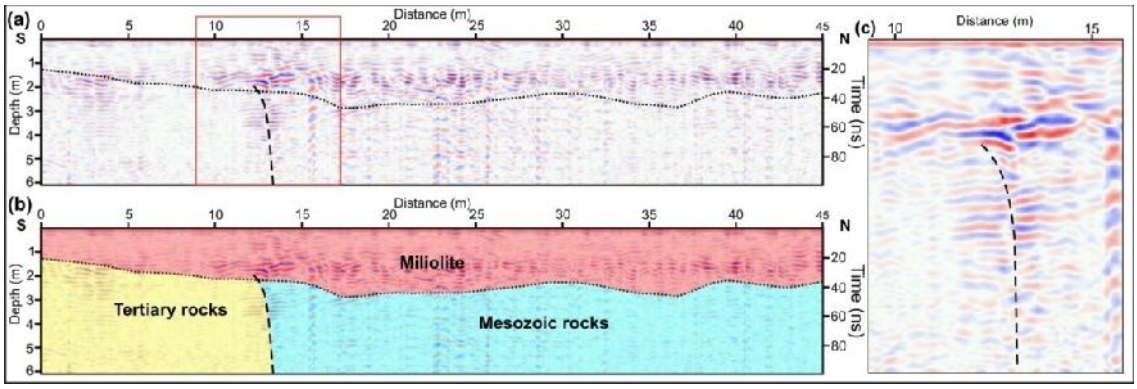

Figure 10.13 (a) 200 MHz GPR profile taken to the west of Gedi. **(b)** Interpreted section of the profile shown in a. **(c)** Enlarged area of fault location marked in (a)

In the processed GPR profile, the uppermost part of 0 to ~2 m in depth depicts wavy reflections of high amplitude corresponding to miliolite (Fig. 10.13b). The pattern of the reflections suggests that the thickness of the miliolite reduces southward. Below this, there are two zones of distinct reflection pattern from 0 to ~12.5 and from ~12.5 to 45 m in distance. Mesozoic rocks show high amplitude of reflection and Tertiary rock shows very low amplitude (Fig. 10.14a and b). There is an abrupt change in the pattern and amplitude of GPR reflections observed at a distance of ~12.5 m. We correlate this

with the contact between Mesozoic and Tertiary rocks marking the Gedi Fault. The fault plane is seen a steep north dipping reverse fault that becomes vertical at depth (Fig. 10.13b).

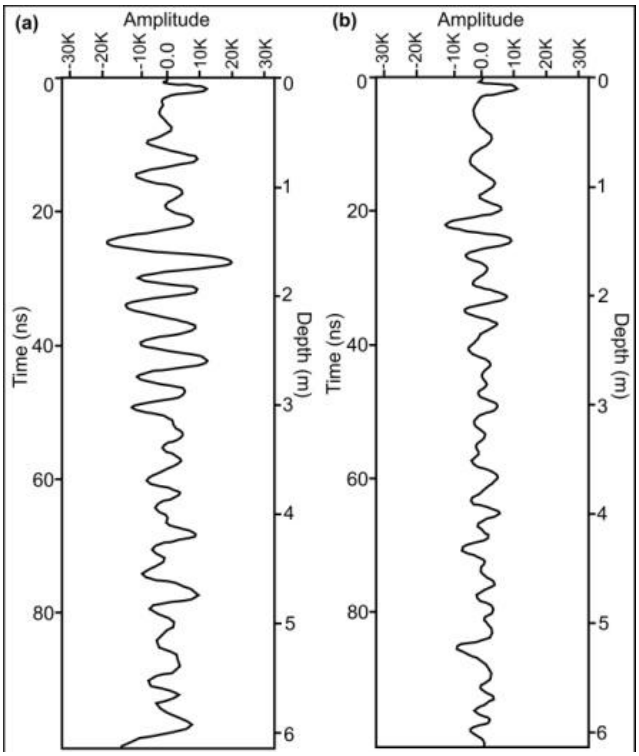

Figure 10.14 (a) Oscilloscope of a single scan emanating from of the Mesozoic rocks at site 5. **(b)** Oscilloscope of a single scan emanating from of the Tertiary rocks at site 4.

Site 6

Site 6 is located in the south of the Bhojnari Dhar village. In the field, the Mesozoic rocks are well exposed in small hills at Bhojnari Dhar and Tertiary rocks occur in the eastern side Bhojnari Dhar. However, the contact between Mesozoic and Tertiary rocks is not exposed. The GPR survey conducted at road-side over the 15 m long S-N trending survey line. The GPR survey carried out using by 80 MHz bistatic antenna in a CO mode (Fig. 10.15a). In the processed profile, the group topmost reflections show inclined and wavy pattern occurring in a cone shape (Fig. 10.15b). This type of reflection may be on account of screed material dumped during the construction of the road. Underlying this, there is high amplitude reflectors occur from 0 to ~6 m in distance, which correlate with the compact Mesozoic rocks. From 0 to 5-6 m distance the reflections are of very low amplitude corresponding to the Tertiary rocks (Fig. 10.15a and Fig. 10.16b). Further northward from 6 m distance the reflections are of significantly high amplitude and also show the change in pattern, corresponding to the Mesozoic rocks (Fig. 10.15a and Fig. 10.16a). The change in the amplitude of the reflection at a distance of ~6

m is because of the contact between the Mesozoic and Tertiary rocks marking the Gedi Fault (Fig. 10.15b). We interpret that the fault plane is vertical in the depth which becomes northward dipping reverse fault near the surface.

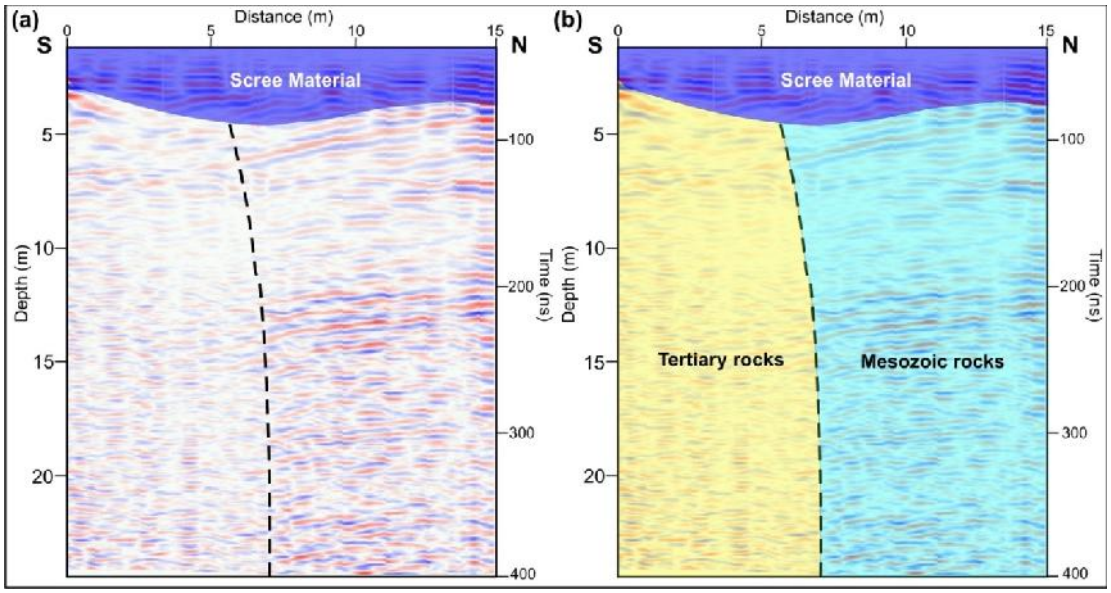

Figure 10.15 (a) 80 MHz GPR profile taken to the south of Bhojnari Dhar. The fault is marked by the amplitude contrast between the Mesozoic rocks and Tertiary sediments. The overlying scree deposit indicated is the road material dumped during construction of the adjacent road. **(b)** Interpreted section of the profile shown in a.

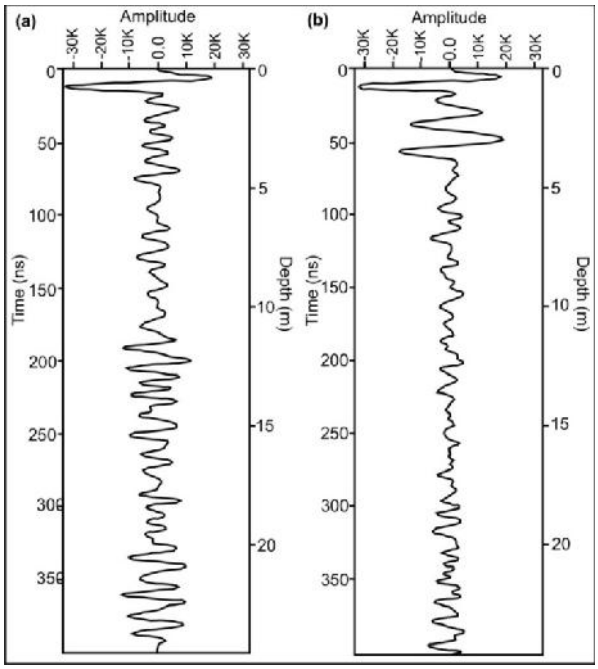

Figure 10.16 (a) Oscilloscope of a single scan emanating from of the Mesozoic rocks at site 6. **(b)** Oscilloscope of a single scan emanating from of the Tertiary rocks at site 5.

The Gedi Fault is a roughly E-W trending fault in the seismically Kachchh palaeorift basin that separates the Desalpar flexure zone comprising Mesozoic rocks to its

north and the Rav basin filled by Tertiary (Miocene) sediments in the south. Teleseismic monitoring of the post-2001 Bhuj earthquake aftershock sequence has revealed increasing seismic activity of low to moderate magnitude. However, there is no data on the precise location and shallow subsurface nature of the Gedi Fault. The present study is based on extensive field and GPR studies along the Gedi Fault with view to delineate its precise neotectonic setting and understand its nature in the light of contemporary seismic activity. The surface and near surface trace of the Gedi Fault is marked by the lithotectonic contact between the Mesozoic rocks of the Desalpar Flexure zone to the north and the Miocene shales in the south. The fault is exposed in patches in the eastern part and in Gangta bet in the westernmost part. In the central and western part, the fault is largely concealed below the thin Quaternary sediment cover consisting of aeolian miliolites and alluvial sediments.

Detailed GPR investigations were carried out at five sites selected after field studies. The GPR data obtained was processed and interpreted based on field observations. In general, all profiles clearly showed the lithological contrast across the fault. The Mesozoic rocks comprising well compacted sandstones yielded consistently high amplitude radar reflections while the Miocene shales showed attenuation of radar waves. The sharp amplitude contrast of the radar waves along a vertical to sub-vertical line is interpreted as the trace of the Gedi Fault. The contact between the Quaternary sediments and the underlying pre-Quaternary rocks was also picked up by GPR.

The GPR data shows that the Gedi Fault is in general a vertical fault at depth which becomes steep northward dipping reverse fault near the surface. The near surface reverse nature of the fault seen in the GPR profiles is corroborated by the field exposures. The fault plane, however, appears to be vertical at depth. The tendency of the Gedi Fault to become reverse near the surface is consistent with the N-S oriented compressional stress regime indicated by the fault plane solutions of the earthquake shocks in recent years. The GPR data also shows that the fault has not propagated upwards into the Quaternary sediment cover in spite of its active nature. This is intriguing given the fact that the focal depths of the post-2001 shocks are less than 15 kms. The low amount of slip that produced low to moderate earthquake shocks may not have been enough to produce a visible offset on the surface. No historic, palaeoseismic, and instrumental records of seismic activity along the Gedi Fault are available for the period before the 2001 Bhuj earthquake. It has been inferred that the present seismic activity along the Gedi Fault is due to stress perturbations caused by the 2001 event (Mandal, 2008) that occurred along the Kachchh Mainland Fault (KMF). The geomorphologic and neotectonic setting

delineated during the present study, however, indicates that the Gedi Fault may have been characterized by low to moderate seismic activity in response to the compressive stresses throughout the late Quaternary. As the Quaternary sediment is not displaced, it is inferred infer that no high magnitude earthquake occurred along the Gedi Fault in late Quaternary. Since the N-S directed compressive stresses are being released periodically through low intensity seismic activity, the probability of a large magnitude earthquake occurring along the Gedi Fault in future is low.

CHAPTER 11

BELA AND KHADIR ISLANDS

The Island Belt uplift consists of four discontinuous landmasses called Pachham, Khadir, Bela and Chorar islands. The islands are surrounded by ranns (local word meaning saline wasteland) characterized by the flat salt-encrusted surface and occurs at few meters above the mean sea level. The ranns are considered to be the uplifted floor of the former gulf (Merh, 2005; Maurya et al. 2008), which was navigable up to ~2 ka as suggested by historical accounts (Oldham, 1926). The rann surface is inundated under a thin sheet of water during the annual monsoon rains and storm tides from the western end where it opens up into the Arabian sea (Roy and Merh, 1981). The term 'island' is therefore used here in a descriptive sense and not in the true sense of the word.

The four islands though occurring as disjointed land masses show comparable geological, structural and geomorphic set up (Biswas, 1977; 1987; 1992; 1993). The general stratigraphy of Khadir and Bela comprises of Mesozoic and Tertiary rocks. Tertiary rocks are exposed only along the southeastern and southwestern fringe of Khadir Island while they cover two-thirds of the Bela island (Fig. 11.1). A stratigraphic comparison of both islands is shown in the Table 11.1. The Cheriya Bet Conglomerate Member is the oldest rock of the Kachchh Basin that is exposed in the northern part of the Khadir island. This is overlain by the Hadibadhang Shale Member followed by the Hadibadhang Sandstone Member. The Ghadada Member occupies most of the island and is capped by the Bhambhanka Member. In Bela island, a comparable succession of Mesozoic rocks is exposed, however, the basal Cheriya Bet Conglomerate Member is not exposed. The Bhanjada island is a stock-like basic intrusive body related to magmatic activity during the end of Mesozoic (Biswas, 1993).

The Mesozoic sequence is unconformably overlain by Tertiary rocks of Chhasra and Sandhan Formation (Fig. 11.1). The Chhasra Formation comprises a Lower Claystone Member and Upper Siltstone Member (Biswas, 1992). The Lower Claystone Member consists of grey and khakhi coloured, laminated to splintery gypseous shale and claystone with thin fossiliferous limestone intercalations. The Upper Siltstone Member consists of micaceous siltstone and laminated khakhi colour silty shale. This Formation is exposed in Bela island only. This is overlain by the Sandhan Formation mostly comprising

sandstones with subordinate amounts of conglomerate, claystone, laminated siltstone and fossiliferous limestone. This formation is exposed in both Bela and Khadir islands.

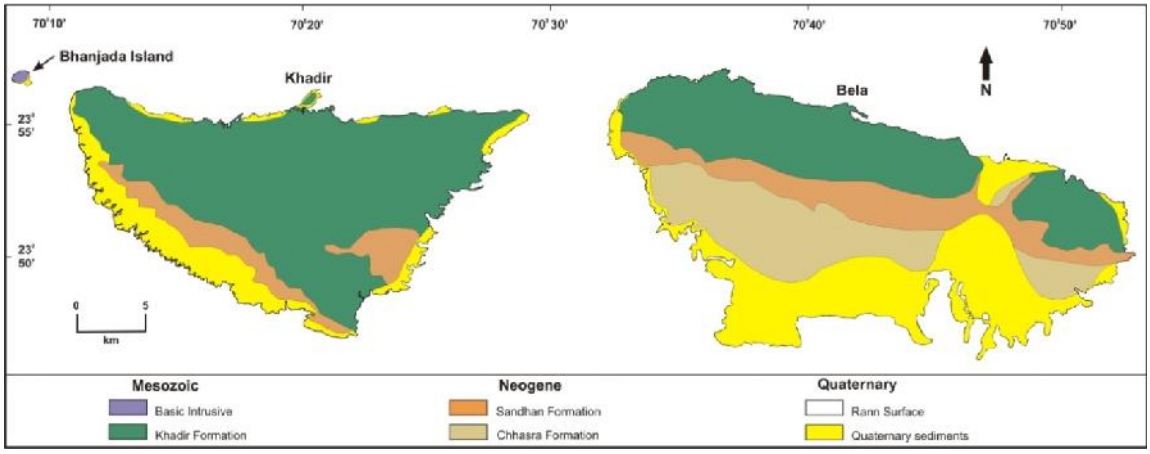

Figure 11.1 Geological map of Bela, Khadir and Bhanjada islands (after Biswas, 1993) with Quaternary deposits around the margins of the islands.

In Bela and Khadir islands, Mesozoic rocks are folded into E-W trending flexures called the Lodrani and the Khadir anticline (Biswas, 1993). The escarpment is formed on the southern limb of the anticlines while the northern limb is eroded away. The straight northern margins of the islands are attributed to the E-W trending Island Belt Fault (IBF) in the north, presently buried below the marine sediments of the rann. The behavior of the IBF in the existing compressional stress regime within the Kachchh basin is not known. Tectonic influences on the landscapes of the various islands and geomorphic evidence of neotectonics have not been documented as yet. The present study describes the tectonogeomorphic characteristics of the Bela, Khadir and Bhanjada islands and provides field based evidence in respect of the active nature of the IBF.

TECTONIC GEOMORPHOLOGY

As a consequence of similar geological and structural set up, the Bela, Khadir and Bhanjada islands show similar landscape characteristics. However, each of these islands also show distinct geomorphic characteristics of their own that have resulted from structural properties. The major geomorphic elements of the islands influenced by the tilted block structure are the northern escarpment and the southward-sloping backslopes that gradually merges with the rann surface (Fig. 11.2).

The IBF scarp

The E-W trending linear escarpment is the most spectacular and prominent feature of the landscape of the Bela, Khadir and Bhanjada islands. All the three islands are marked by prominent subvertical north-facing escarpments that abruptly rise above the

salt encrusted surface of the rann (Fig. 11.2). The escarpment shows the characteristics typical of an active fault scarp and is geomorphic expression of the Island Belt Fault (IBF), located further north below the rann sediments. However, the nature of the escarpment varies in all the three islands (Fig. 11.3a, b, and c).

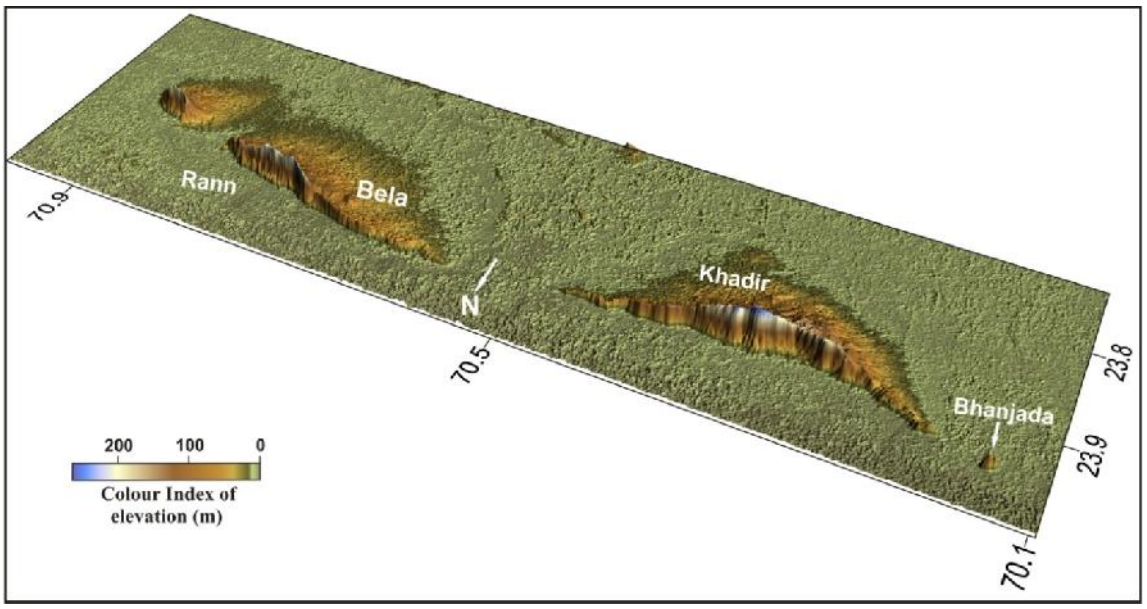

Figure 11.2 Digital Elevation Model (DEM) prepared from Aster Data showing the Bela, Khadir and Bhanjada islands. Note the prominent north facing escarpment and the south oriented backslopes.

Bela escarpment

The northern escarpment of the Bela island attains a maximum height of 246 m in the centre (Fig. 11.4). The scarp is subvertical to vertical and exposes rocks of the Mesozoic formations comprising the island. The escarpment of the Bela island can be divided into two segments separated by a prominent saddle (Fig. 11.3a). The eastern part of the escarpment corresponds to the northern flank of the Mouvana dome which consists of northerly dipping Mesozoic rocks and is therefore gentler. The western part forms the main escarpment and is subvertical to vertical (Fig. 11.5a). The Mesozoic rocks exposed in the face of the escarpment dip southward that form the southern limb of the Lodrani anticline. As described earlier, the northern limb of the anticline is cut by the IBF and is buried under the rann sediments. This imparts an aspect of a cuesta scarp to this part of the Bela escarpment. However, the crest of the escarpment dips on either sides i.e. towards east and west (Fig. 11.3a). This is in conformity with the plunge directions of the E-W trending Lodrani anticline. Throughout its extent from north of Bela to the eastern fringe of the island, most part of the vertical extent of the escarpment presents a undissected wall, a feature typical of scarps that have maintained their youthfulness due

to uplift (Fig. 11.3a). However, at the base, features of marine erosion, carved out by the sea that occupied the rann surface until late Holocene, are found (Fig. 11.5b). The crest of the escarpment forms the main drainage divide which effectively controls the southward courses of the majority of the river courses. However, the northward flowing Nilangadh river has cut a deep gorge that has been formed along a N-S trending transverse fault. The formation of the gorge and the wall like escarpment testifies to the youthful nature of the overall landscape of Bela island.

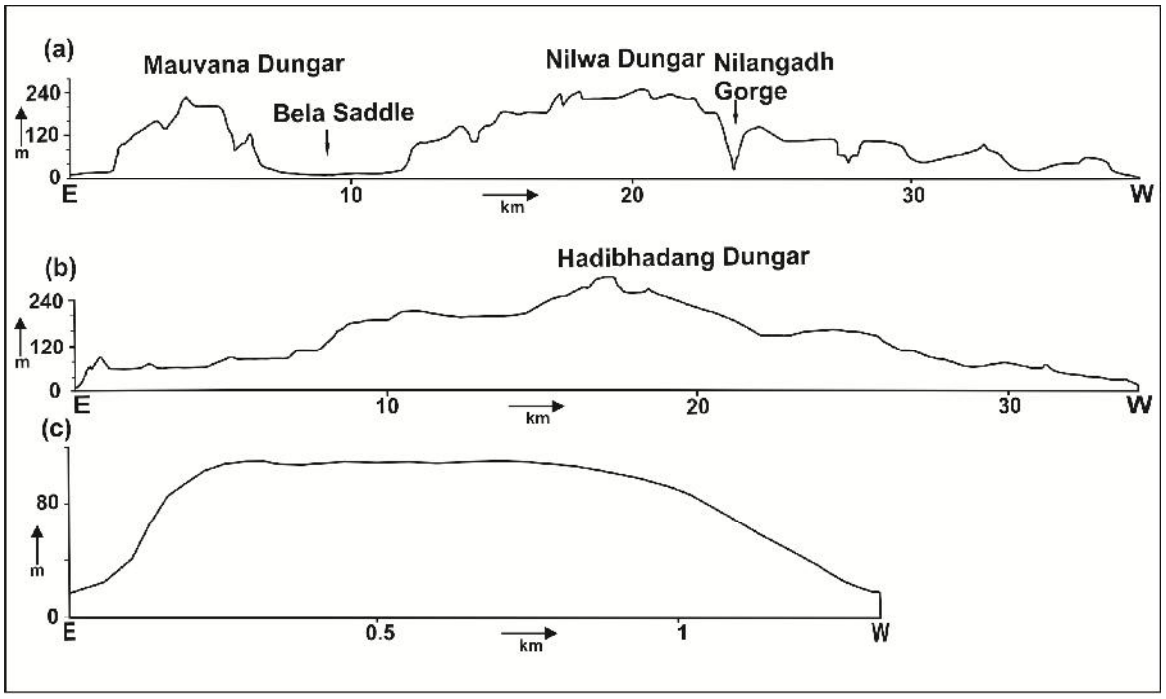

Figure 11.3 E-W topographic profiles drawn over the crest of the northern escarpments of Bela (a), Khadir (b) and Bhanjada (c) islands.

Khadir escarpment

As is the case of Bela island, the northern margin of Khadir island is also characterized by a subvertical to vertical north facing and E-W striking escarpment (Fig. 11.5c and 11.6a. However, unlike the Bela escarpment, the Khadir escarpment is continuous and extends from the eastern margin to the western margin of the island (Fig. 11.3b and 11.6a. The escarpment shows maximum elevation in the central part and lowers towards the east and west (Fig. 11.3b). In plan view, the escarpment is of arcuate shape with the concave side facing the rann in the north (Fig. 11.6a). The escarpment has developed in the southern limb of the Khadir anticline whereas the northern limb has been completely eroded off. The IBF is not exposed anywhere and is presumably buried below the rann sediments in front of the escarpment. This has resulted in a cuesta-like morphology of Khadir island. The Mesozoic sequence exposed in the Khadir escarpment,

can be correlated with those exposed in the Bela escarpment (Biswas, 1993). The escarpment forms major drainage divide which effectively divides the drainage in south flowing north flowing drainages. In general, the Khadir escarpment is steeper and presents a relatively more youthful aspect than the Bela escarpment (Fig. 11.5c). However, the base of the escarpment is wider and therefore the streams arising from the escarpment face flow towards the north to reach the rann surface. This is attributed to the compact conglomerates of the Cheriya bet Formation which form the oldest Mesozoic sediments of the Kachchh basin. All along the base of the scarp marine depositional and erosional landforms are found which were formed during the Holocene when the rann was occupied by shallow sea.

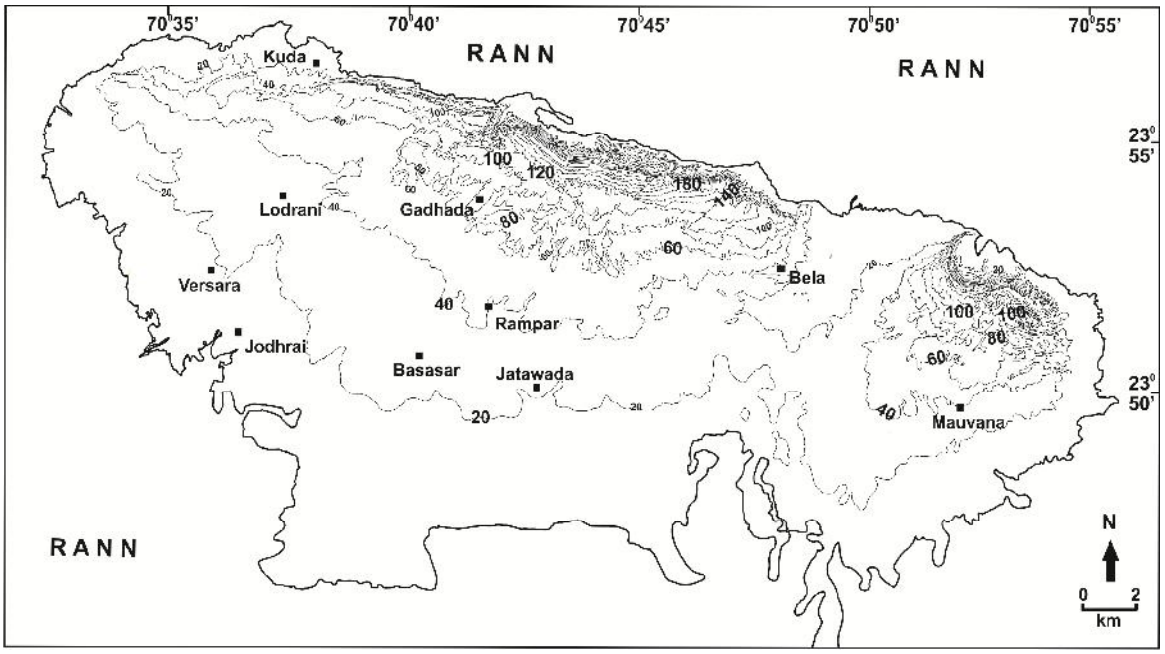

Figure 11.4 Contour map (20 m interval) of the Bela island showing the landscape. Note the steep northern escarpment and the gorge formed across the scarp and increased spacing of the contours on the backslopes

Bhanjada escarpment

Bhanjada island is the smallest in the entire island belt. It consists of igneous intrusive rocks and displays a rugged mountainous topography (Fig. 11.3c) different from that of Bela and Khadir islands, which are made up of south dipping Mesozoic and Tertiary rocks. However, the northern margin of Bhanjada island is also marked by a E-W trending north-facing escarpment (Fig. 11.6b), which suggests that it is also produced by faulting along the IBF. The escarpment is characterized by steep face, although gentler than the Bela and Khadir escarpments. Moreover, the crest of the escarpment is approximately at the same level from east to west whereas the Bela and Khadir escarpments are lowering towards the east and west (Fig. 11.3). This is attributed to the

plunging anticlines as described above. The eastern and southeastern margins of Bhanjada island are marked by raised intertidal flats comparable to those found on the western margin of Khadir Island.

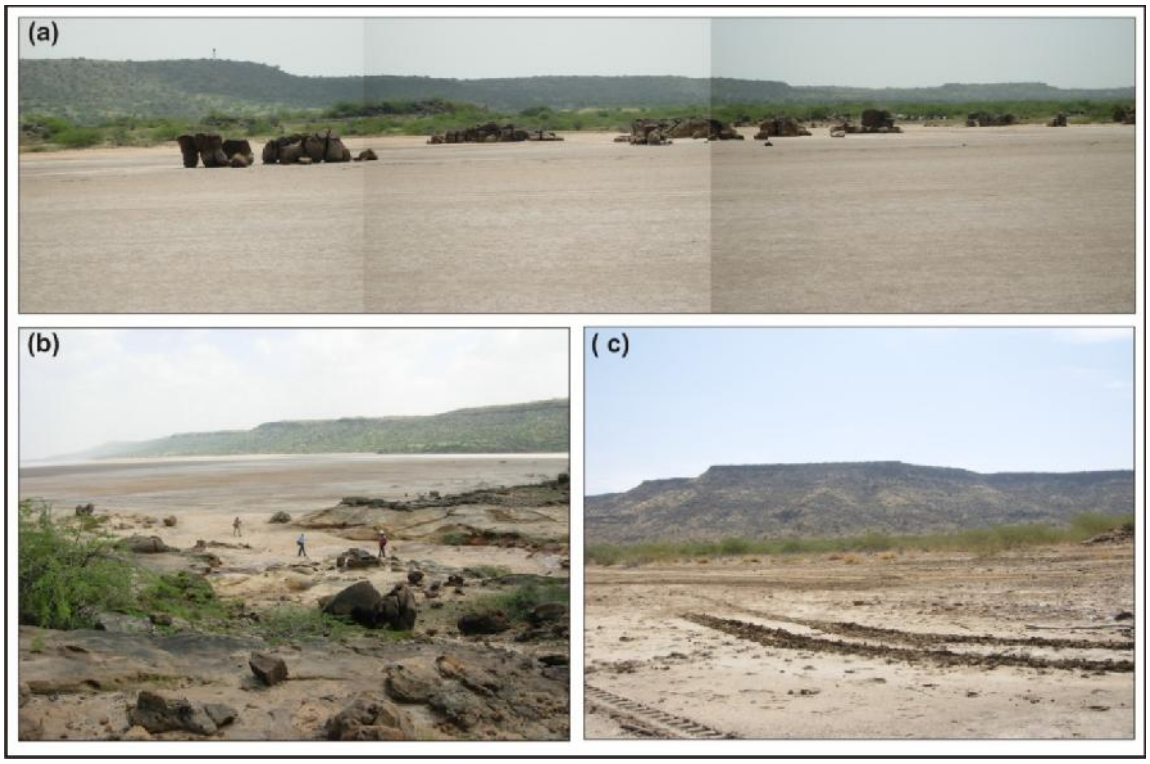

Figure 11.5 (a) Photomosaic of the northern escarpment of the Bela island. In the foreground is the rann surface and the vestiges of the palaeo rocky coast **(b)** Panoramic view showing the marine erosional landscape at the base of the Bela scarp seen in the background **(c)** View of the Khadir scarp. Note the youthful nature of the escarpment.

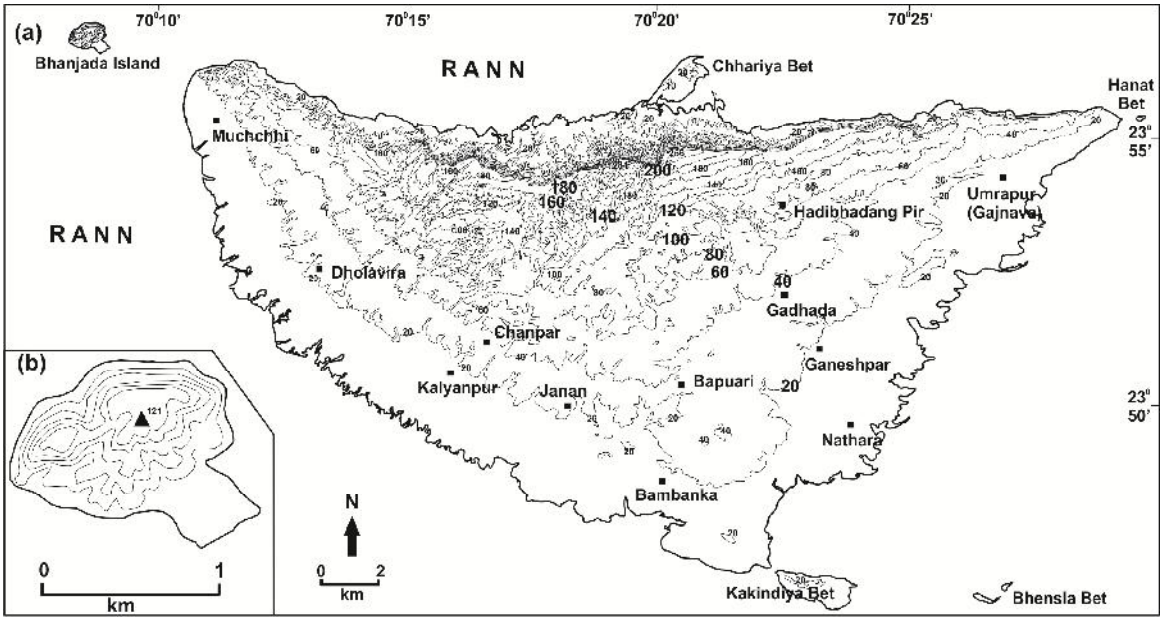

Figure 11.6 Contour map of the Khadir island **(a)** and Bhanjada island **(b)**.

PART-F Neotectonics of the Island Belt Fault (IBF)

South sloping backslopes

The entire extent of Bela and Khadir islands to the south of the crestline of the escarpment consists of southward slopes (Fig. 11.4, 11.6a), controlled by southward dipping Mesozoic and Tertiary rocks. They may be called as dip slopes; however, we prefer to call them backslopes since they are basically formed by faulting along the IBF and the fact that they are developed over the southern limbs of the anticlines. The backslopes are found to be steeper in the northern part whereas they progressively become gentle towards the south, southeast and southwest where they ultimately merge with the flat surface of the rann (Fig. 11.7). The backslope of the Bela island shows two distinct components as seen in the N-S cross profiles (Fig. 11.7a). The upper half (northern part) of the profiles are steeper, while further south they are gentler (Fig. 11.7a). This is attributed to the steeper dips of the Mesozoic rocks and the gentler dips and easily erodible nature of the Tertiary rocks. The knicks of the profiles coincide with the contact region of the Mesozoic and the overlying Tertiary rocks. In Khadir island, the entire backslope is developed over the south-dipping Mesozoic rocks as the Tertiary rocks cover them only along the southeastern and southwestern fringes of the island (Fig. 11.7b). However, the profiles indicate that the backslopes which are steeper in the northern part become progressively gentler southwards. Bhanjada island exhibits typical hilly topography (Fig. 11.6b), nevertheless, the overall southern slope of the surface is clear in the topographic profile (Fig. 11.7c). This, together with the presence of an escarpment at the northern margin provides clear evidence for tilting of the island in response to tectonic movements along the IBF.

The development of backslopes in all islands is attributed to the tilting of Mesozoic and Tertiary rocks in response to the neotectonic movements along the IBF located to the north of the islands. The southward dips of upper Tertiary rocks clearly suggest a component of Quaternary tectonic movements along IBF in the formation of backslopes in these islands.

FLUVIAL GEOMORPHOLOGY

The drainage configuration of Bela and Khadir islands shows remarkable influences of the major structural elements (Fig. 11.8, and 11.9). The islands are drained dominantly by south-flowing rivers that follow the tectonically produced backslopes of the islands to the rann. However, north-flowing river courses also exist which are also direct manifestations of the structure.

PART-F Neotectonics of the Island Belt Fault (IBF)

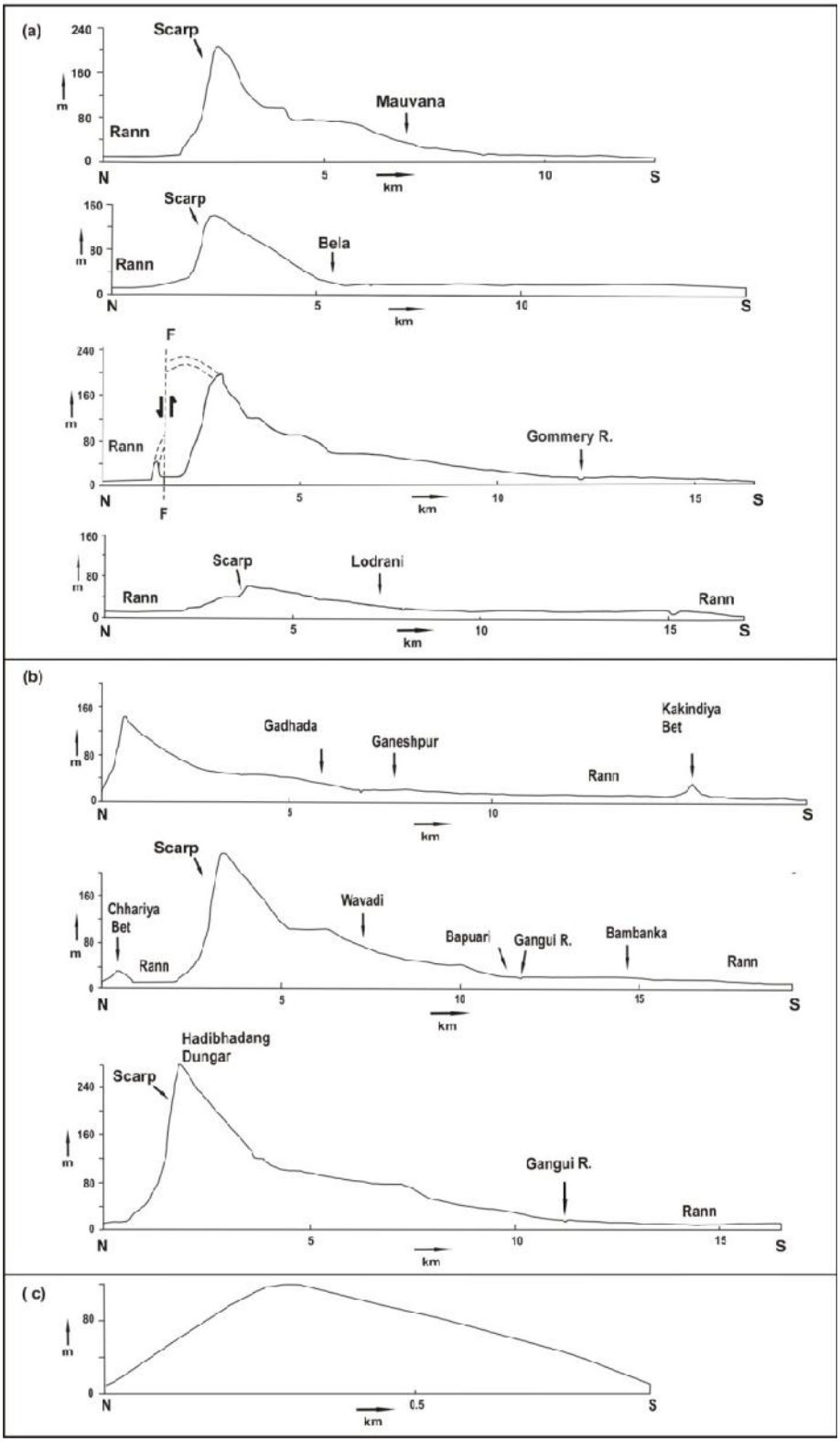

Figure 11.7 N-S topographic sections across Bela (a), Khadir (b) and Bhanjada (c) islands. The tilt block structure of the islands is clearly evident.

Bela island

The drainage configuration of Bela island also correlates well with the structural framework. South flowing rivers form a roughly parallel drainage pattern (Fig. 11.8) on

the backslope. The northeastern part of the island is characterized by radial drainage, controlled by the Muwana dome. The north-flowing river courses comprise the Nilangadh river, the Sharan river and the short streams arising from the crest of the northern escarpment (Fig.11.8). The Nilangadh river is an exception in the sense that it arises on the backslopes and flows northward across the northern escarpment in a deep gorge. This is attributed to a N-S trending transverse fault. The Bela saddle is drained by the Sharan river which originates to the south of the crest of the northern escarpment, flows southeast for some distance before taking a turn towards the north to flow along the saddle into the rann (Fig. 11.8).

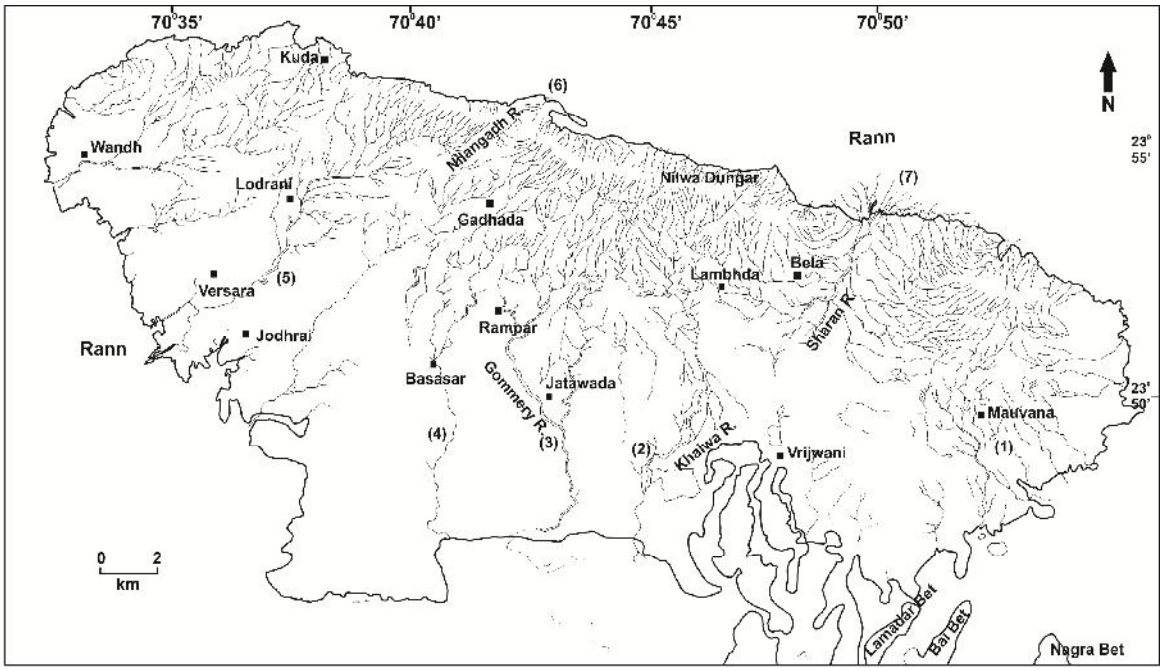

Figure 11.8 Drainage map of the Bela Island. Note the dominant south flowing drainages and the few north flowing drainages. Numbers 1-5 indicate the rivers whose longitudinal profiles of south flowing river shown in Fig. 11.10a; Number 6-7 indicates the river whose longitudinal profile of north flowing river shown in Fig. 11.10b.

All rivers are incised but the south flowing rivers show reduced incision towards the south due to the influence of the active southward tilting of the island. The north-flowing Nilangadh river forms a deep gorge, while the short streams draining the northern face of the escarpment also flow in deeply incised valleys. The south-flowing rivers of Bela Island present steep concave profiles upstream, while downstream the profiles are graded (Fig. 11.10a). The longitudinal profile of the north flowing Nilangardh and Sharan rivers is shown in the Fig. 11.10b. The long profile of the Nilangadh river has a steep concavity, consistent with its deep channel. The long profile of the Sharan river profile is

also concave in the upstream part with prominent knick points, while it is graded downstream (Fig. 11.10b). This is attributed to the fact that its lower reach is located in the saddle i.e. structural low and it flows through relatively erodible Neogene rocks and Quaternary sediments. Overall, the drainage shows obvious influence of the structural framework and active tectonic tilting of the Bela island.

Khadir and Bhanjada islands

The drainage of Khadir island is mostly made up of south flowing rivers that arise very close to the northern escarpment and flow southwards along incised valleys (Fig. 11.9). The south parallel drainage conforms to the southward directed tectonic slopes of the island. The decreasing trend of river incision towards the south points to active titling of Khadir island. The north-flowing drainage comprises short but deeply incised streams draining the face of the northern escarpment (Fig. 11.9). Bhanjada island, though consists of intrusive rocks, also has southward flowing incised rivers. This suggests active southward titling as well in response to the neotectonic activity along the IBF located in the north. The longitudinal profile of rivers flowing over the gentle backslopes of Khadir Island are shown in the Fig. 11.11. All long profiles are steep and concave in the upstream part and relatively gentler in the lower reaches. The experimental studies by (Snow and Slingerland, 1990) reveal that when a river is experiencing uplift in a tilted manner, maximum uplift is towards the upstream side and will result in greater erosion there than downstream to maintain the equilibrium profile. Thus long river profiles of rivers of Khadir and Bela islands support the tilted block type of uplift.

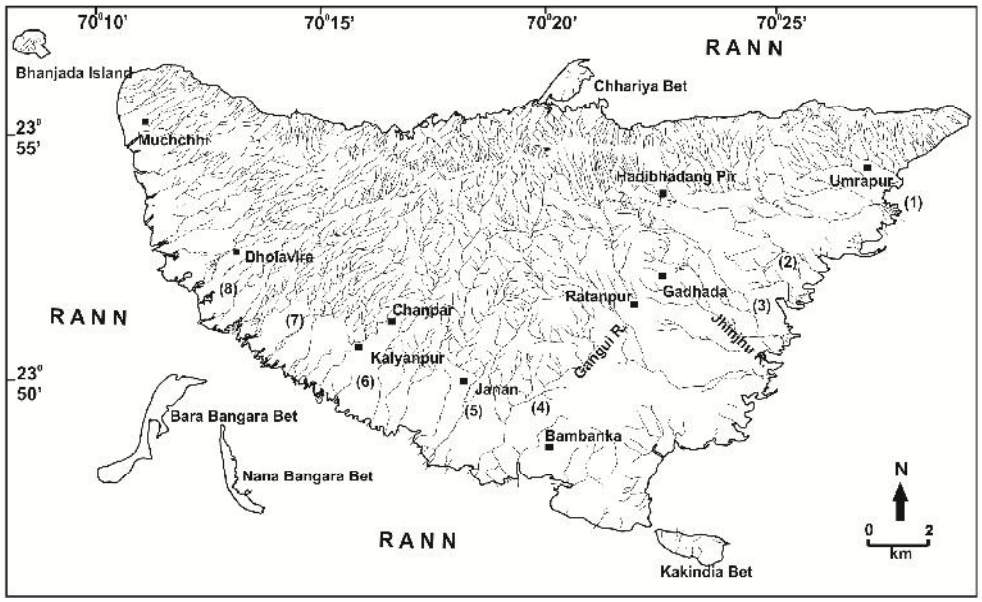

Figure 11.9 Drainage map of the Khadir island. Numbers 1-8 are the rivers whose longitudinal profiles are shown in the Fig. 12.11.

PART-F Neotectonics of the Island Belt Fault (IBF)

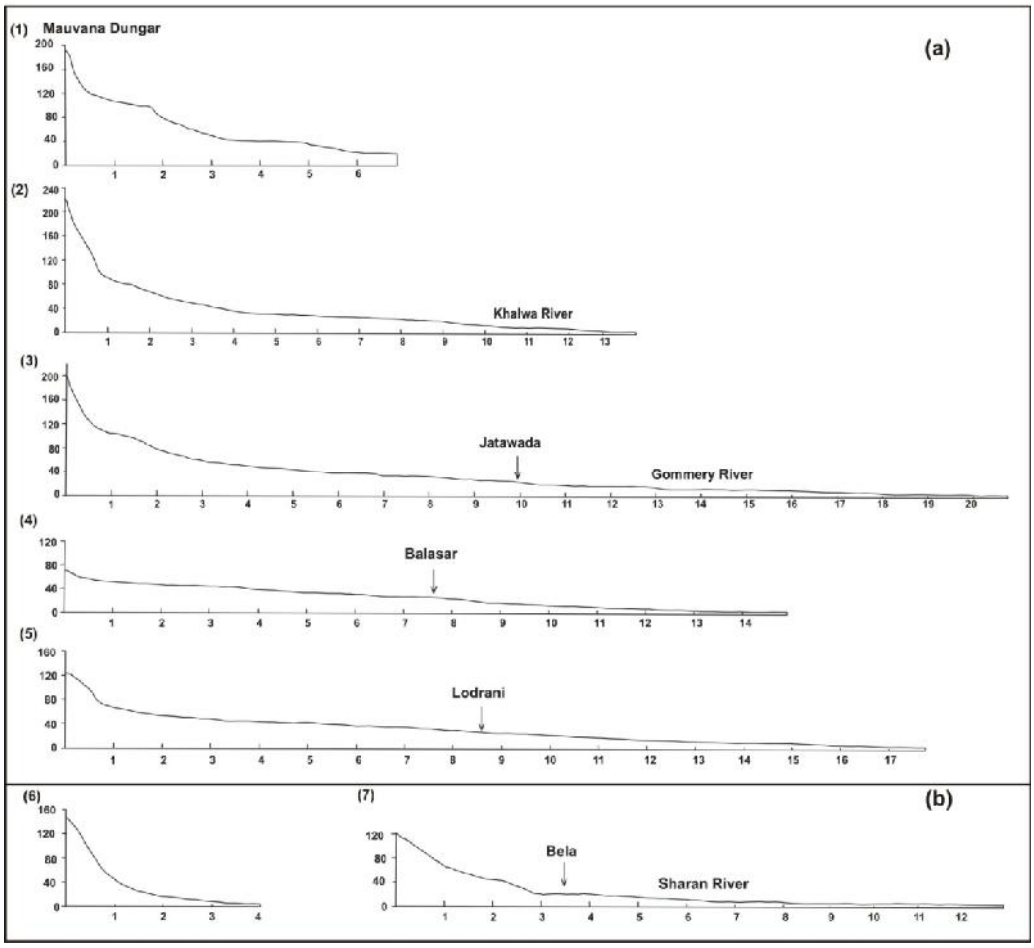

Figure 11.10 Longitudinal river profiles of the Bela island, **(a)** showing the south flowing streams which are draining the southern gentle backslope; **(b)** showing the longitudinal profiles of two north flowing streams.

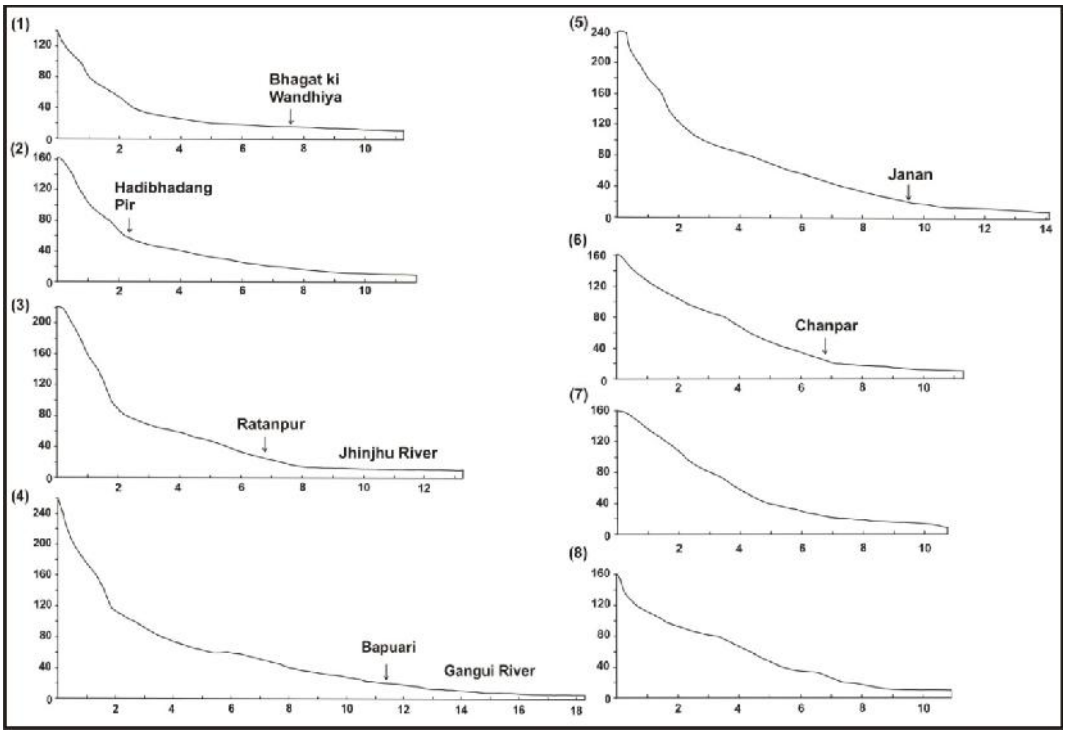

Figure 11.11 Longitudinal river profiles of the rivers of Khadir island.

PART-F Neotectonics of the Island Belt Fault (IBF)

GEOMORPHIC EVIDENCE FOR HOLOCENE UPLIFT

The salt encrusted flat surface of the rann surrounding the islands represent the floor of a former gulf that was connected to the Arabian sea in the west (Merh, 2005). The sea level curve for western India (Hashimi et al. 1995) suggests that the rann was inundated during the Holocene time. Historical accounts and studies in the Little Rann suggest that the rann was occupied by a shallow sea until ~2 ka (Gupta, 1975; Merh, 2005, Maurya et al. 2009). The existence of a shallow sea around Bela, Khadir and Bhanjada islands has resulted in the development of marine depositional and erosional features which provide evidence for uplift during the last ~2 ka.

Raised intertidal flats

The fringes of Bela, Khadir and Bhanjada islands, including the base of the northern escarpments show a thin linear zone of raised discontinuous flat depositional surfaces consisting of Holocene marine deposits. At most places, these flat surfaces gradually merge with the rann surface. However, these surfaces rise up to 4-6 m above the ranns on the landward side. These are composed of sediments that were deposited from a shallow sea up to ~2 ka BP. At western fringe of Khadir island and the eastern fringe of Bhanjada island, the raised depositional surface exhibit vertical cliff faces with 5-6 m sediment thickness (Fig. 11.12). Here, the terraced surface of these deposits show a general slope towards the south. At Khadir island, a gradual reduction in the height of the cliffs towards the south is observed (Fig. 11.12b).

The raised intertidal sediments at Khadir and Bhanjada islands are shown in Fig. 11.13. The base is marked by 20-30 cm thick pebbly to cobbly gravel which unconformably overlies the Mesozoic sedimentary and intrusive rocks in Khadir and Bhanjada islands respectively. The rest of the sections comprise in general by laminated clayey silts (Fig. 11.12b). The uniform beds of clayey silt are broken by the presence of several 2-10 cm thick fine sand layers (Fig. 11.13). The geomorphic setting and the nature of the sediments point to the deposition of these sediments in an intertidal environment. The upper part (~1.5 m) of the section at Khadir shows broad shallow channel-fill structures that also consist of laminated clayey silts. This could be representing the tidal channels that were formed as a consequence of regression and widening of the intertidal zone.

Figure 11.12 **(a)** Distant view of the western margin of the Khadir island. In the foreground is the rann surface. **(b)** Close view of the exposed section of the raised inter-tidal sediments. **(c)** Flat terraced surface of the raised intertidal sediments. In the background is the Bhanjada island. **(d)** View of the terraced surface of raised intertidal sediments at the eastern margin of the Bhanjada island.

Marine Erosional Features

Marine erosional features are found along the base of the north facing escarpments of the islands, where Mesozoic rocks are not overlain by the Holocene marine deposits. These erosional features are notches rocky platform and the sea caves attributed to the marine erosion before ~2 ka (Fig. 11.14). Marine notches are formed in bedrock of coasts near sea level due to either abrasion and/ or dissolution (Pirazzoli, 1986; Rust and Kershaw, 2000). In the tectonically active rocky coasts, marine notches are the precise indicator of rates and pattern of uplift (Rust and Kershaw, 2000). The notches are seen

intermittently along the toe of the scarp, possibly the sheltered zones. The notches show typical morphology as described by Pirazzoli (1986).

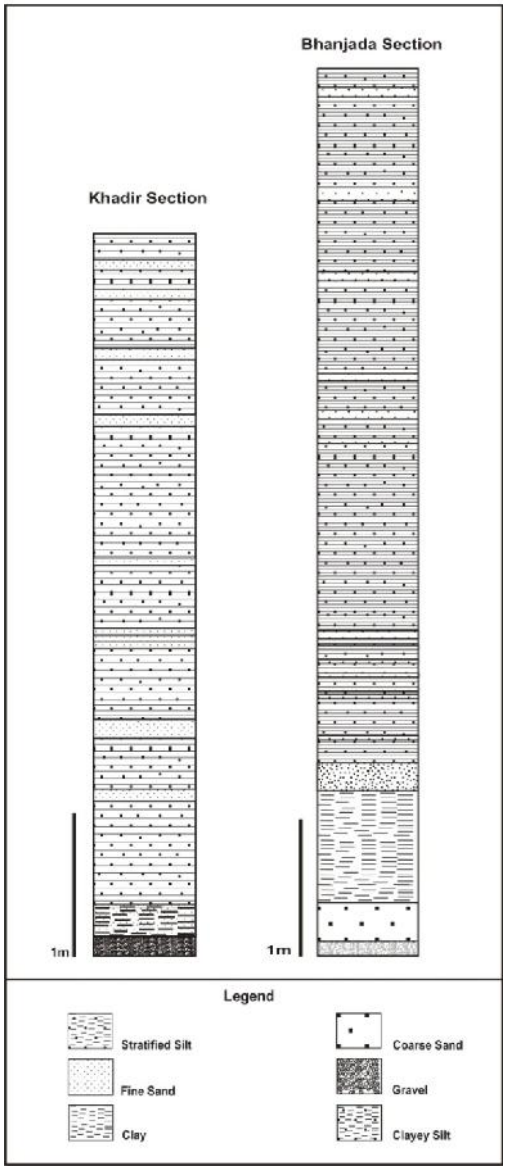

Figure 11.13 Lithologs of raised intertidal sediments at Khadir and Bhanjada islands.

The notches are seen at two levels. The lower notch occurs at a height of ~2m above the rann surface while the upper notch is found at ~4 m (Fig. 11.14a, b, c). The lower notch is wide spread but the upper notch is discontinuous and less prominent. However, it is found to occur at the same level at all places. The two levels of notches clearly suggest uplift of the islands in two phases during middle to late Holocene times. Flat rocky platforms are also found to occur at the base of the escarpments, developed on Mesozoic rocks (Fig. 11.14d). The platforms are easily recognizable as wide flat rocky surfaces at a height of ~4 m above the rann surface. Sea caves of various dimensions are also observed. In general, the formation of these erosional features is attributed to the

Holocene sea that occupied the rann surface and also indicates uplift during the middle to late Holocene in two phases. An uplift of at least 6 m is envisaged since middle Holocene to present.

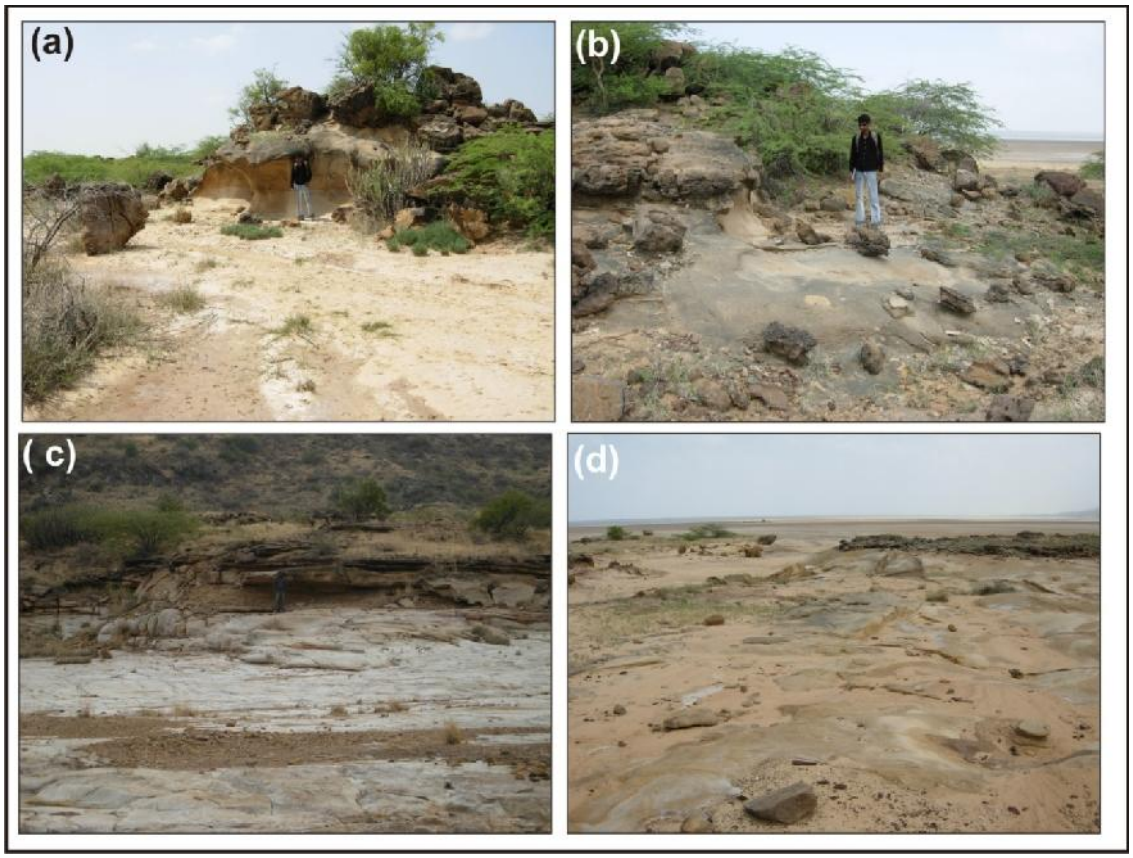

Figure 11.14 **(a)** Lower level marine notch lying north of Bela island; **(b)** Upper level marine notch lying north of Bela island; **(c)** Upper level marine notch lying north of Khadir island; **(d)** Rocky platform developed north of the Khadir island.

CHAPTER 12

PACHHAM ISLAND

The Pachham island is the westernmost island of linear chain of islands viz. Pachham, Bela, Khadir and Chorar islands. These are basically rocky hill masses exposing laterally correlatable Mesozoic and upper Tertiary (Miocene) rocks rising above the flat rann surface (Biswas, 1993). All the four islands including the Pachham island are bounded by the Island Belt Fault (IBF) in the north, which is concealed below a thick cover of Rann sediments. Recent geomorphic studies in the adjacent Khadir and Bela islands indicates that the islands have been uplifted in tilted manner in response tectonic movements along the IBF during the Quaternary (Chowksey et al. 2010).

The Pachham island is made up of two E-W trending hill ranges consisting of compacted and structurally deformed Mesozoic rocks with a intervening structural low (Fig. 12.1a). The northern part of the island is occupied by the Kaladongar hill range while the Goradongar Range marks the southern extremity of the island. The Kaladongar range is a large asymmetric and doubly plunging anticlinal fold with a steep northern limb and a gentle southern limb. The northern limb of the anticline is down faulted against the E-W trending IBF in the north. The fault is morphologically expressed as E-W trending precipitous scarp forming the northern margin of the Pachham island.

The Goradongar hill range is located at the southern periphery of the Pachham island which is composed of a chain of domal and anticlinal hills. The northern margin of the range is marked by north facing scarps representing the Goradongar fault. Due to the fault, the domes and anticline have steeper northern limbs with gentle southern limbs. The hill range is made of Mesozoic rocks classified as the Goradongar Formation which stratigraphically overlies the Kaladongar Formation.

TECTONIC GEOMORPHOLOGY

The geomorphic setup of the Pachham Island shows a remarkable influence of structural setup. The Pachham island is divisible into to morphotectonic units viz. the Kaladongar Hill range and Goradongar Hill range which marks the northern and southern hill range of the Pachham Island respectively (Fig. 12.1a). The Island is bounded in the north and south by Island belt and Goradongar faults. The island is also traversed by a N-S trending basement high named as a Median High forming a hinge of the Kachchh rift

basin (Biswas, 1987, 1993). Geomorphologically, both the faults are represented by E-W trending north facing steep scarps. The backslopes of the Kaladongar range constitutes a major part of the Pachham Island. The two ranges are separated by a synclinal valley described here as the central valley. The Pachham Island is surrounded by the rann surface which has been referred to as a raised floor of the Holocene sea. The presence of the raised intertidal flat on the western margins has been observed which appears similar to the raised intertidal surface at the fringe of Khadir and Bela island described by Chowksey et. al. (2010). The salient characteristics of the major geomorphological features of the Pachham island are described below.

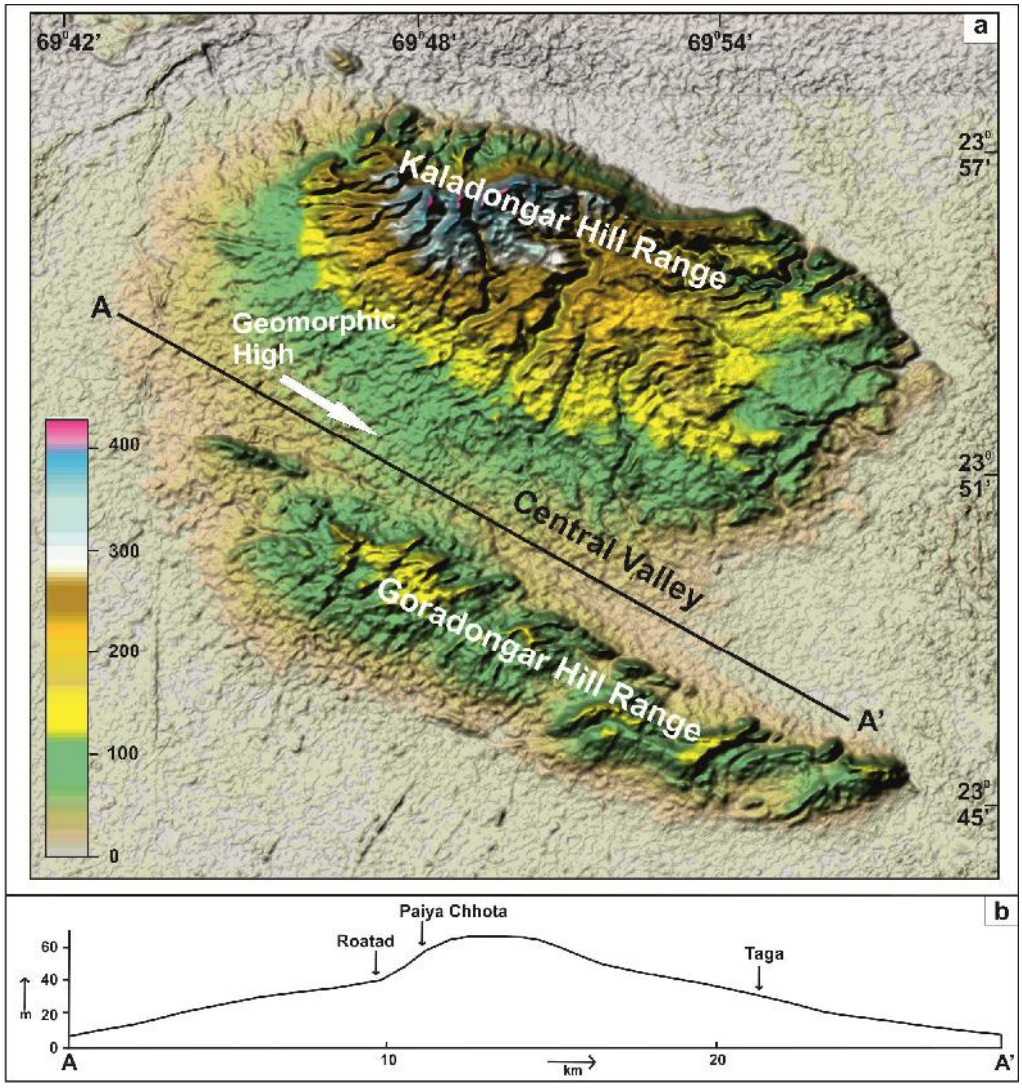

Figure 12.1 (a) DEM of the Pachham island showing the various morphotectonic units. Note the north facing escarpment at the northern margin of the island and the central valley between the two hill ranges. Line AA' is the transect for the topographic profile shown in (b). **(b)** Topographic section along AA' transect shown in (a). Note the prominent geomorphic high in the central part that corresponds to the subsurface Median high.

PART-F Neotectonics of the Island Belt Fault (IBF)

Kaladongar Scarp

The Kaladongar scarp marks the northern limit of the rugged Kaladongar Hill range as well as the Pachham Island. This is represented by a steep north facing surface which abuts against the flat plain rann surface in the north. The scarp is the geomorphic manifestation of the Kaladongar Fault which is buried beneath the rann surface. The scarp is formed in the southern limb of the Kaladongar anticline whose northern limb has been faulted and later eroded (Biswas, 1993). The scarp shows a sinuous pattern in the middle. It attains a maximum height in the centre with decreasing altitude east and westward. This decrease in altitude towards the eastern and western margin is in conformity with the doubly plunging Kaladongar anticline. Babia hill forms the highest elevation point of the Pachham Island as well as the entire Kachchh Basin. The scarp surface is characterized by the short north flowing drainages which rises from its summit and debouches in the Banni plain in the north (Fig. 12.2).

Back slope

The southern margin of the Kaladongar hill range which forms the back slope of the Kaladongar scarp is characterized by a gentle southward dip which later forms the northern margin of the central valley. The back slope represents the southern limb of the Kaladongar anticline. The back slope is mainly characterized by long southward flowing drainages. The slope acts as a large catchment area for the southward flowing parallel drainages. These drainages are serving as the major feeder channel to the axial river like east flowing Pipri river and the west flowing Bandi river which drains the central valley (Fig. 12.2). The drainages have carved out deep valleys in the upland part. The carving of the deep incised valleys in hard strata in an arid zone is a direct manifestation of the neotectonic uplift.

Goradongar scarp

The Goradongar Fault is a replicate of the Kaladongar Fault with its northern side forming the downthrown side. The fault is characterized by the steep northward facing scarps and marks the northern limit of the Goradongar range. Though the Goradongar fault lies further north of the scarp which is mostly canceled under the thick alluvium cover in the central valley and exposed in the eastern part where it is exposed as a vertical fault (Biswas, 1993).. The continuity of the scarp is broken by inter domal saddle zone, some of which are affected by transverse faults. The scarp is formed in the steeper northern flanks of Raimalro anticline, Dhorwar half dome, Juna anticline Ganiapur anticline and Kank hill anticline which together form the Goradongar range. Various

north flowing small streams arise from the scarp and drain towards the central valley (Fig. 12.2).

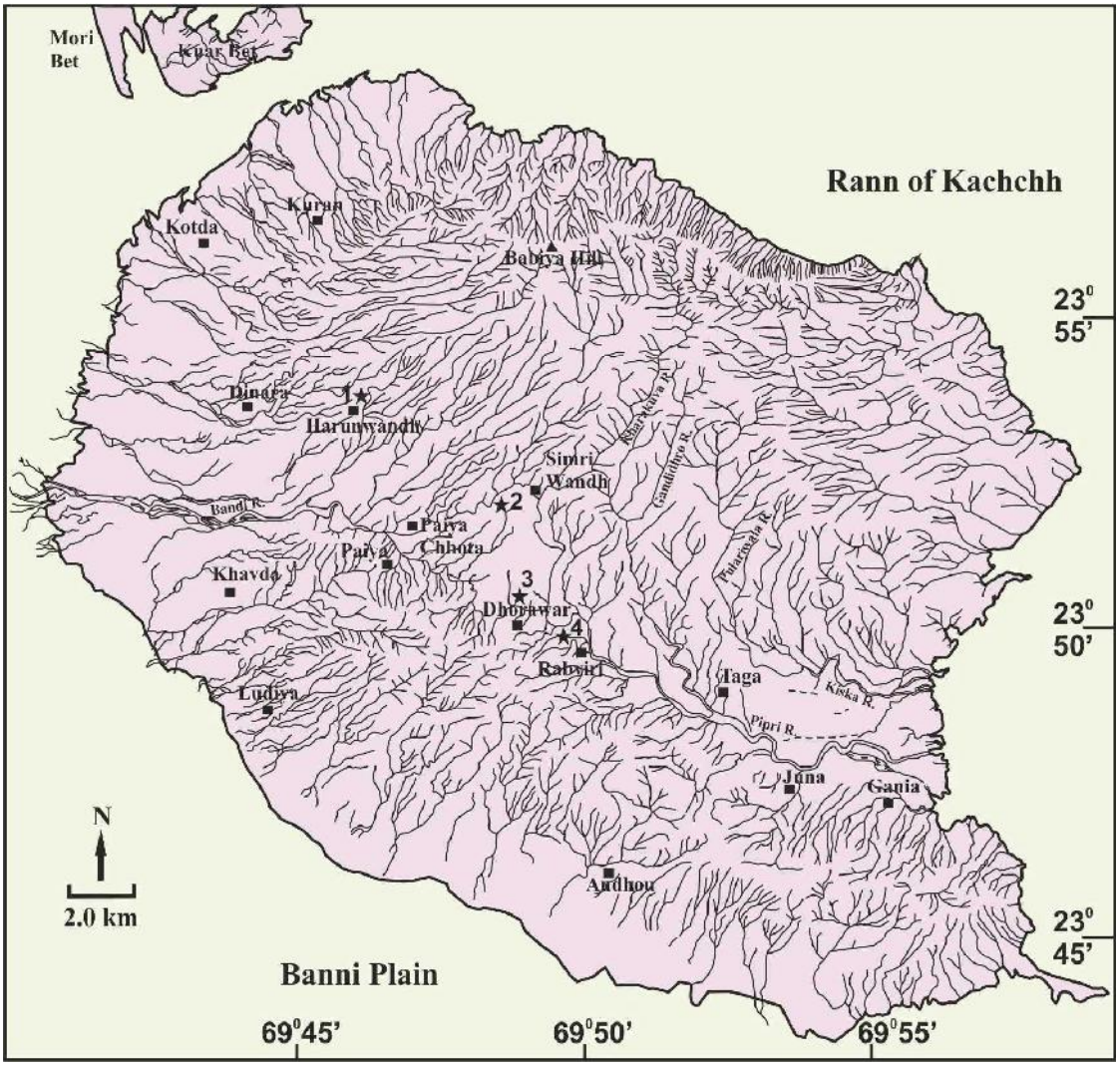

Figure 12.2 Drainage map of the Pachham island. Note the downward south flowing parallel drainages on the backslopes of the Kaladongar hill range and the radial drainage pattern in the Goradongar hill range controlled by the domal structures. Also seen in the bifurcation of the backslope drainage of the Kaladongar hill range into west flowing and east flowing drainages due to the presence of the geomorphic high in the central valley shown in the Fig. 12.1b. Numbers with star indicates the location of the litho-sections shown in the Fig. 12.6 and 12.8.

Central valley

The northern Kaladongar and southern Goradongar Hill range is separated by an E-W trending doubly plunging synclinal low termed as the central valley. The valley appears to be an asymmetric syncline whose northern limb is gentler in comparison to the steep southern limb. The southern limb of the Kaladongar anticline forms the northern limb (Fig. 12.3a) while the steep northern margin of the Goradongar Hill range marks its

southern limb (Fig. 12.3b). The N-S trending Median high which is defined as a basement high passes across the valley in its western part. The surface manifestation of the axial zone of this high can be seen in form of drainage anomaly near the Dhorawar village where the drainages bifurcates in to the east flowing and west flowing drainages (Fig. 12.2). The WNW-ESE cross section profile clearly depicts the geomorphic high with in the central valley (Fig. 12.1b) with the decrease in elevation towards the fringe of the island which is in conformity to the doubly plunging of the synclinal structure. The valley is filled by thick Quaternary sediments overlying Tertiary rocks in the eastern and western margin of the valley. The entrenchment of the drainages near the anomalous high have resulted in the formation of two level of terrace surface which is on account of post depositional uplift along the Median high (Fig. 12.4). Elsewhere in the valley, terrace are developed however deeply incised valley are common feature.

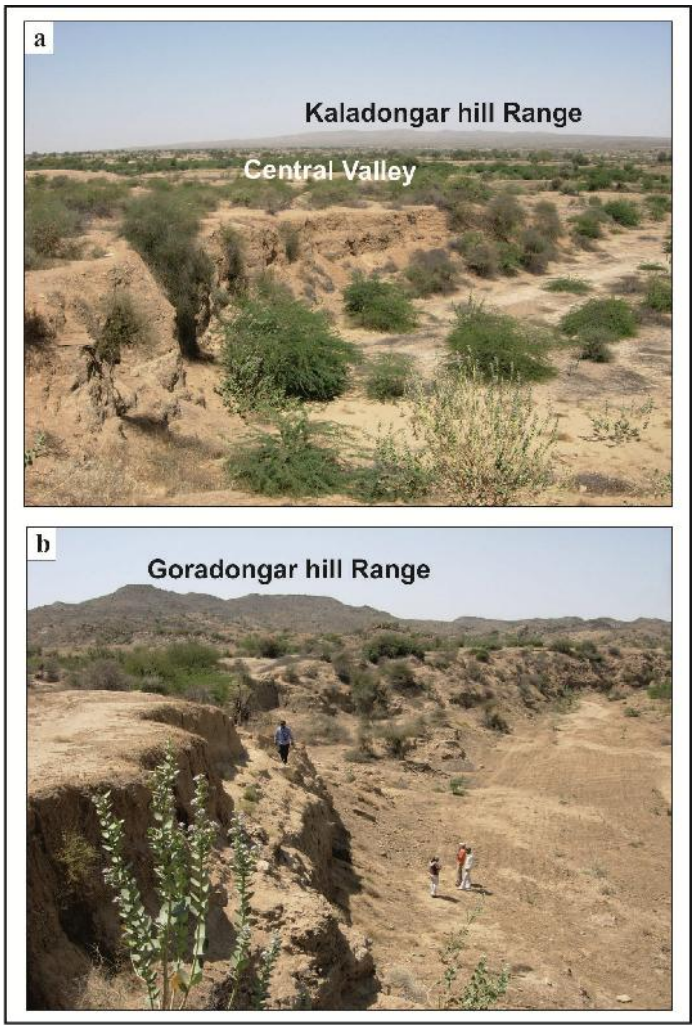

Figure 12.3 (a) Northward view from Goradongar range of the central valley filled with incised Quaternary sediments. Kaladongar hill range can be seen in the background. **(b)** Southward view of the incised cliff section of the Dhorawar stream exposing Quaternary sediments. In the background is the Goradongar hill range.

PART-F Neotectonics of the Island Belt Fault (IBF)

Raised Rann surface:

The rann surface is characterized as a vast saline waste land which was described as a floor of the paleo-arm of the sea which was navigable up to ~2000 years ago (Glennie and Evans, 1976; Merh, 2005). Pachham Island is surrounded by the flat surface of the rann. The fringe of the island shows ~4 m thick uplifted rann sediments which mainly comprises of silty clay to silty sand. The lithology appears to be similar to the raised rann surface as described by Chowksey et al (2010) from the Khadir island. This suggests uplift of the Pachham island during the Holocene time.

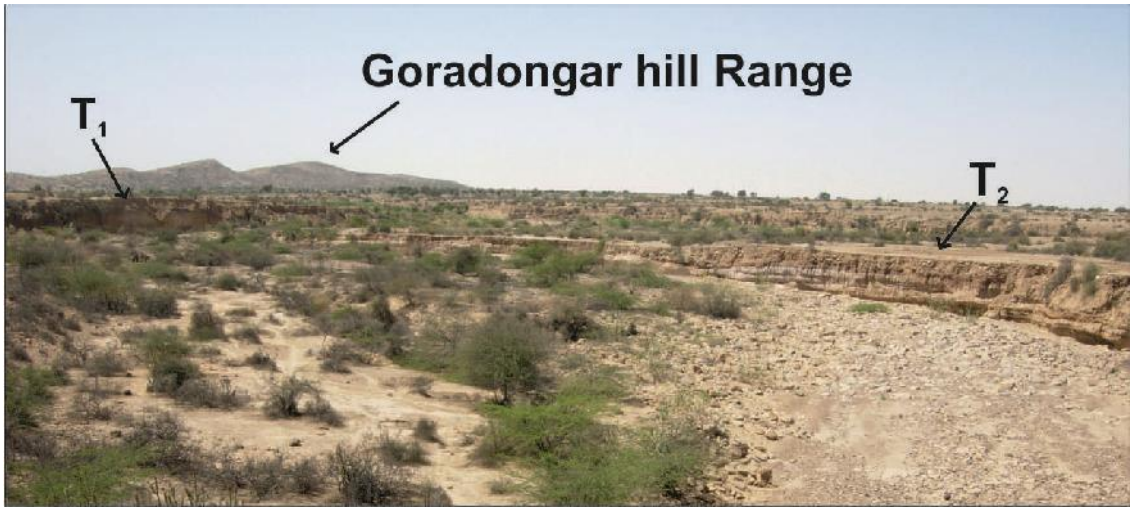

Figure 12.4 Southward view of the incised valley of the Paiya Chhota stream showing two levels of terraces surface. Goradongar hill range is seen in the distant background.

FLUVIAL GEOMORPHOLOGY

The Pachham island is characterized by a short north flowing drainages and long south flowing drainages (Fig. 12.2). The two scarps viz. Kaladongar and Goradongar scarp are acting as a major drainage divide in the north and south of Pachham Island. Parallel drainage is the major characteristic drainage pattern. The Kaladongar scarp is characterized by a short north flowing drainages which rises from the summit of the scarp and drains the scarp face and debouches in the rann. While long and parallel drainages drains the gentle back slope of the Kaladongar hill range. The south flowing drainages forms the major tributaries to the east and west flowing axial rivers like Pipri river and Bandi river respectively which follows the gentle plunge of the central valley towards the east and west respectively.

In the present study the major emphasis is given to the rivers following the back slope of the Kaladongar as it covers a long distance and flow across various E-W trending faults related to the Island Belt Fault to the north (Biswas, 1993). The rivers show deep

entrenchment in the upland as well as its downstream where they have incised the Quaternary as well as the basement rocks. In order to understand the effect of the tectonics on the river longitudinal profile of various south flowing rivers were prepared (Fig. 12.5). The Pipri river is the longest river which in the upstream is known as a Kharakuva river. It rises from the back slope and flows eastward in the central valley. The longitudinal profile of this stream depicts a prominent knick point near Simri Wandh close to which the river channel takes a sudden deflection towards the east. This sharp deflection of the stream is due to the rapid uplift along the buried sub surface structure in form of Median high. As the river enters the central valley the river profile becomes graded. Similar prominent knick point can also be seen near the proximity of the Median high in the south west flowing Paiya Chhota stream (Fig. 12.5). Here three prominent breaks in the river profile can be seen which falls well within the vicinity the Median high and later the profile of the river becomes graded as it gets merge with the west flowing Bandi river. The other south flowing depicts a graded profile as they enter the river valley. Overall, the profiles of all the rivers show distinct convex up segments which suggest the influence of neotectonic uplift along various faults (e.g. Schumm et al. 2000; Keller and Pinter, 2002; Molin and Fubelli, 2005; Menendez et al. 2008; Bull, 2009; Joshi et al. 2013).

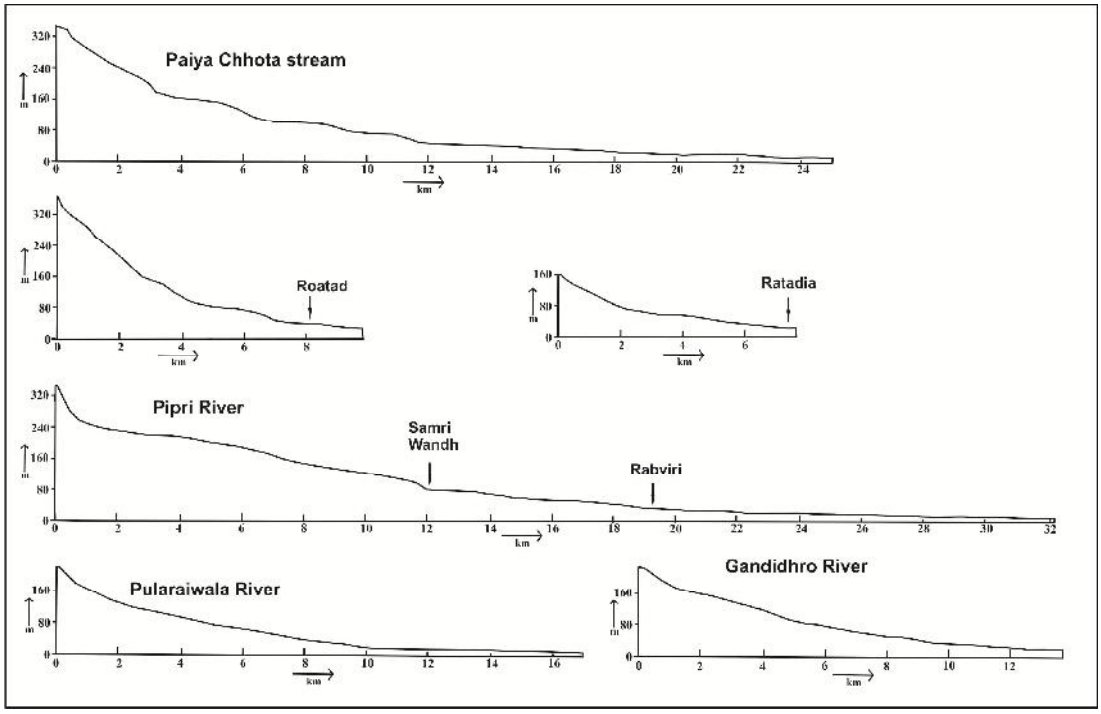

Figure 12.5 Longitudinal river profiles of the south flowing rivers draining the back slopes of the Kaladongar Hill Range. Note the prominent convex up segments in all the profiles.

PART-F Neotectonics of the Island Belt Fault (IBF)

QUATERNARY SEDIMENTS

The central valley has acted as a depo-center for the deposition of Quaternary sediments mainly dominated by fluvial agencies. Tertiary rocks appear to be buried under a thick apron of Quaternary sediments which extends all along the central valley. Good exposures of the Quaternary deposits are seen along the entrenched river sections, which are mostly dominated by colluvial fluvial deposits. The term colluvio-fluvial deposit is used to describe the reworked colluvium generated on account of uplift of the Pachham Island along the principal faults and associated longitudinal faults along the back slope. The Quaternary sediments also comprise of aeolian as well as fluvial miliolites characterized by medium to coarse grained clastic limestone with a higher lithic content (Baskaran et al. 1989). Biswas (1971) have described these as carbonate rich sediments blown by wind from coastal areas and deposited as scattered obstacle dunes along the rocky slopes. The $^{230}Th/^{234}$ U ages of the Kachchh miliolites ranges from 30 to 130 ka (Baskaran et al. 1989; Chakrabarti et al. 1993; Somayajulu, 1993). Reworking of the aeolian miliolite deposits by fluvial processes and their deposition in the valley is categorized separately as valley fill miliolite. The associated coarse grained clast of Mesozoic rocks supports its fluvial origin (Patidar et al. 2007; Thakkar et al. 1999). As miliolite is the only dated Quaternary sediments with a wide extension throughout the Kachchh it can be used for stratigraphic correlation (Chowksey et al. 2011b; Patidar et al. 2007). Thus, on the basis of miliolite Quaternary sediments were divided as Pre miliolite and Post miliolite deposits. Stratigraphically Pre-miliolite deposits lies below the miliolite phase and those lying above the miliolite deposit were termed as Post miliolite. Vertical lithologs from the various entrenched river cliff sections were prepared and were correlated to reconstruct the Quaternary stratigraphy of the Pachham island.

Harunwandh section

A thick Quaternary succession is seen in the entrenched cliff section of the south west flowing river near the Harunwandh village located in the western part of the central valley (Fig. 12.2). The river arises from the southern back slope of the Kaladongar hill range and forms a tributary stream of Bandi river which flows towards the west. As the river enters the central valley it forms a large entrenched meander. This meandering of river is on account of sudden drop in the slope and entrenchment of the Quaternary sediments can be related to tectonic uplift. The upstream part of this stream is characterized by a 5-6 m of entrenched cliff section lying on the left bank. Around ~ 4 m thick Quaternary sediments were exposed in the cliff section overlying the Tertiary rocks

which acts as a basement for Quaternary sediments (Fig. 12.6, litholog 1). The base of the Quaternary sediments is represented by scour and fills structure which represents an erosional contact of 0.8 m thick matrix supported cobble pebble gravel of Quaternary time with the underlying clayey Tertiary rock (Fig. 12.7a). The clasts are generally ill sorted with angular to sub angular clast thus represents a short distance of transport which is in conformity with the geomorphic setting of the deposits. The presence of scour and fill structure at the base along with the clast shape and size reflects a rapid deposition by sediment gravity flow or gravity flow (Rust 1978; Miall, 1996; Strokes and Mather, 2000; Aziz et al. 2003). This unit is overlain by 2 m thick mildly stratified sand with occasional occurrence of the isolated boulder size clasts. The horizontal stratification in the sand represents the planner bed flow regime (Miall, 1996). This unit forms an erosional contact with the overlying 1 m thick bouldery gravel unit. The clast of this unit is ill shorted and have angular to sub angular shape which represents a short transport. The length of boulder in this unit ranges up to 0.5 m showing a normal grading with feeble orientation of the clasts. The boulder clasts are generally supported by sandy matrix. The high sedimentary concentration of angular to sub angular clasts along with a normal grading represents a pseudoplastic viscous debris flow deposited under a low strength flow regime. This unit is overlain by sandy gravel unit with finer clasts of gravel. The top of the section is marked by the aeolian miliolite sand (Fig. 12.7b) it is characterized by horizontal stratification.

On the contrary right bank cliff section of the river in the downstream direction is characterized by the absence of the Tertiary rocks at the base of the cliff section. Here 0.3 m thick sandy gravel forms the basal unit of the Quaternary deposits. The gravels are generally sub rounded to rounded in shape bounded by the sandy matrix. This unit represents their deposition by cohesive, viscous debris flow. This unit is overlain by planer cross stratified gravely sand where the gravels are sub rounded and finer in size. The dominance of the sand with the existence of planer cross stratification represents the dune migration generally associated with the transverse bar of a braided river (Miall, 1996; Smith, 1970; Cant and Walker, 1970). Above this unit lies 0.6 m thick cobble pebble gravel which is characterized by sub angular to sub rounded clast nature. This unit have scored the underlying unit thus forms an erosional contact. The presence of scour and fill structure at the base along with the clast shape and size reflects a rapid deposition by sediment gravity flow or gravity flow (Rust, 1978; Miall, 1996; Strokes and Mather, 2000; Aziz et al. 2003). It is overlain by 1.6 m thick massive and compacted medium sand

in which the compaction is on account of calc content. The massive texture of the sand along with the absence of the sedimentary structure indicates the deposition by sedimentary gravity flows (Miall, 1996; Stokes and Mather, 2000; Coltorti et al. 2010). This unit forms an erosional contact with the overlying matrix supported gravel.

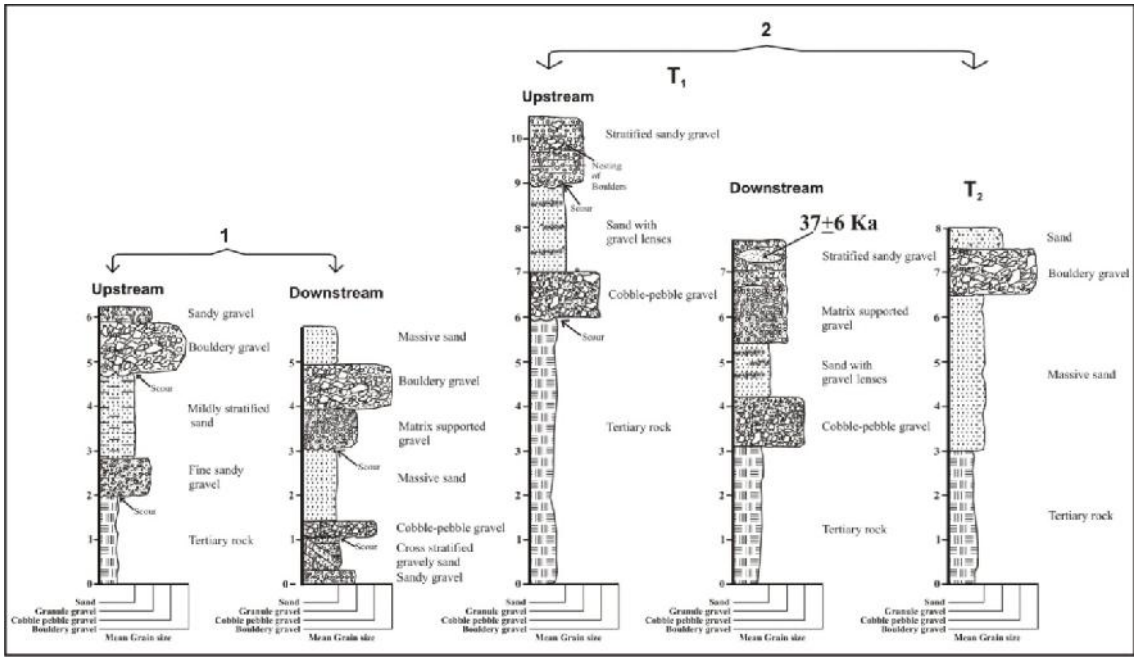

Figure 12.6 Lithologs of the Quaternary sediments occurring over the geomorphic high in the central valley. First two lithologs from left are from Harunwandh stream while the other three are from the Paiya chhota stream. Locations of the section are shown in Fig. 12.2.

The base of this unit is characterized by scour and fills type of structure. Gravels are generally finer with sand acting as a matrix. The presence of scour and fill structure at the base along with the clast shape and size reflects a rapid deposition by sediment gravity flow or gravity flow (Rust, 1978; Miall, 1996; Stokes and Mather, 2000; Aziz et al. 2003). Overall the matrix along with the fabric suggest the deposition under cohesive clast rich debris flow (e.g. Blair and McPherson, 1992; Dorsey and Roering, 2006; Chowksey et al. 2011b). This unit is overlain by 1 m thick bouldery gravel in which the maximum length of boulder range up to 0.6 m and the boulders shows imbrications towards the downstream direction. The gravels are clast supported and gravel imbrication indicates their deposition as a lag deposits (Miall, 1996). The topmost unit of this section is characterized by massive sand with occasional gravel lenses. The massive nature of the sand and presence of gravel lenses suggest their deposition by sediment gravity flow or gravity flow (Rust, 1978; Miall, 1996). Stratigraphically these deposits are lying below the miliolite phase and thus represent the pre-miliolite phase of deposition.

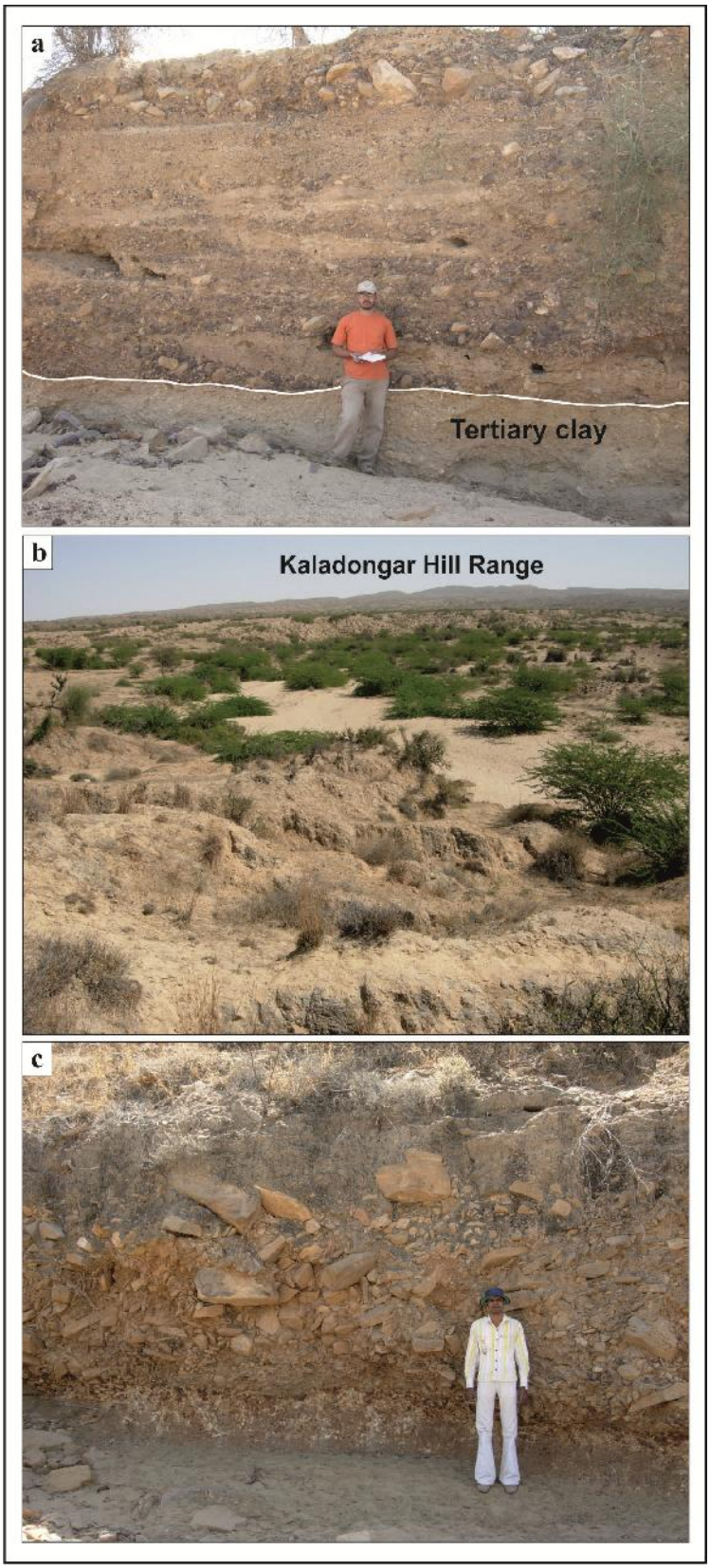

Figure 12.7 (a) A view of the section in the Harunwandh stream showing coarse gravel layers separated by sandy horizons. **(b)** View of the dissected surface developed over aeolian miliolite in the upstream part of the Harunwandh stream. Note sandy present day channel of the river. **(c)** Close view of the unsorted clast supported bouldery gravel overlying the Tertiary rocks at Rabviri to the north of the Goradongar range.

PART-F Neotectonics of the Island Belt Fault (IBF)

Paiya Chhota section:

A deeply entrenched Quaternary sediments section is seen in a stream flowing in south west direction near Paiya Chhota village. This stream arises from the Babia hill which is the highest peak of Kaladongar Hill Range and after draining the gentle southern back slope it enters the central valley. This river has formed a deeply entrenched valley in the upstream hard Mesozoic stratum as well as it dissected the Quaternary sediments before merging into the west flowing Bandi river. As the river enters the central valley the river forms a big entrenched meander where meandering is on account of drop in slope and entrenchment can be related to uplift along the axis of Median high which lies close to its proximity. The river have carved out two different terrace surfaces T_1 and T_2 (Fig. 12.4) where T_1 occurs at a height of ~13 m and comprises of coarse colluvio-fluvial deposits while the younger T_2 surface represents the younger loose and massive sandy sediments which represent the later aggradation phase of the river succeeded by incision phase. Thus T_2 terrace represents the cut and fill terrace.

The upstream entrenched cliff section exposes Quaternary deposits forming terrace T_1 and unconformably overlie the hard Tertiary limestone (Fig. 12.6, litholog 2). The basal unit of the Quaternary deposits is characterized by 1 m thick cobble pebble gravel with sand and fine gravel acting as a matrix. This unit has scored the underlying Tertiary rock and its base represents the score and fills type of structure. The massive nature of the deposits along with the weaker grading suggests it to be deposited by plastic debris flow (Miall, 1996). The presence of score and fill structure at the base suggest a highly viscous and high strength flow regime during deposition. This unit is overlain by a massive sandy unit with subordinate amount of gravel lenses. The massive nature of this sandy unit along with the existence of gravel lenses represents the sediment gravity flow (Miall, 1996; Stokes and Mather, 2000; Coltorti et al. 2010). Above this unit lies 1.5 m thick stratified sandy gravel. Within this unit nesting of boulders are observed. The maximum length of boulders range up to 0.5 m. The gravel is generally fine size and lateral continuity of this unit can be seen in the downstream direction where it also overlies the Tertiary sediments but the scoured base is not seen in the downstream section. The sedimentary fabric along with the horizontal stratification suggests the deposition of this unit by laminated debris flow (Miall, 1996; Pope et al. 2008; Coltorti et al. 2010; Kallmeier et al. 2010). The presence of clusters of boulders within this unit may be on account rolled down of large clusters from the upper slope during the debris flow (Nemec and Kazanci, 1999). This unit is overlain by a ~2 m thick sandy unit with

subordinate amount of gravel lenses. A through lateral continuity of this unit from upstream to downstream is seen with decreasing thickness further downstream. Lack of any sedimentary structure within this sandy unit suggests deposition under sediment gravity flow (Miall, 1996). In the downstream section this unit is overlain by matrix supported gravel. The gravel size varies from medium to fine gravel which is bounded by sandy matrix. This unit cannot be traced out in upstream direction. The absence of this unit in the upstream is on account of its erosion by the overlying stratified sandy gravel unit which forms a scoured base with the underlying sandy unit. This stratified sandy gravel is 1.5 m thick and comprises of nesting of the boulders which shows a downstream feeble orientation. The lateral extension of this unit can be traced out in the further downstream with decreasing thickness from 1.5 m upstream to 1 m downstream. The horizontal stratification suggests the deposition of this unit by laminated debris flow (Miall, 1996; Pope et al. 2008; Coltorti et al. 2010; Kallmeier et al. 2010). The presence of scoured base indicates the high strength viscous flow regime. The presence of clusters of boulders within this unit may be on account rolled down of large clusters from the upper slope during the debris flow (Nemec and Kazanci, 1999). The sample from the sand lens of the topmost unit has been dated by OSL to 37±6 Ka. The sedimentary characteristics and its stratigraphic position are correlatable with the pre miliolitic phase observed in the above described section. The deposition of the above sedimentary unit is followed by incision phase which resulted in the formation of a deeply incised valley and the entrenchment of these deposits.

The T_2 terrace is an incised valley fill terrace which is made up of ~5 m thick Quaternary sediments overlying a 3 m thick Tertiary compacted limestone (Fig 12.6, litholog 2). Medium massive sandy unit of ~3.5 m thick forms the basal unit of Quaternary sediments. This unit represents the aggradational phase of the river in its low energy phase. The massive texture of the sand represents the rapid sediment gravity flow type of deposition (Miall, 1996; Stokes and Mather, 2000; Coltorti et al. 2010). This unit is overlain by 1m thick boulder gravel unit which is supported by sandy and fine gravelly matrix. The presence of this unit represents the existence of short interval plastic debris flow regime. This short plastic debris flow regime is once again surpassed by sediment gravity flow which is represented by 0.8 m thick massive sand unit which forms the top most part of the section. The sedimentary characteristic of this unit is far different than that of sediments exposed in the terrace T_1which are correlatable to pre-miliolite phase.

Thus, on the basis of texture and stratigraphic position the younger sediments of terrace T_2 can be assigned a post miliolite age.

The formation of two levels of terraces indicates two phases of deposition followed by phases of tectonically controlled incision. The post-depositional incision of the pre miliolite sediments comprising terrace T_1 was followed by another aggradation phase during which sediments were dominated by sandy fraction and coarse sediments typically resemble the colluvio-fluvial deposits. This phase represents the post incision phase and thus represents the youngest depositional phase of the Quaternary sediments in the region that was confined to the incised palaeo-valleys. These deposits were later incised by the river and are represented as ~8 m valley fill sediments seen in the T2 terraces. The incision of these sediments corresponds to the youngest phase of uplift.

Dhorawar section

A thick entrenched stream section can be seen in the north of Dhorawar village which is in the close proximity to the axial zone of the Median High which is defined as a paleo high which have played a dominant role throughout the evolution of the Kachchh basin (Biswas, 1987). The stream arises from the Goradongar hill range and flows northward where it merges with the Pipri river. Thick Quaternary sediments can be seen in the entrenched river section cliff. The upstream right cliff section is characterized by 7-8 km thick Quaternary sediments deposited over the hard Mesozoic sandstone (Fig. 12.8, litholog 3). The basal unit of the Quaternary sediments is characterized by 1.3 m boulder gravel where the boulder clast reaches maximum length up to 0.5 m. The clasts are generally angular to sub angular and are clast supported to matrix supported. Higher sediment concentration along with the cohesive matrix with little internal sorting represents hyperconcentrated pseudo debris flow (Miall, 1996). The higher concentration of large clast, texture and absence of any sedimentary structure indicates the cohesionless non-viscous pseudoplastic debris flow (e.g. Blair and McPherson, 1992; Aziz et al. 2003; Pope et al. 2008). This unit is overlain by 1.3 m thick stratified gravel with sandy matrix which represents deposition of this unit by laminated debris flow (Miall, 1996; Pope et al. 2008; Coltorti et al. 2010; Kallmeier et al. 2010). Both the above described unit seems to be missing in the downstream part of the river channel. It is then followed by a bouldery gravel unit which comprises of angular to sub angular clasts supported by sandy or fine gravely matrix. This unit forms the basal unit of the downstream section where the reduction in grain size is noticed with increase in matrix percentage. The sedimentary architect of this unit points towards a cohesionless plastic debris flow. This phase is

overlain by 1.2 m thick massive sand in the upstream whose thickness pinches out to 0.5 m in the downstream direction. The presence of massive texture represents a sediment gravity flow (Miall, 1996). Above this unit in the upstream part lies 0.3 m thick gravel which is supported by sandy matrix. The thickness of this unit increases from 0.3 m in upstream direction to 1.3 m in the downstream direction. The presence of sandy matrix within the gravel along with the absence of any sedimentary structure suggests the cohesive nature of the depositing agent indicating its deposition by sedimentary gravity flows (Rust, 1978; Miall, 1996). The top of the section in the upstream direction is characterized by 0.7 m fluvial miliolite whose thickness increases further downstream where its thickness increases ~1.7 m. Thick lenses of cobble and pebble is also seen within this unit points towards the fluvial origin by reworking of aeolian miliolite in the upstream part. Thus, the Quaternary sediments below this unit can be assigned a pre miliolite age. This unit is overlain by matrix supported gravel which forms the topmost unit of the upstream section which in the downstream direction becomes sand dominated and gravel appears to form lenses with in this unit. This decrease in the grain size from upstream towards the downstream is characteristic feature of deposits associated with the sedimentary gravity flow. The upper most unit in the downstream section is characterized by the ~1.5 m thick massive sand representing the sediment gravity flow of deposition. The massive nature of sand is similar to that of sediments exposed in the terrace T2 of Paiya Chhota stream. As these deposits lies above the miliolite unit thus represents the post miliolite phase of deposition. It is followed by the entrenchment of these deposits by the river on account of tectonic uplift.

Rabviri section

A thick entrenched river cliff section comprising of a thick Quaternary section overlying the Mesozoic rock is seen in a small tributary of the Pipri river close to the Rabviri village. The Quaternary sediments lying in this segment marks the southern margin of the Central valley. The 11 m thick entrenched cliff section can be seen on the right bank of the stream (Fig. 12.8, litholog 4). The section comprises of 4 m thick Mesozoic sandstone forming the base of the above Quaternary deposits. The basal unit of the Quaternary sediment is characterized by chaotic boulder gravel which are generally clasts supported to matrix supported (Fig. 12.7c). The higher concentration of larger clast along with the weak grading and absence of any texture represents the pseudoplastic debris flow deposited as a inertial bedload by turbulent flow regime (Miall, 1996). The clasts are generally angular to sub angular with maximum 0.8 m length of boulders. This

unit is also characterized by sand lenses, which comprises of medium sand with calcrete nodules. This unit is overlain by 2 m thick cobble pebble gravel. The clasts are sub angular to sub rounded which are bounded by sandy matrix. The presence of sandy matrix along with the large clast size points towards the viscous nature of the depositing flow while the absence of any structure along with the clasts nature points towards the deposition by debris flow (Rust, 1978; Miall, 1996). This unit is overlain by 1.2 m thick sandy gravel. The small gravel size along with the higher sandy concentration represents the low strength debris flow. This unit is overlain by bouldery gravel where the boulder size extends upto 0.5 m in length. The bouldery gravel is generally supported by sandy matrix. This unit represents the deposition by the plastic debris flow. This unit is overlain by 1.2 m thick sandy gravel where the gravels are generally finer in size deposited by low strength debris flow. The stratigraphic position as well as sediments nature is correlatable to the pre miliolite deposits of the Dhorawar section, thus pre miliolite age can be assigned to these deposits.

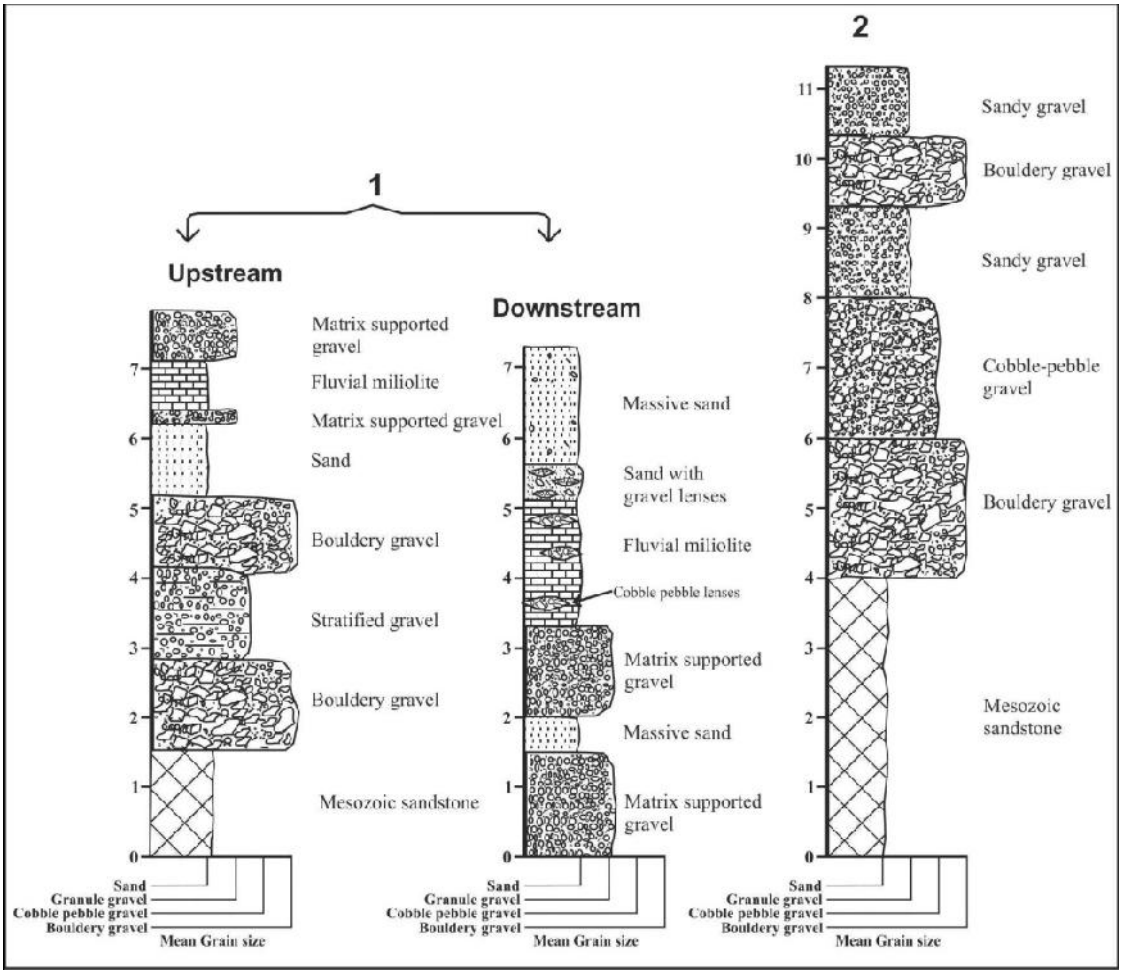

Figure 12.8 Lithologs of the exposed Quaternary sediments Location of the section is shown in the Fig. 12.2.

PART-F Neotectonics of the Island Belt Fault (IBF)

LITHOSTRATIGRAPHY

Quaternary sedimentation by various south flowing rivers arising from the southern backslope of the Kaladongar ranges as well as the various north flowing short streams arising from the Goradongar range have formed a thick sedimentary succession in the central valley. On the basis of the sedimentary characteristic the sediments can be divided into two major units. The first unit comprises of coarse grained sediments characterized by the colluvio-fluvial deposits with varying clast size ranging from boulders to gravel deposited by either debris flow or gravity flow. These deposits represent the reworked colluvium deposits generated on account of the uplift along the principal as well as related longitudinal fault. On the contrary the second unit is dominated by sandy fraction which comprises of the sandy gravel to sand which represents the aggradation phase of the rivers.

An extensive miliolite deposits in the form of either aeolian or fluvial origin is seen all along the central valley. The miliolite are originally a carbonate rich sediments blown by the wind from the coastal area and got deposited as a scattered obstacle dunes along the rocky slopes (Biswas, 1971). The reworking of these sediments by fluvial agencies results in the valley fill type of miliolite deposits. The presence of the big clasts of Mesozoic rocks points to their fluvial origin. The miliolite depositional phase of Kachchh encompasses the middle Pleistocene to late Pleistocene time (Baskaran et al. 1989). $^{230}TH/^{234}U$ dates of these deposits represent a broad range of time duration from 135 ka to 30 ka (Baskaran et al. 1989; Somayajulu, 1993). Thus this unit can serve for correlation of the overlying as well as underlying units. Thus the overlying sediments above this miliolite horizon can be assigned a post miliolite age while the underlying unit can be assigned as a pre-miliolite age.

Thus, on the basis of the field observation, stratigraphic position as well as the sedimentary characteristics the litho-stratigraphy of the Quaternary sediments of the Pachham island has been reconstructed. The oldest Quaternary phase is represented by thick colluvio-fluvial deposits which are dominated by angular to sub angular boulders and gravels deposited by debris flow. These types of deposits represent reworked colluvium which was originally generated on the back slopes of the Kaladongar hill range on account of uplift along the principal fault (IBF) as well as the other sympathetic faults on the backslopes. These deposits got deposited in the central valley in a debris flow type of regime and dispersion of these deposits took place by fanning of these deposits as the consequences of sudden fall in the gradient of the slope. This resulted in deposition of a

thick apron of the sediments which buried the entire valley. This phase is followed by miliolite phase which consists of an aeolian as well as fluvial phase. This phase represents a long span of a time from Middle Pleistocene to late Pleistocene (Baskaran et al. 1989).The aggradation of the streams has resulted in the formation of the valley fill type of miliolite deposits by the reworking of the aeolian miliolite. These valley fill can be differentiated from the aeolian miliolite by the presence of the big clasts of the Mesozoic sandstone and shale. This phase is followed by post miliolite uplift which has resulted in entrenchment of the pre-miliolite phase sediments. The uplift is associated with the major tectonic fabric of Pachham island. This phase is later followed another aggradation phase dominated by the sandy to sandy gravel deposited by sediment-gravity flow. Stratigraphically they lie above the miliolite unit as seen at the top of the Dhoravar river section. Thus, depending upon the sedimentary architect along with the stratigraphic position this phase can be considered as post miliolite phase. This aggradation is later followed by the yet another uplift along the principal fault which resulted in the incision of these sediments. The incision with in the central valley is more near the central part of the central valley in comparison to the eastern and western part of the central valley. Drainage anomaly in form of deflection of the drainages can be easily seen near the Dhoravar village. The incision in this part is also more in comparison to other part of the central valley.

The study suggests that the uplift along a geomorphic high correlates with the axial part of Median high. The presence of drainage anomalies in the vicinity of the axial part of the median high along with the presence of various nick-points and convex up longitudinal profile of the river flowing across the feature confirms the uplift along the buried subsurface feature. The uplift has also resulted in the formation of the deeply entrenched valleys and dissected landscape. The uplift has also raised the Rann surface abutting the Pachham island. The Rann sediments characterize the sedimentary succession of late Holocene time. Thus on account of this it can be said that the last tectonic uplift occurred during the late Holocene time after the deposition of Rann sediments. This uplift has resulted in the formation of the T2 terrace of Paiya Chhota stream.

NEOTECTONIC ACTIVITY ALONG IBF

The architecture of the Kachchh Basin of Middle Jurassic age is mainly governed by E-W trending faults, marking major lines of uplift during the late Cretaceous inversion phase of the basin (Biswas, 1987; 1993). The present-day compressional stress regime

have resulted in repeated seismic activity in the basin like the 1819 Allahband earthquake, the 1956 Anjar earthquake, and the 2001 Bhuj earthquake (Biswas and Khattri, 2002). After the 2001 Bhuj earthquake (Mw 7.7), moderate to low seismicity is observed along several faults that include the Island Belt Fault (IBF) as well (Mandal, 2008). The Ranns of Kachchh mark a structural depression where marine sedimentation took place until ~ 2 ka. The present study, carried out in Bela, Khadir islands and a small island close to the western margin of Khadir proves that active tectonics has played a major role in the geomorphological evolution of these islands. Structurally, all the islands are tilted blocks and this controls their overall geomorphic setup and style of neotectonic activity. The southward directed tilted block structure of the islands is attributed to the periodic reactivation of the IBF. The north-facing precipitous E-W trending escarpments, marking the northern margin of the islands are the most conspicuous geomorphic features and mark the geomorphic expression of the IBF, presently buried under the rann sediments to the north. The fresh and youthful nature of the escarpments suggests continued uplift.

The southerly sloping backslopes of the islands are developed over the south-dipping Mesozoic and Neogene rocks. The backslopes on Mesozoic rocks are steeper while those on Neogene rocks are gentler. The backslopes are drained by south-flowing parallel water courses which arise very close to the crest of the northern escarpments and flow southwards incising through Mesozoic and Neogene rocks. The depth of incision is found to decrease towards the south indicating control of neotectonic titling on drainages. The long profiles of the rivers are steeper and concave up in the upper reaches and gentler in the lower reaches testifying to active tectonic control. Structurally controlled north-flowing rivers are observed in Bela island: the Nilangadh river cuts through the northern escarpment in a gorge and the Sharan river flows through a saddle between the Lodrani anticline and the Muvana dome.

Various coastal geomorphic features are seen at the toe of the northern escarpments of Bela and Khadir islands which are attributed to the sea which occupied the rann until ~ 2 ka. Erosional rocky platforms occur discontinuously at an elevation of 2-4 m above the rann surface all along the base of the Bela and Khadir escarpments. Two levels of notches designated as upper and lower notches are also observed at a height of 4m and 2m respectively. Notches are generally formed at sheltered sites from wave action (Rust and Kershaw, 2000). The preservation of two level of notches can be on account of rapid uplift (Cooper et al. 2005). Sea caves have also been noticed along the base of the escarpments.

PART-F Neotectonics of the Island Belt Fault (IBF)

Raised marine terraces consisting of sediments deposited in inter tidal conditions are documented from the western margin of Khadir and from the eastern margin of Bhanjada island. The cliff sections of these terraces expose 5-6 m of rann sediments. The sediments overlie Mesozoic rocks and dominantly comprise laminated clayey silts. The presence of channel-fills in the upper part of the section at Khadir island suggests existence of shallow tidal channels in the intertidal zone. The formation of the terraces is attributed to tectonic uplift during late Holocene. Tectonic tilting of the islands during this period is testified by the southward decrease in the elevation of terraces.

The geomorphic setup of the Pachham island strongly correlates with the pre-Quaternary tectonic frame work. The central valley formed along the synclinal structure acted as the major sink for the deposition of the Quaternary sediments. The Quaternary sedimentation of Pachham island can be divided into three phases, the first is represented by a coarse colluvio-fluvial depositional phase which was generated by reworking of colluvium attributed to the neotectonic movement along the principal (IBF) and its associated parallel faults. This phase therefore represents the pre miliolite phase of the Quaternary uplift which was followed by the miliolite depositional phase. The post miliolite tectonically driven incision phase occurred due to reactivation of various faults along with the subsurface Medial high resulted eastward and westward division of the drainages and the entrenchment of the river valleys. The subsequent depositional phase was confined within incised paleo valleys. The last tectonic uplift resulted in the formation of the second level of terrace in the central valley and correlates with the uplift of the rann surface during the Holocene.

CHAPTER 13

DISCUSSION

The Kachchh basin is a seismically active pericratonic palaeorift basin located on the western continental margin of India. The landscape of the basin is strongly controlled by E-W tending tectonic fabric (Biswas, 1974). The basin is characterized by several uplifts bounded by roughly E-W trending faults. These are the mainland uplift, Wagad uplift, Desalpar uplift and the Island belt uplift which comprises linearly arranged series of Pachham, Bela, Khadir and Chorar islands. These uplifts are bounded by the Kachchh Mainland Fault (KMF), South Wagad Fault (SWF), Gedi Fault (GF) and the Island Belt Fault (IBF) respectively. The basin exposes of a thick sequence of Mesozoic and Cenozoic sedimentary rocks (Biswas, 1977, 1987). The rift opened during the early Jurassic and witnessed continuous sedimentation during its rifting phase until the late Cretaceous. The rift was inverted at the end of Cretaceous resulting in the formation of intrabasinal uplifts with corresponding structural lows due to movement along faults (Biswas and Khattri, 2002). The lows were filled up by thick transgressive marine sediments during the Neogene and Quaternary periods. During the post-Cretaceous inversion phase, the faults bounding the uplifts were periodically reactivated thereby facilitating the deposition of Cenozoic sediments and evolution of the present day landscape (Biswas, 1987). A characteristic feature of all the faults is the presence of a narrow flexure zone consisting of domes and anticlines on the upthrown side (Biswas, 1987). The Kachchh basin is characterized by major fault bound uplifts which includes the Island Belt Uplift, South Wagad Uplift, Desalpar uplift and the Kachchh Mainland Uplift. These uplifts have prominent geomorphological expression and are bounded by the Island Belt (IBF), South Wagad Fault (SWF), Gedi Fault (GF) and the Kachchh Mainland Fault (KMF) respectively. All faults qualify to be categorised as active as indicated the available data and distribution of earthquakes that have occurred during historic time in the basin.

NEOTECTONIC EVOLUTION OF ACTIVE FAULT ZONES

The occurrence of the 2001 Bhuj earthquake led to intensive monitoring of seismic activities in the Kachchh basin (Chadha, 2010). The continuous aftershock during the post-2001 interval have revealed concentration of earthquakes in the eastern part of

the basin extending from the eastern part of the KMF, to the IBF in the north which has been defined as the Kachchh Seismic Zone (Mandal and Chadha, 2008). The post-2001 Bhuj earthquake low to moderate seismic activity indicates that the earthquakes have been spatially migrating in an unpredictable pattern (Mandal and Chadha, 2008; Mandal, 2009). The Kachchh Seismic Zone shows a large network of complexly interacting faults which have uncertainties as to their mechanical coupling. Therefore it is interpreted that the tectonic loading is shared by the array of potentially active faults in complex ways both spatially and temporally. It has been shown that the faults may turn on and off and stress transfer across large regions may cause remote triggering of faults thought to be inactive (Liu et al., 2011; Pollitz et al., 2003).

The present study was carried out along the active faults with prominent geomorphic expression within the Kachchh Seismic Zone, which includes the KMF, SWF, GF and the IBF. The study is primarily field based and utilizes GPR technique, which is now recognized as a reliable tool for understanding the neotectonic setting of active faults. The main objective of the study was to provide neotectonic controls on the geomorphic evolution of the fault zones, Quaternary stratigraphy, field constraints for the precise location and shallow subsurface characteristics of the faults. The data generated fills an important gap in estimating seismic hazard and mitigation models.

In active fault studies, use of GPR to detect and analyze the nature of active or Quaternary fault zones and faults in shallow subsurface is well known. Displacement along the fault plane could affect the host material in several ways which depends on the type of material and the type of movement along the fault. In such areas, reflections from the faults themselves are less common, but diffractions associated with horizons truncated by faults are common**.** GPR tends to be most successful when two different kinds of rocks came in contact because of the vertical movement along the fault and because of the abrupt change in the electrical property of the material. This lead to the abrupt lateral change in the amplitude and phase of the reflected GPR signals. Features with such characteristics are good target for GPR. In Kachchh Seismic Zone, all faults investigated in the present study, are marked by the contact between Mesozoic rocks and Tertiary rocks which is easily picked up and interpreted in the processed GPR profiles by visible change in the pattern of reflectors. At places, where the fault trace was covered by colluvio-fluvial deposits and aeolian miliolite, these deposits were also imaged in the processed GPR profiles as an undeformed mass of reflectors overlying the reflectors of Mesozoic and Tertiary rocks.

PART-G Interpretation and synthesis

All fault zones show neotectonically controlled deposition of Quaternary sediments, though the stratigraphic development varies (Table 13.1). The KMF zone shows a continuous sediment cover characterized by spatially and vertically heterogeneous assemblage of Quaternary deposits. The confinement and deposition of Quaternary sediments in front of the KMF scarps points to the primary control exerted by neotectonic activity in the generation and deposition of the Quaternary sediments. The Quaternary sediments of the KMF zone show three major aggradation phases. The oldest phase includes the strikingly coarse grained with large boulders and poorly sorted colluvio-fluvial sediments occurring below the miliolites. The sedimentary characteristics indicate deposition, dominantly by debris flows and sediment gravity flows, as small coalescing alluvial fans in the front of the scarps. These deposits suggest pre-miliolite neotectonic activity along the KMF. The second aggradation phase comprises aeolian miliolites and fluvially reworked miliolites that have been previously dated from middle to late Pleistocene. The youngest phase is the post-miliolite phase that is represented by comparatively finer sandy gravels, gravelly sands and sand. The sediment characteristics suggest deposition in shallow braided stream channels under reduced level of neotectonic activity. Neotectonic activity along the KMF during post-miliolite time is evidenced by vertical dips of miliolites and tilting of gravels near the scarps. The tectonically controlled incision and dissection of the Quaternary deposits is the result of neotectonic activity that continues at the present day. The overall nature, sedimentary characteristics and geomorphic setting of the sediments suggest that the KMF remained neotectonically active throughout the Quaternary period.

The South Wagad Fault comprises a series of E-W trending faults cut by transverse faults. The South Wagad Fault is divisible into the Adhoi, Kanthkot, Khanpar, Kharol, Dedarwa, Vekra, and Kanmer faults. A chain of domes and anticlines occur to the north of the fault. In the field fault is marked by the contact between sheared Mesozoic rocks and Tertiary rocks. At most places, the fault zone is blanketed by mounds of thick aeolian miliolite deposits. The present day landscape shows deep gullies, youthful topography, knickpoints, and deflected drainages supporting the ongoing tectonic activity along SWF.

The field investigations along the Gedi Fault (GF) revealed the presence of Quaternary sedimentary cover especially in the central and western part. Field examination of the scanty exposures showed that the fault trace marks the lithotectonic contact between Mesozoic rocks in the north and the Tertiary (Miocene) sediments to the

south. The GPR data indicates that the Gedi Fault is a steep north dipping reverse fault which becomes vertical at depth. Since the fault does not displace the Quaternary deposits and low incision, it is inferred that the Gedi Fault has been characterized by low to moderate seismic activity under compressive stress regime during the late Quaternary.

The GPR studies suggest that the KMF is near vertical northward steeply dipping fault that tends to become a steep south dipping reverse fault in the vicinity of transverse faults. The GPR data of SWF shows that the fault is a steep southward dipping fault. GPR profiles taken in the Gedi Fault (GF) zone indicates that the fault is steeply north dipping reverse fault near the surface that becomes vertical at depth. The integrated approach of GPR surveys and field studies suggest a dominantly N-S oriented compressional stress environment along the KMF, SWF and GF. The segmented nature and change in the behaviour of the fault in different segments indicates that the distribution, accommodation and release of stresses are not uniform along the faults.

The geomorphic set up and landscape of the Bela, Khadir and Bhanjada islands is strongly controlled by the inherited structural framework. Neotectonic tilting of the islands towards south occurred in response to tectonic activity along the E-W trending Island Belt Fault (IBF). Raised marine landforms indicate active Holocene tilting of the islands. The geomorphic setup of the Pachham Island strongly correlates with the pre-Quaternary tectonic frame work. The central valley formed along the synclinal structure acted as the major sink for the deposition of the Quaternary sediments. The Quaternary sediments of the Pachham Island reveal deposition in three phases; the first is represented by a coarse colluvio-fluvial depositional phase which was generated by reworking of colluvium attributed to the neotectonic movement along the principal (IBF) and its associated parallel faults. This phase therefore represents the pre miliolite phase of the Quaternary uplift which was followed by the miliolite depositional phase. The post miliolite tectonically driven incision phase occurred due to reactivation of various faults along with the subsurface Medial high resulted eastward and westward division of the drainages and the entrenchment of the river valleys. The subsequent depositional phase was confined within incised paleo valleys. The last tectonic uplift resulted in the formation of the second level of terrace in the central valley and correlates with the uplift of the rann surface during the Holocene. GPR data could not be obtained along the IBF as the fault trace is buried under thick Rann sediments which is beyond the penetration depth of GPR. However, it has been visualised as a vertical fault (Biswas, 1993).

PART-G Interpretation and synthesis

Table 13.1 Summary of the stratigraphy of the Quaternary sediments occurring in the active fault zones of Kachchh.

KATROL HILL FAULT (KHF) ZONE	KACHCHH MAINLAND FAULT (KMF) ZONE	SOUTH WAGAD FAULT (SWF) ZONE	GEDI FAULT (GF) ZONE	LITHOLOGY	MODE OF OCCURENCE	GEOLOGIC TIME
Scarp-derived colluvium	-	-	-	Angular to sub-angular pebbles and cobbles embedded in sandy to gravelly matrix	At the base of range front scarp	Late Holocene
Alluvial deposits	Alluvial deposits	Alluvial deposits	-	Fine sands, silts and clays	Sporadically along the various north-flowing streams	Middle Holocene
Valley-fill Miliolite	Valley-fill Miliolite	-	-	Sandy sheet of miliolite with boulders and pebbles	Extensively deposited along the river valleys	Late Pleistocene
Aeolian Miliolites	Aeolian Miliolites	Aeolian Miliolites	Aeolian Miliolites	Well-shorted fine grain sand with carbonate rich send	At higher elevations along the southerly directed slopes of the hill range and at the base of the north-facing range front scarps	Middle Pleistocene (Based on U/Th dating- after Baskaran et al. 1989)
Bouldery Colluvio-fluvial deposits	Bouldery Colluvio-fluvial deposits	-	-	Boulder-size fragments of shales and sandstones	At the base of range front scarps	Early to Middle Pleistocene

PART-G Interpretation and synthesis

TOWARDS A NEOTECTONIC MODEL OF KACHCHH

The 2001 Bhuj earthquake proved to be watershed in the seismotectonic studies of the Kachchh basin which have provided wealth of geophysical data for understanding the crustal scale structure of the Kachchh Seismic zone (Kayal et al. 2002; Mandal and Chadha, 2008; Mandal, 2009; Bhatt et al. 2009). The post-2001 event aftershock sequence provide important details on the crustal characteristics in the Kachchh Seismic zone (Mandal and Chadha, 2008; Mandal, 2009). Till 2009, the aftershocks include 13 M $\geq$ 5 events, over 230 M $\geq$ 4 events and more than 4000 M $\geq$ 3 events (Mandal, 2009). The continued aftershock activity triggered the neighbouring Gedi fault (GF) that resulted in the occurrence of the 7th March 2006 event of Mw 5.6 (hypocenter: 23.84 N, 70.72 E, 3.0 km depth) (Mandal et al. 2007a). Focal depths of these aftershocks vary from 2 to 40 km with 90% of the events occurring at 10-35 km depths. It is noted that there were no events along GF and ABF during 2001-2002 (Mandal et al. 2007b). In 2004, the activity along GF increased with the occurrences of two M4, six M3, and five M2 events, (Mandal et al. 2007b). The seismotectonic analysis of the aftershocks explains the crustal properties responsible in different ways. Based on gravity and magnetic studies, Chandrasekhar and Mishra (2002) and Mishra et al. (2005) proposed coupling of regional stress generated by crustal buoyant roots and mafic intrusive acting as stress concentrators. Kayal et al. (2002) observed conjugate rupture propagation with two trends i.e. NE and NW trend and postulated that the main shock generated aftershocks by shear adjustment and fault interactions. Bilham et al. (2003) explained the Bhuj earthquake by flexural stress distribution. Bhatt et al. (2009) attributed the event to the intersection of faults including a new proposed fault, the Bhachau Fault, a model that closely approximates the fault interaction model (Talwani, 1988; Gangopadhyay and Talwani, 2003). However, the suggestion by Mandal et al. (2004b) and Mandal and Chadha (2008) about the presence of a fluid filled fractured rock matrix within a mafic pluton, responsible for accumulating large crustal stress that resulted in a lower crustal intraplate earthquake appears to be more plausible explanation.

The present study has provided critical data on neotectonic evolution of the active faults falling within the currently hyperactive Kachchh Seismic Zone as suggested by the post-2001 earthquake aftershock sequence. The study has provided important constraints on neotectonic, precise location and nature of the faults in the shallow subsurface. The Quaternary sediments confined within the fault zones clearly indicate the role of dominantly vertical movements in the landscape evolution. A comparative evaluation

based on geologic parameters of the fault zones studied is attempted along with the Katrol Hill Fault, whose neotectonic evolution is relatively well studied (Patidar et al. 2007; 2008; Kundu et al. 2010). The shallow near-surface fault properties as inferred from the field and GPR investigations were used to evolve a model. The downward extrapolation of the faults to deeper levels is based on the previous information available on the pre-Quaternary basin characteristics and fault evolution mainly provided by Biswas (1982; 1987; 1993) and Biswas and Khattri (2002). The inferred disposition of the faults is at variance with some of the tectonic models proposed during the last decade.

Recent models explaining the structural set up of the basin show all faults major intrabasinal uplift bounding faults as thrusts that merge downward into a decollement surface. In this context, the pre-Quaternary history of the Kachchh basin is directly relevant for understanding the neotectonic reactivation and evolution of the faults as they define the fundamental structural grain of the basin which has been subjected to periodic reactivation depending on its orientation and rheological properties. In addition, previous crust forming and thickening/thinning events and volcano-magmatic events have certainly influenced the modern crustal rheology and therefore partly determine susceptibility to reactivation by distant plate boundary-derived compressive forces or other intraplate stresses. This may one of the reasons for recent studies that have attempted to understand the modern deformation regime in the Kachchh basin fallen short of adequately explaining the distribution and kinematics of Quaternary tectonic stresses and their role in geomorphic evolution as they have failed to take into account the crustal preconditions and evolutionary development of the basin.

The various faults of the Kachchh basin were formed during the syn-rift phase under extension stress regime (Biswas, 1987). The basin was inverted in late Cretaceous in response to the collision of the Indian plate with the Eurasian plate in the north (Biswas and Khattri, 2002). During the inversion phase under compressional stresses, the same faults were reactivated in the reverse manner. The unidirectional movement along faults continue to the present day, that has maintained the first order structurally controlled topography and overall differential uplift of the basin (Biswas, 1974). The deformational style that the basin has undergone is very well reflected in the rather simple structure of the pre-Quaternary rocks. The most intense deformation is invariably seen in narrow flexure zones occurring along the upthrown side of the E-W tending faults (Biswas, 1987). The flexures themselves comprise open elongated asymmetrical domes and anticlines whose forelimb steeply dip towards the causative fault while the backlimb is

gentler which quickly assumes dips as low as 5^{o} and even become horizontal within a short distance (Biswas, 1993).

The exhaustive mapping of the rocks of the Kachchh basin reveal that the rocks in most parts of the uplifts are horizontal and may show deformation that can at best be described as mild (Biswas, 1993). This type of structural setting suggests primarily vertical movements along faults under compression that deformed the strata close to the faults with dissipation of stress in a short distance away from the fault. Moreover, the –E-W trending faults are favourably oriented for dip slip reactivation rather than strike slip deformation. This is evident by the large vertical separation along the E-W trending faults and all horizontal separation concentrated along the transverse faults. Consequently, the observed crustal shortening is minimal as a major component of the accumulating stress, were accommodated by vertical movements and negligible horizontal movement in relative terms. Though the amount of crustal shortening in response to the Cenozoic compressive stresses is not yet quantified, the 'mildly' deformed pre-Quaternary rocks and Quaternary sediments rule out the large amount of shortening usually an outcome of orogenic activity as collisional plate boundaries. The complete absence of high intensity deformational features like tight overfolds, recumbent folds and low angle faults, which commonly observed in terrains that have undergone substantial horizontal shortening (e.g. The Himalayas), strongly rule out the possibility of the originally vertical normal faults of the Kachchh basin assuming the characteristics thrust faults. This is confirmed by the available global positioning system (GPS) campaign data that suggests very slow strain accumulation in the basin (Sridevi et. al., 2001).

Overall, the overall low intensity of deformation in the Kachchh basin is in conformity with its location far away from the collisional plate boundary. The data generated along active faults of the Kachchh Seismic Zone in the present study correlate well with the known pre-Quaternary tectonic history of the basin. In the absence of any evidence for significant crustal shortening in the basin, except in the vicinity of the faults, the present study rules out the presence of parallel low angle thrust system and the presence of any low-angle decollement zone in the deeper crust. The results of the present study seems to validate the basement controlled tectonic model advocated previously (Biswas, 1993) which is based on exhaustive field mapping and is able to explain the several other structural and stratigraphic intricacies of the Kachchh basin. The presence of fluids related to the presence of plutonic bodies inferred in the deeper crust in the

Kachchh Seismic Zone also supports the role of basement structure in the contemporary seismicity observed in the region (Mandal and Chadha, 2008).

The present study could not adequately bring out the part played by the transverse faults in influencing the release of stresses and their seismotectonic implication. The fact, that the transverse faults offset all E-W trending faults, which are the primary stress accumulators in the basin, is a significant aspect (Maurya et al. 2003). However, it was observed that some of the geomorphic anomalies like entrenched meanders, deformation of Quaternary sediments, marked variation in the level and thickness of Quaternary depositional surface along with the tendency of KMF to transform into a reverse fault invariably occur in the vicinity of intersection with transverse faults. It has been proposed that intraplate earthquakes occur due to a localized stress build-up in response to plate tectonic forces in the vicinity of intersecting faults which act as stress concentrators within a pre-existing zone of weakness (Talwani, 1988). Studies on intraplate earthquakes spanning the globe have shown that intersecting faults are spatially associated with the observed seismicity (Gangopadhyay and Talwani, 2003). Detailed studies on discontinuous and seismically active faults elsewhere have demonstrated that such faults may show clustering of earthquakes in the vicinity of transverse faults offsetting them and significantly affect the aftershocks and earthquake swarm activity (Bakun and McEvilly, 1979; Eaton et al., 1970; Hill, 1977; Johnson and Hadley, 1976). A similar scenario has been revealed along the KHF three surface faulting events at a single site located very close to a transverse fault (Patidar et al. 2008). This suggests that future earthquake nucleation along the active faults in the region is most likely to be in the zones where the E-W trending faults intersect with the transverse faults.

Recent sand box modelling studies have tried to simulate the complex fault controlled structural pattern of the Kachchh basin. The studies demonstrate the formation of stress normal faults along with linear flexures comparable to the setting of active faults in the basin. Similar experimental results have confirmed that ancient faults determine to a large extent the subsequent fault pattern and fault evolution. However, the degree and mode of the reactivation are strongly controlled by the location of the old fault and by its orientation relative to the new stress field. However, the structural pattern observed in sand box model may not be replicated in the field due various geological parameters involved. A remarkable difference between the natural example and the analogue models is the formation of backthrust, easily simulated in the sand models and but may absent in the field (Viola et al. 2004). This is revealed in the studies carried out by Viola et al.

(2004) to simulate the structural pattern of the Giudicarie fault system in the Italian Alps, where there is no field evidence for such a major backthrust.

However many analogue sand experiments simulating the push of a rigid indenter into a sand pack have shown that the formation of backthrusts is inhibited by the backstop represented by the thick indenter (Malavieille, 1984; Calassou et al., 1993; Bonini et al., 1999). The most probable explanation given for the Giudicarie fault system is that the rheological difference between the two blocks involved in faulting that may have played a 'backstop' role (Viola et al. 2004). Given its lithological composition (massive gneisses and amphibolites), the Austroalpine basement is mechanically more competent than the adjacent sedimentary cover of the Southern Alps which inhibited the development of backthrust (Viola et al. 2004). The E-W trending faults of the Kachchh Seismic Zone exhibit a similar kind of setting where the fault planes demarcate the mechanically rigid block (Mesozoic rocks) on the upthrown side and the markedly softer block (Tertiary rocks) on the downthrown side. This could be the main cause for the absence of backthrust along all active faults of Kachchh. The geometrically opposite arrangement of the blocks with significantly different mechanical strength may also be a crucial factor in the accumulation and release of tectonic stresses and the consequent seismic activity. With compression causing push from the south and the presence of magmatic bodies in the subsurface (Mandal and Chadha, 2008), the most favourable arrangement of the thermo-mechanically contrasting blocks is provided by the KMF and the IBF where the stronger block is located on the southern upthrown side which pushes against the markedly softer Tertiary lithologies to the north. The stress condition created along these faults is more suited for substantial dip slip along the fault plane. This is in conformity with the tendency of the KMF to become reverse at places, high relief range bounding scarp, high magnitude 2001 event and moderate magnitude 1956 event and a large dense concentration of the aftershocks along it (Mandal, 2009).

The SWF and the Gedi Fault (GF) exhibit a reverse arrangement of the block with differing mechanical strength. These faults are characterised by the presence of the rigid block comprising Mesozoic rocks to the north and the softer Tertiary rocks to the south. This setting is relatively unfavourable for stress accumulation and release. The near and in front location of the eastward propagating KMF means that less amounts of stresses may be accumulating along the SWF. Moreover, a substantial part of the stresses that should have accumulated along the SWF is absorbed by the E-W trending warping of the mechanically softer Samakhiali-Lakadia plain aided by the compressive stresses and

continuing uplift of the Northern Hill range from the shallow subsurface. This is in conformity with the low relief SWF scarps, absence of colluvio-fluvial deposition and relatively lesser concentration of mostly low magnitude aftershocks (Mandal and Chadha, 2008). The Gedi Fault (GF) shows a similar thermo-mechanical setting which conforms with the mostly low magnitude with few intermediate magnitude aftershocks (Mandal, 2009). The consistently reverse nature of Gedi Fault in the shallow subsurface suggests that the fault has accumulated far greater amount of stresses than the SWF. All stresses however accumulated along the GF as there are no faults close proximity to share the tectonic loading.

POSSIBLE CAUSE OF HIGH SEISMICITY IN KACHCHH BASIN

The widespread distribution of historical seismicity and post-2001 earthquake aftershock indicate that the Kachchh basin has accommodated a large amount of intraplate deformation that has occurred in the western continental margin. The concentration of medium to high magnitude seismic events in the basin also suggest that the deformation is predominantly occurring in the Kachchh basin which is sandwiched between the Saurashtra horst to the south and the Precambrian rocks of the Aravalli mountain ranges in the south. Crustal reactivation within the Kachchh basin may have been facilitated by a number of crustal preconditions. Firstly, the Kachchh region was the site of significant crustal extension leading to the formation of a rift basin along the already existing Precambrian structural trends. Secondly, the basin was the site of regionally widespread and volumetrically significant late Cretaceous basaltic volcanism. The volcanic activity may have thermally weakened the crust predisposing it to subsequent structural reactivation during the inversion phase of the basin following the collision of the Indian plate with the Eurasian plate. In addition, the development of thick accumulations of sedimentary deposits in rift basins within a region of extended crust is also capable of producing variations in Moho temperatures that may contribute to localization of intraplate deformation (Sandiford and Hand, 1998). Thus the Kachchh basin crust appears to have been favourably preconditioned for reactivation in that it is comprised of a non-cratonic terrene with inherent crustal anisotropy and structural weak zones, which was further mechanically weakened and thinned by Mesozoic rift basin development and was thermally weakened by widespread by the regionally extensive late Cretaceous extrusive volcanic activity.

PART-G Interpretation and synthesis

Overall, for these reasons, the Kachchh basin can be considered as the 'soft' part of the western continental margin of the Indian plate and thus particularly susceptible to reactivation in response to a distant collision. The favourable preconditions for reactivation of intrabasinal faults of the Kachchh basin includes a thermo-mechanically weak upper crust sandwiched between the rigid Saurashtra horst in the south and the Aravalli basement blocks to the north (below the aeolian cover of the Thar desert and the Nagar Parkar ridge). This contrasts with the adjacent regions which have been more resistant to reactivation as they comprise mechanically stronger crust and behave as rigid crustal blocks.

The E-W trending latitudinal network of intrabasinal faults within the entire basin defines a narrow of deformation zone giving rise to typical of basin and range type of geomorphic province. The narrow zone of deformation is attributed mainly to adjustment to N-S compression in the form of vertical movements. This is because the E-W trend of the major faults is favourably oriented for dip slip reactivation. The strike slip component of the accumulating stresses appears to be mainly absorbed by the transverse faults offsetting the E-W trending faults. The almost perpendicular relationship between direction of maximum horizontal stress and the pre-existing basement structural trends is the fundamental control on the fault evolution during the post-rift inversion phase. Along-strike growth and joining of restraining bends is an outcome of the dominantly uplifting processes occurring in the basin. The transformation of vertical normal faults to high angle reverse faults is a process that occurred throughout Quaternary and is still continuing as evidenced by the GPR data.

The widespread distribution of the epicentres of the available historical earthquake data and the post-2001 earthquake shocks are consistent with a diffusely deforming basin interior region with tectonic loading shared amongst the E-W trending network of faults with complex structural setting. Therefore, earthquake prediction is likely to be more complex than in plate boundary settings and extrapolation of derived Late Quaternary palaeoseismic events is not straightforward. It is widely recognized that development of intraplate mountain belts in continental interior regions may be linked to distant plate boundary effects, especially plate margin collisions (Molnar and Tapponnier, 1975; Tapponnier et al., 1982). Recent studies (Cunningham, 2013) on the ongoing modern mountain building processes within the Gobi Corridor in response to compressional forces derived from the Indo-Eurasia collision to the south demonstrates that reactivation

of ancient accretionary and collisional orogens within continental interiors can play an important role in continental evolution and the life cycle of orogenic belts.

CHAPTER 14

CONCLUSIONS

The present field and GPR based study along the active fault zones of Kachchh has led to the following conclusions.

1. The KMF zone is marked by high relief north facing range bounding fault scarps with typical basin and range setting. The scarps are developed in steeper northern limb of the flexures. The KMF is a strongly segmented fault and is divisible into six morphotectonic segments bounded by transverse faults. From west to east these are- the Nirona-Jhura segment (segment-I), Kunaria-Lodai segment (segment-II), Lodai-Jawaharnagar segment (segment-III), Jawaharnagar-Khirsara segment (segment-IV), Khirsara-Devisar segment (segment-V) and the Amarapar-Sikra segment (segment-VI). The height of the fault scarp gradually decreases towards the east and finally disappears at the eastern margin of Segment-V. The segment-VI includes the eastward extending part of the KMF mapped in the present study through field and GPR investigations.

2. The KMF is well exposed between Khirsara and Devisar as a near vertical north dipping lithotectonic contact between the steeply dipping Mesozoic rocks in the south and the Tertiary (Neogene) rocks to the north. Except this part, the KMF is buried below the thick continuous Quaternary sediment cover that overlap the fault zone and abut against the north facing rocks.

3. The Quaternary sediments comprise colluvio-fluvial deposits, aeolian and valleyfill miliolite and coarse to fine grained alluvial deposits. OSl dating suggests that the sediments of the KMF zone date back to ~100 ka. The major neotectonically controlled aggradational phases in various segments are correlatable. The sediments appear to become progressively thinner, stratigraphically younger and finer towards the east.

4. The GPR investigations has revealed that the KMF is mostly vertical to steep north dipping fault in all the segments. However, the fault plane is found become reversed in the vicinity of the transverse faults. The present study infers that the KMF has been characterised by differential uplift whereby the southern block is uplifted more in comparison to the northern block.

PART-G Interpretation and synthesis

5. The SWF zone is characterised by continuous cover of Quaternary sediments, mostly aeolian miliolites followed by alluvial sediments. The fault shows south facing range bounding fault scarps with intermediate relief similar to basin and range setting. The fault is exposed in patches in the eastern part.

6. The SWF is divisible into segments due to the presence of transverse faults. The GPR studies have revealed the vertical to steep south dipping fault plane of the SWF which marks the tectonic contact between the Mesozoic rocks to the north and the Tertiary (Neogene) rocks to the south.

7. The Samakhiali-Lakadia plain is actively deforming, evidenced by geomorphic and drainage anomalies, in response to the continued tectonic activity along the KMF and the SWF under compression. The plains show a prominent zone of upwarping that has resulted in drainage disruption in the Samakhiali plain and increased incision in the Lakadia plain further east. The upwarping is attributed to the rising up of the Northern Hill Range due to eastward lateral propagation of the KMF.

8. The Gedi Fault (GF) zone is also buried under a continuous Quaternary sediment cover. The sediments are mainly aeolian miliolites and alluvial sediments. The fault is expressed as a low relief scarp as it is almost completely overwhelmed by the Quaternary deposits.

9. The Gedi Fault (GF) is also a segmented fault due to the transverse faults cutting across the E-W trending fault line. The GPR studies have revealed that the GF is high angle north dipping reverse fault which becomes vertical at depth.

10. The IBF is geomorphologically expressed as high relief precipitous E-W trending escarpments at the northern margins of the islands. The IBF is buried under a thick pile of marine sediments of the Great Rann and is presumed to be a vertical fault in conformity with the other E-W trending faults.

11. The Pachham, Khadir and Bela islands reveal active southward tilting due to movements along the IBF. Raised marine erosional features at the base of the escarpment suggest tectonic movements along the IBF in the recent past. Southward tilted raised Rann sediments along margins, pockets of colluvio-fluvial and alluvial deposits on backslopes also indicate neotectonically active nature of the IBF.

PART-G Interpretation and synthesis

12. The surface and shallow subsurface characteristics of the active faults with prominent geomorphic expression in the Kachchh Seismic Zone worked out in the present study reveal variable intensity of neotectonic activity along different faults in compressive stress environment. The KMF shows highest intensity of neotectonic activity followed by IBF, SWF and GF. This broadly correlates with the observed level of historic seismicity and the post-2001 aftershock activity except the IBF along which there is no documented evidence of high magnitude seismic events.

13. The present detailed study did not reveal any evidence of surface rupturing events from the exposed Quaternary sediments along the active fault zones studied. However, this sharply contrasts with the available record from the Katrol Hill Fault (KHF) zone where three major surface faulting events with reverse movements are reported during the last ~30 ka with the last one occurring at 3 ka BP (Patidar et al. 2008; Kundu et al. 2010). In view of the lack of any discernible differences in the surface geological conditions, it is hypothesised that the occurrence of earthquakes at deeper crustal levels may be the main cause for the absence of any record of surface faulting along active faults of the Kachchh seismic zone.

14. Based on the present study and the available data, it is estimated that the KMF is capable of generating high magnitude seismic events, followed by the IBF. In comparison, the possibility of the high magnitude events occurring along the SWF and GF is low.

APPENDIX

FUNDAMENTALS OF GROUND PENETRATING RADAR (GPR)

The Ground Penetrating Radar (GPR) is a high-resolution geophysical technique used to investigate the subsurface architecture. It is a nondestructive geophysical technique that produces high quality subsurface data. Currently the GPR technique is used in the fields of engineering, geophysical, geological, archeological and other near surface investigations like hydrological and geotechnical inspections. This technique provides a continuous cross-section profile of subsurface along with the three dimensional pseudo image with accurate depth estimation (Fig. A.1). GPR works on the principle of seismic technique due to the resemblance between acoustic and electromagnetic prospecting methods (Davis and Annan, 1989; Cassidy, 2009). The main difference between the two techniques is the vectorial character of electromagnetic waves compared to scalar character of the acoustic waves.

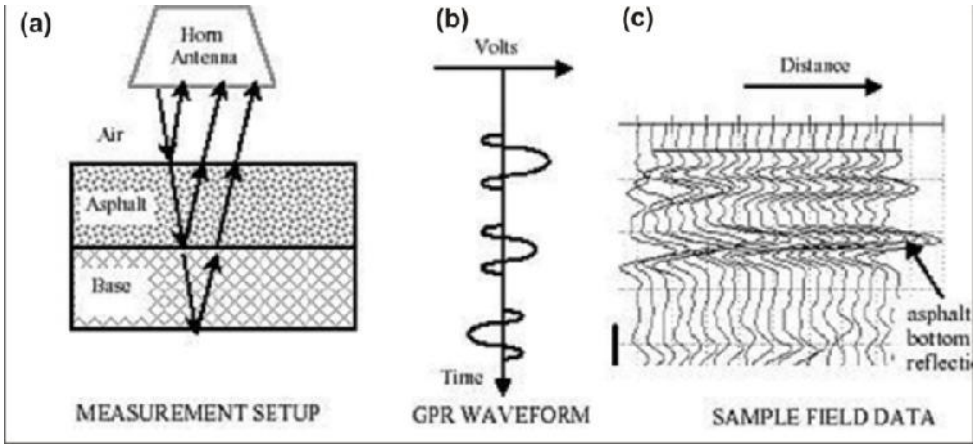

Figure A.1 Mode of GPR data acquisition and the resulting radar profile in wiggle mode. **(a)** Diagram showing the manner of signal penetration and internal architecture of the subsurface reflectors. **(b)** Characteristic of electromagnetic waveform **(c)** Radar reflection profile in wiggle mode.

A GPR survey is usually carried out with one source and one receiver at a fixed distance and also called as a common-offset measurement while in seismic survey a large number of receivers for every source are required, it is known as a multi-offset measurement. Another difference between the two techniques is depth of penetration and resolution of data. GPR which involves electromagnetic wave is generally used to obtain image of the shallow subsurface upto ~50m.While the seismic techniques which uses sound waves can obtain an image of the subsurface (100 to 10000 m). When a wave is

transmitted in the subsurface ground reflections are generated when a wave hits a layer in the subsurface with different characteristic material properties. GPR reflections are generated (Fig. A.1) when a pulse hits an object or layer with different electromagnetic characteristics (Davis and Annan, 1989; Daniels, 2000).

GROUND PENETRATING RADAR (GPR)

The GPR is non-invasive technique that utilizes differences in electromagnetic properties of subsurface objects to produce an image of the subsurface (Davis and Annan, 1989). The basic principle and working of the GPR involves the transmission of high frequency electromagnetic waves into the ground, which is reflected back from the sediment interfaces showing variable electrical properties in the subsurface and is received on the surface and displayed in form of a profile (Fig. A.1). The GPR profile shows horizontal survey distance versus vertical two-way travel time in nanoseconds (1 ns = 10^{-9} second). A ray is defined as a straight line drawn from the transmitter to the edge of the wave front. The interval of time that it takes for the wave to travel from the transmitter antenna to the receiver antenna is simply called the two way travel time. The recording of both pulses over a period of time with receiver antenna system is called a "trace". The spacing between measurement points is called the trace spacing. The trace is the basic measurement for all time-domain GPR surveys. A scan is a trace where a color scale has been applied to different amplitude values. The two-way travel time depends directly upon the depth of investigation it is greater for deeper objects than for shallow objects. The EM waves sense the changes in physical and composition properties of the subsurface material like grain size, water moisture, dielectric permittivity and electric conductivity (Davis and Annan, 1989). The radar waves travel downward at a specific velocity that is determined primarily by the permittivity of the material (Jol and Bristow, 2003). The relationship between the velocity of the waves and material properties is the fundamental basis for using GPR to investigate subsurface. The frequency-dependent medium properties can be obtained from a CMP measurement (Van der Kruk and Slob, 1998). The propagation speed (velocity) of the transmitted waves is controlled by electromagnetic properties of the examining objects (Davis and Annan, 1989). The presence water content, dissolved minerals, expansive clay, heavy minerals in the subsurface materials may produce significant changes in the radar reflection strength (Topp et al., 1980; Olhoeft, 1984; Beares and Haeni, 1991).

The clayey sediments are normally known to show higher attenuation of radar signal, especially of higher frequencies, thereby affecting penetration as they possess high water retention capacity and low electrical resistivity. Small scale textural variations in the subsurface sediments are consequence of change in permittivity and are sufficient to cause reflections of radar signals (Van Dam and Schlager, 2000). The generalized values of electrical properties of some common earth materials (Table A.1) are present by Neal, (2004). These values of dielectric permittivity control the penetration of radar waves. Higher the dielectric permittivity lowers the penetration of radar signals. Neal (2004) indicated that the changes in the subsurface material will affect the index of refraction, and reflected energy will be produced related to the contrast in the dielectric constant across a boundary between two materials (Table A.2).

Table A.1 Showing typical electric properties of common geological materials (Neal, 2004). Note the relative dielectric permittivity and electromagnetic wave velocity is controlled by water content.

Medium	**Relative dielectric Permittivity (E_r)**	`	**Conductivity (mS m^{-1})**	**Attenuation (dB m^{-1})**
Air	1	0.3	0	0
Fresh water	80	0.03	0.5	0.1
Seawater	80	0.01	30,000	1000
Unsaturated sand	2.55-7.5	0.1-0.2	0.01	0.01-0.14
Saturated sand	20-31.6	0.05-0.08	0.1-1	0.03-0.5
Unsaturated sand and gravel	3.5-6.5	0.09-0.13	0.007-0.06	0.01-0.1
Saturated sand gravel	15.5-17.5	0.06	0.7-9	0.03-0.5
Unsaturated silt	2.5-5	0.09-0.12	1-100	1-300
Saturated silt	22-30	0.05-0.07	100	1-300
Unsaturated clay	2.5-5	0.09-0.12	2-20	0.28-300
Saturated clay	15-40	0.05-0.07	20-1000	0.28-300
Unsaturated till	7.4-21.1	0.1-0.12	2.5-10	-
Saturated till	24-34	0.1-0.12	2-5	-
Freshwater peat	57-80	0.03-0.06	<40	0.3
Bedrock	4-6	0.12-0.13	10^{-5} -40	7 X 10^{-6} -24

Table A.2 Reflection coefficient modeling for typical changes in sediment water content, porosity, lithology and grain shape. The reflection coefficients indicate the proportion of energy theoretically reflected from an interface (Neal, 2004).

Layer 1 Layer 2	Porosity (%)	E_r	Reflection coefficient (+1 to -1)	Geological significance
Dry sand	35	3.1		
Saturated sand	35	20.7	-0.44	Water table
Dry sand	35	3.1		5% porosity change in dry sand
Dry sand	30	3.27	-0.013	
Saturated sand	35	20.7		5% porosity change in saturated sand
Saturated sand	30	17.7	+0.04	
Saturated sand	35	20.7		lithology change to high-porosity peat
Peat	70	46.5	-0.2	
Dry sand	35	3.1		dry heavy-mineral placer deposit
Dry heavy-mineral sand	35	19.9	-0.43	
Saturated sand	35	20.7		saturated heavy-mineral placer deposit
Saturated heavy- mineral sand	35	53	-0.23	
Round grains	33	23.5		
Platey grains	33	16.9	+0.08	grain-shape change
Isotropic grain packing	33	22.5		orientation change for platey grains
Anisotropic grain packing	33	16.9	+0.7	

Criteria for selection of antenna

The present study is carried out using SIR-20 digital radar instrument manufactured by Geophysical Survey Systems Inc. (GSSI), USA with center wave frequencies of 16-200 MHz (Fig. A.2a,b). The GPR system comprises of five main

components; control unit, transmitter, receiver antennas and data storage or display module.

The selection of the antenna is based on the depth of investigation. A high frequency waveform (short wavelength) will provide a more detailed or higher resolution image than a low frequency waveform, but the higher frequencies are attenuated or absorbed at a greater rate (Jol and Bristow, 2003).

GPR operation is digitally controlled by the console (main unit) attached with laptop and another electronic module which connect to the antennas by fiber optic cable. The data is usually recorded in digital format for post-survey processing and display. Distance control along a traverse line are provided by a range of various means which may include, a well calibrated odometers based survey wheel, accurate positioning of profile length, manually marking into the data by an electronic push-button during profiling and differential GPS reading along the transect line.

Depth to which GPR can image below the surface directly dependants on three main factors; the centre frequency of the antenna, the number of interfaces that generate reflections and the dielectric contrast at each interface and the rate at which the signal is attenuated as it travels downward (Jol, 1995). As the GPR pulse arrives at each interface, a portion of it is returned to the surface and the rest continues into the next layer (Daniels, 2000). As the number of interfaces increase, the proportion of energy that propagates down gets reduced. In addition, the greater proportion of energy that is reflected back to the surface at each interface, the less energy that is available to propagate deeper into the ground. This limits the depth of investigation because the reflections of interest get masked by the clutter of the chaotic returns. The conductivity of the investigated material has a major influence on the depth penetration. As the conductivity increases, the material acts more like a conductor than a semi-conductor (Saarenketo, 1998). The frequency used is also important since the resolution of the system and the rate of signal attenuation is proportional to the frequency of the GPR system.

Resolution is controlled by wavelength of the propagating electromagnetic wave in the ground. The vertical resolution depends on the frequency used and the physical properties of the subsurface while the horizontal resolution is a function of the spacing between traces and the footprint of the radar pulse. The wave theory suggests that the greatest vertical resolution that can be expected is 1/4 of the size of a wavelet (Davis and Annan, 1989). The size of the wavelets that are recorded in a GPR profile is a function of the pulse width of the original transmitted pulse. There is strong relationship between

frequency and wavelength (equation B). Lower the frequency greater the wavelength and higher the frequency shorter the wavelength (Davis and Annan, 1989). If we are looking for small targets at shallower depth higher frequency GPR antenna gives adequate resolution but for larger targets like the position of the subsurface water table, lower frequencies should be used. Selection of the operating frequency for a radar survey should be object oriented.

Data acquisition

The methodology of GPR technique involves the data acquisition, processing and interpretation. There are different methods for obtaining GPR data acquisition. The data is recorded on a visual readout or in a digital format in a laptop attached with the Main unit (Jol and Bristow, 2003). The measurements from GPR can be made by two different ways. In continuous manner the shielded monostatic antenna is dragged along a transect line to record a high-resolution continuous cross-section of the subsurface (Fig. A.2a, c). The monostatic antenna contains a pre-fixed unmovable configuration of transmitter and receiver inside a shielded cover, that can be attached with an odometer based survey wheel to determine the horizontal survey distance (Fig. A.2a). GPR survey data by monostatic antenna can be carried out in two different ways: time mode and distance mode. In both the manners GPR antenna is moved along the ground or tow behind a vehicle. The time mode survey comprises the data recording in continuous manner without using the survey wheel. The data recorded in this manner measures vertical and horizontal both the axis in time. But in the distance mode a calibrated survey wheel is attached with antenna to calculate the horizontal survey distance.

The second manner comprises a transmitter and receiver as separate entities and the measurements are made by manually shifting the points along the surface. This is known as bistatic antenna configuration (Fig. A.2d). The data collection with unshielded bistatic antennas are quite time consuming and gives low resolution images of subsurface compared to monostatic antenna but the center frequency of the bistatic antenna can be changed to achieve greater depth penetration. The fixed-mode (point mode) arrangement has the advantage of flexibility where as the moving-mode (free run) has the advantage of rapid data acquisition. Different acquisition set-up can be used to obtain information of the subsurface using multi low-frequencies antennas.

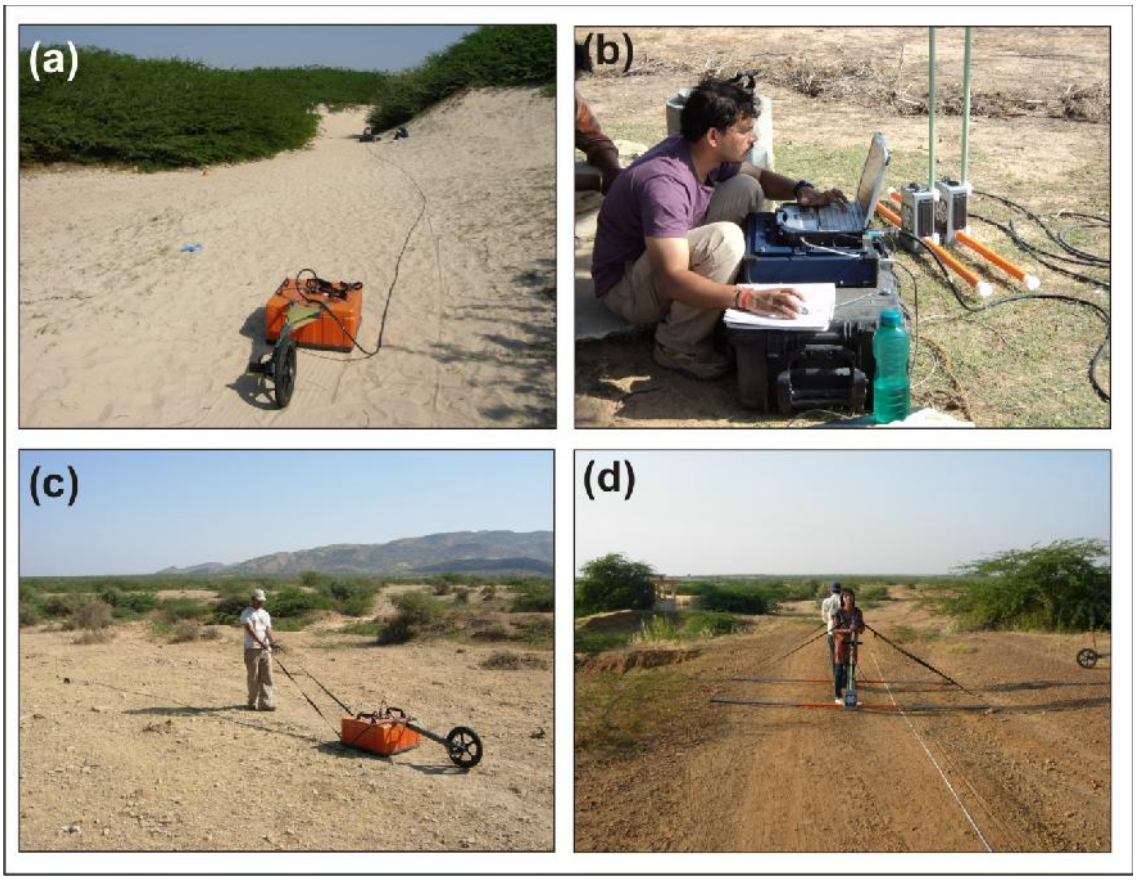

Figure A.2 (a) Monostatic antenna of 200 MHz frequency attached with survey wheel; **(b)** Main unit (Console) attached with the laptop to visualize the data during acquisition; **(c)** GPR survey by a 200 MHz monostatic antenna in a continuous mode; **(d)** GPR survey by Multiple Low Frequency (MLF) bistatic antenna in a point mode.

Different type of survey methods are given below:

Common-offset gather

This technique involves the collection of repeated measurements in stacked form along a survey line and is known as Common-offset measurement. The Common-offset GPR profiling is commonly used for geological applications to map the continuity of the features at depth. Generally, GPR is used in a common-offset configuration to detect subsurface anomalies and to delineate the lateral and vertical changes in subsurface. The source and receiver antennas are separated by a fixed distance, and measurements are carried out by gradually shifting the antennas over the points with common-offset distance (Fig. A.3a). This method is fast and therefore relatively cheap, but a major drawback can be the lack of wave speed information of the subsurface. However, when an object having contrasting electrical properties is present in the subsurface, a hyperbolic reflection occurs in the GPR data. From this hyperbola, the wave speed in the subsurface can be estimated as described in Van der Kruk and Slob (1998).

Common-mid point (CMP)

Common midpoint survey (CMP) is a GPR technique to estimate the subsurface velocity structure of the study area. It is generally used to analyze the variable velocity and density layers of the shallow subsurface (Huisman et al., 2003; Jol and Bristow 2003). The CMP profiles are obtained in a point mode with the help of bistatic antennas, where the orientation of the antennas is perpendicular to the electric field polarization. The measurements are taken by manually shifting to transmitter and receiver from a mid point to opposite directions up to a maximum distance. In this technique the high pulses of EM energy are radiated downward at every shooting point and the receiver records the signals in stacked form. The stacking of the signals facilitates to reduce the signal to noise ratio. In the CMP mode the transmitted EM waves repeatedly travel through same material but the offset distance between the antennas are changed (Fig. A.3b). It provides a plot between antennas separation (offset distance between antennas) and two way travel time. The strongest reflections at the top of the data are the direct air waves and the direct ground waves. The CMP data can identified from the alignment of these two reflections which represent to direct propagation of radar waves from transmitter to receiver through air and top skin of the ground (Neal, 2004). The calculated velocity obtained by this method is used to convert the time window into the depth scale and in advanced GPR data processing (Yilmaz, 2001; Huisman et al., 2003).

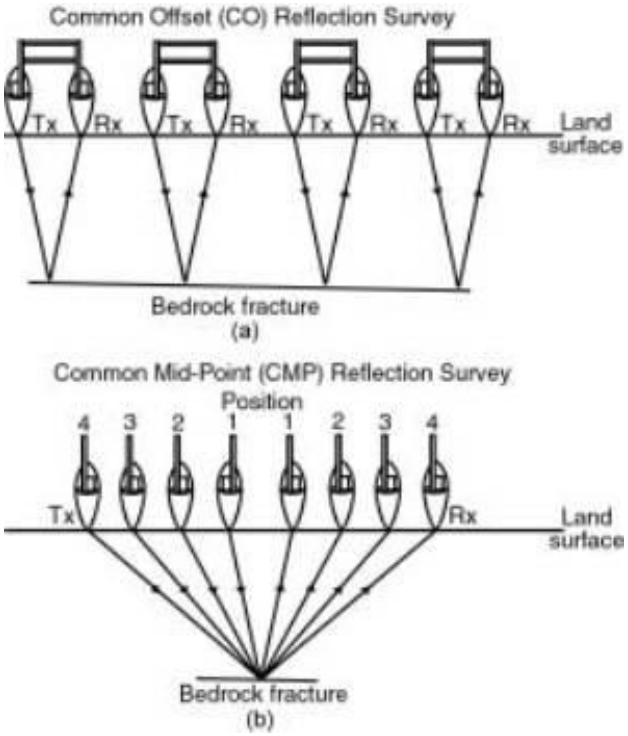

Figure A.3 (a) the configuration for Common Offset (CO) survey; **(b)** the configuration for the Common Mid Point (CMP) survey.

Wide-angle-reflection-refraction (WARR)

This is the Common source method in which the transmitter is fixed and the receiver is gradually shifted opposite to source with common step size. The common receiver method allows shifting of the position of transmitter away from stable receiver antenna (Fig. A.4). The Common source and Common receiver methods of GPR data collection are also known as wide-angle-reflection-refraction (WARR) technique and is generally used to make out the penetration speed (velocity) of the radar waves. This technique is generally used in the areas having rugged topography where it is not easy to place an antenna at fixed position and shifting to other along a line at discrete points. The acquisition fundamentals of this technique are similar to the previously described CMP method.

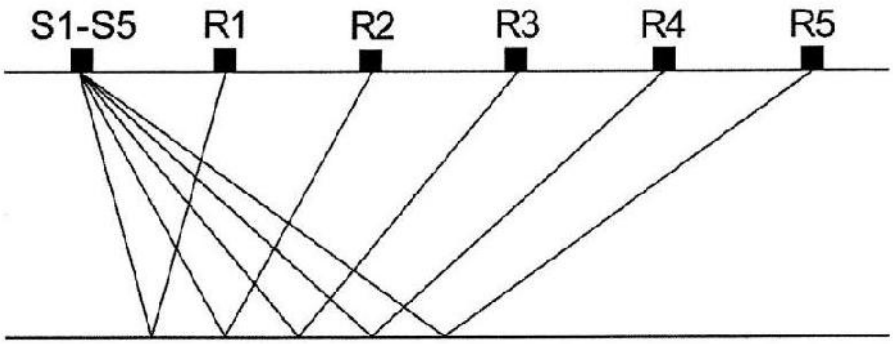

Figure A.4 Antenna configuration used in the Wide-angle-reflection-refraction (WARR). Here the transmitter (S) is kept fixed and the receiver is gradually shifted opposite to source with common step size.

3-D GPR surveying

Three-dimensional GPR surveying is complex but an interesting method to recognize the shallow subsurface geological setup. It provides the vertical and lateral dimensions of buried object or structure present in the subsurface. Three-dimensional displays have an advantage of looking at the entire survey site at once. It allows the creation of plan views at different depths as well as perspective views by cutting the 3D solid cube in slices (Patidar et al., 2006). To obtain a three-dimensional image of the subsurface, numerous measurements are carried out along parallel survey lines to record reflected and diffracted electromagnetic waves (Fig. A.5).

The software used for 3D GPR data processing interpolates the 2D parallel profiles into the systematic format to create the 3D solid cube. In practice, several parallel survey lines are measured with common offset present between the source and receiver antenna. This offset should be same for inline (parallel to the survey line) and crossline directions (perpendicular to the survey line). The quality and resolution of 3D GPR data

depends upon the grid layout, sampling and scanning speed of the antenna and the electromagnetic properties of the surveying medium (Daniels, 2000). Surface normalization operations should be performed prior to data interpretation when the 3D grid lines are situated over the undulated terrain. The sampling intervals should not be too sparse which may result in loss of subsurface information. Accurate positioning of sets of profiles, selection of viewing angle for presentation, combination of frequency cutoff filters, thickness of time slice and suitable colour range are some important criterions to be followed during data analysis (Young and Sun, 1998).

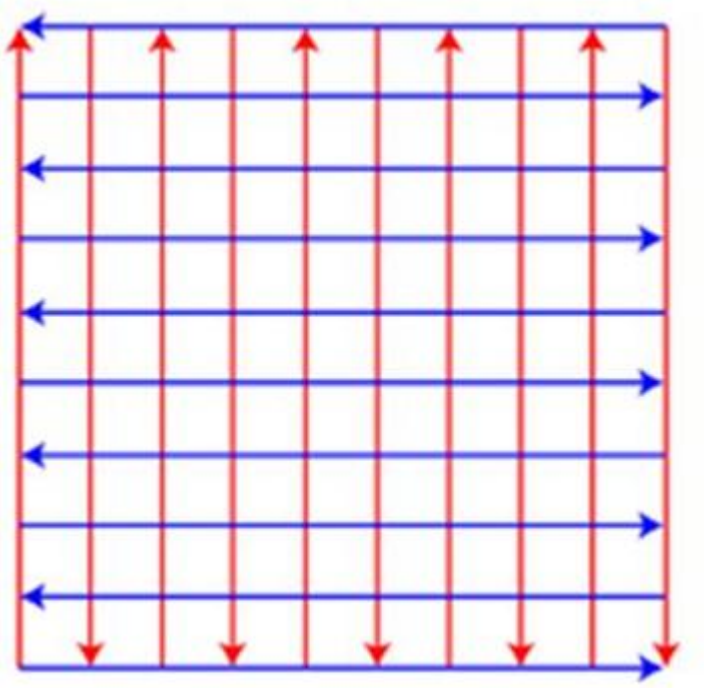

Figure A.5 A typical GPR survey pattern for carrying out the 3D GPR data acquisition.

Data processing

Appropriate processing is required to remove the unwanted signals from the data generated either by subsurface or surface anomalies, while some GPR data can be left unprocessed (Neal, 2004). The processing and analysis of GPR data needs understanding of fundamentals of geophysics (Yilmaz, 2001). There is lot of similarity in data acquisition procedures of GPR surveys and seismic reflection surveys, so many techniques of seismic data processing can directly be applied to process the GPR data (Young et al., 1995; Fisher et al., 1996). In many cases very little processing is required to locate the target of interest. The GPR technique involves the propagation of electromagnetic waves (EM) of specific central frequency in the subsurface where it may interact with subsurface materials in a variety of ways like, attenuation, reflection,

refraction and diffraction. The raw GPR data may not show the true subsurface image because of external noises produced by electronic bodies, geometrical inhomogeneity of the subsurface materials, concrete structures, metallic bodies and many other things. All the radar data do not require all kinds of processing algorithms. It is based on the accuracy of data sets and subsurface conditions. Processing of GPR data involves modification in raw data; so that it is more easily visualized and interpreted but the selection of processing parameters should be based on the physical modeling and theoretical background of the geophysics and not on the users whims (Jol and Bristow, 2003; Olhoeft, 2000).

The step may include the header file parameters editing using field notes, which contain the information about the data collection parameters, range of time window, scanning and sampling speed and some background information. The next step is to apply the time-zero correction for shifting the traces along the time axis (ns) to correct the misalignment of the first break in radar profile (Neal, 2004). It is important for accurate depth estimation for subsurface reflections. Similarly, the distance normalization operation is applied to reduce the difference of antenna towing speed and to get accuracy of horizontal scale for GPR profile (RADAN for Windows, 2000). This operation calculates the number of scans between every horizontal meter and then equally divides them throughout the distance to get actual scanning speed of the receiver. Some GPR profiles collected in adverse conditions require special processing.

Amplitude and Gain adjustments to the data

The presence of the clay rich horizon in the subsurface may results in the attenuation of the radar signals (Jol, 1995). This will results in lowering of the amplitude of the reflected reflections at the receiving end. Attenuation of the GPR signals depends on the dielectric conductivity of the examining substances and may be on account of malfunctioning of the equipment (Davis and Annan, 1989). The data quality can be enhanced by applying gain adjustments of each trace. To correct the spherical dispersion and enhance the quality of radar signals, automatic gain control (AGC) function is applied. AGC function computes the signal amplitude of individual trace over a time window and amplified to signal with average point (Annan, 1999). Linear gain and Exponential gain can also be used to enhance the quality of the lower reflection amplitudes.

Static adjustments to the data

Many time the GPR survey is carried out over an inclined surface which may leads to significant distortion of the subsurface images if uncorrected (Fisher et al., 1996). This problem is made worse because the radiated energy from a transmitter always propagates outwards from the antenna at right angles to the surface (Neal, 2004). The topographic corrections require the repositioning of traces at their original place which can be carried out by the Surface normalization operation shifted to traces along the time axis using GPS track profiles or field elevation data, which is very necessary to calculate the accurate depth of subsurface feature for a better interpretation of the sedimentary facies and structural discontinuities.

Filtering of radar data

The main purpose of filtering is to remove unwanted background noise caused by the subsurface anomalies or due to surface distractions (Kruk and Slob, 2004). Filtering strategies can include band pass (removing frequencies in a certain range), low pass (removing low-frequency signals), and high pass filtering (removing high-frequency signals). But, the over filtering of the data may leads to the generation of the artifacts.

Migration

Migration is one of the important procedures to convert diffracted GPR signals to their correct position (Olhoeft, 2000). According to Young and Sun (1998) the migration function is applied to rearrange the true position of steeply dipping subsurface reflections and hyperbolic diffractions. Generally the buried metallic objects, boulders, strata of higher electric conductivity or overhead objects like; hi-tension electric lines, tress, mobiles phones and concrete structures scattered to radar signals and appear as a strong hyperbolic return in the GPR profiles. The shape of the hyperbola depends on the velocity of the reflected waves (Young and Sun, 1998).

Generally the migration can be carried out in two ways, time migration and depth migration (Yilmaz, 2001). Time migration is suitable for the areas having small to moderate lateral velocity variations where as depth migration suits for the area having large variations in lateral velocity.

Deconvolution

This function is applied to eliminate the effect of ringing from GPR data (Todoeschuck et al., 1992). Ringing generally occurs on account of multiple reflections "ringing" which mask original radar reflections. The ringing multiples associated with water layers and weathered subsurface horizon can be wipeout by passing the data

through Deconvolution (Neal, 2004). This process is quite difficult procedure and may not produce the good results. Although, it may be very useful where reverberation is a major problem. Proper care should be taken while performing the Deconvolution during processing and perhaps it should not be used as an essential processing step (Neal, 2004).

Velocity analysis

The velocity analysis generally involves determining the propagation speed of the radar waves in the subsurface materials, then converting the reflection travel times into the depths. The electromagnetic energy generally travels at the speed of light ($0.3 mns^{-1}$) in a free space media. And its velocity in the subsurface usually ranges from 0.01-$0.16 mns^{-1}$ (Table A.1). Velocity determination can be carried out by three different methods: Common-Mid Point (CMP) velocity survey, Point-Source reflection analysis and direct water depth measurements or core depth logging. The first two methods are generally more effective for determining velocities of the upper surface geological layers. The data acquired by Common-Mid Point (CMP) method gives more direct image of the subsurface velocity structure and is very common for determining the subsurface velocity of wavy. This method provides accurate results determining the precise depths of subsurface reflectors. The velocity of the electromagnetic waves can be determined from equation A, where as the signal wavelength can be calculated from equation B: described by Benson (1995).

$$v = \frac{c}{\sqrt{E_r}} \quad \ldots\ldots\ldots \textbf{(A)}$$

where:

v = The velocity of the wave through the subsurface material.

c = The speed of light (30 cm/nanosecond).

E_r = The relative dielectric constant.

$$\lambda = \frac{v}{f} \quad \ldots\ldots\ldots \textbf{(B)}$$

where:

λ = Wavelength.

v = The velocity of the wave through the subsurface material.

f = Frequency.

Existence of moisture in subsurface sediments limits the penetration of radar waves. As shown in Table A.1, water has highest dielectric permeability as compare to

other geological material. The velocity increases at frequencies grater then 1000 Mhz because of the relaxation of the water molecules (Davis and Annan, 1989). The attenuation of radar signals are also occurs when the heterogeneous subsurface medium are scanned by higher frequencies.

Time-depth conversion

Velocity of the subsurface plays an important role in order to determine the depth of the anomaly precisely. The radar reflections in the GPR survey directly depends on the dielectric and conductivity of the subsurface material (Davis and Annan, 1989). Common-Midpoint Survey (CMP) with bistatic antennas helps in determining the velocity of the radar wave in the subsurface media which indeed can be used for determining the dielectric constant of the beneath material. In general during the acquisition a tentative dielectric constant is used depending on the field understanding which can be changed in the later stage by the value obtained by velocity analysis. According to Benson (1995) the depth of subsurface reflector can be determined by the equation given below.

$$d_r = \frac{v t_r}{2} \quad \ldots\ldots\ldots \text{(C)}$$

where:

d_r = The depth to the reflector.

v = The velocity of the wave through the subsurface material.

t_r = The two-way travel time to the reflector (taken from the GPR trace).

Data interpretation

The interpretation of GPR data is the most ambiguous part of this modern geophysical technique (Yilmaz, 2001). It is based on the characterization of specific signal patterns received from the subsurface anomalies obtained from the propagating media. Important aspect of the interpretation of the GPR data is to distinguish the true reflections or clutters from external objects (Jol and Bristow, 2003). A record of the field conditions and survey strategies helps a great deal during the interpretation. At times the raw GPR data does not represent the real picture of the subsurface due to occurrence of diffraction of radar wave from complex buried structures, which may appear as a random or multiple reflections and may require some special processing steps (Annan, 1999; Daniels, 2000). The concept of radar stratigraphic interpretation is derived from the

principles of seismic stratigraphy seismic stratigraphy and can be directly applied to GPR interpretation (Jol and Smith, 1991; Neal, 2004).

The presence of water in sediments strongly affect the radar reflections because the water content shows higher dielectric constant than air filled sediments (Ekes and Hickin, 2001; Sridhar and Patidar, 2005).

Interpretation of fault plane/zone in GPR profile is a tuff task and in some cases requires some special processing steps like, Migration and Deconvolution along with some a good field understanding (Gross et al. 2004). The arrival time of direct ground waves is a function of ground surface propagation velocity (Kruk and Slob, 2004). The interpretation of GPR data should be object oriented because sometime much interference are incorporated with the data, which cannot be removed by processing. Over filtering in order to clean the data may results in generation of artifacts.

The reflection patterns of the processed profile is to be critically evaluated in terms of parameters like: thickness and intensity variations of the reflected signals, changes in the dip of the reflections, termination or displacement of the reflections along a plane, reductions in amplitude strength, presence of diffraction hyperbolas, frequency variation along the vertical trace and many other complementary reflection patterns. GPR data can be analyzed in many different ways depending on the aims and objective of the interpretation.

Utility and Limitations of GPR

GPR is one of the important tools, ideally suited for obtaining realistic high resolution subsurface image up to the 50 m.

- The instrument is compact and easy to handle compared to the logistic requirement of other geophysical survey instruments, hence can be easily transported and operated in far off places.
- There is no need for digging electrodes for measuring subsurface reflections by GPR.
- The GPR can detect small structures, palaeo-liquefaction features from the contrast between dielectric permittivity of sand and clay which is not possible by any other geophysical technique (Maurya et al., 2005).
- The GPR study provides a great help in delineating the shallow subsurface nature of the seismically active faults.

- GPR has provided a new dimension in the field of Archeology and civil engineering.

The main disadvantages of the GPR technology are as follows:

- In the areas having significant structural relief, data may get contaminated by echoes and multiple reflections and can create confusion during processing and interpretation.
- Presence of conducting material like saline water, clays and heavy minerals can strongly influence the GPR depth penetration.
- The method is time consuming which requires a lot of time in setting the acquisition parameters.

REFERENCES

ANNAN, A. P., (1999) Practical Processing of GPR Data, Proceedings of the Second Government Workshop on Ground Penetrating Radar. Sensor and Software Inc. Mississauga, ON, Canada. pp. 1-15.

ANDERSON, K.B., SPOTILA, J.A., and HOLE J.A., (2003) Application of geomorphic analysis and ground penetrating radar to characterization of paleoseismic sites in dynamic alluvial environments: an example from southern California. Tetonophysics, v. 368, pp. 25-32.

AZIZ, H. A., RUBIO, E. S., CALVO, J. P., HILGEN, F. J. and KRIJGSMAN, W., (2003) Palaeoenvironmental reconstruction of a middle Miocene alluvial fan to cyclic shallow lacustrine depositional system in the Calatayud Basin (NE Spain); Sedimentology v. 50, pp. 211–236.

BAKUN, W. H. and MCEVILLY, T. V., (1979) Earthquakes near Parkfield, California: Comparing the 1934 and 1966 sequence. Science, v. 205, pp. 1375–1377.

BASKARAN, M., DESHPANDE, S. V., RAJAGURU, S. N. and SOMAYAJULU, B. L. K., (1989) Geochronology of miliolite rocks of Kutch, western India; J. Geol. Soc. India v. 33 pp.588–593.

BELEUSSOV, V. V., (1962) Basic problems in Geo-tectonics. Mc Graw Hill Co. Inc., 816p

BENSON, A. K., (1995) Application of ground penetrating radar in assessing some geological hazards: examples of ground water contamination, faults, cavities. Journal of Applied Geophysics, v. 33, pp. 177-193.

BERES, M. and HAENI, F. P., (1991) Application of Ground Penetrating Radar Methods in Hydrogeologic Studies. Groundwater, v. 29, pp. 375-386.

BERES, M., HUGGENBERGER, P., GREEN, A. G. and HORSTMEYER, H., (1999) Using two and three-dimensional georadar methods to characterize glaciofluvial architecture. Sediment. Geol., v.129, pp.1–24.

BHATT, K. M., HÖRDT, A., KUMAR, S., (2009) Seismicity analysis of the Kachchh aftershock zone and tectonic implication for 26 Jan 2001 Bhuj earthquake. Tectonophysics, v 465, 75–83.

BILHAM, R., (1998) Slip parameters of the Rann of Kachchh, India, 16 June 1819 earthquake quantified from contemporary accounts; In: Coastal Tectonics (eds) Stewart I S, Vita-Finzi C; Geol. Soc London. v.146, pp.295–318.

BILHAM, R., BENDICK, R. and WALLACE, K., (2003) Flexure of the Indian plate and intra plate earthquakes. Proc. Ind. Acad. Sci. Earth Planet Sci. v. 112, pp. 315-329.

BISWAS, S. K., (1965) A new classification of the Tertiary rocks of Kutch, W. India. Bull. Geol. Min. Met. Soc. Ind., v. 35, pp. 1-6.

BISWAS, S. K. (1971) The miliolite rocks of Kutch and Kathiawar; Sedim. Geol. v. 5 pp. 147–164.

BISWAS, S.K., (1973) A note on the mode of eruption of the Deccan Trap lavas with special reference to Kutch. JGSI, v. 14, pp. 134-141.

BISWAS, S. K., (1974) Landscape of Kutch – A morphotectonic analysis; Indian J. Earth Sci. v. 1(2), pp.177–190.

BISWAS, S.K., (1977) Mesozoic Rock Stratigraphy of Kutch. Quart. Jour. Geol. Min. Metal. Soc. Ind. v. 49, pp. 1-52.

BISWAS, S. K., (1982) Rift basins in western margin of India and their hydrocarbon prospects with special reference to Kutch Basin. Jour. of Amer. Asso. Petro. Geol., v. 10, pp. 1497-1513.

BISWAS, S.K., (1992) Tertiary stratigraphy of Kutch. Jour. of Palento. Soc. India. v. 37, pp. 1-29

BISWAS, S. K., (1993) Geology of Kutch, K.D. Malaviya Institute of Petroleum Exploration, Dehradun, pp. 450.

BISWAS, S. K., (2005) A review of structure and tectonics of Kutch basin, western India, with special reference to earthquakes. Current Science, v. 88, pp. 1592-1600.

BISWAS, S. K., and KHATTRI, K. N., (2002) A geological study of earthquakes in Kachchh, Gujarat, India. J. Geol. Soc. India, v. 60, pp. 131–142.

BISWAS, S. K., (1987) Regional tectonic framework structure and evolution of the western margin Basin of India. Tectonophysics, v. 135, pp. 307–327.

BISWAS, S. K. and RAJU, D. S. N., (1973) the rock stratigraphic classification on the Tertiary sediments of Kutch. Bull. ONGC. v. 10(1&2), pp. 37-46.

BISWAS, S. K. and DESHPANDE, S. V., (1970) Geologic and Tectonic maps of Kachchh. Bull. Oil and Natural Gas Commission. v. 7, pp. 115-116.

BLAIR, T. C. and McPHERSON, J. G., (1992) The Trollheim alluvial fan and facies model revisited; Geol. Soc. Am. Bull. v. 104, pp. 762–769.

BONINI, M., MORATTI, G. and SANI, F., (1999) - Evolution and depocentre migration in thrust-top basins: inferences from the Messinian Velona Basin (Northern Apennines, Italy). Tectonophysics, v. 304, pp. 95-108.

BULL, W.B., (2009) Tectonically Active Landscapes, Wiley-Blackwell, Oxford. pp. 326.

BURNES, A., (1835) Memoir on the eastern Branch of the River Indus, giving an account of the alteration produced on it by an earthquake, also a theory of the formation of the Runn and some conjectures on the route of Alexander the Great; drawn up in the years 1827-1828, R. Asiatic Soc. Trans., v. 3, pp. 550-588.

BRISTOW, C. S., (1995) Facies analysis in the Lower Greensand using ground penetrating radar. Jour. of the Geol. Soc., London. v. 152, pp. 591-598.

BROOKFILED, M. E., (1998) The evolution of the great river systems of southern Asia during the Cenozoic India-Asia collision: rivers draining southwards. v. 22(3-4), pp. 285-312.

CAI, J., MCMECHAN, G. A. and FISHER, M. A., (1996) Application of ground penetrating radar to investigation of near surface fault properties in the San Francisco Bay region. Bulletin of the Seismo. Soc. Amer. v. 86, pp. 1459-1470.

CALASSOU, S., LARROQUE, C., MALAVIEILLE, J. (1993) Transfer zones of deformation in thrust wedges: An experimental study. Tectonophysics. v. 221(3-4), pp. 325-344.

CANT, D. J. and WALKER R. G., (1976) Development of a braided-fluvial facies model for the Devonian Battery Point Sandstone, Québec, Canadian Journal of Earth Sciences. v. 13(1), pp. 102-119.

CARPENTIER, S. F. A., GREEN, A. G., DOETSCH, J., DORN, C., KAISER, A. E., CAMPBELL, F., HORSTMEYER, H. and FINNEMORE, M., (2012) Recent deformation of quaternary sediments as inferred from GPR images and shallow P-wave velocity tomograms: northwest Canterbury plains, New Zealand J. Appl. Geophys. v.81, pp.2–15.

CASSIDY, N. J., (2009) Ground penetrating radar theory and application. In Ground Penetrating Radar: Processing, Modeling and Analysis (ed. Jol, H. M.), Elsevier, pp. 141–172.

CHADHA, R. K. (2010) Seismic Hazard in India–Practical Aspects and Initiatives During IYPE, T. Beer(ed.),Geophysical Hazards, International Year of Planet Earth, Springer Science+Business Media B.V. pp. 151-159

CHAKRABARTI, A., SOMAYAJULU, B. L. K., BASKARAN, M. and KUMAR, B., (1993) Quaternary miliolites of Kutch and Saurashtra, western India: Depositional environments in the light of physical sedimentary structures, biogenic structures and geochronological setting of the rocks; Senckenbergina Maritima. v. 23, pp. 7–28.

CHAMYAL, L. S., MAURYA, D. M., BHANDARI, S., and RAJ, R., (2002) Late Quaternary geomorphic evolution of the lower Narmada valley, western India: implications for neotectonic activity along the Narmada–Son fault. Geomorphology. v. 46, pp. 177–202.

CHANDRA, U., (1977) Earthquake of Peninsular India- a seismotectonic study. Bull. Seismol. Soc. Amer. v. 67, pp. 1387-1413.

CHANDRASHEKAR, D.V. and MISHRA, D. C., (2002) Some geodynamic aspects of Kutch basin and seismicity: An insight from gravity studies. Curr. Sci., v. 83, pp. 492-498.

CHEN, Y., LI, Y., ZHANG, Y., ZHANG, M., ZHANG, J., YI, C. and LIU, G., (2011) Late Quaternary deposition and incision sequences of the Golmud River and their environmental implications; Quat. Int. v. 236, pp. 48–56.

CHOW, J., ANGELIER, J., HUA, J. J., LEE, J.C. and SUN, R., (2001) Paleoseismic event and active faulting from ground penetrating radar and high resolution seismic reflection profiles across the Chihshang fault, eastern Taiwan. Tectonophysics, v. 333, pp. 241–259.

CHOWKSEY, V., MAURYA, D. M., KHONDE, N. and CHAMYAL, L. S. (2010) Tectonic geomorphology and evidence for active tilting of the Bela, Khadir and Bhanjada islands in the seismically active Kachchh palaeorift graben, Western India Z. Geomorphologie. v. 54, pp. 467–90.

CHOWKSEY, V., JOSHI, P., MAURYA, D. M. and CHAMYAL, L. S. (2011a) Ground penetrating radar characterization of fault-generated Quaternary colluvio-fluvial deposits along the seismically active Kachchh Mainland Fault, Western India. Current Science. v. 100 pp. 915–921.

CHOWKSEY, V., MAURYA, D. M., JOSHI, P., KHONDE, N., DAS, A. and CHAMYAL, L. S., (2011b) Lithostratigraphic development and neotectonic significance of the Quaternary sediments along the Kachchh Mainland Fault (KMF) zone, western India. J. Earth Sys. Sci. v. 120, pp. 979–99.

CHRISTIE, M., TSOFLIAS, G. P., STOCKLI, D. F. and BLACK, R., (2009) Assessing fault displacement and of-fault deformation in an extensional tectonic setting using 3-D ground penetrating radar imaging. J. Appl. Geophys. v. 68, pp. 9–16.

CHUNG, W.Y. and GAO, G., (1995) Source parameters of the Anjar earthquake of July 21, 1956, India and its seismotectonic implications for the Kutch rift basin. Tectonophysics. v. 242, pp. 281–292.

COOPER, F. J., ROBERTS, G. P., and UNDERWOOD, C. J., (2005) A comparison of 10^3-10^5 year uplift rates on the South Alkyonides Fault, central Greece: Holocene climate stability and the formation of coastal notches. Geophysical Research Letters , v. 33, pp.1-6.

COLTORTI, M., FAZIA, J. D., RIOS, F. P. and TITO, G. (2010) The Nuagapua alluvial fan sequence: Early and Late Holocene human-induced changes in the Bolivian Chaco?. Proc. Geologists' Assoc. v.121 pp. 218–228.

CUNNINGHAM, D., (2013) Mountain building processes in intracontinental oblique deformation belts: Lesson from the Gobi Corridor, Central Asia. Jour. Stru. Geol. v. 46, pp.255-282.

DAVIS, J. L. and ANNAN, A. P., (1989) Ground-penetrating radar for high resolution mapping of soil and rock stratigraphy. Geophy. Prospect., v. 37, pp. 531–551.

DEMANET, D., RENARDY, F., VANNESTE, K., JONGMANS, D., CAMELBEECK, T. and MEGHRAOUI, M., (2001) The use of geophysical prospecting for imaging active faults in the Roer Graben, Belgium Geophysics. v. 66 pp.78–89.

DANIELS, J. J., (2000) Ground Penetrating Radar Fundamentals. (Prepared as an appendix to a report to the U.S.EPA, Region V, Nov, 2000), available at <http://www.geology.ohio-state.edu

DENITH, M., O'NEILL, A. and CLARK, D. (2010) Ground penetrating radar as a means of studying palaeofault scarps in a deeply weathered terrain, southwestern Western Australia. Jour. Appl. Geophys. v. 72, pp. 92–101.

DEYNOUX, M., CINER, A., MONOD, O., KARABIYIKOGLU, M., MANATSCHAL, G. and TUZCU, S. (2005) Facies architecture and depositional evolution of alluvial fan to fan-delta complexes in the tectonically active Miocene Koprucay Basin, Isparta Angle, Turkey; Sed. Geol. v. 173, pp. 315–343.

DORSEY, R. J. and ROERING, J. J., (2006) Quaternary landscape evolution in the San Jacinto fault zone, peninsular ranges of southern California: Transient response to strike-slip fault initiation; Geomorphology. v. 73, pp. 16–32.

EATON, J. P., O'NEILL, M. E. and MURDOCK, J. N., (1970) Aftershocks of the 1966 Parkfield-Cholame, California, earthquake: A detailed study. Bulletin of Seismological Society of America. v. 60, pp. 1151–1197.

EKES, C. and HICKIN, E. J., (2001) Ground penetrating radar facies of the paraglacial Cheekye Fan, southwestern British Columbia, Canada. Sed. Geol. v.143, pp. 199–217.

FARR, T. G. and KOBRICK, M., (2000) Shuttle radar topography mission produces a wealth of data. Eos, Transactions American Geophysical Union. v.81(48), pp. 583-585.

FERRY, M., MEGHRAOUI, M., GIRARD, J., ROCKWELL, T. K., KOZACI, O., AKYUZ, S. and BARKA, A., (2004) Ground penetrating radar investigations along the North Anatolian fault near Izmit, Turkey: constraints on the right-lateral movement and slip history Geology. v. 32 pp. 85–88.

FISHER, S. C., STEWART, R. R. and JOL, H. M., (1996) Ground penetrating radar (GPR) data enhancement using seismic techniques. Jour. Eng. Env. Geophy. v. 1, pp. 88-96.

FIORE, J., PUGIN, A. and BERES, M., (2002) Sedimentological and GPR studies of subglacial deposits in the Joux Valley (Vaud, Switzerland): backset accretion in an esker followed by an erosive jökulhlaup. Géogra. Phys. Quat. v. 56, pp.19–32.

GANAS, A., PAVLIDES, S., KARASTATHIS, V., 2005. DEM-based morphometry of range-front escarpments in Attica, central Greece, and its relation to fault slip rates. Geomorphology. v. 65, pp. 301–319.

GANGOPADHYAY, A. and TALWANI, P., (2003) Symptomatic Features of Intraplate Earthquakes. Seismological Research Letters. v. 74(6), pp. 863-883.

GARCIA, A. F., ZHU, Z., KU, T. L., GALDEANO, C. S., CHADWICK, O. A. and CHAC O. N., MONTERO, J., (2003) Tectonically driven landscape development within the eastern Alpujarran Corridor, Betic Cordillera, SE Spain (Almeria); Geomorphology. v. 50 pp. 83–110.

GARZIONE, C. N., DECELLES, P. G., HODKINSON, D. G., OJHA, T. P. and UPRETI, B. N., (2003) East-west extension and Miocene environmental change in the southern Tibetan plateau: Thakkhola graben, central Nepal; Geol. Soc. Am. Bull. v. 115, pp. 3–20.

GHOSH, D. N. (1969) Biostratigraphic classification of the Patcham-Chari sequence at the Jumara dome section. Proc. 56th Ind. Sci. Cong., paert III, pp. 214.

GLENNIE, K. W. and EVANS, G. (1976) A reconnaissance of the recent sediments of the Ranns of Kutch, India. Sedimentology. v. 23, pp. 625–64.

GREEN, A. G., GROSS, R., HOLLIGER, K., HORSTMEYER, H., BALDWIN, J., (2003) Result of 3-D georadar surveying and trenching the San Andreas fault near its northern landward limit. Tectonophysics. v. 365, pp. 7-23.

Grohmann, C. H., (2004) Morphometric analysis in geographic information systems: applications of free software GRASS and R. v. 30(9-10), pp-1055-1067.

GROSS, R., GREEN, A.G. and HORSTMEYER, H., (2004) Location and geometry of the Wellington Fault (New Zealand) defined by detailed three-dimensional georadar data. Jour. Geophy. Res. (Solid Earth-Red), v. 109(B5), art. no. B05401.

GUPTA, H. K., RAO, P. N., RASTOGI, B. K. and SARKAR, D., (2001) The Deadliest Intraplate Earthquake. v. 291, pp. 2101-2102.

GUPTA, S. K., (1975) Silting of the Rann of the Kutch during the Holocene. Ind. Jour of Earth Sci. v. 2, pp. 163-175.

HACK, J.T., (1973) Stream-profile analysis and stream-gradient index. U.S. Geological Survey Journal of Research. v. 1, pp. 421–429.

HARE, P. W. and GARDNER, T.W., (1985) Geomorphic indicators of vertical neotectonism along converging plate margins, Nicoya Peninsula, Costa Rica In:M. Morisawa & J.T.Hack (eds): Tectonic geomorphology: Proceedings of the 15th GeomorphologySymposiaSeries. Binghamton, 1985, pp.76-104.

HASHIMI, N. H., NIGAM, R., NAIR, R. R. and RAJGOPALAN, G. (1995) Holocene sea level fluctuations on western Indian continental margin: An update. Jour. Geol. Soc. of India. v. 46 pp. 157-162.

HEIN, F. J. and WALKER, R. G., (1977) Bar evolution and development of stratification in the gravelly braided Kicking Horse River, British Columbia; Canadian J. Earth Sci. v. 14, pp. 562–570.

HILL, D. P., (1977) A model for earthquake swarms. Jour. Geophy. Res., v. 82, pp. 1347–1352.

HORTON, R. E., (1932) Drainage basin characteristics. Amer. Geophys. Union, Trans. v.13, pp. 348–352.

HUMPHREY, N. F. and KONRAD, S. K. (2000) River incision or diversion in response to bedrock uplift. Geology. v. 28 pp. 43–46.

JOHNSON, C. E. and HADLEY, D. M., (1976) Tectonic implications of the Brawley earthquake swarm, Imperial Valley, California, 1975. Bulletin Seismological Society America, v. 66, pp. 1132–1144.

JOL, H. M., SMITH, D. G., (1991) Ground Penetrating Radar of northern lacustrine deltas. Canadian Journal of Earth Sciences, v. 28, pp. 1939–1947.

JOL, H. M. (1995) Ground penetrating radar antenna frequencies and transmitter powers compared for penetration depth, resolution and reflection continuity Geophys. Prosp. v. 43, pp. 693–709

JOL, H. M. and BRISTOW, C. S.,(2003) GPR in sediments: advice on data collection, basic processing and interpretation, a good practice guide. In *GPR in Sediments* (eds Bristow, C. S. and Jol, H. M.), Spec. Publ. Geol. Soc. Lon., 2003, v. 211, pp. 9–27.

JOSHI, P., MAURYA, D. M., CHOWKSEY, V. and CHAMYAL, L. S. (2012) Proc. 14th Int. Conf. on Ground Penetrating Radar (Shanghai). v.3, pp. 850.

JOSHI, P. N., MAURYA, D. M., CHAMYAL, L. S., (2013) Morphotectonic segmentation and spatial variability of neotectonic activity along the Narmada–Son Fault, Western India: Remote sensing and GIS analysis, Geomorphology, v. 180, PP. 292-306.

KALLMEIER, E., BREITKREUZ, C., KIERSNOWSKI, H. and GEIßLER, M. (2010) Issues associated with the distinction between climatic and tectonic controls on Permian alluvial fan deposits from the Kotzen and Barnim Basins (North German Basin); Sed. Geol. v. 223 pp.15–34.

KELLER, E.A. and PINTER, N., (2002) Active Tectonics. Earthquakes, Uplift and Landscape. Prentice Hall, New Jersey, pp. 362.

KAYAL, J. R., ZHAO, D., MISHRA, O. P., DE, R., SINGH, O.P. (2002) The 2001 Bhuj earthquake: tomographic evidence for fluid at the hypocenter and its implications for rupture nucleation. Geophys. Res. Lett. v. 29, pp. 51-54.

KAR, A., (1995) Geomorphology of the western India. Mem. Geol. Soc. India, v.32, pp.168–190.

KHONDE, N., MAURYA, D. M., SINGH, A. D., CHOWKSEY, V. and CHAMYAL, L. S. (2011) Environmental significance of raised rann sediments along the margins of Khadir, Bhanjada and Kuar bet islands in Great Rann of Kachchh, Western India Curr. Sci. v. 101 pp. 1429–1434

KOSTIC, B., BECHT, A. and AIGNER, T., (2005) 3-D sedimentary architecture of a Quaternary gravel delta (SW-Germany): Implications for hydrostratigraphy. Sed. Geol. v. 181, pp.143–171.

KOSTIC, B. and AIGNER, T., (2007) Sedimentary architecture and 3D ground-penetrating radar analysis of gravelly meandering river deposits (Neckar Valley, SW Germany). Sedimentology, v. 54, pp. 789–808.

KRUK, J. V. D. and SLOB, E. C., (2004) Reduction of reflection from above surface objects in GPR data. Jour. Appl. Geophy. v. 55, pp. 271-278.

KUNDU, H. K., THAKKAR, M. G., BISWAS, R. H. and SINGHVI, A. K., (2010) Optical dating of sediments in khari river basin and slip rate along Katrol Hill Fault (KHF), Kachchh, India. Geochronometria. v. 37, pp 21-28.

LEEDER, M. R., SEGER, M. J. and STARK, C. P. (1991) Sedimentation and tectonic geomorphology adjacent to major active and inactive normal faults, southern Greece; J. Geol. Soc. Lon. v. 148, pp. 331–343.

LIU, M., STEIN, S., WANG, H., (2011) 2000 years of migrating earthquakes in north China: how earthquakes in midcontinents differ from those at plate boundaries. Lithosphere. v. 3(2), pp. 128-132.

MALAVIEILLE, J., (1984) Modelisation experimentale des chevauchements imbrique´ s: application aux chaıˆnes de montagnes. Bulletin Societe´ Ge´ ologique de France. v. 7, pp. 129–138.

MANDAL, P., RASTOGI, B.K., SATYANARAYANA, H.V.S., KOUSALYA, M., VIJAYRAGHAVAN, R., SATYAMURTHY, C., RAJU, I.P., SARMA, A.N.S. and KUMAR, N. (2004a) Characterization of the causative fault system for the 2001 Bhuj earthquake of Mw 7.7. Tectonophysics, v.378, pp.105-121.

MANDAL, P., RASTOGI, B.K., SATYANARAYANA, H.V.S., KOUSALYA, M., 2004b. Results from Local Earthquake velocity tomography: implications toward the source process involved in generating the 2001 Bhuj Earthquake in the Lower Crust beneath Kachchh (India). Bull. Seism. Soc. Am., v. 94 (2), pp. 633–649.

MANDAL, P., CHADHA, R. K., RAJU, I. P., KUMAR, N., SATYAMURTY, C., NARSAIAH, R. and MAJI, A., (2007a) Coulomb static stress variations in the Kachchh, Gujarat, India: Implications for the occurrences of two recent earthquakes (Mw 5.6) in the 2001 Bhuj earthquake region. Geophys. Jour. Internat., v.169, pp. 281-285.

MANDAL, P., CHADHA, R. K., RAJU, I. P., KUMAR, N., SATYAMURTY, C. and NARSAIAH, R., (2007b) Are the occurrences of the 7th March 2006 Mw 5.6 event along the GEDI fault and the 3rd February 2006 Mw 4.58 event along the Island Belt fault triggered by the five years continued occurrence of aftershocks of the 2001 Mw 7.7 Bhuj event? Curr. Sci., v. 92(8), pp.1114-1124.

MANDAL, P. (2008) Stress rotation in the Kachchh rift zone, Gujarat, India. Pure Appl. Geophys. v. 165. pp. 1307–1324

MANDAL, P., (2009) Estimation of Static Stress Changes after the 2001 Bhuj Earthquake: Implications towards the Northward Spatial Migration of the Seismic Activity in Kachchh, Gujarat, Jour. Geol. Soc. India, v. 74, pp. 487-497.

MANDAL, P. and CHADHA, R. K., (2008) Three-dimensional velocity imaging of the Kachchh seismic zone, Gujarat, India. Tectonophysics. v. 452, pp. 1–16.

MANDAL, P. and PANDAY, O. P., (2010) Relocation of aftershocks of the 2001 Bhuj earthquake: a new insight into seismotectonics of the Kachchh seismic zone, Gujarat, India J. Geodyn. v.49, pp.254–60

MAURYA, D. M., THAKKAR, M. G. and CHAMYAL, L. S. (2003a) Implications of transverse fault system on tectonic evolution of Mainland Kachchh, Western India. Curr. Sci. v. 85, pp. 661–667.

MAURYA, D. M., BHANDARI, S., THAKKAR, M. G. and CHAMYAL, L. S. (2003b) Late Quaternary fluvial sequences of southern Mainland Kachchh, western India; Curr. Sci. v. 84, pp.1056–1064.

MAURYA, D. M., PATIDAR, A. K., MULCHANDANI, N., GOYAL, B., THAKKAR, M. G., BHANDARI, S., VAID, S. I., BHATT, N. P. and CHAMYAL, L. S. (2005) Need for initiating ground penetrating radar studies along active faults in India: An example from Kachchh. Current Science. v. 88, pp. 231-240.

MAURYA, D.M., GOYAL, B., PATIDAR, A.K., MULCHANDANI, N., THAKKAR, M.G. and CHAMYAL, L.S., (2006) Ground Penetrating Radar imaging of two large sand blow craters related to the 2001 Bhuj earthquake, Kachchh, Western India. Jour. Appl. Geophy. v. 60, pp. 142-152.

MAURYA, D .M., THAKKAR, M. G., PATIDAR, A. K., BHANDARI, S., GOYAL, B. and CHAMYAL, L. S., (2008) Late Quaternary geomorphic evolution of the coastal zone of Kachchh, western India; J. Coasstal Res. v.24, pp. 746–758.

MAURYA, D. M., Thakkar, M. G., Khonde, N., and Chamyal L. S. (2009) Geomorphology of the Little Rann of Kachchh, W. India: Implication for basin architecture and Holocene palaeo-oceanographic conditions. Zeischrift fur Geomorphologie, v. 53, pp. 69-80.

MAURYA, D. M., CHOWKSEY, V., JOSHI, PARUL, N. AND CHAMYAL, L. S. (2013) Application of Ground Penetrating Radar for delineating neotectonic setting and shallow subsurface nature of the seismically active Gedi Fault, Kachchh, Western India. Jour. Geophysics and Engineering, DOI:10.1088/1742-2132/10/3/034006

MAYER, L., (1990) Introduction to Quantitative Geomorphology. Prentice Hall, Englewood, 380p.

MCCALPIN, J. P. and THAKKAR, M.G., (2003) 2001 Bhuj-Kachchh earthquake: surface faulting and its relation with neotectonics and regional structures, Gujarat, Western India, In: D. Pantoshi, K. Berrymann, R.Yeats and Y. Kinugasa (Eds.), Ten years of Paleoseismology in the ILP, progress and prospects, Annals of Geophysics. v. 46 (5), pp. 937-956.

MCCLYMONT, A. F., GREEN, A. G., KAISER, A., HORSTMEYER, H. and LANGRIDGE, R. (2010) Shallow fault segmentation of the alpine fault zone, New Zealand revealed from 2- and 3D GPR surveying J. Appl. Geoph. v.70, pp. 343–54.

McCLYMONT, A. F., GREEN, A. G., STREICH, R., HORSTMEYER, H., TRONICKE, G., NOBES, D. C., PETTINGA, J., CAMPBELL, J. and LANGRIDGE, R. (2008) Visualization of active faults using geometric attributes of 3D GPR data: an example from the alpine fault zone, New Zealand Geophysics v.73, pp. B11–23

MENÉNDEZ, I., SILVA, P.G., MARTÍN-BETANCOR, M., PÉREZ-TORRADO, F. J., GUILLOU, H., SCAILLET, S., (2008) Fluvial dissection, isostatic uplift, and geomorphological evolution of volcanic islands (Gran Canaria, Canary Islands, Spain), Geomorphology. v. 102, pp. 189–203.

MESCHEDE, M., ASPIRON, U. and REICHERTER, K., (1997) Visualization of tectonic structures in shallow-depth high-resolution ground penetrating radar (GPR) profiles. Terra Nova. v. 9, pp. 167-170.

MCPHERSON, J. G., SHANMUGAM, G. and MOIOLA, R. J. (1987) Fan deltas and braid deltas: Varieties of coarse-grained deltas; Geol.Soc.Am.Bull. v. 99, pp. 331–340.

MERH, S. S., (2005) The Great rann of Kachchh: perception of a field geologist. Jour. Geol. Soc. India. v. 65 pp. 9–25

MERRITTS, D. and VINCENT, K. R., (1989) Geomorphic response of coastal streams to low, intermediate, and high rates of uplift, Medocino triple junction region, northern California Geological Society of America Bull. v. 101(11), pp. 1373-1388.

MESCHEDE, M., ASPIRON, U. and REICHERTER, K., (1997) Visualization of tectonic structures in shallow-depth high-resolution ground penetrating radar (GPR) profiles Terra Nova. v.9, pp. 167–170

MIALL, A. D. (1977) A review of the braided-river depositional environment. Earth Sci. Rev. v. 13, pp. 1–62.

MIALL, A. D., (1996) The geology of fluvial deposits. Springer, Berlin, 582p.

MILLER, V. C., (1953) A quantitative geomorphic study of drainage basin characteristics in the Clinch mountain area. NR Technical Report 3: Va. and Tenn. Office Naval Research Project.

MISRA, D. C., CHANDRASEKHAR, D. V., SINGH, B., (2005). Tectonic and crustal structures related to Bhuj earthquake of January 26, 2001: based on gravity and magnetic surveys constrained from seismic and seismological studies. Tectonophysics. v. 396, pp. 195-207.

MOLNAR, P. and TAPPONNIER, P. (1975) Cenozoic tectonics of Asia: Effects of a continental collision. Science, New Series, v. 189(4201), pp. 419-426.

MOLIN, P., FUBELLI, G., (2005) Morphometric evidence of the topographic growth of the Central Apennines. Geografia Fisica e Dinamica Quaternaria. v. 28, pp. 47–61.

MULCHANDANI, N., PATIDAR, A. K., VAID, S. I. and MAURYA, D.M. (2007) Late Cenozoic geomorphic evolution in response to inversion tectonics, Kim river basin, Western India. Journal of Asian Earthsciences, v. 30, pp. 33-52.

NEAL, A., (2004) Ground-penetrating radar and its use in sedimentology: principles, problems and progress. Earth Sci. Rev., v.66, pp.161–330.

NELSON, R. E., (1846) Notice of an earthquake and a probable subsidence of the land in the district of Cutch, near the mouth of the Koree, or eastern branch of the Indus, in June 1845. Quart. J. Geol. Soc. London, v. 2, pp. 103.

NEMEC, W. and KAZANCI, N., (1999) Quaternary colluviums in west-central Anatolia:sedimentary facies and paleoclimatic significance, Sedimentology. v. 46, pp. 139-170.

OLDHAM, R. D., (1898). A note on the Allah Bund in the northwest of the Runn of Cutch, Memoirs Geological Survey of India, v. 28, pp. 27–30.

OLDHAM, R. D., (1926) The Cutch (Kachh) Earthquake of 16th June 1819 With a Revision of Great Earthquake of 12th June, 1897. Memoire Geological Survey of India. v. 46, pp. 1–77

OLHOEFT, G. R., (1984) Application and limitations of ground penetrating radar. 54th Annual international Meeting and exposition of the society of exploration Geophysicists, December, 2-6, Atlanta, Georgia, Expanded Abstract with Biographies, pp. 147-148.

OLHOEFT, G. R., (2000) Maximizing the information return from ground penetrating radar. Jour. App. Geophy. v. 43(2-4), pp. 175–187

OVERMEEREN, R. A. V., (1998) Radar facies of unconsolidated sediments in The Netherlands: a radar stratigraphy interpretation method for hydrogeology. J. Appl. Geophy., v.40, pp.1–18.

PATIDAR, A. K., MAURYA, D. M., THAKKAR, M. G. and CHAMYAL, L. S. (2006) Shallow subsurface characterization of active faults using Ground Penetrating Radar: example of Katrol Hill Fault (KHF), Kachchh, western India. 11th International Conference on Ground Penetrating Radar, (GPR 2006), The Ohio State University, Columbus, USA.

PATIDAR, A. K., MAURYA, D. M., THAKKAR, M. G. and CHAMYAL, L. S. (2007) Fluvial geomorphology and neotectonic activity based on field and GPR data, Katrol hill range, Kachchh, western India; Quat. Int. v. 159, pp.74–92.

PATIDAR, A. K., MAURYA, D. M., THAKKAR, M. G, and CHAMYAL, L. S., (2008) Evidence of neotectonic reactivation of the Katrol Hill Fault during late Quaternary and its GPR characterization; Curr. Sci. v. 94, pp.338–346.

PAUSELLI, C., FEDERICO, C., FRIGERI, A., OROSEI, R., BARCHI, M. R. and BASILE, G. (2010) Ground penetrating radar investigations to study active faults in the Norcia basin (central Italy) J. Appl. Geophys. v. 72, pp.39–45.

PIKE, R.J., WILSON, S.E., (1971) Elevation–relief ratio, hypsometric integral and geomorphic area–altitude analysis. Geol. Soc. Amer. Bull. v. 82, pp. 1079–1084.

PIRAZZOLI, P. A., (1986) Marine notches. In: vande Plassche, O.(ed). Sea-level Research: a Manual for the Collection and Evaluation of Data, Geo Books, Norwich, UK. pp. 361-400.

POPE, R., WILKINSON, K., SKOURTSOS, E., TRIANTAPHYLLOU, M. and FERRIER, G. (2008) Clarifying stages of alluvial fan evolution along the Sfakian piedmont, southern Crete: New evidence from analysis of post-incisive soils and OSL dating. Geomorphology. v. 94, pp. 206–225.

POLLITZ, F., VERGNOLLE, M., CALAIS, E., (2003) Fault interaction and stress triggering of twentieth century earthquakes in Mongolia. Jor. Geophy. Res. B: Solid Earth 108.ETG 16-1-ETG 16-14.

QUITTMEYER, R. C. and JACOB, K. H., (1979) Historical and modern seismicity of Pakistan, Afganistan, northern and southern Iran. Bull. Seismol. Soc. Am., v. 69, pp. 773-823.

RAJENDRAN, C.P. and RAJENDRAN, K., (2001) Characteristics of deformation and past seismicity associated with the 1819 Kutch earthquake, northwestern India. Bull. Seismol. Soc. Am. v. 91(3), pp. 407-426.

RAJENDRAN K, RAJENDRAN C P, THAKKAR M and TUTTLE M P (2001) The 2001 Kutch (Bhuj) earthquake: Coseismic surface features and their significance. Current Science. v. 80(11), pp. 1397-1405.

RAJENDRAN, C. P., RAJENDRAN, K., THAKKAR, M. G. and GOYAL, B. (2008) Assessing the previous activity at the source zone of the 2001 Bhuj earthquake based on the near-source and distant paleoseismological indicators J. Geophys. Res. v.113, pp.B05311

RAJNATH, (1932) A contribution to the stratigraphy of Cutch. Quart. Journ. Geol. Min. Met. Soc. Ind, v. 4, pp. 161-174

RASHED, M., KAWAMURA, D., NEMOTO, H., MIYATA, T. and NAKAGAWA, K. (2003) Ground penetrating radar investigations across the Uemachi fault, Osaka, Japan J. Appl. Geophys. v. 53, pp.63-75

ROY, B. and MERH, S. S., (1981) The Great Rann of Kutch—an intriguing Quaternary terrain. Recent Researches in Geology. Hindustan Publishing Corporation, India. pp. 100-108.

RUST, B. R., (1978) Depositional models for braided alluvium, In: Fluvial Sedimentology (ed.) Miall A D, Can. Soc. Petrol. Geol. Mem. v.5, pp.605–625.

RUST, R., and KERSHAW, S., (2000). Holocene tectonic uplift pattern in northeastern Sicily: evidence from marine notches in coastal outcrop. Mar. Geol. v. 167(1-2), pp. 105-126.

SANDIFORD, M. and HAND, M., (1998) Controls on the locus of intraplate deformation in central Australia. Earth and Plan. Sci. Lett. v. 162(1-4), pp. 97-110.

SALVI, S., CINTI, F. R., COLINI, L., ADDEZIO, G. D., DOUMAZ, F. and PETTINELLI, E. (2003) Investigation of the active Celano-L'Aquila fault system, Abruzzi (central Appennines, Italy) with combined ground penetrating radar and palaeoseismic trenching. Geophysical Journal International. v. 155, pp. 805-818.

SAARENKETO, T. (1998) Electrical properties of water in clay and silty soils. Jour. Appl. Geoph. v. 40(1-3), pp. 73-88

SASS, O. and KRAUTBLATTER, M., (2007) Debris flow-dominated and rockfall-dominated talus slopes: Genetic models derived from GPR measurements. Geomorphology. v. 86, pp.176–192.

SCHUMN, S. A., (1956) Evolution of drainage systems and slopes in badlands at Perth Amboy, New Jersey. Geol. Soc. Am. Bull. v. 67, pp.597-646.

SCHUMM, S. A., DUMONT, J. F. and HOLBROOK, J. M., (2000) Active tectonics and alluvial rivers. Cambridge University Press. pp. 274.

SMITH, D. G. AND JOL, H. M., (1995) Wasatch fault (Utah), detected and displacement characterized by ground-penetrating radar. Environ. Eng. Geosci., v.1, pp.489–496.

SMITH, N. D., (1970) The Braided Stream Depositional Environment: Comparison of the Platte River with Some Silurian Clastic Rocks, North-Central Appalachians, Geol. Soc. Of America Bulletin, v. 81(10), pp. 2993-3014.

SLATER, L. and NIEMI, T.M., (2003) Ground-penetrating radar investigation of active faults along the Dead Sea Transform and implication for seismic hazards within city of Aqaba, Jordan. Tectonophysics, v. 368, pp. 33-50.

SNOW, R. S. and SLINGERLAND,R. L.(1990) Stream Profile Adjustment to Crustal Warping: Nonlinear Results from a Simple Model. The Journal of Geology. v. 98, pp. 699-708.

SOMAYAJULU, B. L. K., (1993) Age and mineralogy of the miliolites of Saurashtra and Kachchh, Gujarat; Curr. Sci. v. 64, pp. 926–928.

SRIDEVI, J., MUKAL, M., PARVEZ, I. A., ANANDA, M. B., KUMAR, P. D. K GUAR, V., (2001) Estimate of coseismic displacement and post seismic deformation using global positioning system geodesy for Bhuj earthquake of 26 Jan 2001. Curr, Sci. v. 82, pp.748–752.

SRIDHAR, A. and PATIDAR, A., (2005) Ground penetrating radar studies of a point-bar in the Mahi River Basin, Gujarat. Current Science, v. 89, pp. 183-189.

STOKES, M. and MATHER, A. E., (2000) Response of Plio-Pleistocene alluvial systems to tectonically induced base level changes, Vera Basin, SE Spain; J. Geol. Soc. Lon. v. 157, pp.303–316.

STRAHLER, A.N., (1952) Hypsometric (area-altitude) analysis of erosional topography. Geol. Soc. Am. Bull. v. 63, pp. 1117–1142.

STRAHLER, A. N., (1964). Quantitative geomorphology of drainage basins and channel networks. In: Chow, V. T., (ed), Handbook of applied hydrology. McGraw Hill Book Company, New York, Section 4-11.

SUN, J. and YOUNG, R. A. (1995) Recognizing surface scattering in ground-penetrating radar data. Geophysics. v. 60, pp. 1378–85.

TALWANI, P., (1988) The Intersection Model for Intraplate Earthquakes. Seismological Research Letters. v. 59(4), pp. 305-310.

THAKKAR, M. G., MAURYA, D. M., RAJ, R. and CHAMYAL, L. S., (1999) Quaternary tectonic history and Terrain evolution of the area around Bhuj, mainland Kachchh, western India. J. Geol. Soc. India, v. 53, pp. 601–610.

THAKUR, V.C. and WESNOUSKY, S.G., (2002) Seismotectonics of 26 January, 2001 Bhuj earthquake affected region. Curr. Sci., v. 82(4), pp. 396-399.

TODOESCHUCK, J. P., LAFLECHE, P. T., JENSEN, O. G., JUDGE, A. S. and PILON, J. A., (1992) Deconvolution of ground probing radar data. In Pilon, J.A. (eds.) Ground Penetrating Radar. Geological Survey of Canada Paper. v. 90(4), pp. 227-230.

TAPPONNIER, P., PELTZER, G., LE DAIN, A.Y., ARMIJO, R., COBBOLD, P., 1982. Propagatingextrusion tectonics in Asia: new insights from simple experiments with plasticine. Geology 10, 611-616.

TOPP, G. C., DAVIS, J. L. and ANNAN, A. P. (1980) Electromagnetic determination of soil water content: mesurements in coaxial transmission lines. Water Resource Research, v. 16, pp. 574-582.

VAN DAM, R. L. and SCHLAGER, W. (2000) Identifying causes of groundpenetrating radar reflections using time-domain reflectometry and sedimentological analyses. Sedimentology. v. 47, pp. 435–449.

VAN DER KRUK, J. and SLOB, E. C., (1998) Determination of the E□ective Source Wavelet, Proceedings Seventh international conference on Ground-Penetrating Radar, Lawrence, Kansas, USA, May 27-30, 1998, pp. 625-630.

VAN DER KRUK, J., SLOB, E. C., and Fokkema, J. T., (1999), Background of Ground Penetrating Radar measurements, Geologie en Mijnbouw. v. 77, pp. 177-188.

VIOLA, G., ODONNE, F., and MANCKTELOW, N.S. (2004) Analogue modelling of reverse fault reactivation in strike–slip and transpressive regimes: application to the Giudicarie fault system, Italian Eastern Alps. Jour. of Str. Geol. v. 36, pp. 401-418.

WALLACE, S. C., NOBES, D. C., DAVIS, K. J., BURBANK, D. W. and WHITE, A. (2010) Three-dimensional GPR imaging of the Benmore anticline and step-over of the Ostler fault, South Island, New Zealand Geophys. Jour. Int. v.180, pp. 465–74.

WYNNE, A. B., (1872) The geology of Kachchh. Mem. Geol. Surv. India. v. 9, pp. 289.

YILMAZ, O., (2001) Seismic Data Analysis. Soc. Expl. Geophysics, Tulsa.

YOUNG, R.A. and SUN, J. (1998) Extracting a Radar Reflection from a Cluttered Environment Using 3-D Interpretation. Journal of Environmental and Engineering Geophysics, v. 3, pp. 21-131.

YOUNG, R. A., DENG, Z. and SUN, J., (1995) Interactive processing of GPR data. The Leading Edge. v. 14, pp. 275-280.

LIST OF PUBLICATIONS OF VIKAS CHOWKSEY

INTERNATIONAL

1. MAURYA, D.M., **CHOWKSEY, V.**, JOSHI, P. and CHAMYAL, L.S. (In press) Application of Ground Penetrating Radar for delineating neotectonic setting and shallow subsurface nature of the seismically active Gedi Fault, Kachchh, Western India. **Journal of Geophysics and Engineering**
2. SHUKLA, S. B., **CHOWKSEY, V.**, PRIZOMWALA, S., UKEY, V., BHATT, N. P. and MAURYA, D. M. (In press) Internal sedimentary architecture and coastal dynamics as revealed by Ground Penetrating Radar (GPR), Kachchh coast, western India. **Acta Geophysica.**
3. JOSHI, P., MAURYA, D. M., **CHOWKSEY, V.** and CHAMYAL, L.S. (2012) Shallow subsurface mapping of active faults using GPR in the seismically active Kachchh palaeorift basin, western India: Implication for neotectonic activity. **Proc. 14th Inter. Conf. on Ground Penetrating Radar, 2012,** Shanghai, China, pp. 850-855.
4. **CHOWKSEY, V.**, MAURYA, D. M., KHONDE, N. and CHAMYAL, L.S. (2010) Tectonic geomorphology and evidence for active tilting of the Bela, Khadir and Bhanjada islands in the seismically active Kachchh palaeorift graben, Western India. **Zeischrift fur Geomorphologie,** v. 54, pp. 467-490.

NATIONAL

5. **CHOWKSEY, V.,** MAURYA, D. M., KHONDE, N., JOSHI, P. and CHAMYAL, L.S. (Comm) Active tectonic control on landscape and Quaternary sedimentation in the Pachham Island, Kachchh, Western India. **Jour. Geol. Soc. India** (Comm.)
6. MAURYA, D. M., KHONDE, N., DAS, A., **CHOWKSEY, V**. and CHAMYAL, L. S. (2013) Subsurface lithostratigraphy of the Great Rann of Kachchh from preliminary textural analysis of two continuous cores. **Current Science**, v.104, pp.1071-1077.
7. **CHOWKSEY, V**., MAURYA, D. M., JOSHI, P., KHONDE, N., DAS, A. and CHAMYAL, L.S. (2011) Lithostratigraphic development and neotectonic significance of the Quaternary sediments along the Kachchh Mainland Fault (KMF) zone, Western India. **Jour. Earth System Science**, v.120, pp. 979-999.
8. KHONDE, N., MAURYA, D. M., SINGH A. D., **CHOWKSEY, V.** and CHAMYAL L. S. (2011) Environmental significance of raised rann sediments along the margins of the Khadir, Bhanjada and Kuar bet islands in the Great Rann of Kachchh, western India. **Current Science**, v. 101, pp. 1429-1434.
9. **CHOWKSEY, V**., JOSHI, P., MAURYA, D. M. and CHAMYAL, L. S. (2011) Application of Ground Penetrating Radar (GPR) for characterization of fault-generated Quaternary colluvio-fluvial deposits along the seismically active Kachchh Mainland Fault (KMF), Western India. **Current Science**, v.100, pp. 915-921.
10. KHONDE, N., MAURYA, D. M., **CHOWKSEY, V**., THAKKAR, M. G. and CHAMYAL, L. S. (2010) Tectonic geomorphology of the Chang river basin in SE Wagad, Kachchh, Western India. In: Geological processes and climate change (Eds. D. S. Singh and N. L. Chhabra), Macmillan Publisher India Ltd. pp. 151-162.